Aus dem Institut für Molekulare Onkologie,
Direktor: Prof. Dr. Thorsten Stiewe
des Fachbereichs Medizin der Philipps-Universität Marburg

Functional characterization of the *TP53* mutome using CRISPR/Cas9 saturating mutagenesis

Inaugural-Dissertation
zur Erlangung des Doktorgrades der Naturwissenschaften
dem Fachbereich Medizin der Philipps-Universität Marburg
vorgelegt von

Mariia Klimovich
aus Sankt Petersburg

Marburg, 2021

Angenommen vom Fachbereich Medizin der Philipps-Universität Marburg am:

Gedruckt mit Genehmigung des Fachbereichs.

Dekanin: Prof. Dr. Denise Hilfiker-Kleiner
Referent: Prof. Dr. Thorsten Stiewe
Korreferent: Prof. Dr. Malte Buchholz

For my best friend and
husband Boris & my sister

"Change is the essential process of all existence."

(Mister Spock)

Lists of abbreviations

ARF	Alternative reading frame
ATM	Ataxia Telangiectasia Mutated
ATP	Adenosine triphosphate
ATR	Ataxia Telangiectasia and Rad3-related protein
BAX	BCL2-Associated X Protein
BBC3/PUMA	BCL2 Binding Component 3
Bcl-2	B-cell lymphoma 2
Bcl-xL	B-cell lymphoma-extra large
BRCA1	BReast CAncer 1, early-onset
CDKN1A/CDKN2A	Cyclin-Dependent Kinase Inhibitor 1A (p21) / 2A (p14ARF/p16)
CHK2	Checkpoint kinase 2
CRISPR	Clustered Regularly Interspaced Short Palindromic Repeats
DBD	DNA binding domain
DN-effect	Dominant-negative effect
DTT	Dithiothreitol
GADD45	Growth Arrest and DNA Damage
GOF	Gain of function
Hsp70	Heat Shock Protein 70 kDa
Hsp90	Heat Shock Protein 90 kDa
LOF/pLOF	Loss of function/partial-loss of function
MDM2	Mouse double minute 2 homolog
MDM4/MDMX	Mouse double minute 4
mRNA	messenger RNA
NGS	Next generation sequencing
NOXA	Phorbol-12-Myristate-13-Acetate-Induced Protein 1
PAI1	Plasminogen activator inhibitor-1
PAM	Protospacer adjacent motif
PML	Promyelocytic leukemia protein
Rb	Retinoblastoma

SESN1/SESN2	Sestrin 1 / Sestrin 2
Suv39h	Histone-lysine N-methyltransferase

Amino acids table

A	Alanine
C	Cysteine
D	Aspartic acid
E	Glutamic acid
F	Phenylalanine
G	Glycine
H	Histidine
I	Isoleucine
K	Lysine
L	Leucine
M	Methionine
N	Asparagine
P	Proline
Q	Glutamine
R	Arginine
S	Serine
T	Threonine
V	Valine
W	Tryptophan
Y	Tyrosine

Abstract

TP53 is an essential tumor suppressor gene which is inactivated in every second tumor. Most frequently *TP53* is disabled by missense mutations which result in the expression of a mutant p53 protein. Mutant p53 protein is unable to prevent uncontrolled proliferation and can additionally increase cancer growth by dominant negative and gain of function effects. Mutations in *TP53* are frequently associated with aggressive tumor growth, chemotherapy resistance and shortened survival. Therefore, the *TP53* gene status has important clinical implication. Moreover, information about *TP53* mutations will be essential for application of emerging p53-targeted therapeutics: Mdm2 inhibitors and p53 reactivators.

Eight most frequent hotspot mutations account for nearly 30% of all missense *TP53* variants found in tumors and are extensively studied. Hotspot *TP53* mutations lead to production of a transcriptionally inactive loss of function protein. The rest 70% of *TP53*-mutated tumors contain one of >2000 distinct mutant p53 variants, most of which are uncharacterized. Such a broad spectrum of mutants makes prediction of their impact on disease outcome a very challenging task. Therefore, for advancing personalized cancer treatment it would be of utmost importance to study how the hundreds of individual p53 mutations influence a therapy response. Functional characterization of hundreds of mutations in a gene of interest is a tall order task which requires time-consuming *in vitro* and *in vivo* experiments. Thus, an experimental approach for a massive parallel phenotypic screening of mutations in *TP53* gene would be of a great value.

In the present work we took advantage of the CRISPR-Cas9 gene editing technology to develop the CSMS – CRISPR-based saturated mutagenesis screening of *TP53* gene, an improved system for massive parallel functional screening of p53 mutants.

We have established rapid and flexible protocol of targeting p53 mutations into endogenous *TP53* locus using CRISPR-Cas9-induced homology-directed repair. We have validated CSMS by performing saturation mutagenesis of the short protein motif and demonstrated outstanding performance. We have scaled our protocol up to establish a high-throughput method that allows precise functional characterization of thousands of p53 variants. We have tested effects of p53 mutations on response to Mdm2 inhibitors and irradiation and revealed excellent correlation of screening

results with known structural, functional and clinical data. Furthermore, we have demonstrated that CMSM is able to highlight even subtle functional difference between mutants and identify partially loss of function mutants. Manipulating the endogenous *TP53* locus allowed us to study effects of mutation in non-coding regions, which was previously unachievable. A detailed comparison of our data with the previously published studies provided compelling evidence, that the procedure established in our study is significantly more accurate in categorization of pathogenic *TP53* mutations.

In summary, we have attested CSMS as a powerful tool to catalogue *TP53* mutations. This tool can be used in the future to increase the utility of mutations in *TP53* as clinical biomarkers.

Zusammenfassung

TP53 ist ein essentieller Tumorsuppressor, der in jedem zweiten Tumor inaktiviert vorliegt. In den meisten Fällen ist die Ursache hierfür eine *missense* Mutation, welche zur Expression eines veränderten p53-Proteins führt.

Das mutierte p53 Protein ist nicht in der Lage eine unkontrollierte Proliferation zu verhindern und kann das Tumorwachstum im Falle von dominant-negativen oder *gain of function* Mutationen sogar aktiv unterstützen.

Mutationen im *TP53* Gen sind häufig assoziiert mit einem aggressiven Tumorwachstum, Chemoresistenz und einer kürzeren Überlebensspanne der Patienten. Aus diesem Grund ist der p53 Genstatus von hoher klinischer Relevanz. Darüber hinaus sind Informationen zu verschiedenen TP53 Mutationen essentiell für die Applikation vergleichsweise neuer Therapiestrategien, welche gezielt an p53 ansetzen: Mdm2-Inhibitoren und p53-Reaktivatoren.

Die acht häufigsten so genannten *Hotspot* Mutationen versachen nahezu 30% aller in Tumoren gefundenen p53 *missense*-Mutationen und werden daher umfassend untersucht. Diese *Hots*pot Mutationen führen zur Produktion von transkriptionell inaktiven *loss-of-function* Proteinen. Die restlichen 70% der *TP53* Mutationen bestehen aus mehr als 2000 unterschiedlichen p53 Varianten, von denen die meisten bisher nicht charakterisiert sind. Neben Tumor-assoziierten *non-Hotspot* Mutationen macht diese Vielzahl an Mutanten eine Vorhersage über ihren Einfluss auf die Erkrankung zu einer großen Herausforderung.

Aus diesem Grund wäre es für eine verbesserte personalisierte Krebstherapie von großer Wichtigkeit, heraus zu finden, wie hunderte verschiedener individueller p53 Mutationen die Therapieantwort beeinflussen.

Die funktionelle Charakterisierung hunderter Mutationen eines Gens ist eine umfassende Aufgabe, die zeitaufwendige *in vitro* und *in vivo* Studien beinhaltet. Daher wäre ein experimenteller Ansatz von großem Vorteil, welcher es erlaubt, umfangreiche phänotypische *Screenings* von p53 Mutanten parallel durchzuführen.

In der vorliegenden Arbeit wurde das CRISPR-Cas9 System genutzt um das CRISPR-basierte gesättigte Mutagenese Screening (*CRISPR-based saturated mutagenesis screening* – CSMS) des TP53 Gens zu entwickeln, ein verbessertes System zum parallelen umfangreichen phänotypischen Untersuchung von p53

Mutanten. Wir haben damit ein schnelles und flexibles Protokoll entwickelt, um unter Einsatz des CRISPR-Cas9-induzierten *homology-directed repair* (Homologie-gerichtete Reparatur) p53 Mutationen in den endogenen *TP53* Genlocus einzubringen. Das CSMS wurde mittels getättigter Mutagenese des kurzen Protein Motivs validiert und erwies sich als überaus erfolgreiche Methode. Wir haben unser Protokoll soweit verbessert, um eine Hochdurchsatz-Methode zu entwickeln, welche eine exakte funktionelle Charakterisierung von tausenden p53 Varianten ermöglicht.

Wir haben die Effekte von p53 Mutationen auf das Ansprechen auf Mdm2-Inhibitoren und Bestrahlung untersucht und dabei eine herausragenden Korrelation zwischen den Ergebnissen des *Screenings* und bekannten strukturellen, funktionalen und klinischen Daten feststellen können.

Darüber hinaus konnten wir zeigen, dass CSMS in der Lage ist selbst kleinste funktionelle Unterschiede zwischen Mutationen aufzuzeigen und partielle *loss-of-function* Mutanten identifizieren kann.

Die Manipulation des endogenen *TP53* Genlocus erlaubt es uns, die Effekte von Mutationen in nicht-kodierenden Regionen zu untersuchen, was bisher unmöglich war. Ein genauer Vergleich unserer Daten mit bisher publizierten Studien bewies, dass die in unserer Studie etablierte Methode eine deutlich genauere Kategoriosierung pathogener p53 Mutationen ermöglicht.

Zusammegefasst können wir bestätigen, dass CSMS ein leistungsfähiges Instrument zur Katalogisierung von *TP53* Mutationen darstellt. Diese Methode kann zukünftig genutzt werden, um den Nutzen von Mutationen im *TP53* Gen als klinischen Biomarker zu verbessern.

1. Introduction

1.1 *TP53* is a key tumor suppressor

TP53 is the most frequently mutated gene in human cancer. On average, the *TP53* gene is altered in every second tumor. In some cancer entities (e.g., ovarian and uterine cancers), *TP53* is mutated in more than 80% of cases (Leroy et al. 2014b; Donehower et al. 2019). The importance of *TP53* as a tumor suppressor is exemplified by the hereditary cancer predisposition disorder, Li-Fraumeni syndrome. Germline *TP53* mutations were identified in most individuals with Li-Fraumeni syndrome (Guha and Malkin 2017).

TP53 encodes a transcription factor that controls a network of hundreds of genes: p53 reacts to various extrinsic and intrinsic stimuli (DNA damage, oxidative stress, activation of oncogenes, nutrient deprivation, telomere shortening) and regulates cell fate by inducing various responses: cell cycle arrest, apoptosis, senescence, DNA repair and others (Williams and Schumacher 2016). Deregulation of the p53 network is a universal hallmark of cancer. The p53-mediated response can be dampened in cancer cells either by mutations in the *TP53* gene itself or by alterations in the genes encoding negative or positive p53 regulators like MDM2 and CDNK2A (p14ARF). Mutations in *TP53* are frequently associated with poor clinical prognosis, aggressive tumor growth, metastasis, and therapy resistance (Olivier et al. 2010).

p53 protein prevents the spreading of genetically altered cells via two core programs: apoptosis and cell cycle arrest (Donehower et al. 2019). P53-driven apoptosis involves the transcriptional induction of target genes, including *BAX, PMAIP1* (Noxa), and *BBC3* (Puma), which ultimately leads to permeabilization of the mitochondrial outer membrane, release of cytochrome c from mitochondria, activation of caspases, and cell death (Riley et al. 2008; Zilfou and Lowe 2009; Aubrey et al. 2018b). Furthermore, p53-dependent transcription-independent initiation of apoptosis was described in numerous studies (Moll et al. 2005; Haupt et al. 2003; Kim et al. 1999; Ho et al. 2019). Besides apoptosis, p53 can engage other cell death pathways: necrosis (Baumann 2012), ferroptosis (Le Jiang et al. 2015), pyroptosis (Ranjan and

Iwakuma 2016), anoikis (Ghosh et al. 2010), and necroptosis (Muller and Vousden 2014; Xie et al. 2013).

Under moderate stress p53 engages a reversible cell cycle arrest and DNA repair, thereby limiting the propagation of oncogenic mutations. The key mechanism of p53-mediated cell cycle arrest relies on the activation of the *CDKN1A* gene, whose product p21 inhibits cyclin-dependent kinases (CDKs) to halt cell cycle progression. Inhibition of CDKs prevents the hyperphosphorylation of Rb and thereby induces cell cycle arrest. Upon certain conditions (oncogene activation, persistent DNA damage), p53 response leads to an irreversible block of cell division (senescence) through transcriptional activation of target genes such as *CDKN1A*, *PAI1*, *SUV39H,* and *PML* (Riley et al. 2008; Kortlever et al. 2006). p53 regulates cellular metabolism by controlling the expression of anti-oxidative genes *SESN1, SESN2, GPX,* and regulators of glycolysis (TIGAR) (Liu et al. 2008; Sablina et al. 2005).

Activation of p53-driven response can be lethal for the cell. Therefore, in normal cells it is tightly controlled. In unstressed cells, p53 is continuously produced but is immediately complexed with MDM2 and MDMX proteins via the N-terminal domain (Marine and Jochemsen 2004). The E3-ubiquitin-ligase MDM2 labels p53 with polyubiquitin, promoting its nuclear export and proteasomal degradation (Haupt et al. 1997; Tollini et al. 2014; Sane and Rezvani 2017; Boehme and Blattner 2009).

MDM2-dependent degradation of p53 is interrupted by stress stimuli. DNA damage-induced phosphorylation of MDM2 and p53 by CHK1, CHK2, ATM, and ATR protein kinases prevents ubiquitination of p53 (Kruse and Gu 2009). Additionally, MDM2-p53 interaction can be disrupted by the p14ARF protein in response to hyperproliferative signaling from oncogenes (Pomerantz et al. 1998; Zhang et al. 1998; Kamijo et al. 1998). Since elevated levels of p53 are toxic to the cell, the duration of p53 accumulation is controlled by a negative feedback loop: the *MDM2* gene itself is a transcriptional target of p53. Therefore, stabilization of p53 induces MDM2 expression and dampens p53 activity (Wu et al. 1993).

Taken together, p53 is a key regulator of cellular fate with multifaceted functions and complex dynamics. It effectively prevents propagation of stressed and genetically altered cells. Deregulation of the p53 response is an imperative for any cancer cell.

1.2 *TP53* structure

The p53 protein contains 393 amino acids and is divided into several domains: the N-terminal domain (1-62 aa) and the adjacent proline-rich domain (63-97 aa) are essential for transactivation (Fig. 1A) (Baptiste et al. 2002; Zhu et al. 2000). The central DNA-binding core domain (DBD) (102-292 aa) mediates sequence-specific binding to response elements located in promotors of target genes. The binding of four p53 subunits to DNA is facilitated by a tetramerization domain (323-356 aa). The C-terminal domain (364-393 aa) supports DNA binding (Laptenko et al. 2015). Moreover, it can be subjected to multiple post-translational modifications and essential for regulating cellular levels of p53 (Gu and Zhu 2012; Joerger and Fersht 2007).

1.3 p53 mutations and their consequences

1.3.1 *Loss of function (LOF) mutations*

Unlike most other tumor suppressor genes, which are frequently inactivated by deletions, frameshift, or nonsense mutations, approximately 70% of *TP53* alterations found in human cancers are missense mutations (Fig. 1B) (Levine and Vosburgh 2008; Muller and Vousden 2013; Donehower et al. 2019).

The primary consequence of *TP53* mutations is the loss of normal tumor-suppressive functions due to impaired DNA binding or protein misfolding, which confers critical selective advantage during tumor progression. However, disruption of protein functionality could also be achieved by nonsense or frameshift mutations. The unusual mutational spectrum of the *TP53* gene (prevalence of missense over nonsense or frameshift mutations) has two explanations. First, the selection of missense variants exerts neomorphic pro-oncogenic functions that foster more aggressive cancer growth (gain of function, GOF) (Brosh and Rotter 2009; Baugh et al. 2018). Second, missense mutants exhibit a dominant-negative effect (DNE), nonmutational inactivation of the second wild-type allele (Srivastava et al. 1993; Lee et al. 2012). Missense mutations in *TP53* generate a vast diversity of more than2000 mutant proteins. Mutations in *TP53* have been traditionally considered equally damaging. However, increasing experimental evidence suggests that missense

mutations generate a “rainbow” of mutant proteins with distinct characteristics (Sabapathy and Lane 2018; Walerych et al. 2015).

Consistent with the indispensable role of transactivation for normal p53 functions, most cancer patients carry mutations of the DNA-binding domain (Leroy et al. 2014b). Among them, eight mutations are found in nearly 10% of all human tumors with p53 missense mutations and are referred to as hotspot mutations (R175H, G245S, R248W, R273C, R273H, R282W, R248Q, and R249S) (Baugh et al. 2018). All hotspot mutants represent classical LOF mutations because they are completely unable to transactivate target genes and suppress cellular growth (Campomenosi et al. 2001; Kotler et al. 2018). Deleterious effects of hotspot mutations on tumor suppression are well exemplified by animal models: mice with heterozygous

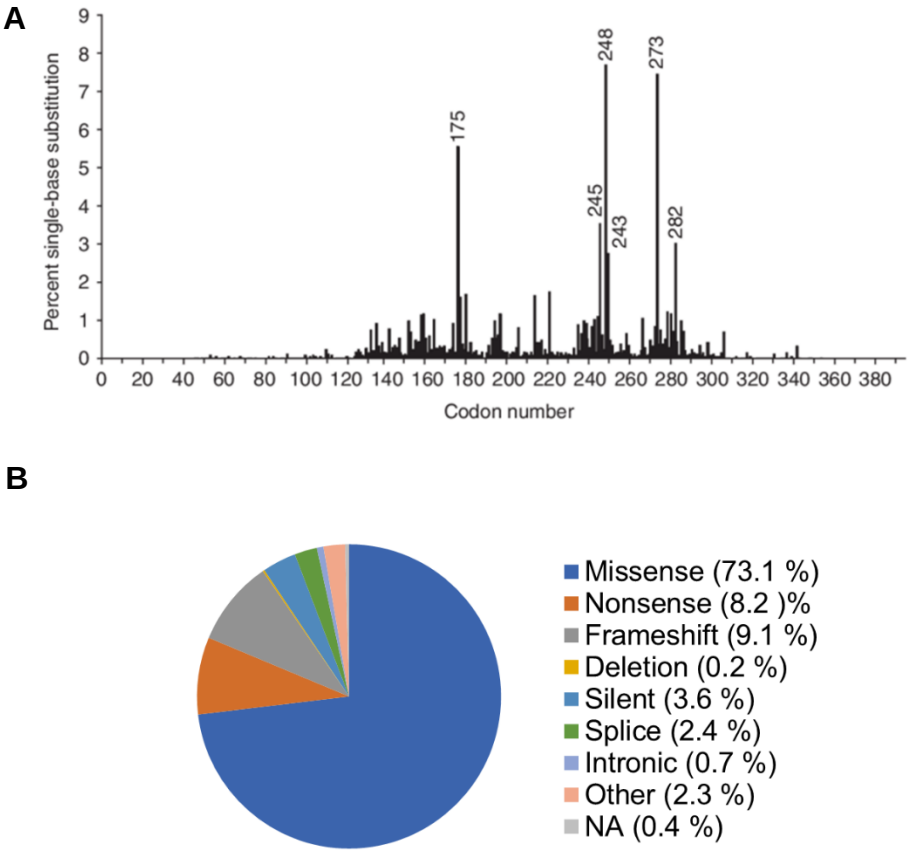

Figure 1. Mutational spectrum of TP53

A. Distribution of missense *TP53* mutations (N=27847). **B.** Frequencies of distinct classes of *TP53* mutations (N=28866). Data source: IARC database, R20, July 2019.

germline hotspot mutations (*Trp53*$^{+/mut}$) show the same (for example, R172H and R270H) or even stronger (R248Q) predisposition to the development of sporadic tumors as *Trp53*$^{+/-}$ animals (Olive et al. 2004; Hanel et al. 2013)

Hotspot mutations are divided into two classes: contact and structural. Contact mutations (R273H and R248W) affect residues that directly interact with DNA, whereas structural mutations (R175H, G245S, R249S, and R282H) hit residues essential for the maintenance of p53 structure (Joerger and Fersht 2007; Ang et al. 2006; Joerger et al. 2006). Mutation R248Q fits both categories (Wong et al. 1999). In contrast to contact p53 mutants that retain normal folding, structural mutants unfold at body temperature and tend to aggregate. Many non-hotspot variants were predicted to impair p53 function via structural alterations (Baugh et al. 2018).

Several studies from our group have described non-hotspot p53 variants that do not fit into the aforementioned classes because they neither decrease protein stability nor affect residues contacting DNA. These mutations impair another essential property of p53: DNA binding cooperativity. The binding of p53 monomers to DNA promotes the formation of tetramers via protein-protein interactions between the H1-helices of the DNA-binding domains (Weinberg et al. 2004). Mutations at residues E180 and R181 disrupt salt bridges between adjacent monomers, weaken cooperative binding with DNA and reduce p53-mediated tumor suppression (Kitayner et al. 2006; Dehner et al. 2005; Timofeev et al. 2013; Schlereth et al. 2010a; Schlereth et al. 2013). Such cooperativity mutations promote tumorigenesis in mice and are found in sporadic cancers as well as in Li-Fraumeni syndrome individuals with hereditary cancer susceptibility (Schlereth et al. 2010a; Timofeev et al. 2013; Timofeev et al. 2019).

1.3.2 *Partial loss of function mutations*

Comprehensive studies of the hotspot *TP53* mutations have undoubtedly demonstrated their complete loss of functional properties. Accordingly, all p53 mutants were regarded as equally non-functional. Nowadays, it is increasingly recognized that p53 mutations generate a spectrum of proteins with various degrees of residual functionality (Sabapathy and Lane 2018; Manfredi 2019). Some of the non-hotspot p53 mutants, which were overlooked by earlier studies, retain the ability

to transactivate particular target genes, representing, therefore, “separation-of-function” or “partial loss of function” (partial-LOF) mutants (Kato et al. 2003; Menendez et al. 2006; Jordan et al. 2010). A good example is the tumor-derived mutant R175P. Its murine equivalent R172P is devoid of pro-apoptotic activity but retains the ability to induce cell cycle arrest, maintains chromosome stability, and partially suppresses tumorigenesis (Liu et al. 2004).

The other example of partial-LOF mutants is cooperativity mutations located in the H1 helix, two of which were extensively studied by our group. The mutant E177R (the equivalent of human E180R) is unable to induce apoptosis but efficiently activates cell cycle arrest, controls oxidative stress, and partially protects mice from tumorigenesis (Timofeev et al. 2013). The other mutant R178E (the equivalent of human R181E) is transcriptionally inactive but can still drive mighty chemotherapy response *in vivo* via a non-transcriptional mechanism (Timofeev et al. 2019). These studies pinpoint the chance that many of the non-hotspot mutants retain residual activities. Whether partial-LOF mutants can be exploited for cancer therapy is unknown. Since non-hotspot mutations account for 70% of all missense variants found in cancers, this question deserves deeper investigation.

1.3.3 *Gain of function mutations*

Besides losing transactivating ability, some mutant p53 variants (for example, R175H, R273H, R248Q, R248W, and others) can actively fuel malignant growth by acquiring novel oncogenic functions (gain of function, GOF) (Muller and Vousden 2014; Kim and Lozano 2018; Mello and Attardi 2013). Experimentally, GOF properties of some mutants were initially demonstrated upon their overexpression in p53-null cells, where they conferred enhanced cell growth and tumorigenicity (Dittmer et al. 1993). Studies of such GOF-mutants in *in vivo* models have demonstrated that they provide a strong survival advantage to cancer cells, creating oncogene-like addiction, confer enhanced metastatic and invasive potential, drug resistance, drive angiogenesis, and epigenetic reprogramming (Basu et al. 2018; Morton et al. 2010; Muller and Vousden 2013; Vogiatzi et al. 2016; Lang et al. 2004; Olive et al. 2004; Hanel et al. 2013; Do et al. 2012; Hientz et al. 2017; Blandino et al. 1999; Buganim et al. 2006; Aschauer and Muller 2016; Schulz-Heddergott and Moll 2018; Alexandrova et al. 2015).

Mechanistically, GOF properties are still incompletely understood and seem to involve, among others, aberrant interactions of mutant p53 with transcriptional cofactors (e.g., NF-Y, YAP, NF-κB, E2F1, Sp-1, Ets-1), which result in transactivation of non-canonical target genes (Vogiatzi et al. 2016; Chin et al. 1992; Frazier et al. 1998; Lee et al. 2000; Ludes-Meyers et al. 1996; Quante et al. 2012; Freed-Pastor et al. 2012; Weisz et al. 2007). Interestingly, GOF activity was demonstrated for several non-missense p53 mutants. For example, truncating mutations in exon 6 generate proteins that are devoid of transactivating function and induce epithelial-mesenchymal transition and grant prometastatic features via binding to cyclophilin D in mitochondria (Shirole et al. 2016).

GOF effects can also be driven by interactions of mutant p53 with its two homologs, p63 and p73 (Li and Prives 2007; Hall and Muller 2019). The two transcription factors normally exhibit tumor-suppressive properties. The binding of mutant p53 to p63 and p73 can lead to improper binding to target gene promoters and downregulation of proapoptotic functions (Muller and Vousden 2014; Li and Prives 2007).

1.3.4 *Dominant-negative effect*

Monoallelic missense *TP53* mutations can compromise functions of the wild-type *TP53* allele. This phenomenon is known as a dominant-negative effect (DN-effect) and was demonstrated upon coexpression of mutant and wild-type p53 proteins (Vries et al. 2002; Srivastava S. et al. 1993; Kern et al. 1992; Shaulian et al. 1992; Sun et al. 1993). DN-effect has also been demonstrated in mouse models: co-expression of one mutant *Trp53* allele with wild-type protein accelerates cancerogenesis compared to *Trp53*$^{+/-}$ animals (Michele Harvey et al. 1995; Geng Liu et al. 2000; Vries et al. 2002; Giacomelli et al. 2018). Similarly, Li-Fraumeni syndrome patients carrying missense *TP53* mutations are diagnosed with cancer earlier in life than patients with truncating mutations (Jillian M Birch et al. 1998). Of note, the DN-effect was shown to be mutant-specific: the degree of residual transactivation of target genes by wild-type p53 depends on the particular co-expressed mutant (Paola Monti et al. 2002). The DN-effect is mechanistically explained by the formation of non-functional tetramers composed of both normal and mutant subunits, which results in decreased concentration of functional tetramers

and unfolding of the wild-type protein (Milner and Medcalf 1991; DiGiammarino et al. 2002).

Even though the DN-effect and GOF properties were conclusively demonstrated in multiple *in vitro* and animal studies, their relevance for the progression of human tumors is still under debate. Two recent studies have conclusively shown that the majority of the hundreds of tested missense mutations exert a dominant-negative effect in multiple cancer cell lines (Boettcher et al. 2019; Giacomelli et al. 2018). However, one of these reports found no evidence of GOF properties (e.g., growth stimulation or drug resistance) for hotspot mutants in leukemia cell lines (Boettcher et al. 2019). A recent analysis of the TCGA dataset revealed that 90% of tumors have biallelic *TP53* loss, suggesting that the DN-effect alone is unable to completely impair p53-mediated tumor suppression (Donehower et al. 2019). In line with this, a recent study in the mouse lymphoma model demonstrated that DNE does not globally impair functions of the wild-type protein but rather selectively suppresses only a subset of target genes, which is sufficient for deregulation of tumor-suppressive circuits and transformation of premalignant cells in cooperation with c-Myc (Aubrey et al. 2018a).

Presumably, both GOF-effect and DNE are relevant for oncogenesis. However, they can operate at distinct cancer progression stages and be strongly dependent on the particular mutant, genetic, and cellular contexts. Therefore, the importance of both phenomena for cancer patients still needs to be firmly established.

1.3.5 *Importance of functional characterization of non-hotspot mutations*

The prevalence of eight hotspot mutations over the others prompted a comprehensive characterization of these variants in multiple *in vivo* and *in vitro* models (Lang et al. 2004; Olive et al. 2004; Hanel et al. 2013; Muller and Vousden 2013; Muller et al. 2011; Liu et al. 2016; Xu et al. 2014; Achatz and Zambetti 2016). At the same time, functional consequences of non-hotspot missense p53 mutations remain poorly characterized. While some of these mutants exhibit full loss of function (identical to null allele), many others can retain particular wild-type properties, exhibit DN or neomorphic GOF effects (Freed-Pastor and Prives 2012; Muller and Vousden 2014; Shirole et al. 2016). GOF activities of mutant p53 vary between particular

mutants, depend on oncogenic context and tissue type (Olive et al. 2004; Lang et al. 2004; Stein et al. 2020). Together with a vast array of LOF and partial LOF mutations, they create tremendous diversity of protein variants, many of which can represent potential targets for distinct therapeutic modalities (Liu et al. 2015; Parrales and Iwakuma 2015; Sur et al. 2009; Martins et al. 2006; Muller and Vousden 2014). The fact that only eight mutations among more than 2000 are well-characterized emphasizes the high demand for a comprehensive functional characterization of non-hotspot p53 mutants.

1.4 *TP53* isoforms and non-coding mutations

The human *TP53* locus encodes 12 protein isoforms. Isoforms are generated by alternative splicing, alternative initiation of transcription or translation (Surget et al. 2013; Joruiz and Bourdon 2016). The existence of p53 isoforms adds another level of complexity to the p53 network. For example, canonical full-length p53 isoform (p53α) is produced from mRNA with complete exclusion of intron 9. Partial retention of this intron generates two isoforms (p53β and γ) with a truncated C-terminal domain. p53 isoforms are expressed in a tissue-specific manner, and their functional importance is still far from being fully understood. In normal cells, p53 isoforms are believed to finetune the p53 network, while in malignant cells, they may inhibit functions of the full-length protein, e.g., via a dominant-negative effect or by promoting aggregation (Vieler and Sanyal 2018). Deregulated expression of p53 isoforms was found to participate in many pathological conditions: premature aging, inflammation, developmental disorders, and many human cancer entities (Muhlinen et al. 2018; Cooks et al. 2014; Marcel et al. 2011). For example, overexpression of the p53 isoform Δ133p53α, produced from an internal promoter in intron 4, was described in colorectal cancer, serous ovarian cancer, breast cancer, and cholangiocarcinoma (Vieler and Sanyal 2018; Joruiz and Bourdon 2016; Khoury and Bourdon 2011; Surget et al. 2013).

Non-coding variants can change the balance between p53 isoforms. Mutations localized in the intron 4 affect the alternative promoter and impair the synthesis of several p53 isoforms (Leroy et al. 2014b; Leroy et al. 2017). Mutations at the boundary between intron 6 and exon 7 lead to the production of the shortened p53Ψ

isoform, which drives the reprogramming of cells into a premetastatic state (Senturk et al. 2014). Moreover, multiple synonymous and non-synonymous germline variants were discovered in intron 9, which encodes alternative exons for p53β and p53γ isoforms. Although the clinical significance of these variants is unclear, it is possible that they may determine expression levels of distinct p53 isoforms (Silden et al. 2013; Solomon et al. 2014; Graupner et al. 2009). In summary, mutations in the non-coding sequence of *TP53* deserve more comprehensive characterization.

1.4.1 *Splice mutations*

Although missense mutations in *TP53* exons are most frequent, much more rare alterations in non-coding regions can also alter p53 protein synthesis and have, therefore, clinical significance. For example, recurrent rearrangements in the first intron are frequently found in osteosarcomas, and mutations at splice sites in introns 1 and 9 are associated with Li-Fraumeni syndrome (Chen et al. 2014; Ribi et al. 2015; Verselis et al. 2000). Splice-site mutations result in the expression of aberrant transcript variants and shortened polypeptides. The production of truncated p53 isoforms was reported in colorectal cancer (Smeby et al. 2019), chronic lymphocytic leukemia (Bromidge et al. 2000), lung cancer (Takahashi et al. 1990), and other cancer entities (Holmila et al. 2003). Besides, recent study reported a novel type of *TP53* alterations: splice-site-creating mutations (Jayasinghe et al. 2018). Finally, mutations in exonic splicing enhancers and silencers can impair mRNA splicing (Gorlov et al. 2004; Wang et al. 2004; Laverdière et al. 2000).

Hence, *TP53* variants affecting splicing can have important clinical implications and require more comprehensive characterization.

1.5 Clinical significance of *TP53* mutations

Some germline mutations in *TP53* undoubtedly predispose individuals to cancer development (Malkin et al. 1990; Gonzalez et al. 2009). Tumors developing in animals harboring p53 genomic mutations demonstrate early onset, aggressive metastatic growth, and therapy resistance (Zuber et al. 2009; Lozano 2010). In cancer patients, *TP53* mutations are also associated with poor prognosis and therapy resistance in multiple studies. One of the best examples of the clinical value

of *TP53* status is chronic lymphocytic leukemia (CLL). Although the frequency of *TP53* variants is very low in asymptomatic patients, the presence of *TP53* variants is often associated with poor prognosis characterized by advanced clinical stage, rapid disease progression, chemoresistance, and shorter overall survival (Leroy et al. 2017). Besides, *TP53* mutational status in acute myeloid leukemia (AML) is an important predictor for the therapy outcome (Hunter and Sallman 2019).

Nevertheless, the clinical significance of p53 mutation status remains controversial (Robles and Harris 2010). The majority of studies demonstrate an association between *TP53* mutations and poor survival for patients with breast, hematopoietic, head and neck, and liver cancers (Zhang et al. 2017). Conversely, roughly half of the studies in bladder, brain, lung, colon, esophagus, and ovarian cancer patients failed to identify such association (Robles and Harris 2010). Likewise, a report based on the TCGA dataset analysis has also demonstrated that the presence of the *TP53* mutation alone has poor prognostic value for many cancer types (Olivier et al. 2007). By contrast, a mutant *TP53*-associated gene expression signature was a much more informative outcome predictor (Donehower et al. 2019). The controversial diagnostic utility of *TP53* mutational status for clinical prognosis can be partially explained by the immense complexity of the p53 network and the multitude of mutations. This underscores the need for comprehensive functional analysis of the full mutational spectra to increase the predictive value of *TP53* mutational status (Sinn et al. 2020).

1.6 IARC *TP53* and UMD databases

The immense diversity of *TP53* mutations and clinical value of *TP53* mutational status substantiated the need of tools to classify and sort information on p53 variants retrieved from thousands of publications and medical reports. Nowadays, two regularly updated databases of *TP53* variants are available: the IARC *TP53* database (www.iarc.fr/P53) and the UMD-p53 database (Universal Mutation Database) (http://p53.curie.fr/ and www.umd.necker.fr:2001/). The IARC *TP53* database has been launched in 1989 (Olivier et al. 2002; Bouaoun et al. 2016; Hollstein et al. 1994; Hernandez-Boussard et al. 1999). The currently available version R20 July 2019 comprises data on 29900 somatic mutations and 9200 variants. The UMD-p53 database was released in 1994, and the last 2017_R2

version includes data on the *TP53* status of more than 80400 tumors and 6870 *TP53* variants (Cariello et al. 1994; Leroy et al. 2014a). Both databases contain information about germline and somatic mutations, common *TP53* polymorphisms in human populations, *TP53* status in human cell lines. Besides information on mutation frequencies, databases contain functional annotations retrieved from the literature, including three high-content studies (Kato et al. 2003; Kotler et al. 2018; Giacomelli et al. 2018). IARC *TP53* and UMD databases are essential sources of information on p53 mutations for scientists and clinicians.

1.7 Targeting p53 for cancer therapy

1.7.1 *Reactivation of wild-type p53 with MDM2 and MDMX inhibitors*

In approximately 50% of all tumors, the wild-type *TP53* gene is retained (Donehower et al. 2019). In such tumors, cellular levels of p53 protein are kept low due to constant proteasomal degradation of p53 promoted by E3 ubiquitin ligases (most notably, MDM2) (Kruse and Gu 2009). Tumors with retained wild-type p53 need to enforce this negative feedback loop to avoid lethal activation of p53 by oncogenic signaling. Therefore, the amplification of *MDM2* and the inactivation of the *CDNK2A* gene, encoding the MDM2-inhibiting protein p14ARF, are common genetic alterations of wild-type p53 tumors (Mina et al. 2017; Donehower et al. 2019). The central role of MDM2 in the degradation of wild-type p53 encouraged the development of inhibitors of MDM2 and its homolog MDMX as a means for reactivation of the p53 pathway in cancers without *TP53* alterations. In 2021, 25 clinical trials of 10 MDM2 and MDMX inhibitors were registered at clinicaltrials.gov.

The prototypic compound for MDM2-inhibitors is nutlin-3a, a cis-imidazoline that occupies the p53-binding pocket of MDM2 and disrupts the p53-MDM2 interaction (Vassilev et al. 2004). Inhibition of p53-MDM2 interaction with nutlin leads to p53 stabilization, cell cycle arrest, and apoptosis (Khoo et al. 2014). More potent nutlin derivatives (e.g., RG7112 and RG7388 by Roche) are extensively tested in preclinical and clinical studies, alone or in combination with other drugs (e.g., chemotherapy, BH3 mimetics, or monoclonal antibodies) (Ding et al. 2013; Tovar et al. 2013; Andreeff et al. 2016; Tisato et al. 2017). Another drug, SAR405838 (MI-773, Sanofi), forms the MI-773-MDM2 complex by mimicking three key amino acid

residues of p53 involved in MDM2 binding. Additionally, the compound induces refolding of the unstructured N-terminus of MDM2, which further enhances interactions between the molecule and the protein and enhances the binding affinity (Jiaxiong Lu et al. 2016; Wang et al. 2014). At present, two clinical trials were completed with MI-773 (NCT01636479 and NCT01985191). AMG 232 (Amgen) is a piperidinone inhibitor of the MDM2-p53 interaction. AMG 232 is tested in clinical trials on melanoma, glioblastoma, and acute myeloid leukemia (NCT02110355, NCT01723020, NCT02016729) (Sun et al. 2007). Besides the drugs listed above, several other compounds are currently under clinical development: MK-8242 (Merck), CGM097, and HDM201 (Novartis).

Recently, the MDM2 homolog MDMX (or MDM4) also gained attention as a therapeutic target. MDMX has non-overlapping functions with MDM2. It lacks the E3 ubiquitin-ligase activity and negatively regulates p53 via direct interaction and sequestration, and forms regulatory complexes with MDM2 (Tollini et al. 2014). Reports on amplification of *MDMX* in some tumors raise concerns that MDM2 inhibition alone may be ineffective in such patients (Donehower et al. 2019; Riemenschneider et al. 1999; Yu et al. 2014a; Danovi et al. 2004; Bao et al. 2016). This prompted the development of a novel class of dual MDM2/MDMX inhibitors (Wu et al. 2015; Bernal et al. 2010; Chang et al. 2013; Chen et al. 2017). One member of this class of molecules is RO-5963 (Graves et al. 2012). RO-5963 is a cell-permeable indolyl-hydantoin compound that simultaneously hinders binding of both MDM2 and MDMX with p53 and activates p53 signaling and apoptosis in cells with high levels of MDMX. Besides inhibiting MDMX-p53 interaction, additional strategies of targeting MDMX are explored, for example, inducing protein degradation and inhibiting its expression (Yu et al. 2020).

Although MDM2 inhibitors were developed to treat cancers with wild-type *TP53,* there is evidence that they may have some activity against mutant *TP53*-expressing tumors. For example, apoptosis-deficient mutants E177R and R178E reveal lethal activities during embryonic development in an *Mdm2*-null background, highlighting the fact that even variants with strongly compromised pro-apoptotic function can exert cytotoxic action upon excessive stabilization (Klimovich et al. 2019). Moreover, treatment of cells expressing transcriptionally-inactive mutant R178E with a

combination of nutlin and doxorubicin unleashes residual cytoplasmic activities of the mutant and kills cells by apoptosis (Timofeev et al. 2019). In clinical trials, some activity of RG7112 was reported for a few leukemia patients with p53 mutations (Andreeff et al. 2016). Thus, MDM2 inhibitors may potentially have clinical utility for the treatment of tumors with certain p53 mutants.

Another unexplored possibility is that treatment of patients carrying p53 mutation with MDM2 inhibitors may have a detrimental effect due to excessive stabilization of mutant p53 and amplification of their GOF or DN-effect (Alexandrova et al. 2017a; Yue et al. 2017). Therefore, MDM2 inhibitors need to be tested in the context of the whole mutational spectra to fully understand the hidden benefits and potential side effects of these compounds.

1.7.2 *Mutant p53 reactivators*

Since p53 is most frequently inactivated by missense mutations, the mutant protein is retained in cancer cells. This opens an opportunity to harness mutant p53 for therapy. Two major strategies are pursued: the first approach involves the restoration of wild-type-like conformation and functions of the improperly folded mutant protein. This concept was supported by numerous studies demonstrating that re-expression of p53 kills p53-negative cells (Feldser et al. 2010; Junttila et al. 2010; Martins et al. 2006; Xue et al. 2007). Many mutant p53 variants are unfolded at body temperature. Experiments with temperature-sensitive p53 mutants demonstrated that stabilization of protein conformation turns unfolded p53 back into a wild-type state (Friedlander et al. 1996; Michalovitz et al. 1990). Therefore the development of small molecular compounds leading to stabilization and functional rescue of mutant p53 was actively pursued, and more than a dozen compounds were developed in the past decades, some of which are listed in Table 1 (Bykov et al. 2017). Mechanistically, many mutant p53-reactivators rely on the same principle: they bind covalently to the mutant protein, elevating its thermostability and shifting the equilibrium toward a native conformation by mass action (Bullock and Fersht 2001). The most advanced compound of this class is APR-246 (PRIMA-Met). APR-246 is a prodrug that is converted to the Michael acceptor methylene quinuclidinone (MQ) (Bykov et al. 2005; Bykov et al. 2016). MQ covalently binds to cysteines (Cys124 and 277) in p53, followed by protein refolding and restoration of wild-type function

Table 1. Overview of mutant p53-reactivating compounds (Bykov et al. 2017)

Compound	Chemical name and/or class	Mechanism	Clinical development	Year
Cys-targeting compounds				
CP-31398	Styrylquinazoline	Michael acceptor	Experimental and/or preclinical	1999
PRIMA-1	Quinuclidinone	Converted to MQ, which binds p53 by Michael addition	Experimental and/or preclinical	2002
APR-246	Quinuclidinone	Converted to MQ, which binds p53 by Michael addition	Phase Ib/II for ovarian cancer, MDS and oesophageal cancer	2005
MIRA-1	Maleimide	Michael acceptor	Experimental and/or preclinical	2005
STIMA-1	Styrylquinazoline	Michael acceptor	Experimental and/or preclinical	2008
3-Benzoylacrylic acid	Benzoylacrylate	Binds p53 by Michael addition	Experimental and/or preclinical	2010
KSS-9	Piperlongumine	Microtubule poison; redox; Michael acceptor	Experimental and/or preclinical	2016
PK11007	Sulfonylpyrimidine	Binds p53 by nucleophilic aromatic substitution	Experimental and/or preclinical	2016
Zn^{2+} chelators				
ZMC1	Thiosemicarbazone	Zn^{2+} chelator	Experimental and/or preclinical	2012
COTI-2	Thiosemicarbazone	Zn^{2+} chelator	Phase I for gynaecological tumours and head and neck cancer	2016
Peptides				
pCAPs	Peptides	Bind p53; promote refolding	Experimental and/or preclinical	2016
Reacp53	Peptide	Disrupts mutant-p53 aggregates	Experimental and/or preclinical	2016
Other types of compounds				
RETRA	2-(4,5-Dihydro-1,3- thiazol-2-ylthio)-1- (3,4-dihydroxyphenyl) ethanone	Disrupts mutant-p53–p73 complexes	Experimental and/or preclinical	2008
PK083	Carbazole	Binds and stabilizes p53-Y220C	Experimental and/or preclinical	2008
P53R3	Quinazoline	Restores DNA binding to mutant p53	Experimental and/or preclinical	2008
SCH529074	Piperazinylquinazoline	Binds p53	Experimental and/or preclinical	2010
PK7088	Pyrazole	Binds and stabilizes p53-Y220C	Experimental and/or preclinical	2013
Stictic acid		Binds p53 in silico	Experimental and/or preclinical	2013
Chetomin	Epidithiodioxopiperazine	HSP40-mediated refolding of p53-R175H	Experimental and/or preclinical	2015

(Wassman et al. 2013; Lambert et al. 2009; Zhang et al. 2018). The drug has demonstrated cytotoxic activity against tumors with the p53 mutations R175H and R273H (Bykov et al. 2016). APR-246 demonstrated a favorable safety in phase I clinical trials in patients with hematological tumors (NCT03931291, NCT03588078, NCT03072043) and in phase II trials in prostate cancer patients (NCT00900614). APR-246 in combination with azacitidine showed robust clinical efficacy in *TP53* mutant MDS/AML patients (NCT03745716) (Sallman 2020; Cluzeau et al. 2019). Further clinical trials are currently ongoing. Notably, MQ has been reported to inhibit thioredoxin reductase 1 (Trxr1) and deplete the cellular pool of glutathione, thereby killing mutant p53-expressing cells, which are more vulnerable to oxidative damage (Liu et al. 2017; Peng et al. 2013). These reports highlight that some mutant p53 reactivators have low selectivity and may exert a plethora of side effects, questioning whether observed clinical effects are indeed dependent on mutant *TP53* refolding. Other examples of p53 reactivators sharing the same mode of action are shown in Table 1 (Bykov et al. 2017). While some p53 reactivators target a broader spectrum of mutants by stabilizing their conformation (e.g., CP-

31398 was shown to refold V173A, S241F, R249S, and R273H), other compounds were explicitly designed to target single mutants, e.g., PK7088 refolds only p53 Y220C by filling a surface cleft left by the mutation of tyrosine and stabilizing the native conformation (Parrales and Iwakuma 2015; Boeckler et al. 2008). Another class of p53 reactivators is zinc chelators. Zinc (Zn^{2+}) ions are required for correct folding of p53, DNA binding, and transactivation (Loh 2010; Butler and Loh 2003, 2007). Zn^{2+} stabilizes two loops in the DBD by tetrahedral coordination by Cys176-His179 and Cys238-Cys242. Zinc-free DBD is unfolded at body temperature (Butler and Loh 2003). Incubation of cells with Zn^{2+} chelators results in the transition of p53 into unfolded inactive conformation, which can be reversed back to normal by supplementing cells with Zn^{2+} (Hainaut and Milner 1993). The binding of Zn^{2+} can be perturbed by several mutations, including the most frequent hotspot variant R175H (Cho et al. 1994). Supplementation of mutant p53-expressing cells with an excess of Zn^{2+} can partially rescue DNA binding, supporting the idea of using zinc administration for mutant p53 reactivation (Puca et al. 2011). However, supplementation with free zinc is not a feasible strategy because a relatively small excess of zinc also induces p53 denaturation (Butler and Loh 2007). A thiosemicarbazone compound ZMC-1 (zinc metallochaperone) functions as a zinc ion buffer, providing an optimal concentration of intracellular Zn^{2+} ions and supporting correct p53 folding without direct binding to the protein (Blanden et al. 2015). Accordingly, ZMC-1 was shown to selectively inhibit the growth of cells harboring p53 mutants with impaired zinc-binding (e.g., R175H, C238S, C242F, and C176F) (Yu et al. 2014b).

1.7.3 *Mutant p53 degrading drugs*

The universal characteristic of the majority of mutant p53-expressing tumors is the massive accumulation of the mutant protein. Therefore intensive p53 immunostaining is a reliable surrogate marker of p53 mutations, widely used by pathologists (Bartek et al. 1990; Yemelyanova et al. 2011; Köbel et al. 2016). Importantly, mutant p53 is not accumulated when expressed in non-transformed cells or in normal tissues of transgenic (mutant knock-in) mice (Lang et al. 2004; Olive et al. 2004). Therefore, stabilization of mutant p53 is a specific hallmark of cancer cells and considered required for its oncogenic GOF activities (Mantovani et

al. 2019). Several mechanisms drive the accumulation of mutant p53. First, lack of transactivation and impaired ubiquitination by MDM2 and CHIP lead to disfunction of the p53-MDM2 feedback loop. Furthermore, short MDM2 isoforms frequently produced in cancer cells can inhibit the ubiquitination of mutant p53 (Zheng et al. 2013; Sigalas et al. 1996; Jacob et al. 2013). Second, Hsp90 and Hsp70 chaperons bind to mutant p53 and protect it from aggregation and MDM2-dependent ubiquitination (Frum R.A. 2014; Li et al. 2011; Blagosklonny et al. 1996; Whitesell et al. 1998). Finally, co-chaperone proteins from the BAG family were shown to interact with mutant p53, protect it from degradation and promote GOF (Yue et al. 2016; Yue et al. 2015).

Excessive stabilization of mutant p53 creates an oncogene-like addiction to GOF mutants (Parrales and Iwakuma 2015; Schulz-Heddergott and Moll 2018; Sabapathy 2015). Targeting this addiction by inhibition or genetic ablation of mutant p53 counteracts cancer growth *in vitro* and *in vivo* (Schulz-Heddergott and Moll 2018; Freed-Pastor et al. 2012; Weissmueller et al. 2014; Walerych et al. 2016; Alexandrova et al. 2015; Schulz-Heddergott et al. 2018; Zhu et al. 2015). Hence, elimination of mutant p53 from cancer cells by promoting its degradation is a reasonable therapeutic approach. Inhibition of HSP90 with ganetespib or combination of 17AAG (HSP90 inhibitor) with SAHA (HDAC 6 inhibitor) was shown to deplete mutant p53 levels and significantly extended the survival of mice carrying T cell lymphomas expressing p53 R172H and R248Q (Alexandrova et al. 2015). Moreover, ganetespib synergized with chemotherapy to eliminate mutant p53-expressing tumors (Alexandrova et al. 2017b). A combination of ganetespib with paclitaxel was tested in cancer patients (Ray-Coquard et al. 2019).

Another mechanism of mutant p53 stabilization implicates the Hsp40 family member DNAJA1, which shelters mutant p53 from CHIP-mediated degradation in conjunction with the mevalonate pathway intermediate mevalonate-5-phosphate (Parrales et al. 2016). Interestingly, inhibition of the mevalonate pathway with HMG-CoA reductase inhibitors (statins), the most common cholesterol-lowering drugs, was shown to decrease levels of several mutant p53 variants (Parrales et al. 2016; Xu et al. 2019). Statins were also shown to prevent HSP90-mediated mutant p53 stabilization and induce MDM2-dependent degradation (Ingallina et al. 2017). Mutant p53 directly

activates the mevalonate pathway by interacting with SREBP2, which supports the malignant behavior of cancer cells via activation of Ras, Rho, and YAP/TAZ (Sorrentino et al. 2014). Therefore, statins directly counteract mutant p53 by reducing oncogenic signaling (Parrales et al. 2018). Statins have shown cytotoxicity in lung cancer cells (Chou et al. 2019). Moreover, moderate efficacy was evident in autochthonous T-lymphomas expressing two different GOF mutant p53 alleles. (Tutuska et al. 2020). Whether statin therapy can be translated into clinical benefit for patients with p53-mutant cancer, remains to be established (Chae et al. 2015; Blandino and Di Agostino 2018).

1.7.4 *Targeting mutant p53 aggregation*

Mutant p53 is improperly folded and forms amyloid aggregates in cancer cell lines and human tumor samples (Silva et al. 2014; Xu et al. 2011; Levy et al. 2011; Oliveira et al. 2020). Disaggregation is a prospective approach for the rescue of normal functions of mutant p53. This concept was tested in high-grade serous ovarian carcinomas by designing the peptide Reacp53 that disrupts p53 aggregates and shifts the dynamic equilibrium towards a correctly folded form, recovering a wild-type-like protein. Reacp53 restores the p53 functions in hotspot mutants R175 and R248 and improves survival of animals xenografted with ovarian carcinoma (Soragni et al. 2016).

1.7.5 *Targeting interactions between mutant p53 and p73*

Several p53 GOF mutants strongly bind and inactivate the p53 family member p73 that has many overlapping functions with p53. The mutant p53-p73 heterotetramers block p73 function supporting proliferation and chemoresistance (Schulz-Heddergott and Moll 2018). The disruption of the mutant p53-p73 complex would restore p73 functions. RETRA (“reactivation of transcriptional reporter activity”) disrupts such complexes and restores p73-mediated transcription and cell death (Kravchenko et al. 2008; Hong et al. 2014; Hepburn 2007).

Pharmacological targeting of mutant p53 was proven to be very challenging, and despite substantial efforts, no drugs have been approved for clinical application so far. All currently available compounds were shown to act on a specific small set of hotspot mutants (Parrales and Iwakuma 2015). How suitable these emerging

therapeutics are to the broader spectrum of p53 mutants is unknown. Therefore, the development of a mutant p53 screening system allowing for parallel testing of multiple p53-targeting compounds in the context of the full mutational spectrum is of high translational value.

1.8 Experimental systems for functional studies of p53 mutations

Mouse models were extensively used to study p53. Animal experiments gave supporting evidence for the development of p53-targeting therapies. Despite their utility, only a small amount of mouse models with germline p53 mutations corresponding to human ones were generated (e.g., *Trp53*R172P, *Trp53*R172H, and *Trp53*R270H) (Liu et al. 2004; Geng Liu et al. 2000; Olive et al. 2004). Mouse models carrying the human variants R248W, R248Q, or G245S, are also available (Hanel et al. 2013). These models gave invaluable insight into p53 biology. However, mouse models have lots of limitations, first of all, the limited number of available genotypes. Therefore, they are unsuitable for studying the vast diversity of mutant p53 protein variants.

Cell lines are widely used to investigate mutant p53. Not surprisingly, mutation occurrence in cell lines reflects their frequency in human cancers: among more than 2000 mutant p53 cell lines listed in the IARC-p53 database, more than 500 contain mutations in one of 8 hotspot codons. Mutations occurrence among cell lines is strongly biased towards hotspot mutations probably due to survival benefit during *in vitro* culture, whereas non-hotspot mutants are strongly underrepresented. Cell lines lack for majority of non-hotspot mutations, therefore they can be characterized only using engineered cell lines. Since every cell line has a unique genetic background and carries mutations in many genes, comparisons of large groups of cell lines would be needed to reveal phenotypic effects of multiple p53 mutants. Therefore, for the detailed studies of large sets of mutations, a common isogenic background is needed.

1.8.1 *Systematic analysis of the p53 mutome*

The tremendous diversity of p53 variants, a wide range of biological effects of mutant proteins (DN, LOF, and GOF), as well as lack of suitable models for most of the

mutants, prompted the development of high-throughput screening approaches aimed to characterize the full mutational continuum. The first attempt to gain a deep insight into the complexity of p53 mutations was made in 2001 (Campomenosi et al, 2001), followed by Kato and co-authors in 2003 (Kato S. et al. 2003). 2314 mutant p53 variants were tested in a yeast-based reporter assay for their ability to activate transcription from p53 response elements of different target genes (*MDM2, PMAIP1, BAX, CDKN1a, GADD45, AIP1, 14-3-3δ*). This work confirmed that the majority of mutations localized in the DNA binding domain completely impair transactivation. The other domains turned out to be much more resistant to mutagenesis. Importantly, this assay also demonstrated that many non-spot variants exhibit only partial loss of transactivation, suggesting that the p53 mutome is functionally much more diverse than previously appreciated. This publication demonstrated the value of deep mutational scanning for functional and structural studies of p53 and served since then as the most important source of functional annotation for most of the p53 variants identified in patients and listed in databases (IARC p53, UMD, and ClinVar).

A later study from the Kato group highlighted an important disadvantage of the transactivation reporter-based screening system (Kakudo Y. et al. 2005). Testing a panel of 179 mutants in p53-negative Saos-2 cells surprisingly revealed that the transactivating properties of many mutants did not correlate with their ability to induce apoptosis. This implied that the functional impact of p53 mutations is not a direct result of target genes transactivation, supporting the importance of transactivation-independent apoptosis. In support of this, wild-type p53 was shown to directly interact with pro- and anti-apoptotic proteins (Bak, Bax, Bcl-xL, and Bcl-2) and induce mitochondrial outer membrane permeabilization and consecutive apoptosis independently of target genes transactivation (Chipuk et al. 2004; Mihara et al. 2003). These findings were recently corroborated by the description of a transactivation-deficient mutant, which is nevertheless able to induce apoptosis in response to chemotherapy *in vivo* (Timofeev et al. 2019). This study highlighted the problem: comprehensive profiling of p53 variants requires not just a measurement of the transactivating potential but rather quantification of their impact on cell fitness.

Advances in next-generation sequencing have allowed the implementation of high-throughput functional screening of p53 variants in mammalian cells. Three recent

publications reported the application of lentiviral cDNA libraries containing thousands of p53 variants introduced into human cells (Kotler et al. 2018; Giacomelli et al. 2018; Boettcher et al. 2019). Next-generation sequencing was used as a readout to quantify changes in mutation abundance. The first study assessed enrichment or dropout of mutations after the prolonged cultivation of p53-deficient H1299 lung cancer cells infected with the lentiviral library and demonstrated a profound correlation between functional effects of p53 mutations, structural features, and evolutionary conservation. This experimental system was able to delineate wild-type-like and LOF mutations accurately. Moreover, passaging of the library infected cells *in vivo* revealed preferential enrichment of some cancer-associated variants, highlighting the GOF activities of selected mutants.

The second study (Giacomelli et al. 2018) assayed human A549 lung cancer cells infected with a lentiviral library of p53 variants and treated them with nutlin in two configurations. For the assessment of the dominant-negative effect, cells carrying wild-type p53 locus were infected. LOF mutants were identified after delivery of the library into p53-knockout A549 cells. This work has demonstrated that 80% of the mutants tested exert DN-effect on the wild-type allele.

The third study (Boettcher et al. 2019) utilized a p53 wild-type AML cell line MOLM-13 engineered to express a p21-GFP reporter. After introducing a saturated library of p53 missense mutants sorting of cells showing weak GFP fluorescence allowed to isolate p53 variants that exert a dominant-negative effect on the normal p53. Similar to the previous report, this work also revealed that the vast majority of DBD-mutants exert a strong DN-effect on the wild-type protein.

Interestingly, the aforementioned studies reported conflicting results regarding the GOF effects of p53 mutants. Kotler et al. have assessed the enrichment of mutants from their library in three settings: standard cell culture conditions, 3D-culture in spheroids, and *in vivo* growth upon subcutaneous injection in NSG mice. Strikingly, enrichment of variants from *in vivo* experiments did not correlate with both *in vitro* systems. Among mutations recovered from the tumors formed in mice, 10 mutants belong to the most frequent cancer-associated variants, suggesting that they elicit GOF effects in the *in vivo* model. Notably, enrichment of variants was highly

correlated between standard and 3D culture conditions in vitro. These results clearly demonstrate that GOF effects are strongly dependent on selective forces that operate only in a particular context.

Conversely, the other two studies did not find any evidence of GOF for any of the mutants tested. Such discrepancies in reporting GOF activities of p53 mutants point out that the functional consequences of p53 mutations are strongly dependent on the experimental system used to uncover them. This emphasizes the need for the development of more advanced screening systems.

The elegant studies by S. Kato, E. Kotler, A. Giacomelli, and S. Boettcher have made important advances in exploring the diversity of mutant p53 variants. However, these studies have several disadvantages:

- the study of Kato and coauthors (Kato et al., 2012) was performed in yeast cells that naturally lack p53 and, in turn, the complete network of p53 regulators and posttranslational modifications, making the system overtly non-physiological; moreover, the screening was focused on only 8 short response elements from p53 target genes: MDM2, p53R2, BAX, Noxa, GADD-45, AIP1, 14-3-3δ, WAF1, whereas the transcriptional network of p53 includes hundreds of genes controlled by complex enhancer-promoter interactions (Sullivan et al. 2018; Bieging and Attardi 2012)

- the more recent studies utilized lentiviral cDNA libraries to express p53 in human cells. In the conditions of p53 overexpression from a strong lentiviral promoter, cellular effects may have been exaggerated;

- using cDNA makes it impossible to test non-coding intronic variants and mutations of splice-sites;

- expression of p53 from cDNA simplifies the complexity of p53 isoforms;

- another drawback of using cDNA is the non-physiological regulation of expression by a lentiviral promoter and lack of post-transcriptional regulation via miRNA binding to sites in the 3'UTR (Kafri et al. 2000; Brendel et al. 2012; Matoulkova et al. 2012; Bottini et al. 2017; Kotagama et al. 2015; Vislovukh et al. 2014).

To overcome these inherent drawbacks of the cDNA-based screening system, mutations need to be introduced into the endogenous genomic locus. The discovery

of CRISPR and tremendous progress in the development of gene-editing technology makes this task feasible.

1.9 Genome editing using CRISPR-Cas

The discovery of the CRISPR (clustered regularly interspaced short palindromic repeats) system has led to a giant leap in the field of genome editing and dramatically simplified genome engineering and mutagenesis. In 2013, two groups (of Feng Zhang and George Church) simultaneously published the description of genome editing using the CRISPR/Cas9 system in human cells (Le Cong et al. 2013; Mali et al. 2013). By the end of 2014, nearly 1000 papers mentioning CRISPR had been published. Nowadays, the CRISPR/Cas system is involved in clinical trials worldwide and demonstrated successful treatment of sickle cell disease in the patient (Ledford 2020).

The CRISPR-Cas system originates from genomes of prokaryotic organisms such as archaea and bacteria (Wiedenheft et al. 2012). The system serves as a defense mechanism against infections by bacteriophages. Riboprotein complexes encoded by CRISPR recognize and cleave DNA from bacteriophages, preventing the entry of foreign genetic material. CRISPR-Cas systems from various bacterial species were used to develop highly efficient programmable endonucleases suitable for site-specific DNA cleavage in any living organism.

The most widely used CRISPR-Cas9 system that was also implemented in the present work was derived from *Streptococcus pyogenes.* The *S. pyogenes* CRISPR-Cas9 complex comprises two RNA molecules: (crRNA and tracrRNA) and the Cas9 nuclease (Fig. 2A) (Barrangou 2015; Deltcheva et al. 2011). Two RNAs are fused in a chimeric single-guide RNA (sgRNA) in most currently employed systems (Jinek et al. 2012). sgRNA targets the nuclease to the specific DNA sequence in the genome. Most of the 100 bp-long sequences of the sgRNA are invariant; the binding specificity of the complex is determined by the 20 bp-long fragments on the 5'-end of the sgRNA. Therefore, the specificity of the Cas9 protein can be easily changed by replacing the 20 bp fragment in the sgRNA (Fig.2B).

Cleavage of DNA by the Cas9 enzyme requires a specific motif in the proximity of the recognition sequence, the protospacer adjacent motif (PAM). The PAM sequence recognized by the Cas9 nuclease is NGG and is located 3 nucleotides downstream of the cleavage site. Cas9 binds to the target sequence determined by sgRNA homology and makes a blunt double-strand break in DNA between the 17th and 18th bases of the target sequence (Jinek et al. 2012) (Fig. 2C). The DNA repair machinery immediately recognizes a double-strand break. Genome editing exploits two distinct DNA repair mechanisms: non-homologous end-joining (NHEJ) and homology-directed repair (HDR) (Fig. 2A,C). NHEJ occurs in the absence of the homologous DNA molecule and forms random short insertions or deletions (indels), leading to frameshifts and ultimately to knockout of the gene (Fig. 2C). When the DNA template homologous to the double strand break site is provided in the form of a homologous chromosome, plasmid DNA or oligonucleotide, the HDR mechanism can proceed (Fig. 2C). HDR replaces a damaged DNA segment with a template sequence, seamlessly introducing the template into the genome. If the HDR template contains desired modifications, they are integrated into the genome. Therefore, unlike the inaccurate NHEJ mechanism, which generates random indels, HDR enables precise editing of genomic DNA by introducing single mutations or substantially large inserts into the genome in the proximity of the cleavage site. Importantly, NHEJ and HDR mechanisms are competing with each other (Sargent et al. 1997). NHEJ is a preferential repair pathway, making the selection of cells which have undergone HDR a substantial challenge during gene editing. Additional obstacle for the efficient gene editing is p53-mediated DNA damage response induced by double strand breaks. Besides limiting the frequency of HDR-mediated transgene integration, DNA damage response promotes selection of cells with inactivating mutations in *TP53* (Enache et al. 2020; Haapaniemi et al. 2018; Ihry et al. 2018). Inactivation of p53 during editing enhances editing efficiency and protects *TP53* locus from acquisition of random alterations.

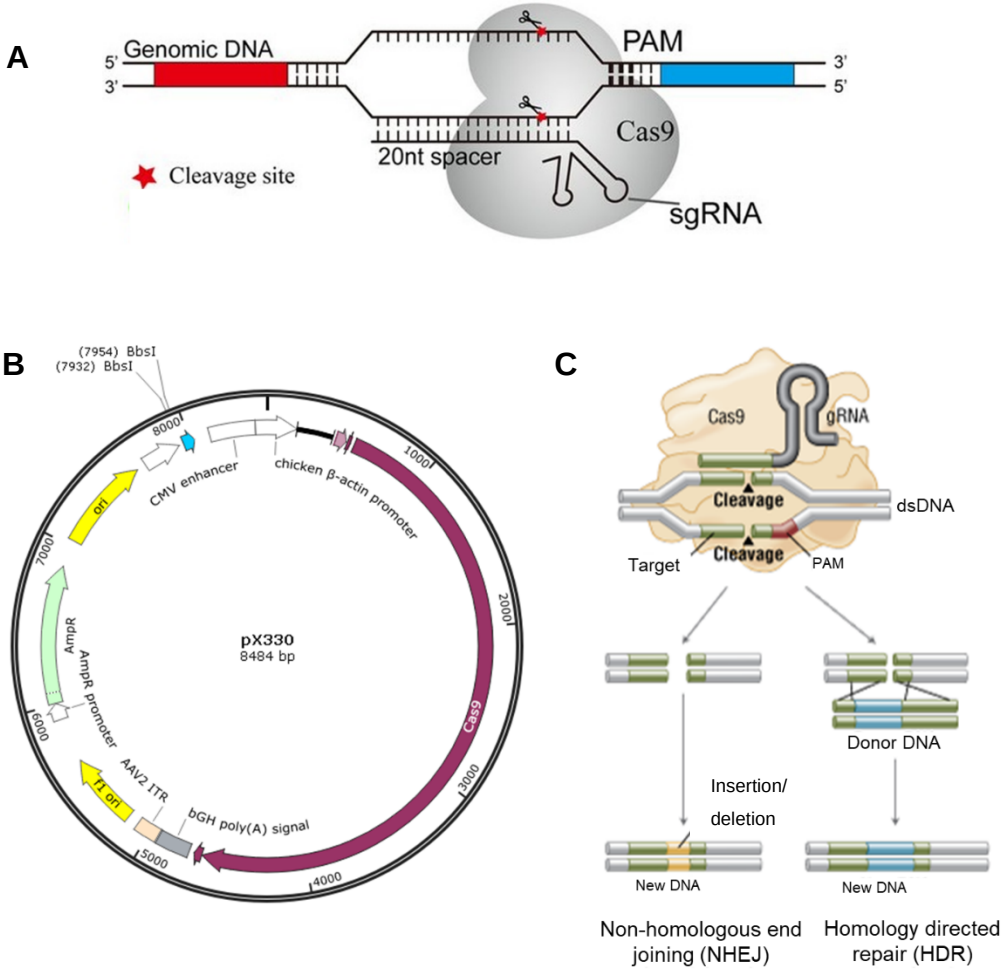

Figure 2. CRISPR-Cas9-mediated genome editing

A. Structure of the *S. pyogenes* Cas9-sgRNA RNA-guided nuclease complex *Figure adapted from Yu Wang et al., Applied and Environmental Microbiology 2018.* **B.** A plasmid for the expression of the human codon-optimized SpCas9 and chimeric single guide RNA (sgRNA). BbsI recognition sites indicate the cloning site for the sgRNA. Modified from https://www.addgene.org/42230. **C.** Cas9 protein forms a complex with a sgRNA, binds the target site, and cleaves genomic DNA creating a double-strand break (DSB) 3-4 nucleotides upstream of the PAM sequence. DSB is repaired by the non-homologous end-joining (NHEJ) or homology-directed repair (HDR). As a result of NHEJ, random insertions and deletions are generated. HDR results in the precise integration of the provided donor template which has sequence homology with the target region. Figure modified from https://www.neb-online.de/genome-editing/.

1.10 Saturation mutagenesis

Saturation mutagenesis is a technique applied in functional studies and protein engineering, in which a codon at a certain position is exchanged with all possible amino acids. Generation of scanning site saturation libraries enables the interrogation of every possible alteration in the given protein (Fig. 3A,B).

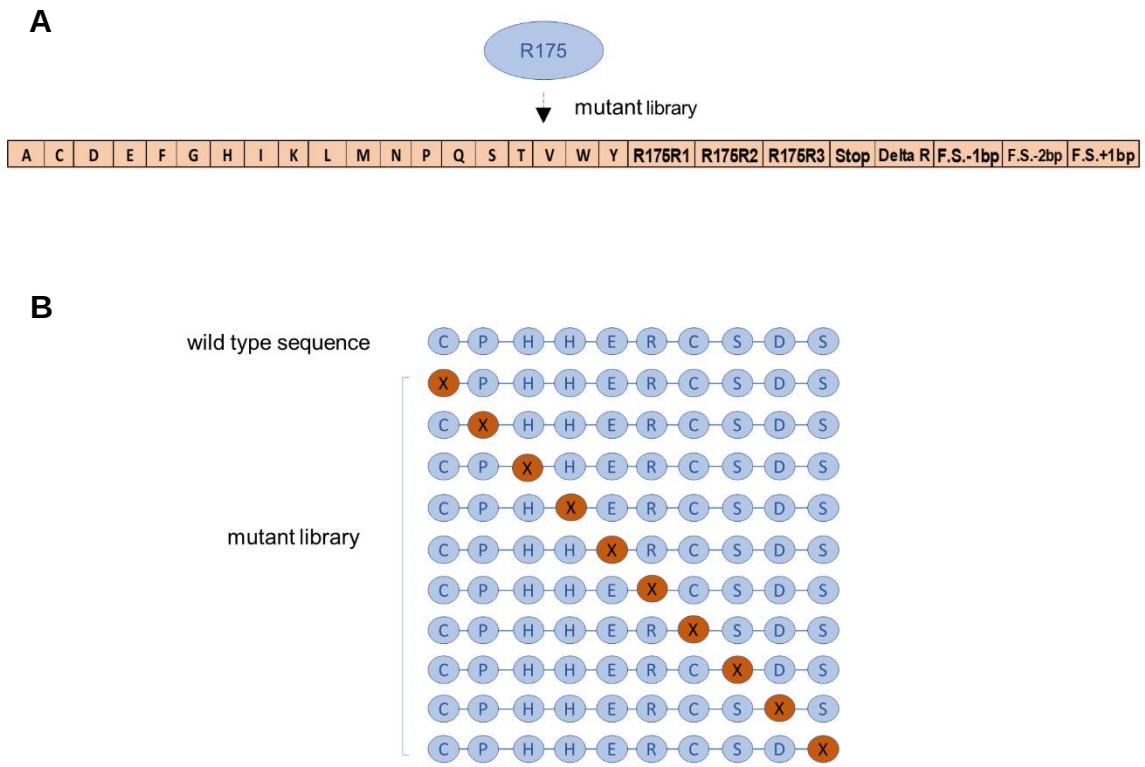

Figure. 3 Schematic of the saturation mutagenesis principle employed in the work shown for the R175 and H1 helix libraries

A. A single site-saturation library for the codon R175 included mutations to all 19 amino acids, 3 synonymous mutations, stop codon, codon deletion, and 3 frameshifts. **B.** Amino acid sequence of the p53 H1 helix. Each position (shown as X) was mutated to the 19 amino acids, one synonymous mutation, and a stop codon.

This approach was implemented in studies of numerous genes, including tumor suppressors (PTEN) (Mighell et al. 2018). However, before the advent of the CRISPR-Cas9 era, saturation mutagenesis in mammalian cells was possible only *in trans* (by episomal expression of mutagenic libraries from plasmid or lentiviral vectors) (Siloto and Weselake 2012). Nowadays, the CRISPR-Cas9 system has been widely implemented for targeted genome editing allowing to perform site-

saturation mutagenesis at almost any genomic locus using HDR (Findlay et al. 2014; Ma et al. 2017; Canver et al. 2020).

A good example of the CRISPR-Cas-guided HDR-based saturated mutagenesis is a comprehensive mutational screening of nearly 4000 variants in the *BRCA1* gene (Gregory M. Findlay et al. 2018). The study revealed many new pathogenic variants in the gene and showcased the utility of CRISPR-based mutagenesis for functional studies. CRISPR-Cas9 system was recently implemented to introduce the most frequent hotspot mutations into *TP53* locus of leukemia cell lines (Boettcher et al. 2019). However, no reports on systematical mutagenesis of the endogenous TP53 locus were published so far to our knowledge.

We aimed to take advantage of CRISPR-Cas9-induced genome editing to design an improved system for high-content phenotypic characterization of *TP53* mutations, considering the limitation of the prior studies.

1.11 Aim

The aim of the present study was to develop a system for massive parallel phenotypic analysis of p53 mutations in the context of the endogenous *TP53* locus. To achieve this goal, we set several objectives:

1. Establish a protocol for the generation of site-saturation libraries of the *TP53* gene. Develop an efficient strategy using CRISPR-Cas9-induced HDR to target variant libraries into the endogenous genomic locus of human cancer cells to produce isogenic cellular libraries.
2. Develop a workflow for the high-content quantification of anti-proliferative capacity and specific tumor-suppressive functions (apoptosis, cell cycle arrest) of p53 variants.
3. Validate the system using libraries of increasing complexity. Compare the phenotypical impact of variants with previously published experimental evidence and clinical data from the public databases (IARC TP53 and UMD).
4. Assess the impact of p53 mutations on the sensitivity of cancer cells to therapeutic agents activating wild-type or mutant p53.

5. Explore phenotypic consequences of intronic mutations to showcase the advantages of the employed strategy.
6. Perform a comprehensive analysis of thousands of p53 DNA binding domain variants and compare the resulting phenotypic catalog with earlier studies and public resources.

2. Material and methods

2.1 Materials:

2.1.1 *Bacterial strains*

Name	Source
DH10B ElectroMAX	LifeTechnologies
OneShot Mach1-T1®	LifeTechnologies

2.1.2 *Plasmids*

Backbone	Name	Insert	Source
pENTR™/D-TOPO®	pENTR™/D-TOPO®		LifeTechnologies
pENTR™/D-TOPO®	pENTR_HA1	*TP53* ex4-int4	Present work
pENTR™/D-TOPO®	pENTR_HA2_GGate	*TP53* ex4-int6	Present work
HR700PA-1	HR700PA-1		System Biosciences
HR700PA-1	HR700_HA1_HA2_GGate_H1 helix	*TP53* ex4-int4 *TP53* ex4-int6	Present work
HR700PA-1	HR700_HA1_HA2_EE	*TP53* ex4-int4 *TP53* int4-EE-int6	Present work
HR700PA-1	HR700_R175_golden_gate	*TP53* ex4-int4 *TP53* int4-int6	Present work
HR700PA-1	HR700_Exon5_golden_gate	*TP53* ex4-int4 *TP53* int4-int6	Present work
pCR-BluntII-TOPO®			LifeTechnologies
pCR-BluntII-TOPO	pCR-Blunt II-TOPO_HA2_GoldenGate_R175		Present work
px330-U6-Chimeric_BB-CBh-hSpCas9	px330-sgRNA_in5_p53wt	gRNA *TP53* intron5	AG Stiewe
px330-U6-Chimeric_BB-CBh-hSpCas9	px330-sgRNA_in5_p53+T	gRNA *TP53* intron5+T	Present work
HR700PA-1	HR_R175	R175 mutant library	Present work
HR700PA-1	HR_H1 helix	H1 helix mutant library	Present work

HR700PA-1	HR_Exon5	Exon 5 mutant library	Present work
px330-U6-Chimeric_BB-CBh-hSpCas9	px330-sgRNA_Puro	gRNA Puromycin	AG Stiewe

2.1.3 *Cell lines*

Cell line	p53 status
HCT-116 (human colon carcinoma)	+/+
HCT-116 $^{\Delta/TP53E}$	Δ/LSL-editable
HCT-116 $^{\Delta/LSL\text{-}R175\text{-}Lib}$	Δ/LSL-R175-mutation library
HCT-116 $^{\Delta/R175\text{-}Lib}$	Δ/R175-mutation library
HCT-116 $^{\Delta/LSL\text{-}H1\ helix\text{-}Lib}$	Δ/LSL-H1 helix-mutation library
HCT-116 $^{\Delta/H1\ helix\text{-}Lib}$	Δ/H1 helix-mutation library
HCT-116 $^{\Delta/LSL\text{-}Exon5\text{-}Library}$	Δ/LSL-Exon 5-mutation library
HCT-116 $^{\Delta p53\text{-}L}$	Δ/Δ (deletion from exon 2 to exon 9)
HCT-116 $^{+/LSL}$	+/LSL
HCT-116 $^{\Delta/LSL\text{-}Splicing\text{-}Lib}$	Δ/LSL-Splicing-library
HCT-116 $^{\Delta/\ Splicing\text{-}Lib}$	Δ/Splicing-library

2.1.4 *Oligonucleotides*

Name	Sense (5'-3')	Antisense (5'-3')
1	HA1_f_CACC_BsrGI	CACCTATATGTACAAGAGGCTGCTCCCCCCGTG
2	HA1_r_BsaI_S	TATAGAGACCGATGGATAAAAGCCCAAATTC
3	HA2_f_CACC_MluI_L	CACCACGCGTCCATCACACCCTCAGCATCTC
4	HA2_r_SalI	TATAGTCGACGAGATGGAATCTCGCTCTGTC
5	P53Int4-for1	CCCTTTGGCTTCCTGTCAGTG
6	CRISPR_seq_for	AGCAACAGATGGAAGGCCTC
7	MCS2_HR700PA_1_f	GGGGGCTGTCCCTAGATCTATAA
8	TP53Exon5 fwd	GTTGATTCCACACCCCCGCC
9	TP53Exon6 rev	GGGCACCACCACACTATGTC
10	Ex7 hp53_2 rev	GATGGTGGTACAGTCAGAGCC
11	TP53_ex5_NGS_BC11_r	AGAACCAGAAGACTTGCCAACTGGCCAAGACCT

12	TP53_mutPAM_f_BCO1	CGTACAAGAGACAAGCAATCAGTGAGGAATCAGAGGCCTCC
13	TP53_mutPAM_f_BCO3	CGTACTAGCAGACAGCAATCAGTGAGGAATCAGAGGCCTCC
14	TP53_mutPAM_f_BCO5	TCTTGAGTATCTGTAGCAATCAGTGAGGAATCAGAGGCCTCC
15	TP53_mutPAM_f_BCO3+1bp	ACGTACTAGCAGACAGCAATCAGTGAGGAATCAGAGGCCTCC
16	TP53_mutPAM_f_BCO5+2bp	GCTCTTGAGTATCTGTAGCAATCAGTGAGGAATCAGAGGCCTCC
17	TP53_ex5_NGS_BC11_r-1bp	GAACCAGAAGACTTGCCAACTGGCCAAGACCT
18	TP53_ex5_NGS_BC11_r-2bp	AACCAGAAGACTTGCCAACTGGCCAAGACCT
19	H1_helix_R175_BbsI	[PHOS]CATGACGGAGGTTGTGAGGCGGTCTTCCCACCATGAGCGCTGCTGAAGACG
20	BbsI_H1_1	[PHOS]CGGAGGTTGTGAGGCGCTGGTCTTCCCATGAGCGCTGCTCAGAT
21	BbsI_H1_2	[PHOS]GGTCTTCCCATGAGCGCTGCTGAAGACGCGATGGTGAGCAGCTG
22	EE_Ggate_f	GCGCTGCCCCCACCATGAGGAATGCTCAGATAGC
23	EE_Ggate_r	CATCGCTATCTGAGCATTCCTCATGGTGGGGGCA
24	Intron_4_mut_oligo_13nt_fwd	CAATATGAAGACCTCTGTCTCCTTC
25	Intron_4_mut_oligo_13nt_rev	ATATATGAAGACTCTCCAGCCCCAG
26	p53_Intron4_BbsI_1	GCCCTGACTTTCAACTCTGTCTGTCTTCTCTTCCTACAGTACTCCCCTG
27	p53_Intron5_BbsI_2	GATAGCGATGGTGAGCAGAAGACGCTGGAGAGACGACAGGG
28	p53_cDNA_rev	GCCAACCTCAGGCGGCTCAT

2.1.5 *sgRNAs*

Name	Sense (5'-3')	Antisense (5'-3')
gRNA in5wt	CACCGTCAGTGAGGAATCAGAGGCC	AAACGGCCTCTGATTCCTCACTGAC
gRNA in5del	CACCGAGAGCAATCAGTGGGGACCC	AAACGGGTCCCCACTGATTGCTCTC
gRNA in5+T	CACCGTGAGGAATCAGAGGACCTG	AAACCAGGTCCTCTGATTCCTCAC
gRNA Puro	CACCGCACGCCGGAGAGCGTCGAAG	AAACCTTCGACGCTCTCCGGCGTGC

2.1.6 *MiSeq kit*

Name	Source
NEBNext ChIP-Seq Library Prep Master Mix Set for Illumina E6240	New England BioLabs
NEBNext Multiplex Oligos for Illumina (Index Primer Set 1) E7335	

2.1.7 *Enzymes*

Name	Source
AfeI	New England Biolabs
BbsI	
BsrGI	
BsaI	
MluI	
NdeI	
NotI-HF	
SalI-HF	
SfiI	
T7 Endonuclease I	
Q5® Hot Start High-Fidelity DNA Polymerase	
GoTaq® G2 DNA Polymerase	Promega
T4 DNA Ligase	LifeTechnologies

2.1.8 *Antibodies*

Primary antibodies

Antigen	Clone	Host	Clone type	Dilution for WB	Source
β-actin	AC-15	mouse	monoclonal	1:10000	Abcam
p53	DO1	mouse	monoclonal	1:10000	Dr. B. Vojtesek
p21		rabbit	polyclonal	1:200	SantaCruz Biotech

Secondary antibodies

Antigen	Host	Clone type	Dilution for WB	Source
Alexa Fluor 488-linked anti-mouse-IgG	goat	monoclonal	1:60	Life Technologies
HRP-linked anti-mouse IgG	sheep	monoclonal	1:10000	GE Healthcare
HRP-linked anti-rabbit IgG	donkey	polyclonal	1:10000	GE Healthcare

2.1.9 *Chemicals (drugs, antibiotics)*

Name	Source
MI-773	Selleckchem
nutlin-3a	Sigma-Aldrich
RG7388	MedChem Express
MEL23	Merck
AMG 232	MedChem Express
RO-5963	Merck-Millipore
puromycin dichloride	Thermo Fisher

2.2 Methods

2.2.1 *Molecular cloning procedures*

Site directed mutagenesis

Site directed mutagenesis was performed using QuikChange Lightning Multi Site-Directed Mutagenesis Kit – Academic according to manufacturer's protocol (#210513, Agilent).

Splicing, R175 and H1 helix libraries design

P53 variant libraries were prepared by cloning of double-stranded oligonucleotides containing individual mutations into vector HR-2-Golden-Gate. Individual single-stranded 26, 37 and 34 bp oligonucleotides for the Splicing, R175 and H1 helix libraries correspondingly were synthesized by Eurofins*. Pairs of single-stranded oligonucleotides (sense and antisense) were reannealed to generate double-stranded fragments with sticky ends.

Exon5 library design

To prepare the HDR template library a pool of 3843 230 nucleotide-long single-stranded oligonucleotides was manufactured by Agilent using array-based synthesis (SurePrint technology)*****. Each oligonucleotide was spanning the region Chr. 17: 7,675,045 - 7,675,261 (assembly hg28) and contained a single codon substitution. The pool of single-stranded oligonucleotides was converted into double-stranded using PCR with primers #26 and #27 containing BbsI recognition sequences at 5'-ends (see primer table in Materials and methods). The resulting PCR fragments were cloned into the modified HR-Golden Gate cloning vector.

Golden Gate cloning

Oligonucleotides reannealing was performed in 96-well PCR plates (Engler et al. 2008). Each pair of oligonucleotides was mixed in individual well and after reannealing all double-stranded oligonucleotides were pooled together in 2 ml eppendorf tube.

Reannealing buffer:

- 10 µl 1M Tris-HCl pH=7.5
- 10 µl 5M NaCl

- 980 µl H_2O

Reannealing reaction (in PCR tubes):

- 16 µl reannealing buffer
- 2 µl 10 µM sense oligonucleotide (dilute stock of oligo 10 times)
- 2 µl 10 µM antisense oligonucleotide (dilute stock of oligo 10 times)

Cycling parameters were: 95ºC 5 min, afterwards cooling down 1 degree per 30 seconds up to 21ºC.

***** *The list of all mutant libraries, sequences and raw data see on the USB stick.*

For library assembly, Golden Gate cloning reaction included the following components:

2.5 µl reannealed oligo

1 µl HR-2-Golden-Gate vector (1µg)

1 µl BbsI NEB (10U)

0.5 µl DNA ligase NEB (30 U)

2 µl 10x buffer 2.1 NEB

1 µl 10 mM ATP (NEB or Fermentas)

1 µl 100 mM DTT

H_2O up to 20 µl

Cycling parameters:

37°C 2 min
20°C 5 min
} 50x

65°C 25 min

4°C ∞

Golden Gate cloning reaction (in PCR tubes) was setup in three tubes. Samples were then pooled together before transformed into bacteria.

TOPO cloning

Cloning of PCR products was performed using pENTR/D-TOPO or Zero Blunt TOPO PCR cloning kits according to manufacturer's protocol (#K240020, #450245 Thermo Fisher correspondingly).

Bacterial culture and plasmid DNA isolation

Transformation of cloning product was performed into electrocompetent bacteria. Frozen bacteria were thawed on ice and mixed with 1-2 µl of the cloning product. Bacteria were then transferred into a cooled electroporation cuvette and pulsed with 1.8 kV pulse in a Micropulser (BioRad). Bacteria were incubated in 500 µl of LB medium for 30-40 minutes at 37°C under shaking at 250 rpm. 100-200 µl of transformed bacteria were plated on LB agar plates supplemented with antibiotics for selection of positive clones. Agar plates were incubated overnight at 37°C and

clones were picked for small scale plasmid preparations. Following reagents were used:

- LB medium: 5 g/l NaCl, 5 g/l yeast extract, 10 g/l Bactotryptone
- Agar Plates: 1.5% agar-agar in LB medium with Kanamycin (50µg/ml) or Ampicillin (100µg/ml)

Preparation of plasmid DNA for the libraries

Plasmid DNA was prepared at 3 distinct scales for R175, H1 helix or Exon 5 libraries.

Transformation of cloning product was performed into the electrocompetent bacteria. 2, 3 or 10 frozen bacteria aliquots were thawed on ice and mixed with 1-2 µl of the cloning product for R175, H1 helix or Exon 5 libraries respectively. Bacteria were then transferred into a cooled electroporation cuvette and pulsed with 1.8 kV pulse in a Micropulser (BioRad). Bacteria were incubated in 1 ml, 2ml or 5 ml LB media respectively for 30-40 minutes at 37°C upon shaking at 250 rpm. 100-200 µl of transformed bacteria were plated respectively on 5, 15 or 40 15 cm LB agar plates supplemented with antibiotics for selection of positive clones. Agar plates were incubated overnight at 37°C. Bacterial colonies were scraped from all plates using a rubber cell scrapper, resuspended in LB medium and used for medium scale plasmid preparations.

Small scale plasmid isolation (Mini-prep)

To screen for appropriate clones by control restriction digest and Sanger sequencing, small-scale plasmid preparation was performed by alkaline lysis method using following solutions:

- P1 buffer: 50 mM Tris HCl pH 7.5, 10 mM EDTA pH 8.0, 100 µg/ml RNaseA
- P2 buffer: 200 mM NaOH, 1% SDS
- P3 buffer: 3 M potassium acetate pH 5.5

Overnight cultures were inoculated into LB medium supplemented with Kanamycin (50µg/ml) or Ampicillin (100µg/ml). 2 ml of the overnight culture were centrifuged and resuspended in 300 µl P1 buffer. After addition of 300 µl P2 buffer bacteria were lysed for 5 min on ice. 300 µl of buffer P3 were added to neutralize the reaction. The suspension was centrifuged (10 min at 13 000 g) and supernatant was transferred

into a fresh tube. DNA was precipitated with 700 µl isopropanol and pelleted by centrifugation at 13 000 g for 30 min at 4°C. Pellets were washed once with 70% ethanol, dried at 37 °C for 10-20 min and resuspended in 50 µl ddH2O. DNA yield and quality were assessed using Nanodrop ND-1000.

Medium scale plasmid isolation (Midi-prep)

Medium scale plasmid preparation was performed to obtain highly purified plasmid DNA for transfection of eukaryotic cells or further cloning steps. Mini-prep cultures of scrapped bacterial colonies were used to inoculate 100 ml of LB medium containing proper antibiotics. Plasmid DNA purification from overnight cultures was performed by anion-exchange chromatography using Nucleobond Xtra Midi Kit (Macherey-Nagel #740410.100) according to manufacturer´s protocol.

2.2.2 *Cell culture*

HCT-116 cells were cultured in Dulbecco's modified Eagle's medium (DMEM) supplemented with 10% fetal bovine serum (FBS), 1% penicillin (10.000 U/ml)/streptomycin (10 mg/ml) and 0,4% amphotericin B (250 g/ml). Cells were kept at 37°C with 5% CO2 in humidified incubator. Passaging of cells was performed when cells reached confluency. Cells were washed once with 1xPBS and then incubated with 2% trypsin-EDTA solution for 5 min, resuspended in medium, washed once´and plated. Cell were counted using Beckman Culter Z-series counter. Following reagents were used:

- DMEM high glucose, sodium pyruvate, with L-glutamine (#41966, Life Technologies)
- FBS (#F0804, Sigma-Aldrich)
- Amphotericin B (#A2942, Sigma-Aldrich)
- Pen-Strep 100 units/ml penicillin, 100 µg/ml streptomycin (#15140-122, Life Technologies)
- 1x PBS Dulbecco's phosphate-buffered saline without Ca2+, Mg2+ (#14190 Life Technologies)
- Trypsin 10x Trypsin-EDTA solution (#T4174, Sigma-Aldrich)

2.2.3 *Establishing of the HCT-116 $^{\Delta/TP53E}$ cell line*

Transient transfection

Cells were plated 24 hours before transfection into appropriate tissue culture dish at 60% confluency. Number of plated cells was adjusted according to the library size to achieve a ratio of 1000-10000 cells per each mutation. Before transfection cells were washed once with serum-free DMEM. Transfection was performed in serum-free DMEM without additives. Lipofectamine 2000 Reagent (#11668027, LifeTechnologies) and DNA were diluted in Opti-MEM reduced serum medium and transfection was performed according to the manufacturer´s protocol. The amount of reagents for the transfection is shown in the table below. Medium was changed to complete DMEM 4-5 hours after transfection.

Dish	Total volume, ml	Opti-MEM, ml	Plasmid DNA, µg	Lipofectamine 2000, µl
6 well	2	0.2	2.5	4.6
10 cm	10	1	12.5	23
15 cm	20	2	25	46

Three days after transfection cells were treated with 1 µg/ml puromycin for 5 days. After 5 days medium was changed to complete DMEM.

Infection with Cre-recombinase adenovirus

For reactivation of the silenced *TP53* allele after editing cells were transduced with adenovirus expressing Cre-recombinase (Ad5CMVCre VVC-U of Iowa-5, University of Iowa Healthcare). Cells were plated 24 hours before infection at 60% confluency into an appropriate cell culture dish. Infection was performed with concentration sufficient to infect 50% of cells determined by titration. Cells were incubated with virus 30 minutes; cells were carefully swirled every 10 minutes. After that medium was changed to complete DMEM. Cells were cultured 10-14 days until complete loss of GFP signal indicating complete Cre-mediated recombination in most of the cells.

2.2.4 *Flow cytometry and cell sorting*

To assess the efficiency of Cre-mediated recombination GFP expression in infected cells was tested by flow cytometry. GFP signal was quantified in the FL1-A channel on a BD Accuri C6 flow cytometer. Data were analyzed using BD Accuri C6 software.

Annexin V positive and negative cells were sorted with MoFlo Astrios sorter (Beckman Coulter, AY16010) using the Summit 6.3.1 software.

2.2.5 *Cell imaging*

96-well plates were imaged hourly in the IncuCyte S3 time-lapse microscopy system (Sartorius) equipped with an IncuCyte Zoom 10× Plan Fluor objective (Sartorius). Imaging was performed up to 72 h at 37°C. The graphs were generated using the time plot feature in the graph/export menu of the IncuCyte Zoom software. Raw data were exported in the MS Excel and GraphPad Prism to calculate the confluency.

2.2.6 *X-ray irradiation*

Cells were irradiated in 60% confluency using an X-RAD 320iX tube with settings of 320 kV voltage and current of 8 mA with the dose rate ~1Gy/min.

2.2.7 *Western blotting*

Protein extraction

Proteins of interest were detected by western blot technique. Protein extracts were prepared by lysing the cells in an appropriate amount of NP40 lysis buffer supplemented with protease inhibitor. After three rounds of freezing in liquid nitrogen and thawing in warm water bath lysates were centrifuged for 20 min at 13 000 g and supernatant was transferred into a new tube.

Protein concentration was measured using Bradford-based Bio-Rad Protein Assay (#5000006) following manufacturer’s instructions.

Protein lysates were denatured by adding LDS sample buffer and reducing agent (#NP0007, #NP0009, Thermo Fisher) followed by heating at 95°C for 5 minutes.

Protein electrophoresis and blotting

Denatured protein lysates were loaded on precast gels (NuPAGE Novex 4-12% Bis-Tris). Gels were run under constant voltage (100-150 V) in NuPAGE SDS MOPS running buffer for 1-2 hrs.

Proteins were transferred from gels to nitrocellulose membranes in XCell II Blotting modules. Blotting was performed in NuPAGE Transfer Buffer supplemented with 15% methanol at constant voltage (100V) and current limit of 500 mA for 60-90 minutes, depending on protein size. All antibodies were diluted in TBST containing 5% nonfat dry milk. To avoid unspecific binding of primary antibodies, membranes were blocked in TBST containing 10% nonfat dry milk prior to overnight incubation with primary antibodies at 4°C. After three washings with TBST, HRP- or Alexa Fluor-488-coupled secondary antibodies were incubated for 1 hour at room temperature, followed by 3 washing steps with TBST. Chemiluminescent and fluorescent signals were detected by the Gel Doc XR System (Biorad). Following reagents were used:

- NP-40 lysis buffer:

  50 mM Tris-HCl pH 7,4

  150 mM NaCl

  5 mM EDTA pH 8,0

  2% NP-40
- Protease inhibitor cocktail complete (#04693116001, Roche)
- Loading buffer 1x LDS sample buffer (#NP0008, Life Technologies)
- 1x Reducing agent (#NP0009, Life Technologies)
- SDS-Page gels NuPAGE Novex Bis-Tris Mini and Midi Gels (#WG1402BOX, Life Technologies)
- Running buffer NuPAGE MOPS SDS Running Buffer (#NP0001, Life Technologies)
- Protein ladder PageRuler Prestained Protein Ladder (#26616, Thermo Scientific)
- Transfer buffer NuPAGE® Transfer Buffer (#NP00061, (Life Technologies)
- Nitrocellulose membrane (#RPN303D, GE Healthcare)
- TBS 15 mM NaCl, 5 mM Tris HCl pH 7.5

- TBST 1x TBS with 0.1% Tween 20
- Nonfat dry milk Skim Milk Powder (Sigma #70166)
- HRP substrate Western Bright Chemiluminescence Substrate Sirius (Biozym #541021)

2.2.8 *Extraction of genomic DNA*

Purification of genomic (g)DNA from cells was performed according to manufacturer's protocol using either the QIAamp DNA blood Mini Kit or Blood & Cell Culture DNA Max Kit (#51104 or #13362, Qiagen). DNA quality and yield were evaluated using microvolume spectrophotometer (Nanodrop ND-1000).

2.2.9 *Extraction of RNA*

Before isolation of total RNA cells were washed once with PBS, lysed directly on the cell culture dish by adding 600 µl RLT buffer (#79216, Qiagen) and scraped from the dish. RNA was isolated from cell lysates with the RNeasy Mini Kit (#74106, Qiagen) according to manufacturer´s protocol using the QIAcube (Qiagen). RNA quality and yield were evaluated by microvolume spectrophotometer (Nanodrop ND-1000).

cDNA synthesis

Total RNA was reverse transcribed using the SuperScript VILO cDNA synthesis kit (#11754, Life Technologies) according to the manufacturer's protocol. cDNA was diluted up to concentration 5 ng RNA/µl and used for qPCR.

Reagents	Amount
RNA	500 ng
5x VILO Script mix	2 µl
10x SuperScript enzyme	1 µl
ddH2O	up to 10 µl

Cycling parameters:

25°C 10 min

42°C 60 min

85°C 5 min

4°C ∞

2.2.10 *PCR*

Genotyping of cell lines with PCR

Screening for correct genetic modifications during engineering of cell lines was performed by PCR using GoTaq polymerase (M3005, Promega) according to the following protocol:

Reagents	Amount
Template ng/reaction	150 ng
10 µM sense oligonucleotide	1 µl
10 µM antisense oligonucleotide	1 µl
PCR buffer	4 µl
dNTPs	0.4 µl
DMSO	1 µl
GoTaq polymerase 10U	0.2 µl
H_2O, ul	up to 20 µl

Cycling parameters:

95 °C - 2 min
95 °C - 0:30 min
56 °C – 1min/kb min } 35 cycles
72 °C - 0:30 min
72 °C - 5 min
4 °C - ∞

The presence of fragment was analyzed by agarose gel electrophoresis using 1,5-2% agarose gel and RedSafe DNA stain (#21141, Chembio).

Amplification of oligonucleotides for the exon 5 library

Amplification was performed using primers #24 and 25 with 13 bp homology regions and additional BbsI recognition sequences. Fragments were purified using QIAquick PCR Purification Kit (#28106, Qiagen) and used for the Golden Gate cloning procedure.

Reagents	Amount
Template	5 pg
10 µM sense oligonucleotide	1 µl
10 µM antisense oligonucleotide	1 µl
PCR buffer	4 µl
dNTPs	0.4 µl
DMSO	1 µl
GoTaq polymerase 10U	0,2 µl
H_2O	up to 20 µl

Cycling parameters:

95 °C - 2 min
95 °C - 0:30 min
56 °C – 0:30 min } 35 cycles
72 °C - 0:30 min
72 °C - 5 min
4 °C - ∞

PCR for amplicon library preparation

Preparation of amplicon libraries for next generation sequencing was performed using nested PCR. Nested PCR using two sets of primers enabled exclusive amplification of the mutation-carrying *TP53* allele.

The first PCR reaction was used to amplify a region from intron 4 to exon 7 from both p53 alleles and exclude amplification of non-recombined alleles. Amount of gDNA used for amplification was adjusted in order to ensure proper coverage of each mutant corresponded to 1,5; 0,45; 1,5 and 10 µg per replicate for splicing-, R175-, H1 helix and Exon 5-libraries respectively. Therefore, PCR was performed in 10, 3, 10 and 70 parallel reactions for respective libraries. Afterwards PCR products of PCR reaction were pooled together and 40, 20, 40 and 280 µl of splicing-, R175-, H1 helix- and Exon 5-library respectively were purified with QIAquick PCR Purification Kit (#28106, Qiagen) according to manufacturer's instructions and eluted in 30 µl H_2O.

Reagents	Amount
Template	150 ng
10 µM sense oligonucleotide	1 µl
10 µM antisense oligonucleotide	1 µl
PCR buffer	4 µl
10 mM dNTPs	0.4 µl
DMSO	1 µl
GoTaq polymerase 10 U	0.2 µl
H_2O	up to 20 µl

Cycling parameters:

95 °C - 2 min
95 °C - 0:30 min
59 °C – 1:30 min
72 °C - 0:30 min } 20-25 cycles
72 °C - 5 min
4 °C - ∞

The presence and concentration of 1,48 kb PCR product was detected by capillary electrophoresis using DNA Screening Kit QIAxcel and QIAxcel Advanced instrument (#929004 and #9001941, Qiagen).

Second reaction was performed for specific amplification of the targeted mutation-carrying allele splicing-, R175- and H1 helix libraries (primers #12-16 and #11, 17, 18) or 270 bp long primers #12-16 and #24) for the Exon5 library. Primers #12-16 specifically bind to mutated PAM sequence and carries internal barcodes used to identify reads from corresponding replicates in sequencing data. Primers #11, 17, 18 bind in exon 5 for splicing-, R175 and H1 helix libraries. Primer #24 binds in intron 4 for the Exon 5 library. The specificity of the PCR reaction was improved by reducing amount of $MgCl_2$ and dNTPs. To reduce amounts of PCR errors amplification was performed in 5; 3; 5 or 10 parallel reactions for splicing-; R175-; H1 helix- and Exon 5 library respectively. Afterwards PCR reaction products were pooled together and purified with QIAquick PCR Purification Kit (#28106, Qiagen) according to

manufacturer's instructions and eluted in 30 µl H_2O. The second round of purification was performed with Agencourt AMPure XP (63881, Beckman Coulter).

Reagents	Amount
Template pg/reaction	5 pg
10 µM sense oligonucleotide	1 µl
10 µM antisense oligonucleotide	1 µl
$MgCl_2$, 25 mM	1 µl
10x Mg^{2+}-free PCR buffer	2 µl
10 mM dNTPs	0.1 µl
DMSO	1 µl
GoTaq polymerase 10U	0.2 µl
H_2O	up to 20 µl

Cycling parameters:
95 °C - 2 min
95 °C - 0:30 min
66 °C – 0:30 min
72 °C - 0:30 min
} 22 cycles
72 °C - 5 min
4 °C - ∞

Concentration of 1,48 kb PCR product was detected by capillary electrophoresis DNA Screening Kit QIAxcel using QIAxcel Advanced Instrument (#929004 and #9001941, Qiagen).

Triplicate samples were pooled together at equal concentrations (3.3 ng) and used for NGS sequencing library preparation.

2.2.11 *Compound treatment*

All substances were dissolved in DMSO and stored according to manufacturer's recommendations. Compounds were titrated to determine the half maximal inhibitory concentration (IC50). Briefly, cells were treated with a range of concentrations of compounds and viability was determined after 3 days using Cell Titer Glo assay (#G7573, Promega). IC50 values were calculated using GraphPad Prism 8.0 software. Library-carrying cells were treated with compounds at their corresponding IC50 concentrations for 2-16 days and harvested for DNA isolation.

2.2.12 *Preparation of the amplicon library for next generation sequencing*

Quantification of the mutation abundance in genomic DNA from library-expressing cells was performed using massive parallel sequencing (next generation sequencing, NGS) of amplicon libraries. Sequencing libraries were prepared from amplicons using NEBNext ChIP-Seq Library Prep Master Mix Set for Illumina and NEBNext Multiplex Oligos for Illumina (Index Primer Set 1) (E6240L and E7335S, New England Biolabs) according to manufacturer's protocol. Samples were sequenced using MiSeq Reagent Kit v2 Nano or MiSeq Reagent Kit v3 (Illumina) on the MiSeq system.

2.2.13 *Data analysis and software*

GraphPad Prism 8.0

Statistical analysis, IC50 calculations, and preparation of figures were performed in GraphPad Prism 8.0 software. Pearson and Spearman correlation coefficients were calculated regarding the Normality test in GraphPad Prism 8.0. Methods used to infer statistical significance are shown in figure legends and in the text.

TP53 databases

Information about p53 mutant frequencies was taken from the UMD database. Scores from *in silico* predictors (SIFT, Polyphen2, REVEL, BayesDel, Mutassessor, Provean) were retrieved from the UMD database as well. Align-GVGD scores were retrieved from http://agvgd.hci.utah.edu/agvgd_input.php.

Bioinformatics

Edited regions of p53 were analyzed using paired-end AmpliconSeq workflow. Sequenced paired-end reads were further demultiplexed according to the combination of forward/reverse barcoded primer sequences found in the reads.

Primer sequences were identified using CutAdapt (version 2.7) with a parametrization that allowed for a maximal hamming distance of 2 and discarded truncated adapter sequences ensuring that at most two mismatches were accepted. Subsequently, primers were trimmed from the reads and corresponding mate pairs were merged using NGMerge (version 0.3) using "stiched" mode with enabled checking for dovetailing with 3' overhangs.

Merged reads were then compared to a set of *in silico* precompiled edited coding sequences. Since the genome editing should potentially create sequences that differ from the wild-type sequence only by a single base pair, merged reads were simply checked for identity to the expected reads and tallied. If no correspondence was found reads were discarded.

Relative read counts were obtained by dividing the raw counts by the sum of all expected sequences omitting wild-type and non-matched read counts.

Principal component analysis (PCA) was performed ClustVis software (https://biit.cs.ut.ee/clustvis/). Values of reporter genes activity extracted from the

study of Kato and colleagues (Kato et al., 2002) were uploaded on the website and processed using default parameters.

Evolutionary conservation scores were extracted from the ConSurf database (https://consurf.tau.ac.il/) using p53 structure 1TUP as a query.

3. Results

3.1 CRISPR-mediated Saturation Mutagenesis Screen (CSMS)

We aimed to improve the existing methodologies for high-content analysis of *TP53* mutants and developed the CRISPR-mediated Saturation Mutagenesis Screen (CSMS). We have employed recent advances in the CRISPR-Cas9-mediated genome editing to target the library of mutants into endogenous *TP53* locus via homologous recombination.

A brief description of the method is shown in Fig. 4. First, the wild-type *TP53* locus in the cell line is exchanged for the mutant allele using CRISPR-Cas9-mediated homology-directed repair. For this purpose, cells expressing wild-type p53 are co-transfected with two plasmids. The first plasmid encodes the *TP53*-specific CRISPR-nuclease. The second plasmid or plasmid pool contains the *TP53* gene fragments with multiple mutations (one mutation per construct) and represents a library of donor templates for homology-directed repair. After co-transfection, CRISPR-nuclease cleaves DNA in the *TP53* locus. The double-strand break is repaired by HDR using the provided library as donor templates. As a result, the wild-type *TP53* allele is exchanged for one of the mutated alleles from the library, and the pool of isogenic cells containing multiple *TP53* alterations is generated. Afterward, library-expressing cells are treated with p53-activating stimuli (e.g., MDM2-inhibitor or DNA damaging agent).

Activation of p53 mutants with preserved wild-type function promotes cell cycle arrest or apoptosis, which results in depletion of cells harboring such mutations from the pool. Conversely, cells carrying LOF mutants stay unresponsive to the p53-activating stimuli and proliferate, becoming enriched in the population. Thus, counting the number of cells expressing a mutant before and after treatment enables measuring antiproliferative properties of each protein variant. The stronger the mutation is enriched after p53 activation, the less functional the mutant protein is. The abundance of cells carrying particular mutants in the population is quantified using massive parallel sequencing (next generation sequencing, NGS) of the *TP53* locus. Sequencing data from untreated (control) and treated samples are compared to identify enriched and depleted variants (Fig. 4). Finally, the enrichment score is

calculated for each mutant as a measure of p53 protein functionality: low enrichment score of depleted variants reflects preserved wt-like function, whereas high

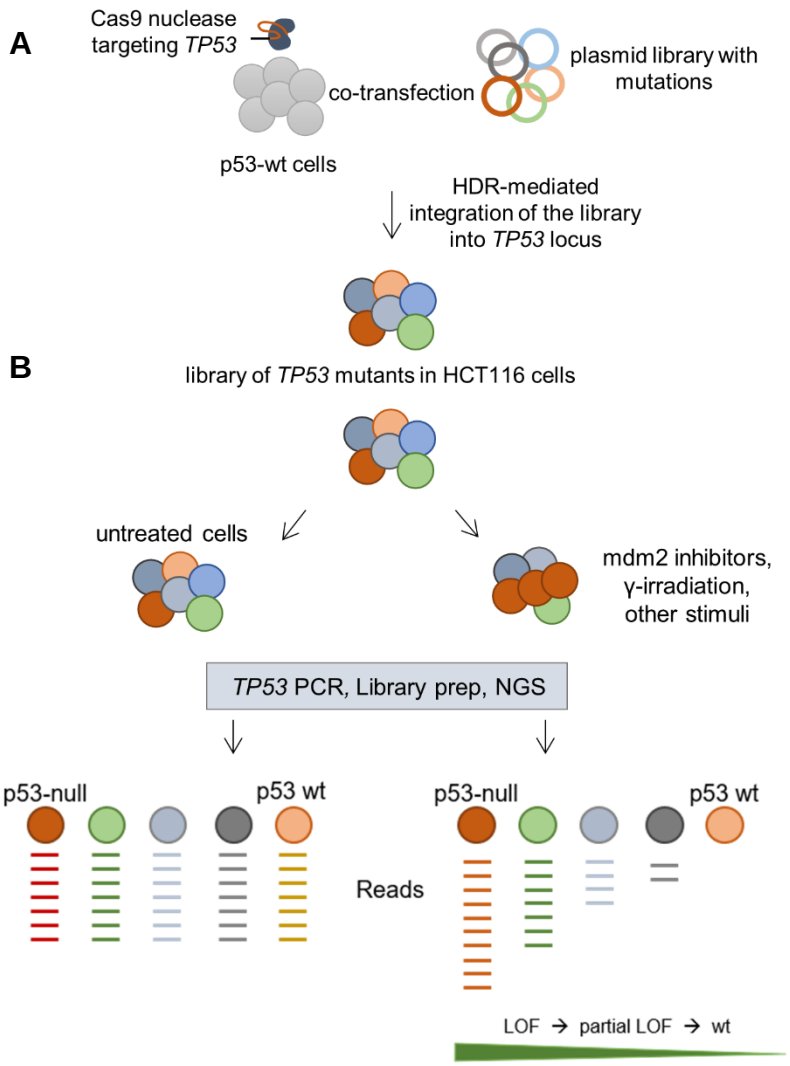

Figure 4. Experimental design of the CSMS

A. Cells are co-transfected with a CRISPR/Cas9 nuclease targeting *TP53* locus and vectors carrying a mutant library. CRISPR nuclease cleaves DNA in the *TP53* locus. Double-strand breaks are repaired by HDR. Cells utilize provided library as homology recombination templates and integrate mutations into the locus. **B.** CSMS employs massive parallel measurement of the impact of p53 mutations on cellular fitness. Cells expressing the library of p53 variants are subjected to p53-activating stimuli and harvested later for DNA isolation, allele-specific PCR, and sequencing library preparation. The relative abundance of each variant is quantified using next-generation sequencing and compared between treated and untreated samples. Wild type-like mutations are depleted after the treatment, LOF mutations are strongly enriched after the treatment, partially-LOF mutations show intermediate enrichment.

enrichment score of enriched variants indicates loss of function.

We aimed to conduct initial proof-of-concept experiments by performing saturation mutagenesis of the most frequently mutated hotspot codon R175 because functional outcomes of most mutations at this position are well studied (Freed-Pastor and Prives 2012; Walerych et al. 2015; Timofeev et al. 2019; Freed-Pastor et al. 2012; Yu et al. 2012; Xu et al. 2014). We have further expanded our analysis to the R175-adjacent region (H1 helix) and, finally, to the complete 5th exon of *TP53* (approximately 22% of all *TP53* mutations affect the 5th exon).

3.2 *TP53* targeting strategy

For the development of the CSMS-system, we have chosen the colorectal cancer cell line HCT-116. HCT-116 cells respond to DNA damage and treatment with MDM2 inhibitors with p53 stabilization, induction of p53 target genes, and undergo cell cycle arrest and apoptosis. These cells have been widely used during the last decade for studying the biology of p53 (Polyak et al. 1996; Sur et al. 2009). The cell line is diploid and contains two intact *TP53* copies (Liu and Bodmer 2006). This allows inactivating one allele and manipulating the other in a hemizygous configuration to avoid interference from the second allele and establish clear genotype-phenotype correlations. Moreover, the functionality of both *TP53* alleles ensures that mutations will be engineered in the normal genomic context with functional regulatory elements. In this section the general concept is described, the experimental details are explained in detail in following sections.

Insertional mutagenesis mediated by homologous recombination has inherently low efficiency (Maruyama et al. 2015). An additional factor limiting the efficiency of CRISPR-mediated gene editing is p53 activation: Cas9-induced double-strand breaks activate the p53-dependent DNA damage response and proliferation arrest in the edited cells (Haapaniemi et al. 2018). To overcome these limitations and enhance HDR-mediated targeting, we have devised a cell line with an editable *TP53*-locus (HCT-116$^{\Delta/TP53E}$), which enabled us to perform mutagenesis with unprecedented efficiency. The schematic view of the *TP53* targeting strategy is shown on Fig. 5. One *TP53* allele in this cell line (*TP53*$^{\Delta}$) is permanently inactivated to ensure that each cell will express a single mutant after editing. The second allele undergoes CRISPR-mediated editing and is therefore called “editable” (*TP53*^{E}). It is

temporarily inactivated to disable p53-mediated DNA damage response provoked by CRISPR-Cas9. After completion of the gene editing, this allele is reactivated to express the mutant protein (Fig.5).

We have created the cell line with described characteristics using two rounds of CRISPR-mediated genome editing. Initially, we were attempting to inactivate one *TP53* allele by deleting it with a pair of two CRISPR-nucleases that target upstream and downstream sequences in the gene locus, respectively. However, resulting cell lines revealed instability and rapidly inactivated the remaining wild-type allele via loss of heterozygosity (LOH). Interestingly, we found that relatively small deletions in the 5th intron completely impaired p53 mRNA splicing and protein translation. This fact allowed us to knock out one *TP53* copy with a small intronic deletion and generate a

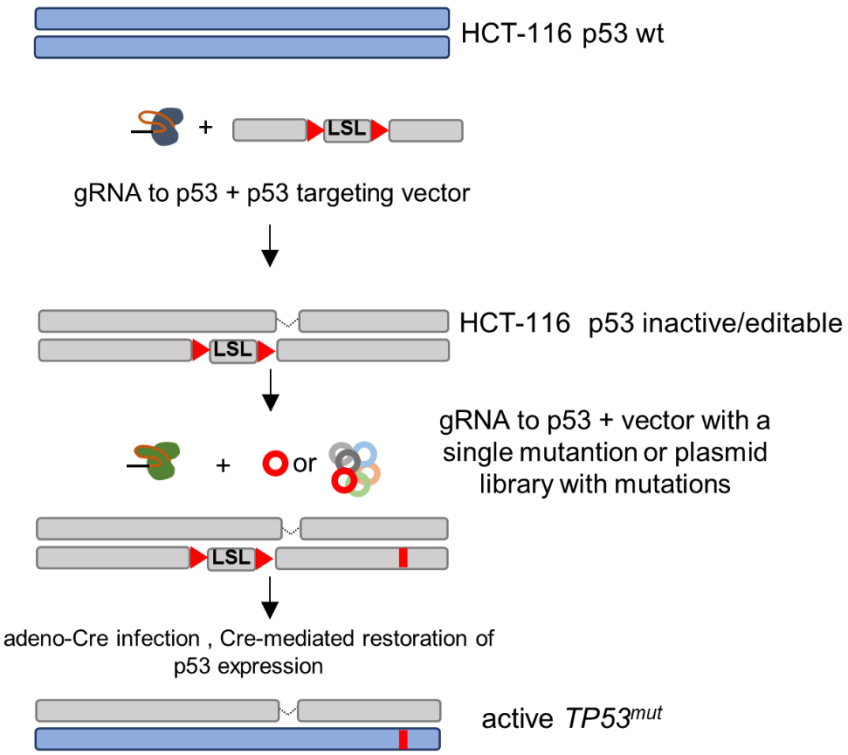

Figure 5. Simplified scheme of *TP53* targeting strategy

Cells are co-transfected with a CRISPR/Cas9 nuclease targeting *TP53* locus and a vector carrying the LSL-cassette. After CRISPR/Cas9 overexpression the first p53 allele is permanently inactivated by deletion. The second allele is temporary inactivated by the integration of LSL-cassette. Next, this cell line undergoes transient transfection with CRISPR/Cas9 nuclease targeting *TP53* locus in the LSL-allele and vector carrying a single p53 mutation or a plasmid mutant library. After infection with adeno-Cre LSL-cassette is excised and mutant p53 expression is restored.

genetically stable cell line with a single active *TP53* copy.

Therefore, in the first editing round, we have used a single CRISPR-nuclease to induce a deletion in the intron 5 of one *TP53* allele. In the same gene editing step, we have integrated the transcription termination cassette (lox-stop-lox, LSL carrying green fluorescent protein (*GFP*) and the puromycin selection marker) into the 4th intron of the second *TP53* allele using homologous recombination.

HDR-mediated integration of the LSL cassette into the *TP53* locus created the conditionally silenced allele and enabled the selection of targeted cells using puromycin resistance or GFP expression. Additionally, erroneous repair of the 5th intron by Cas9-nuclease in the edited conditional allele (*TP53^{E}*) has generated a single nucleotide variant (SNV). The SNV was used as an allele-specific recognition site for CRISPR-nuclease in the second gene editing round.

In the second step of editing, we have employed the allele-specific CRISPR-nuclease to induce double-strand breaks exclusively in the *TP53^{E}* allele and to target the library of *TP53* variants into the locus. Lack of p53 expression (the second allele is permanently inactivated) enabled to increase the editing rate due to dampened DNA-damage response.

After the second editing round, the silenced conditional *TP53^{E}* allele was turned back into an active state by Cre-recombinase expression, which excised the LSL cassette. As a result, a population of cells expressing a single mutant or a pool (library) of mutants from a single *TP53* allele was generated.

To validate the system, we decided to perform mutagenesis of the small region of the gene. Therefore, initially we have focused on the most frequently mutated codon R175. Next, we have explored the adjacent region (H1 hellix) which contains several functionally important conserved residues (e.g. C176, H179, E180, R181). Later we have performed mutagenesis of the complete 5th exon of the *TP53* gene. Targeting of the exon 5 is described in section 3.10.

3.3 Generation of the targeting vector for homologous recombination-driven *TP53* editing

To engineer the endogenous *TP53* locus we have designed a series of plasmid templates for homologous recombination (targeting vectors). One vector was used to generate the editable *TP53* allele; the others were utilized for the mutagenesis.

For conversion of the wild-type *TP53* allele into the editable one we have designed the targeting vector (HR-1) consisting of the following components:

- the HA700PA-1 backbone (Fig. 6A),

- two homology arms spanning the region between 4th exon and 6th intron of *TP53* (chr. 17:7.676.244-7.674.422, GRCh38 assembly),

- lox-STOP-lox (LSL) cassette in the 4th intron, composed of two LoxP sites flanking the puromycin N-acetyl transferase gene (*pac,* confers puromycin resistance), green fluorescent protein gene (GFP), the transcription termination sequence (STOP) and insulator sequences (to prevent activation of endogenous genes by the EF1

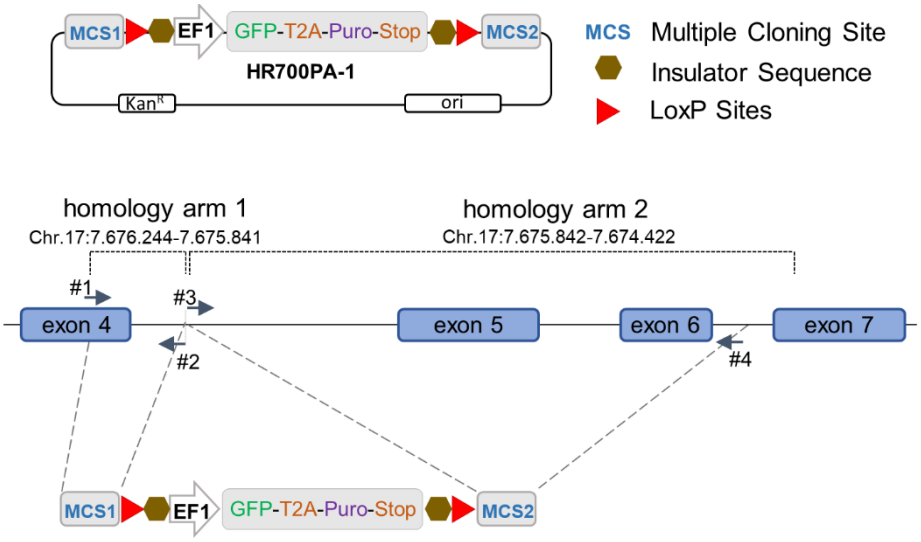

Figure 6. Schematics of the targeting vector for HDR-mediated *TP53* editing

A. Vector HR700PA-1 contains two polylinkers (MCS) for cloning of the homology arms and the LSL cassette (used for selection of targeted cells, harbors GFP and puromycin resistance genes and the transcription terminator sequence (STOP) flanked by insulators and LoxP sites). Integration of the LSL cassette into the *TP53* locus leads to silencing of p53 expression. **B.** Assembly of the HR-1 targeting vector. *TP53* homology arms were amplified from genomic DNA and cloned into MCS 1 and 2. The location of primers for amplification of homology arms is shown with arrowheads. Coordinates are according to the GRCh38 human genome assembly.

promoter in the proximity of the integration site).

Homology arm one spanning 3'-end of the exon 4 and 5'-end of the intron 4 (chr.17:

7.676.224-7.675.841) was amplified by PCR from genomic DNA of HCT-116 cells. The amplicon was digested with BsaI and BsrGI and ligated into the multiple cloning site (MCS1) of the HR700-1A vector (Fig. 6B) (primers #1, 2). Homology arm two spanning the region between exon 4 and intron 6 (chr.17: 7.675.842-7.674.422) was amplified using primers to the 3'-end of intron 4 and 5'-end of the intron 6 and cloned via SalI and MluI digestion and ligation into MCS2 of the HR700-1A vector with previously cloned homology arm one (primers #3, 4) (Fig. 6B).

3.4 Establishment of the *TP53*-hemizygous HCT-116$^{\Delta/TP53E}$ cell line using HR-1 targeting vector

The efficacy of homologous recombination strongly depends on the distance between the homology arm and the double-strand break (Elliott et al. 1998). To ensure the complete replacement of the endogenous H1 helix region at the end of exon 5 with the mutants' library, we have located the targeting site for the Cas9 nuclease in direct proximity of this region in intron 5 (Fig. 7A).

In the first step, we have co-transfected parental HCT-116 cells with a plasmid encoding Cas9 nuclease with intron 5-specific single guide RNA (sgRNA) (pX330-sgRNAp53i5) and an HR-1 targeting vector. Cells with an integrated targeting vector were selected with puromycin (Fig. 7A). Then resistant transfectants were treated with MDM2-inhibitor nutlin for 14 days to enrich the population for p53-null cells, which either harbor *TP53* allele temporarily inactivated by the LSL-cassette, or inactivating deletion or both. This nutlin-enriched population was subcloned to select a cell line with the desired configuration of *TP53* alleles. For this purpose, cells were plated at clonal density, single-cell clones were isolated, and gDNA from the clones was analyzed for the correctly integrated targeting vector using PCR. Forward primer #7 (Fig. 7B) was located in the LoxP site in the targeting vector, whereas reverse primer #10 (Fig. 7B) was placed in the 7th exon, located downstream of the right homology arm. Therefore, amplification proceeded only with template DNA from clones with on-target integration of the targeting vector (Fig. 7B,C). Clones 1, 3, and 5 with confirmed on-target integration of the HR-1 vector were amplified and infected with the Cre-recombinase-expressing adenovirus (adeno-Cre) to excise the LSL cassette and restore p53 expression. Two weeks after infection, cells were treated for 24 hours with 10 µM nutlin to activate p53 and analyzed with western blotting

together with lysates from non-infected cells. As shown in Fig. 7D, clones have responded to adeno-Cre infection differently. Clone 3 showed no reactivation of p53 upon adeno-Cre infection and nutlin treatment, suggesting complete inactivation of both alleles. Clone 5 revealed high levels of p53 in the absence of Cre, indicating that at least one allele was spared by editing. Finally, clone 1 was identical to p53-knockout cells under basal conditions (lanes 5 and 6) but demonstrated Cre-dependent restoration of p53 expression (lanes 7 and 8), implying that at least one *TP53* allele contained an integrated targeted vector with the LSL cassette. Moreover, similarly to p53 wild-type cells, clone 1 revealed nutlin-dependent p53 stabilization and expression of the p21 protein, as expected for the cell line carrying the conditional p53 allele.

To confirm that the *TP53* locus in the engineered cell line had the desired configuration, we have designed a series of PCR primers to generate amplicons covering the region between 4^{th} and 6^{th} exons. The location of amplicons and sequencing results are shown in Fig. 7E.

First, we have amplified DNA with primers #5 and #10 (upper part of Fig. 7E). This primer pair amplified the 1,6 kb long fragment from the intact intron 4. Integration of the LSL cassette would generate the 4.6 kb long fragment; therefore, the targeted allele was not amplified. Sanger sequencing of the 5'-end of the amplicon showed the intact sequence of the *TP53* intron 4 without the integration of the LSL cassette (upper left chromatogram, the dashed line shows the boundary between intron 4 and LSL cassette in the targeting vector). The sequence of the 3'-end of the same amplicon contained 15-bp deletion at the CRISPR-nuclease recognition site (upper right chromatogram). Since cells did not express detectable levels of p53 in the absence of adeno-Cre (Fig. 7D, lanes 5 and 6) we have concluded that the first allele in the engineered cell line contained inactivating deletion and designated this allele as $TP53^{\Delta}$.

Next, we have selectively amplified the second, targeted allele with primers #6 and #10 (primer #6 is specific to the *pac* gene) (Fig. 7E). The sequencing of the resulting amplicon confirmed integration of the targeting vector in the *TP53* locus (5' end of the amplicon was identical to the *pac* sequence from the vector, lower left chromatogram). Since the treatment of cells with Cre-recombinase led to re-

expression of p53 (Fig. 7D, lanes 7 and 8), we concluded that the second allele was converted into a conditional allele by the integration of the targeting vector. Notably, the sequencing of the 3'-end of the same amplicon revealed a single nucleotide insertion in the 5th intron (lower right chromatogram). This single nucleotide variant (SNV) was exploited as a target site for allele-specific CRISPR-nuclease in the second editing step. We have designated the second allele in the cell line as editable (*TP53*^{E}).

The stability of the cell line properties was confirmed by analyzing three independent subclones of clone 1 from Fig. 7F for their ability to restore p53 expression upon adeno-Cre infection and upregulate p21 after nutlin treatment (Fig. 7F). The established cell line Δ/*TP53*E.1 was designated as HCT-116$^{\Delta/TP53E}$ and was utilized in all consecutive experiments.

Western blotting (Fig. 7F) revealed that HCT-116$^{\Delta/TP53E}$ cells show markedly lower p53 and p21 expression after adeno-Cre infection and nutlin treatment than the parental cell line (compare lanes 1 and 3 with lanes 7 and 8). P53 is a known haploinsufficient tumor suppressor. In line, the lack of one gene copy was shown to significantly decrease mRNA and protein levels in HCT-116 cells (Lynch and Milner 2006). Insufficient expression of p53 could potentially lead to reduced activity and, consequently, to improper classification of wild-type-like variants. We have addressed this issue in Discussion.

The selection of cells after homologous recombination is essential to ensure a high yield of edited cells. HCT-116$^{\Delta/TP53E}$ cells already contained a puromycin resistance gene in the *TP53*^{E} allele. To enable the puromycin selection of the targeted cells carrying the library in the second round of editing, we have inactivated the *pac* gene using CRISPR/Cas9. We have designed a single guide RNA specific to the *pac* gene, cloned it into pX330 vector, and transfected into HCT-116$^{\Delta/TP53E}$ cells. (Fig. 7G). We expected that double-strand breaks induced by the *pac*-specific Cas9 nuclease would be repaired via NHEJ generating inactivating indels. For the selection of cells with inactivating *pac* mutations, single-cell clones were isolated and tested for puromycin sensitivity. One clone with restored puromycin sensitivity was established and used in further experiments (Fig. 7H).

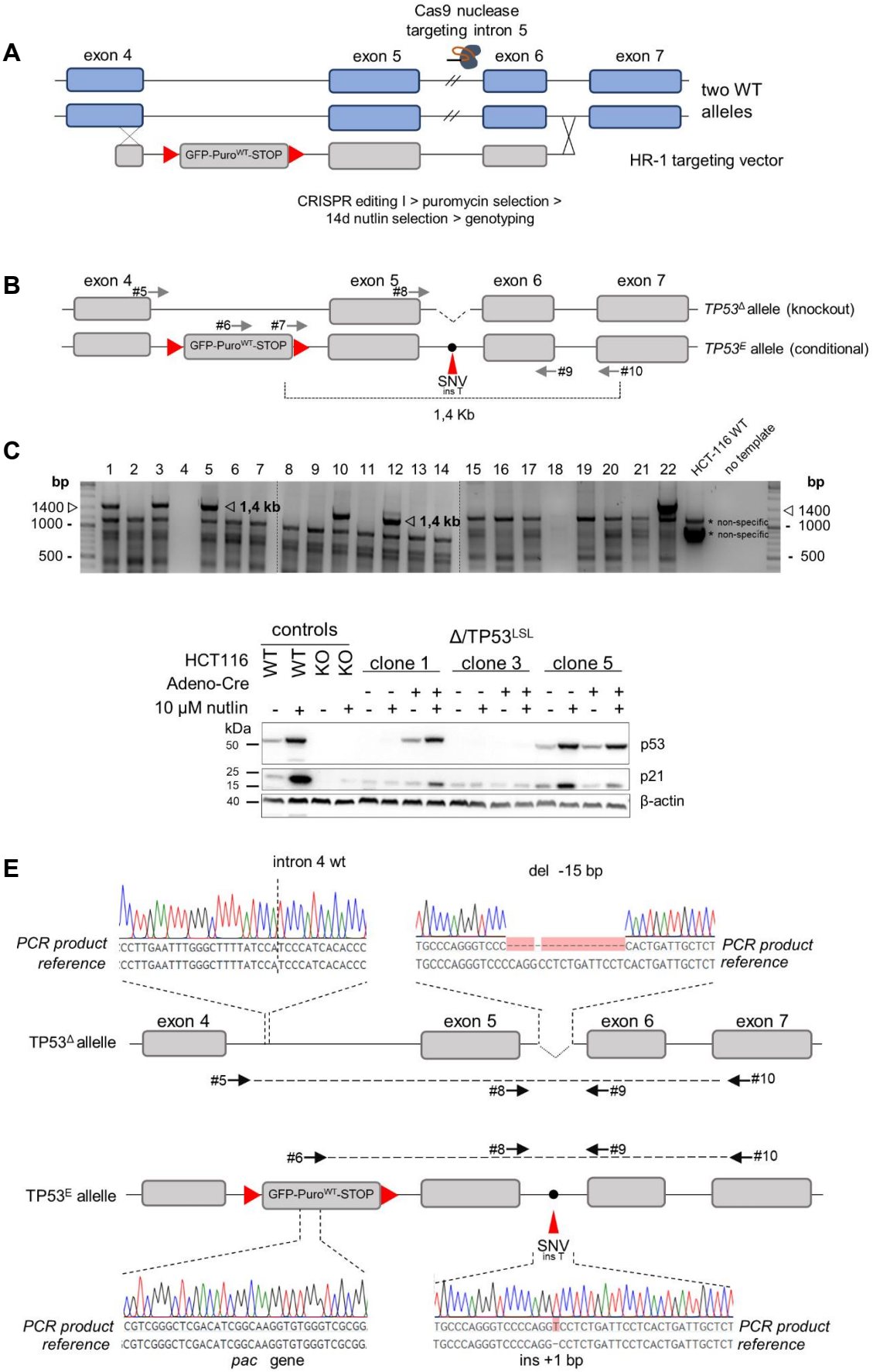
A
Cas9 nuclease
targeting intron 5
exon 4
exon 5
exon 6
exon 7
two WT
alleles
GFP-Puro^WT-STOP
HR-1 targeting vector
CRISPR editing I > puromycin selection >
14d nutlin selection > genotyping
B
exon 4
exon 5
exon 6
exon 7
#5
#8
#6
#7
TP53Δ allele (knockout)
GFP-Puro^WT-STOP
TP53E allele (conditional)
#9
#10
SNV
ins T
1,4 Kb
C
HCT-116 WT
no template
bp
1 2 3 4 5 6 7 8 9 10 11 12 13 14 15 16 17 18 19 20 21 22
1400
1000
500
1,4 kb
1,4 kb
* non-specific
* non-specific
controls
Δ/TP53LSL
HCT116
WT
WT
KO
KO
clone 1
clone 3
clone 5
Adeno-Cre
10 μM nutlin
kDa
50
25
15
40
p53
p21
β-actin
E
intron 4 wt
del -15 bp
PCR product
reference
CCTTGAATTTGGGCTTTTATCCATCCCATCACACCC
CCTTGAATTTGGGCTTTTATCCATCCCATCACACCC
TGCCCAGGGTCCC----------CACTGATTGCTCT
TGCCCAGGGTCCCCAGGCCTCTGATTCCTCACTGATTGCTCT
PCR product
reference
TP53Δ allele
exon 4
exon 5
exon 6
exon 7
#5
#8
#9
#10
#6
#8
#9
#10
TP53E allele
GFP-Puro^WT-STOP
SNV
ins T
PCR product
reference
CGTCGGGCTCGACATCGGCAAGGTGTGGGTCGCGG
CGTCGGGCTCGACATCGGCAAGGTGTGGGTCGCGG
pac gene
TGCCCAGGGTCCCCAGGTCCTCTGATTCCTCACTGATTGCTCT
TGCCCAGGGTCCCCAGG-CCTCTGATTCCTCACTGATTGCTCT
PCR product
reference
ins +1 bp

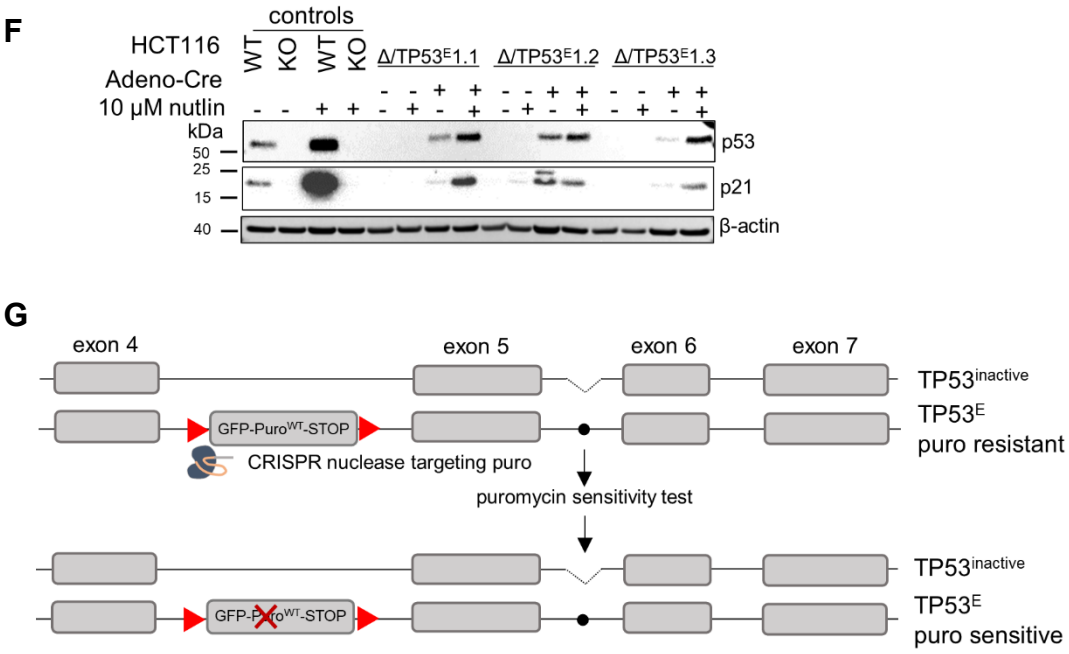

Figure 7. Establishment of the *TP53*-hemizygous cell line HCT-116$^{\Delta/TP53E}$ for highly efficient editing of the *TP53* locus

A. HCT-116 cells were co-transfected with the plasmid encoding CRISPR nuclease targeting intron 5 of *TP53* and donor template for homologous recombination (HR-1). Blue rectangles represent active alleles, grey – inactive. Transfected cells were selected with puromycin. Afterward cells with the functional p53 were eliminated by nutlin treatment. Single-cell clones were established and genotyped. **B.** The desired configuration of the *TP53* locus after targeting. Primers used for genotyping of single-cell clones are shown as arrowheads. Primers #7 and #10 were used for the identification of clones with correct integration of LSL cassette, primers #8 and #9 - for Sanger sequencing of the intron 5, primer #5 was used for Sanger sequencing of the intron 4, primers #6 and #10 were used for amplification of the LSL cassette, primer #6 was used for Sanger sequencing of the LSL cassette. Black dot – single nucleotide variant (SNV), +T insertion in the targeted conditional allele. Red triangles: Lox-P sites. **C.** Identification of single-cell clones with the correct integration of the targeting vector using PCR with primer #7 to LSL cassette and #10 to the exon 7. Single cell clones are labeled from 1 to 22. 1.4 kb PCR fragments corresponding to targeted *TP53* alleles are labeled. Parental HCT-116 cells serve as a negative control. **D.** Western blot analysis of p53 and p21 expression in 3 clones with targeted *TP53* alleles from (C) (designated as Δ/TP53^{LSL}). Cells were infected with adenovirus encoding Cre-recombinase and after 2 weeks were treated with 10 μM nutlin for 24h. Clone 1 demonstrates the Cre-controlled activation of p53 and nutlin-dependent activation of p21.

Figure 7. Continued

E. Sanger sequencing results and schematic representation of two TP53 alleles of the clone 1 (from D). Two upper chromatograms demonstrate the intact intron 4 without vector integration (vertical dashed line shows the end of homology arm 1 and the beginning of the homology arm 2) and the 15 bp inactivating deletion in the 5th intron (dotted line) of one allele (*TP53*$^{\Delta}$). Amplicon was produced using primers #5 and #10 and sequenced using primers #5, 8, and 9. Two lower chromatograms demonstrate the integration of the LSL cassette into the second allele and +T insertion (SNV) in the targeted conditional allele (TP53E). Sequenced amplicons are shown with dashed lines, primers shown with arrows. Amplicon was sequenced using primers #6, 8, and 9. Red triangles: Lox-P sites. **F**. Western blot analysis of p53 and p21 expression in three independent single-cell subclones of the clone 1 from (D) after transduction with adeno-Cre. Cells were treated with 10 μM nutlin for 24h to stabilize p53. Parental cells (WT) and *TP53*-knockout cells (KO) were used as positive and negative controls respectively. β-actin serves as a loading control. **G.** Restoration of the puromycin sensitivity in HCT-116$^{\Delta/TP53E}$ cells via inactivation of the *pac* gene. Cells were transfected with the plasmid encoding sgRNA targeting *pac*, single-cell clones were established and tested for puromycin sensitivity. **H.** Schematics of the *TP53* locus of the HCT-116$^{\Delta/TP53E}$ cell line. The puromycin-sensitive cell line contains one allele inactivated by 15 bp CRISPR-induced deletion in the intron 5. The second allele contains the cassette with the non-functional *pac* gene and GFP in the intron 4 (red cross).

To summarize, the engineered HCT-116$^{\Delta/TP53E}$ cell line has the following properties.

1. One copy of the *TP53* gene is permanently inactivated by a 15-bp deletion in intron 5 to ensure a single active *TP53* allele presents in each cell.
2. The second conditional “editable” *TP53* allele (*TP53*^{E}) is temporarily inactivated by the LSL cassette to allow editing in p53-negative background. After editing is completed, the allele is reactivated by Cre-recombinase, and p53 is re-expressed.
3. *TP53*^{E}-allele can be targeted by the allele-specific CRISPR-nuclease directed against a single-nucleotide variant in intron 5 (Fig. 7H). Thereby monoallelic integration of the library of p53 variants in the following round of genome editing is ensured.

4. The puromycin resistance gene in the HCT-116$^{\Delta/TP53E}$ cell line is disrupted, making cells puromycin-sensitive. Therefore, cells that successfully underwent recombination with the *pac*-containing HDR template can be selected.

3.5 Generation of cell pools expressing p53 variants

To introduce mutations into the *TP53*^{E} allele, we have employed the second round of genome editing. We first aimed to perform mutagenesis of the codon R175 and the adjacent region (H1 helix). To generate the library of targeting vectors carrying mutations, we have utilized the Golden Gate cloning procedure. The protocol enables the rapid single-step cloning of inserts into the vector with almost 100% efficiency (Engler et al. 2008). Golden Gate cloning procedure utilizes the digest of the vector with the Type IIs restriction enzyme, which cleaves DNA outside the recognition site, ensuring seamless cloning. To make the HR-1 targeting vector compatible with this procedure, we have performed site-directed mutagenesis and introduced two recognition sites for the type IIs enzyme BbsI into the vector. Since we first aimed to modify the hotspot codon R175 and the H1 helix domain, we have flanked this region with the recognition sites. Cleavage of this vector with BbsI generates two pairs of incompatible sticky ends that can be ligated only with double-stranded oligonucleotides with corresponding compatible sticky ends (Fig. 8). This precludes circularization of the empty vector and ensures superior cloning efficiency.
Additionally, a dinucleotide mutation was introduced into the vector to destroy the protospacer-adjacent motif (PAM) in the 5th intron in the donor template (TCC to TGG, chr.17:7.674.839-7.674.841). The PAM sequence is essential for the binding of CRISPR nuclease to DNA. Therefore, its mutation in the HDR template prevents cleavage of transfected plasmid and the recombined allele. In addition, the GG dinucleotide was used as the unique primer binding site for the amplification of the *TP53* DNA exclusively from library-carrying cells. Thereby cells that were not targeted and retained the non-edited *TP53*^{E} allele were excluded from further analysis. The resulting vector was named HR-2-Golden Gate.

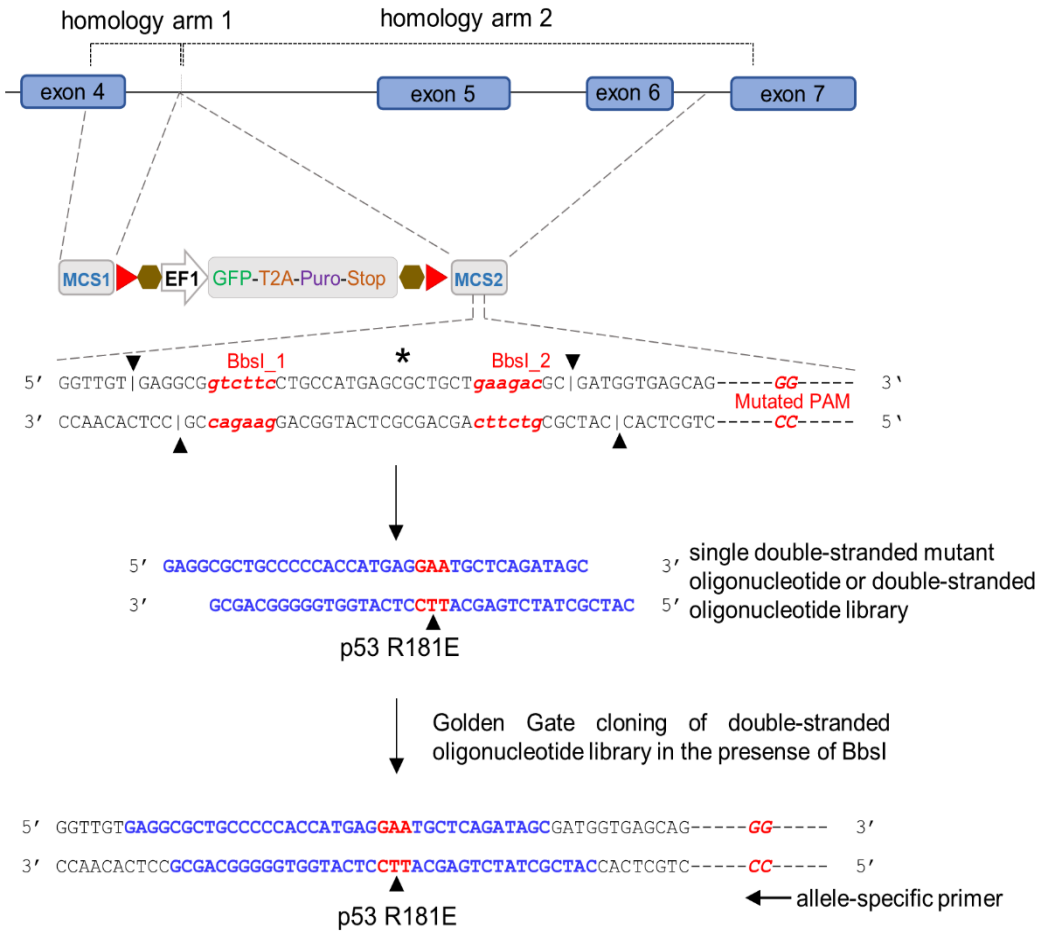

Figure 8. Generation of the HDR template vector for the introduction of the library of H1 helix mutants into *TP53* locus (HR-2-Golden Gate)

To enable Golden Gate cloning of the oligonucleotide library into the targeting vector, two BbsI recognition sites in opposite orientation were introduced into the sequence encoding H1 helix in the right homology arm of the HR-1 targeting vector using site-directed mutagenesis (BbsI recognition sequences are marked in red, cleavage sites are marked with arrowheads). 34 bp double-stranded oligonucleotides with 4-bp overhangs encoding variants of the H1 helix (5th exon) (shown in blue) were cloned into the vector either separately or as a pool using Golden Gate cloning protocol. R181E mutation is shown as an example. HR-2-Golden Gate vector contains a mutated PAM sequence in the intron 5 (GG). GG dinucleotide is used as a primer annealing site for specific amplification of the edited allele (arrow). For mutagenesis of the full exon 5, the vector was redesigned to allow cloning of 230 bp oligonucleotides spanning exon 5 (HR_Exon5) (section 3.10).

As a first step we have introduced single mutations one by one into the modified targeting vector by cloning double-stranded oligonucleotides using the Golden Gate protocol (Fig. 8). To do so, a pair of single-stranded complementary oligonucleotides

with a mutation was designed to form two sticky ends compatible with the BbsI-digested HR-2-Golden Gate vector. Oligonucleotides were annealed and cloned into the HR-2-Golden Gate vector. Cloning product was transformed in *E. coli*; bacteria were plated on LB-agar plates. Plasmid DNA purified from harvested colony and was designated as vector carrying a single p53 mutation. To examine the presence of a *TP53* mutation a fragment was amplified with primers #3 and #4 and sequenced using Sanger sequencing. Co-transfection of cells with the pX330 plasmid encoding the allele-specific sgRNA and targeting vector resulted in HDR-mediated integration of the mutation into the $TP53^{E}$ allele (Fig. 9A). Subsequent puromycin selection generated a mutation-carrying cell line (Fig. 9B). After infection with adeno-Cre the LSL-cassette was excised, restoring the p53 expression (Fig. 9C).

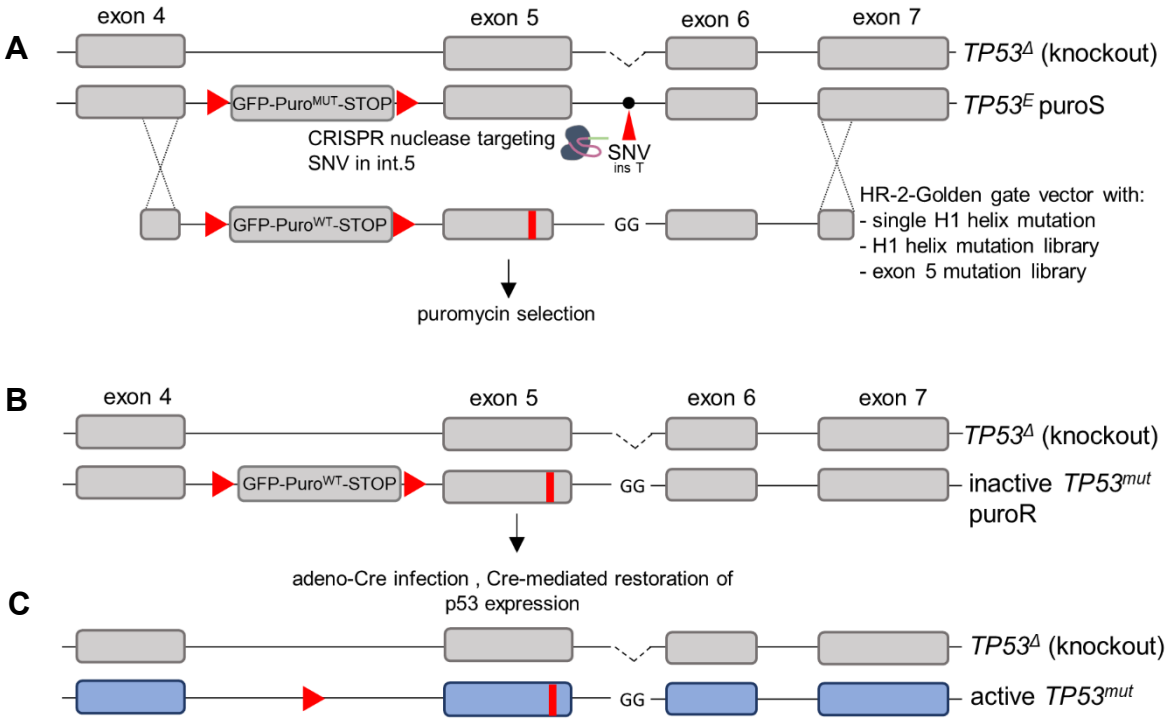

Figure 9. Schematic representation of the introduction of variants into the *TP53*^{E} allele of the HCT-116 $^{\Delta/TP53E}$ cell line using HDR

A. Cells were co-transfected with the plasmid encoding the CRISPR nuclease targeting the 1-bp insertion in the intron 5 of the *TP53*^{E} allele (black dot, SNV) and HR-2-Golden Gate vector carrying a single mutation or a mutagenic library (red rectangle in the exon 5). GG denotes the mutated PAM-sequence which prevents repeated cleavage of the targeted allele and is used as a site for primer binding. **B,C.** Schematic of the conditional allele carrying a single p53 mutation or the variant library before (B) and after (C) Cre-mediated restoration of the p53 expression. Red triangles: Lox-P sites.

3.6 The HCT-116$^{\Delta/TP53E}$ cell line enables highly efficient HDR-mediated mutagenesis of the endogenous *TP53* locus

To test the efficiency of mutagenesis in our system, we have introduced a single inactivating mutation (R181E, CGC > GAA) in the H1 helix-encoding region of the *TP53*^{E} allele, as shown in Fig. 10A. This mutation destroys the AfeI restriction site. Therefore, cells can be easily genotyped using restriction fragment length polymorphism analysis. Following the co-transfection of the pX330-sgRNAp53i5 plasmid encoding the *TP53*^{E}-specific CRISPR nuclease with the HR-vector carrying the R181E donor, template cells were selected with puromycin. Afterward, 13 single-

cell clones were established, and genomic DNA was assayed for HDR template integration. Strikingly, amplicons from 11 clones were resistant to AfeI digestion, suggesting correct modification. Only two clones have retained the initial *TP53*^{E}

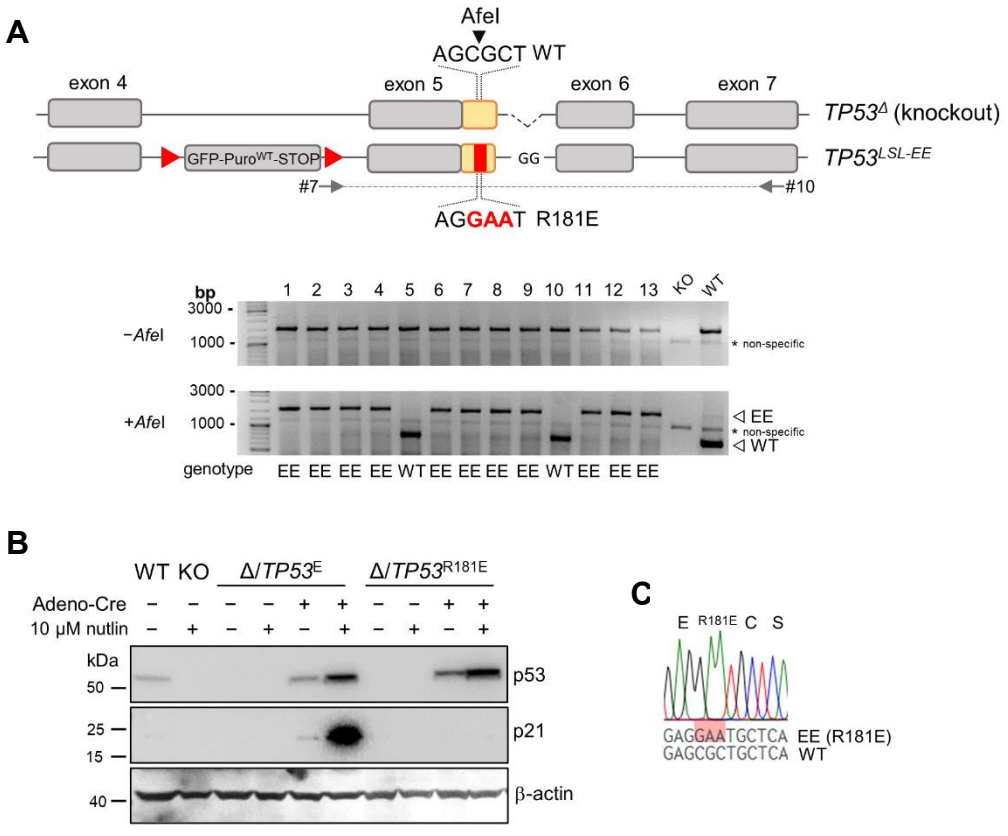

Figure 10. Highly efficient introduction of the R181E mutation into the *TP53* locus of the HCT-116 $^{\Delta/TP53E}$ cell line

A. Schematic of the *TP53* locus in the cell line targeted with the donor template carrying the R181E mutation. AfeI recognition site is disrupted by the mutation (red rectangle). Arrows indicate primers used for the allele-specific PCR. Bottom: PCR-RFLP-genotyping of single-cell clones of HCT-116$^{\Delta/TP53E}$ cells co-transfected with the CRISPR plasmid and the HR-2 Golden Gate-R181E donor template. PCR fragments from 11 of 13 clones were resistant to digest with AfeI, demonstrating targeting efficacy of 75%. KO - cell line with the deletion spanning exons 2 to 9 of TP53, used as a negative control, WT – parental HCT-116 cells serve as a positive control for AfeI digestion. **B.** Western blot analysis of p53 and p21 expression after infection with adeno-Cre in parental (WT), p53-null (KO), and HCT-116 $^{\Delta/TP53E}$ cells as well as in one of the R181E-carrying clones from (A) (untreated and nutlin-treated). **C.** Sanger sequencing confirms the presence of the R181E mutation in the genomic DNA of the engineered cell line.

allele (Fig. 10A). After adeno-Cre infection, expression of p53 was restored, but no p21 activation was evident after nutlin treatment in agreement with transactivation deficiency of the R181E mutant (Fig. 10B) (Timofeev et al. 2019; Schlereth et al. 2010a; Schlereth et al. 2013; Kitayner et al. 2006; Dehner et al. 2005). Finally, successful targeting in 11 clones was confirmed with Sanger sequencing (Fig. 10C).

Later, a panel of 8 mutant cell lines was generated in our group using a similar approach (data courtesy of Julianne Funk, Michelle Neuman, and Pascal Hunold). The presence of desired mutations in all cell lines (R175Stop, R175H, R175P, C176F, H179R, R181L, R181P, and E180R) (Fig. 11A) was validated with Sanger sequencing (Fig. 11B) and western blot after nutlin treatment (Fig. 11C).

Additionally, two other cell lines carrying H1 helix mutants (S183A, S185A, and S183D, S185D) were established using the approach developed in this work. These cell lines were used to explore the importance of H1 helix phosphorylation for tuning the p53 activity (Fig. 11D) (Timofeev et al. 2020).

Summarizing, the HCT-116$^{\Delta/TP53E}$ cell line together with a set of targeting vectors and corresponding protocols established in this work comprise a highly effective system for targeted mutagenesis of the endogenous *TP53* locus.

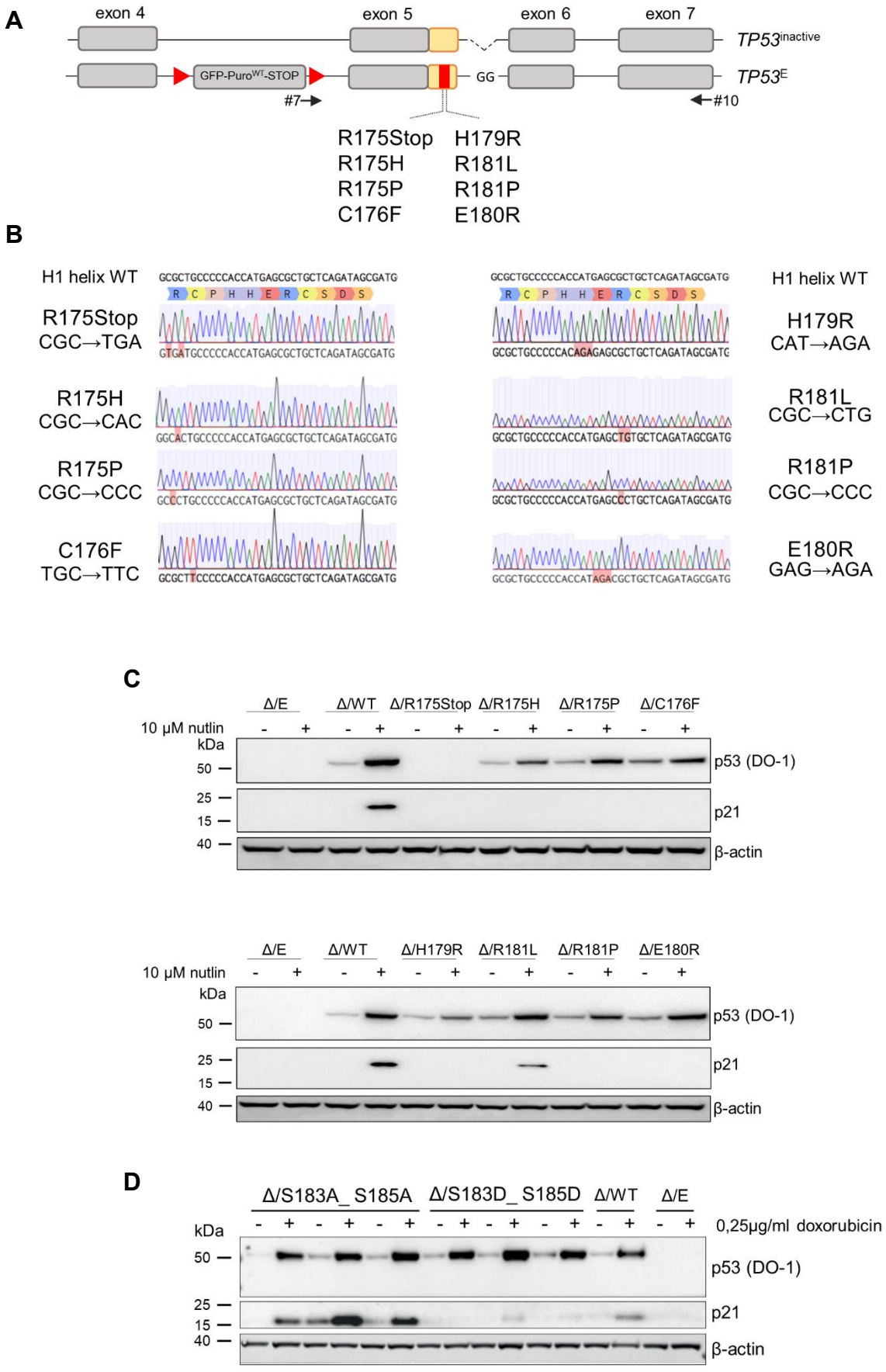
A
exon 4
exon 5
exon 6
exon 7
TP53inactive
GFP-PuroWT-STOP
GG
TP53E
#7
#10
R175Stop
R175H
R175P
C176F
H179R
R181L
R181P
E180R
B
H1 helix WT
R175Stop
CGC→TGA
R175H
CGC→CAC
R175P
CGC→CCC
C176F
TGC→TTC
H179R
CAT→AGA
R181L
CGC→CTG
R181P
CGC→CCC
E180R
GAG→AGA
C
Δ/E
Δ/WT
Δ/R175Stop
Δ/R175H
Δ/R175P
Δ/C176F
10 μM nutlin
kDa
50
25
15
40
p53 (DO-1)
p21
β-actin
Δ/E
Δ/WT
Δ/H179R
Δ/R181L
Δ/R181P
Δ/E180R
10 μM nutlin
kDa
50
25
15
40
p53 (DO-1)
p21
β-actin
D
Δ/S183A_ S185A
Δ/S183D_ S185D
Δ/WT
Δ/E
0,25μg/ml doxorubicin
kDa
50
25
15
40
p53 (DO-1)
p21
β-actin

Figure 11. HCT-116 $^{\Delta/TP53E}$ enables the of the panel of isogenic cell lines with H1 helix mutations

A. Schematic of the *TP53* locus in the HCT-116$^{\Delta/TP53E}$ cell line and the list of mutations introduced. Primers used for Sanger sequencing are shown with arrows. **B.** Sanger sequencing confirming the successful generation of mutant isogenic cell lines. Data courtesy of Julianne Funk and Pascal Hunold. **C.** Western blot analysis of p53 and p21 expression in HCT-116$^{\Delta/TP53E}$ cell (before and after adeno-Cre infection, Δ/E and Δ/WT) and in 8 isogenic cell lines expressing corresponding p53 mutants. No expression of p21 by mutant cell lines under nutlin treatment is evident except cells expressing a known pLOF mutant R181L. Data courtesy of Michelle Neumann **D.** Western blot analysis of p53 and p21 expression in HCT-116$^{\Delta/S183A_S185A}$ and HCT-116$^{\Delta/S183D_S185D}$ cells (in response to doxorubicin, after adeno-Cre infection, Δ/WT and Δ/E cells serve as positive and negative controls). Data courtesy of Oleg Timofeev and Constantin Niederau.

3.7 The HCT-116$^{\Delta/TP53E}$ cell line enables the introduction of multiple mutations into the TP53 locus: construction of the R175 mutagenic library, assessment of the library quality, and targeting efficiency

CSMS approach requires the efficient generation of mutational diversity. To test if the HCT-116$^{\Delta/TP53E}$ cell line is suitable for massive parallel mutagenesis, we have constructed a library representing all possible variants of the hotspot codon R175. The library was composed of 27 oligonucleotides encoding 19 amino acid substitutions, three synonymous mutations (R175R), one stop codon (TGA), R175 deletion, and three frameshift mutations (+1, -1, and -2). The HDR template was prepared by cloning a pool of all double-stranded oligonucleotides into the HR-2-Golden Gate vector. Before establishing a cellular library, we have verified the presence of all variants in the donor vector by NGS. Vector fragments were amplified with primers flanking the R175 region sequence (primers #11 and 12). After sequencing, the number of reads corresponding to each variant was calculated. Normalized read counts were calculated by dividing the number of reads assigned to each variant by the total amount of reads in the sample. The analysis revealed that all variants were presented in the library. Mutation frequencies were normally

distributed (Kolmogorov-Smirnov test p>0.1, skewness 0.74) and none of the variants were lost from the pool, which demonstrates that cloning protocol generates

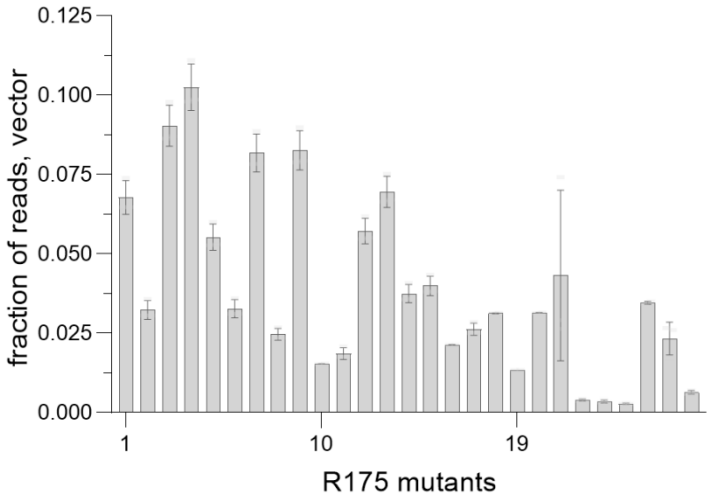

Figure 12. Distribution of variant frequencies across the R175 library

The relative abundance of sequence variants in the plasmid pools carrying saturation R175 mutagenic library in the three independently prepared replicates of the HR-2-Golden-Gate plasmid. Fraction of reads ±SD for each variant is shown.

libraries with fairly uniform coverage (Fig. 12).

After transfection of cells with a plasmid encoding the allele-specific CRISPR-nuclease and a pool of HDR templates and consecutive puromycin selection, a population of library-carrying cells was established.

Next, we have assessed the targeting efficiency. From our experience, adenoviral infection is stressful for cells. Therefore, to exclude stress-induced changes in variant abundance, we have first analyzed cellular libraries before adeno-Cre infection. We have isolated genomic DNA from cells and amplified it using two rounds of PCR.

CRISPR-nucleases always demonstrate some degree of unpredictable off-target cleavage (Wang et al. 2020; Chakrabarti et al. 2019; Tuladhar et al. 2019; Zhang et al. 2015). To exclude the possibility that changes in variant abundance are caused by off-target damage of the irrelevant gene, we have always maintained the amount of input DNA used for sequencing library preparation above a certain threshold. This ensured the amplification of variants from a sufficient number of different cells and minimized random off-target effects. We calculated a minimal amount of genomic DNA for PCR as follows:

$$\text{gDNA amount} = x \cdot 1000 \cdot 6 \text{ pg}$$

where x – the number of mutations in the library, 1000 – desirable representation of each mutant in the sequencing library, 6 pg – the amount of DNA in one diploid cell. The calculated amount was increased by 30% to account for a fraction of non-recombined cells after adeno-Cre infection (amount of non-recombined GFP-expressing cells did not exceed 30% as determined by flow cytometry, data not shown).

In the first PCR round, the *TP53*^{E} allele was amplified using one primer annealing to the LSL cassette and the other annealing to the sequence downstream of the donor template *(*exon 7, primers #7 and #10) (Fig. 13A). Using this primer combination precluded the amplification of HDR templates falsely integrated outside of the *TP53* locus. The second allele (*TP53*$^{\Delta}$) failed to amplify due to the absence of the LSL cassette. The second PCR round with a primer specific to the dinucleotide mutation in the 5th intron (CC > GG) ensured exclusive amplification of DNA from the properly edited allele (primers #11 and 12-14) (Fig. 13B). During all PCR steps, the number of cycles was kept below 20-25 to minimize amplification bias.

PCR products were used to construct the fragment library for massive parallel amplicon sequencing. Before library preparation, PCR fragments were purified, and their concentrations were adjusted. To exclude PCR errors, each sample was amplified in three independent PCR reactions, and then products were pooled. Molecular barcoding was used to enable parallel sequencing of multiple samples. First, three allele-specific primers (#12-14) with unique barcodes were employed (Fig. 13B). Groups of three barcoded samples were combined and additionally barcoded during the library preparation step using the NEBNext kit. Such a strategy enabled parallel sequencing of up to 90 samples. Libraries were sequenced using Illumina Miseq sequencer and analyzed as described in section 2.2.10. To assess the reproducibility of the procedure, all experiments were performed three times, and triplicate samples from every test condition were sequenced. After sequencing, read counts for each variant were calculated and normalized to total read counts in each sample as described above.

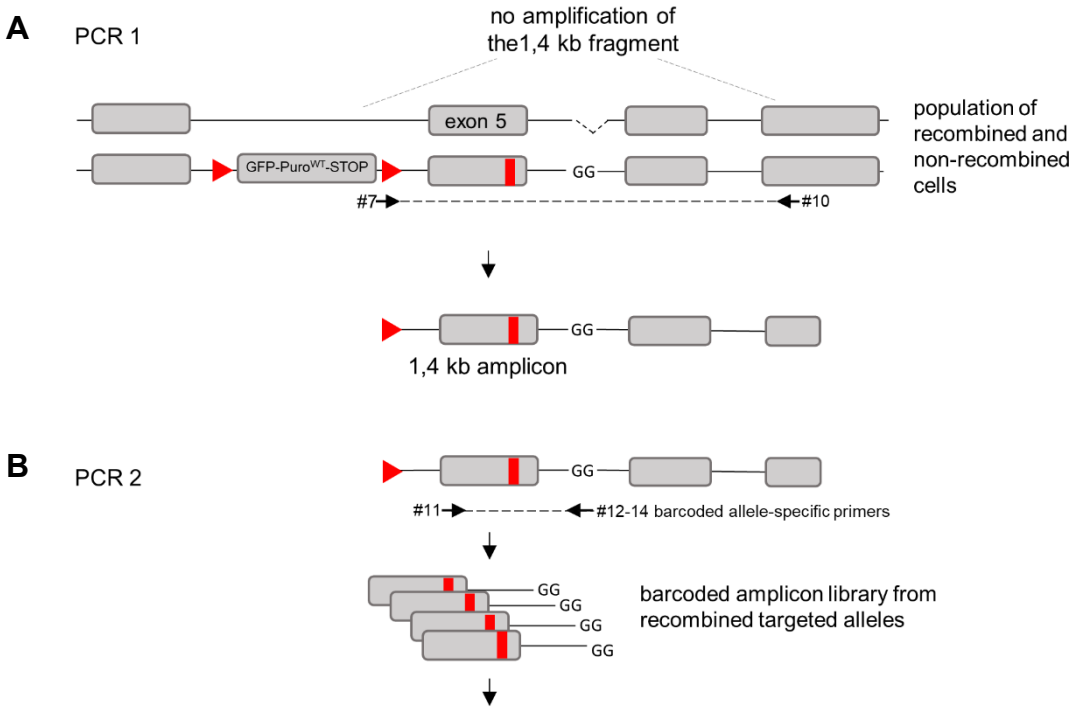

Figure 13. Preparation of the amplicon library before Cre-mediated recombination using nested PCR

A. In the first round of PCR only the *TP53*^{E} allele was amplified due to the specificity of a primer #7 to the LSL cassette. Mutations are shown with a red rectangle. **B.** In the second round of PCR, a primer specific to the GG-dinucleotide in the conditional allele ensured the selective amplification of the targeted allele with the full-length integration of the targeting vector. Cells that have undergone partial targeting (LSL cassette is integrated, the mutation is not integrated) were excluded from amplification. Primers and amplicons are indicated with arrows and dashed lines. Amplicons were purified and used for NGS library preparation.

The distribution of mutations in the cell population before Cre-mediated p53 activation was strongly correlated with the distribution in the targeting vector (r^2=0.94) (Fig. 14A). The abundance of individual mutants was very similar between triplicate preparation of cellular libraries (r^2=0.98) (Fig. 14B). Therefore, our approach reproducibly generates cell libraries with significant mutational diversity in the *TP53* locus.

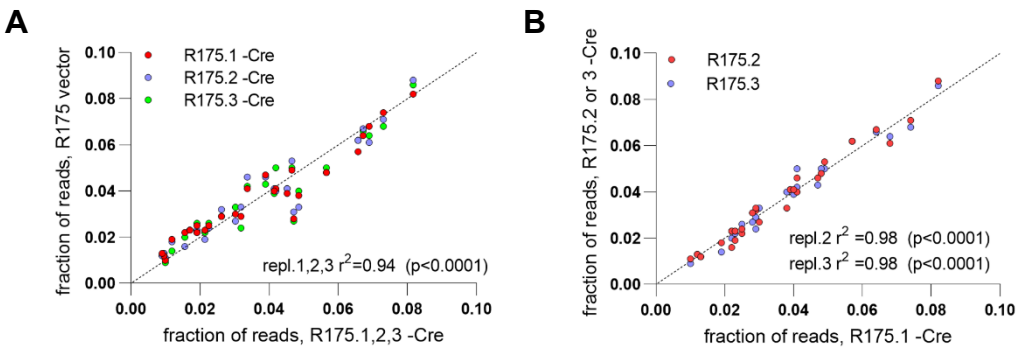

Figure 14. CRISPR-mediated homologous recombination in HCT-116$^{\Delta/TP53E}$ cells results in the reproducible introduction of the R175 site-saturation library into the *TP53* locus

A,B. Correlation of normalized read counts for each of the 27 variants between (A) triplicates of the plasmid library and library-expressing cells before adeno-Cre infection, (B) triplicate cultures of library-expressing cells before adeno-Cre infection. r^2 - squared Pearson correlation coefficient.

Next, cells were infected with adeno-Cre to restore p53 expression from the conditional *TP53*^{E} allele. Fourteen days after infection, genomic DNA was isolated and amplified using two rounds of PCR. In the first PCR round, the Cre-recombined *TP53*^{E} allele was amplified together with the inactive second allele (primers #5 and 10, Fig. 15A). Under the chosen conditions, residual non-recombined *TP53*^{E} alleles containing the LSL cassette failed to amplify due to their large size (Fig. 15A). The second round of PCR with a primer specific to the dinucleotide mutation in the 5th intron (CC > GG) ensured exclusive amplification of DNA from the properly edited and recombined allele (Fig. 15B, primers #11 and 12-14). Sequencing data from triplicate samples were analyzed as described above. Analysis of mutation frequencies in cultures after Cre-mediated p53 activation revealed a strong correlation between triplicates, Rs=0.96 and 0.97, respectively (Fig. 16A). Reassuringly, comparing the relative abundance of variants in cellular libraries before and after Cre-mediated p53 activation also revealed a remarkable correlation (Fig. 16B, Rs=0.85, 0.9 and 0.87 respectively, p<0.0001). These data further demonstrated the reproducibility of the developed mutagenesis procedure and highlighted the stability of library-expressing pools after adeno-Cre infection.

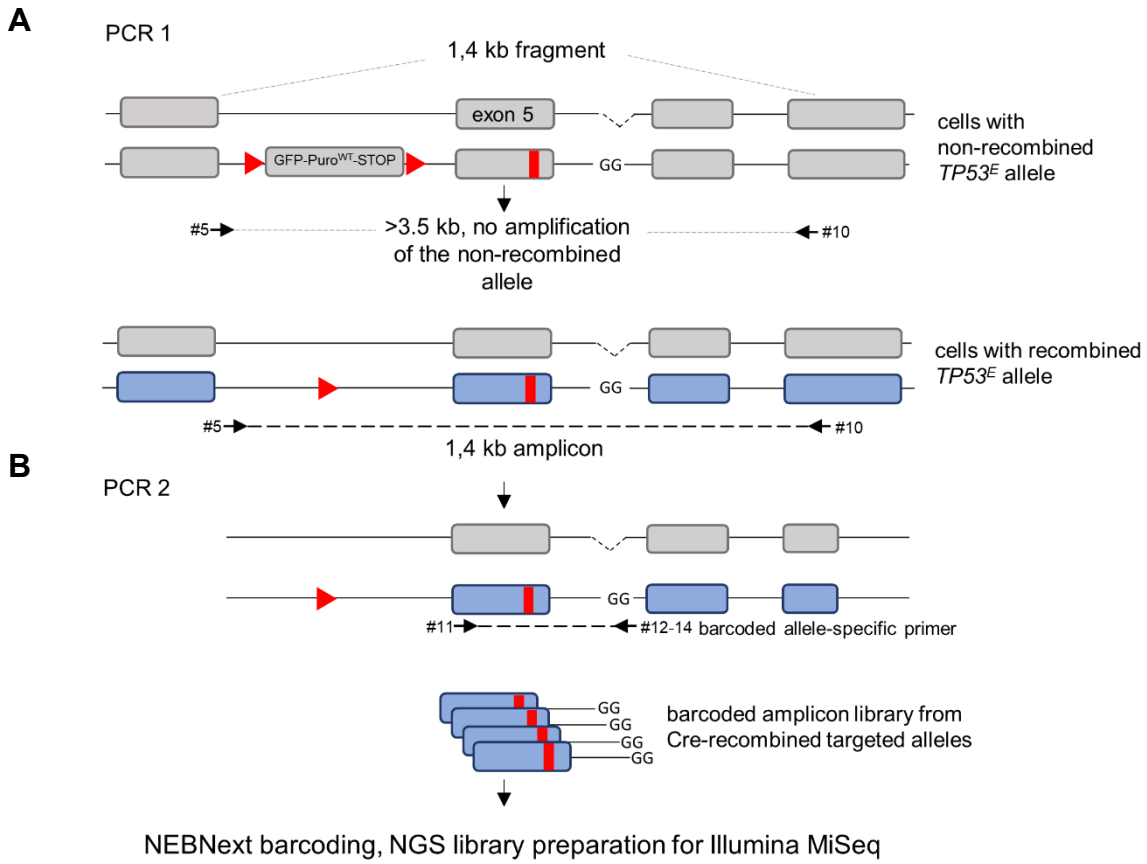

Figure 15. Preparation of the amplicon library after Cre-mediated recombination using nested PCR

A. In the first round of PCR the non-recombined *TP53*^{E} allele (above) was not amplified due to its the large size (3.5 kb) and was excluded from the amplicon library. Recombined *TP53* allele without LSL-cassette and inactive second allele were both amplified (below). The mutation is shown with a red rectangle. **B.** In the second round of PCR a primer specific to the GG-dinucleotide in the conditional allele ensured selective amplification of the targeted allele and exclusion of the second inactive allele. Primers and amplicons are indicated with arrows and dashed lines. Amplicons were purified and used for NGS library preparation.

3.8 System validation: CSMS quantifies anti-proliferative capacity of p53 variants

We have used two metrics to measure the impact of mutations on tumor cell fitness: enrichment score and relative fitness score. The enrichment score (ES) is a measure of the relative enrichment or depletion of the variant in a given sample, where p53 was activated by treatment, compared to the untreated sample. It was calculated as a ratio between normalized read counts (n) in the treated and untreated sample:

ES=$n^{treated}/n^{untreated}$. The relative fitness score (RFS) was calculated as log2-transformed ES ($RFS=log_2ES$).

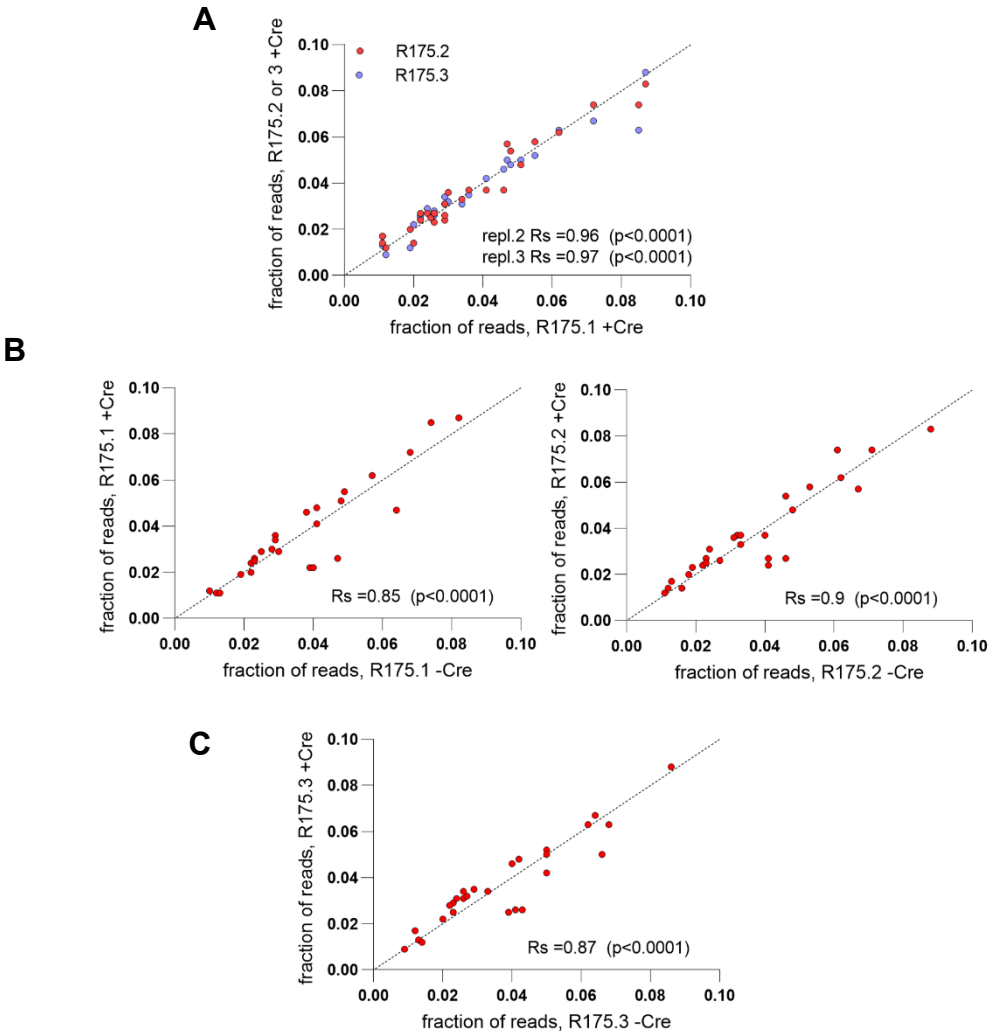

Figure 16. Restoration of the p53 expression after adeno-Cre infection does not change the abundance of the variants.

A. Correlation of normalized read counts for each of the 27 variants in triplicate cultures of library-expressing cells after adeno-Cre infection. r^2 - squared Pearson correlation coefficient. **B.** Correlation of normalized read counts between three independent replicates before and after infection with adeno-Cre. r^2 - squared Pearson correlation coefficient.

It was expected that cells carrying wild-type p53 and mutants with preserved function would respond to p53-activating stimuli with cell cycle arrest or apoptosis. Such variants would be depleted from the population, generating low ES values and negative RFS values. Conversely, cells expressing LOF mutants would remain unaffected and continue to proliferate, leading to the expansion of the variant and

generating high ES or positive RFS values at the endpoint analysis. For most of the calculations, non-log-transformed ES values were used. To ease data interpretation, we used RFS values in heat maps (positive RFS values show enrichment (red color), negative RFS values show depletion (blue color). We have first measured the dynamics of each variant in the R175 library during eight weeks of passaging. We have collected and sequenced DNA samples 2, 4, 6, and 8 weeks after adeno-Cre infection. Analysis of sequencing data revealed modest changes in relative variant abundance after eight weeks of culture (Fig. 17A). Synonymous (wild-type-like) mutations R175R were slightly depleted during passaging (RFS=-0.5), while several missense and nonsense variants were marginally enriched (RFS=0.2-0.3).

Our recent study has demonstrated that HCT-116 cells are highly tolerant to the expression of wild-type p53 and that p53 depletion gives them only a weak proliferative advantage (Klimovich et al. 2019). Therefore, minor changes in the abundance of mutants imply that their expression from the edited allele does not exceed normal physiological levels and that changes observed can be predominantly related to the stress induced by adenoviral infection.

To validate the ability of CSMS to measure the anti-proliferative capacity of p53 mutants, we have activated p53 in library-expressing cells with a panel of MDM2-inhibitors. We have utilized five structurally distinct p53-activating compounds.

Nutlin-3a was chosen as the first-in-class compound and the most extensively tested MDM2 antagonist (>900 citations in Pubmed). To improve the clinical relevance of our data, we have included three compounds that are currently undergoing clinical evaluation: a nutlin derivative with improved potency RG7388 (Hoffmann-La Roche) and two structurally unrelated compounds: the piperidinone AMG 232 (Amgen) and the spirooxindole MI-773 (15, 8, and 2 clinical trials respectively, clinicaltrials.gov). Finally, RO-5963 was added to our drug panel as a member of the class of dual MDM2/MDM-X inhibitors (Graves et al. 2012). Using several structurally distinct compounds allowed us to address several issues. First, to our knowledge, a systematic comparison of the efficacy of structurally distinct MDM2 antagonists against cells expressing multiple mutant p53 variants has not been performed so far. Second, using five distinct compounds could improve the robustness of the screening and address potential off-target effects of the inhibitorsNutlin-3a was

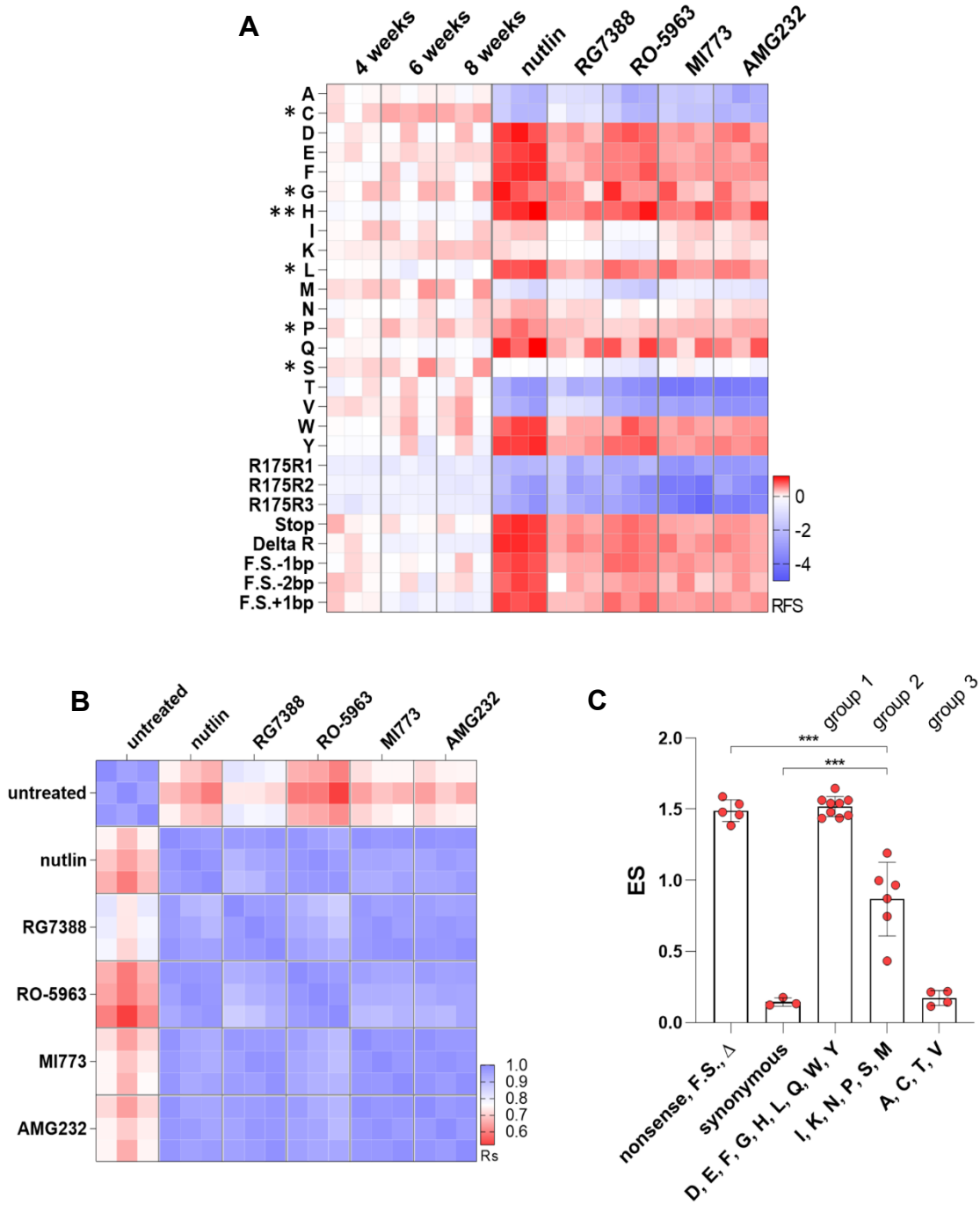

Figure 17. Impact of mutations at the codon R175 on cellular fitness under treatment with MDM2 inhibitors

A. Dynamics of the R175 codon variants in the untreated cellular pool along the 8 weeks time course (3 left columns) and treatment with indicated MDM2 inhibitors (5 right columns). Cells expressing the R175 library after adeno-Cre infection were cultured 2, 4, 6, and 8 weeks or treated with MDM2 inhibitors at IC50 concentrations for 8 days. Relative fitness scores (RFS) calculated relative to 2 weeks for 8 weeks time course experiment or relative to 8 days without treatment for the MDM2 inhibitors treatment experiment.

chosen as the first-in-class compound and the most extensively tested MDM2

Figure 17. Continued

RFS values are shown for triplicates according to the color scale: Red indicates high fitness (retention of the variant), blue indicates low fitness (depletion of the variant). Hereinafter: R175R1,2,3 – synonymous mutations, Stop – premature stop codon, Delta R – R175 deletion, F.S. – frameshifts. * - mutations annotated in the UMD TP53 database (UMD), ** - R175H. **B.** Correlation matrix demonstrating the similarity between cell libraries treated with MDM2 inhibitors. Spearman correlation coefficient of pairwise comparisons is shown according to the color bar. **C.** Enrichment scores of 3 groups of protein variants. Each point is ES of the individual mutation in the nutlin-treated library. Mutants demonstrating high, medium, and low enrichment scores are combined in groups 1, 2, and 3 respectively. ***p<0.0001, ANOVA with Tukey post-test.

antagonist (>900 citations in Pubmed). To improve the clinical relevance of our data, we have included three compounds that are currently undergoing clinical evaluation: a nutlin derivative with improved potency RG7388 (Hoffmann-La Roche) and two structurally unrelated compounds: the piperidinone AMG 232 (Amgen) and the spirooxindole MI-773 (15, 8, and 2 clinical trials respectively, clinicaltrials.gov). Finally, RO-5963 was added to our drug panel as a member of the class of dual MDM2/MDM-X inhibitors (Graves et al. 2012). Using several structurally distinct compounds allowed us to address two issues. First, to our knowledge, a systematic comparison of the efficacy of structurally distinct MDM2 antagonists against cells expressing multiple mutant p53 variants has not been performed so far. Second, using five distinct compounds could improve the robustness of the screening and address potential off-target effects of the inhibitors.

Library-expressing cells were treated for eight days with MDM2-inhibitors at corresponding IC50 concentrations. Then DNA was isolated, and amplicon sequencing was performed. Enrichment scores were calculated relative to untreated samples, as described above. A comparison of enrichment scores derived from replicate libraries revealed a high correlation (Rs>0.9) (Fig. 17A,B), further demonstrating the superior accuracy of the screening protocol. Treatment of the library with MDM2 inhibitors resulted in strong changes in variants abundance, evident from the reduced correlation between untreated and treated samples (Rs<0.8, Fig. 17B). Treatment of cells with five MDM2-inhibitors revealed very similar response patterns exemplified by high correlation between the samples (Fig. 17B). Enrichment scores calculated for each variant did not differ significantly between inhibitors (Friedman test, p=0.058). This indicates that all compounds exert similar effects independently of chemical structure.

Further analysis of the dataset uncovered the differential impact of R175 variants on cellular fitness (Fig. 17A). Expectedly, all three synonymous mutations (R175R) were strongly depleted under treatment with all five compounds (mean ES=0.14±0.02). Conversely, the nonsense mutation (stop codon) and three frame-shift variants were significantly enriched after treatment (mean ES=1.49±0.07), as well as the hotspot mutation R175H (mean ES=1.63±0.1) (Kruskal-Wallis test p<0.0001). Almost equal ES computed for distinct DNA sequences with similar functional impact further verified the robustness of the system (note comparable depletion of all synonymous mutations and equal enrichment of frameshifts and stop codon).

Detailed examination of the data presented in Fig. 17A revealed that all missense R175 variants could be divided into three groups based on their behavior under treatment (Fig. 17C). Nine mutants, including the most frequent cancer-associated variant R175H, were retained in the population comparable to nonsense variants demonstrating apparent LOF phenotype (R175D, E, F, G, H, L, Q, W, and Y, mean ES for nutlin=1.51±0.07 versus 1.49±0.07). Group of six variants (R175I, K, N, P, S, M) showed weak changes upon treatment (mean ES for nutlin=0.95±0.15). The relative abundance of these mutants was significantly different from both nonsense and synonymous mutations, suggesting partial-LOF properties (ANOVA with Tukey test, p<0.0001). Finally, four mutants (R175A, C, T, V) were depleted comparable to

synonymous mutations being, therefore, wild-type like (mean ES for nutlin=0.22±0.11 versus 0.14±0.02) (Fig. 17C). Surprisingly, two tumor-derived variants, R175S and R175C, demonstrated moderate (ES=0.81±0.11) to strong (ES=0.33±0.15) depletion upon treatment with all MDM2 inhibitors classifying them as wild-type-like variants with only little LOF (Fig. 17A). R175C was found in tumor samples as frequently as variant R175L, which was classified as LOF by CSMS (71 and 74 UMD records, respectively). Since recurrent cancer-associated *TP53* mutations are expected to be damaging, both these variants ought to be enriched in our screen.

Supporting this expectation, three *in silico* predictors have classified both variants to be as damaging as other LOF mutants (data were retrieved from UMD database) (Fig. 18A). Such discrepancy raised doubts about the accuracy of the classification made by CSMS. To verify the validity of our classification, we have analyzed data on the transcriptional activity of the six R175 variants as an independent predictor of protein functionality. Specifically, we have retrieved the data from the study of Kato (Kato S. et al. 2003). In this study, the transcriptional activity of hundreds of p53 mutants was measured in the yeast system. The reporter gene was coupled with p53 response elements from the promoters of eight distinct p53 target genes, and reporter expression levels were measured for each mutant. To identify patterns in this multivariate dataset, we have performed principal component analysis using ClustVis software (https://biit.cs.ut.ee/clustvis/) (Fig. 18B). PCA revealed that R175C and R175S were most strongly separated from other variants along with the principal

component 1 axis, suggesting that they have mostly distinct transactivation patterns among all six mutants (Fig. 18B,C). Furthermore, PC1 values exhibited a strong correlation with enrichment score (R^2=0.81), demonstrating that anti-proliferative

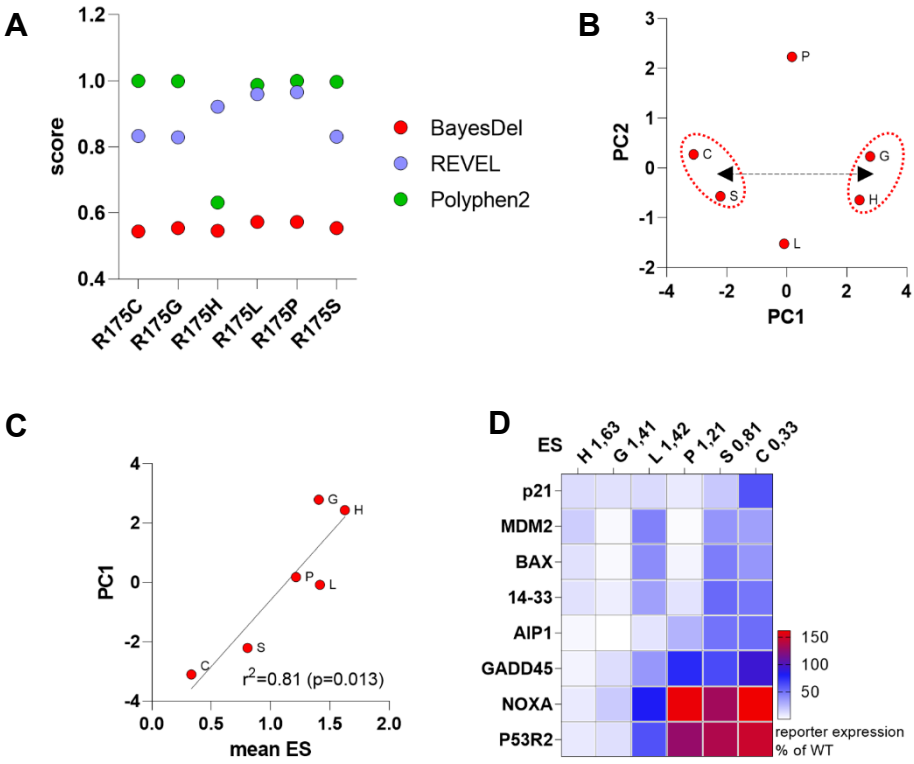

Figure 18. Cancer-associated variants R175S and R175C are functional

A. Prediction of the functionality of R175 mutants made by in silico predictors Polyphen2, REVEL, and BayesDel. All variants are predicted to be equally damaging (scores >0.8 (Polyphen2), >0.5 (REVEL), and >0 (BayesDel) predict the deleterious effect of mutation). **B.** Principal component analysis of the transcriptional activity of R175 mutants. Transcriptional signature for each mutant was extracted from the study of Kato et al., 2003. It is composed of transactivation values of p53 response elements from 8 p53 target genes measured in the yeast reporter assay and normalized to transactivation values of the wild-type protein. Values we subjected to principal component analysis using ClustVis (https://biit.cs.ut.ee/clustvis). Two orthogonal principal components are shown. Large distance between mutants R175C, S, and R175 G, H along the 1st principal component axis reflects a distinct transactivation pattern. Analysis performed by Boris Klimovich. **C.** Correlation between enrichment scores and PC1 values from B. r^2 - squared Pearson correlation coefficient. **D.** Transcriptional activation of individual p53 response elements by R175 mutants. Data are shown as expression levels of the reporter gene normalized to wild type p53 (Kato et al. 2003).

capacity measured by CSMS indeed reflects the transactivating properties of selected p53 mutants (Fig. 18C).

Closer examination of the transactivation of single response elements by individual mutants uncovered a clear pattern (Fig. 18D). Mutants with the highest enrichment scores (R175H, G, and L) showed weak transactivating activity. The mutant with intermediate enrichment (R175P, mean ES=1.21) showed substantial transactivation of three response elements (>50% of wild-type) (Fig. 18D). Finally, mutants R175S and R175C, classified by CSMS as wild-type like, demonstrated strong (>50% of wild-type) induction of reporter gene expression with five and six response elements, respectively. Remarkably, both these mutants activated promoter of the pro-apoptotic gene Noxa stronger than the wild-type protein (132 and 162%, respectively) (Fig. 18D). Thus, CSMS has identified anti-proliferative properties in mutants with preserved transactivating capacity.

Further evidence supporting the validity of our classification can be found in the literature. Mutant R175S (showed weak depletion in CSMS) was shown to activate cell cycle arrest (Ryan and Vousden 1998; Goh et al. 2011; Billant et al. 2017). Similarly, mutant R175C was shown to induce both cell cycle arrest and apoptosis in different cell lines (MCF7, Saos, and PC-3) (Ryan and Vousden 1998; Flaman et al. 1998; Blagosklonny 1997; Ory et al. 1994; Blagosklonny 2002). Finally, cDNA-based screening by Kotler and colleagues has produced scores for the R175C mutant strikingly similar with ours: (RFS for R175C and WT respectively: -2.15 and -2.56 for CSMS and -2.69 and -2.43 for the cDNA screen).

Mutation R175C originates from a C>T transition at a methylated CpG site, which is the most frequent mutation signature of p53 (Giacomelli et al. 2018). Therefore, it is highly plausible that R175C is a non-pathogenic passenger mutation.

Taken together, the CSMS classified six cancer-associated R175 variants in better agreement with previously published data than the commonly used *in silico* tools.

3.8.1 *CSMS dissects the impact of mutations on p53-regulated effector pathways*

Inspired by the good agreement of our results with previous findings, we have continued experimenting with the R175 library to further explore the capabilities of the CSMS. Apart from LOF and wild-type-like mutants, the R175 library screening revealed a group of six mutants with intermediate enrichment (R175I, K, N, P, S, and

M) (group 2 Fig. 17D). Outcomes of p53-mediated response strongly depend on the intensity and duration of treatment. Shorter treatment preferentially induces cell cycle arrest, whereas prolonged treatment leads to apoptosis (Kracikova et al. 2013; Murray-Zmijewski et al. 2008; Paek et al. 2016). Therefore, to gain more detailed mechanistic insight into mutants' properties, we have profiled antiproliferative effects of R175 variants across the range of nutlin concentrations (2.5 – 20 μM nutlin) or treatment durations (2-25 days).

As expected, LOF mutants from group 1 (from Fig. 17D) (R175D, E, F, G, H, L, Q, W, and Y) were strongly enriched even when treated with the lowest concentration of nutlin (2.5 μM) (Fig. 19A,B) and demonstrated progressive enrichment upon increased treatment duration (Fig. 19C,D). Wild-type-like mutants (R175A, C, T, V) revealed rapid depletion from the population even at the lowest concentration of nutlin and after shorter treatment (4-8 days) (Fig. 19B,D).

In striking contrast, five variants from group 2 from Fig. 17D (R175I, K, M, N, S) showed a changing response pattern. In detail, the mutants in the sample treated with 2.5 μM nutlin, demonstrated significant dose-dependent depletion (Fig. 19B). A similar trend was revealed when the mutants-expressing cell library was treated for an extended period: the abundance of five mutants was comparable to LOF mutants after 2-4 days but was significantly decreased upon more extended treatment and reached the level of wt-like variants for two mutants (mean ES at 25 days wt-like: 0.12±0.01, R175M 0.11±0.02, R175S 0.1±0.02, 2-way ANOVA with Sidak's test, $p>0.0001$). Interestingly, the mutant R175P with documented partial-LOF features did not change its abundance in both experiments (Barboza et al. 2006; Liu et al. 2004) but was nevertheless depleted significantly stronger than LOF variants ($p=0.0002$ and 0.0027 for Fig. 19B and D respectively, 2-way ANOVA). Collectively, such behavior revealed partial-LOF properties of the group of six mutants.

These observations uncovered substantial qualitative differences in the response of p53 mutants to MDM2 inhibition. Wild-type-like variants were rapidly cleared from the population even in response to low levels of the stimulus (mean ES at 2.5 μM nutlin= 0.12±0.01, mean ES after two days of treatment 0.36 ±0.08), suggesting that apoptosis is the principal mechanism eliminating variant-carrying cells. Conversely, the persistence of partial-LOF mutants in the population under low concentrations of

nutlin and their depletion under prolonged treatment or elevated concentrations evident from Fig. 19B indicate selective apoptosis defect in these mutants and suggest cell cycle arrest as the principal tumor-suppressive mechanism involved (Fig. 19D).

TP53 mutations that disable specific effector pathways but spare the others have

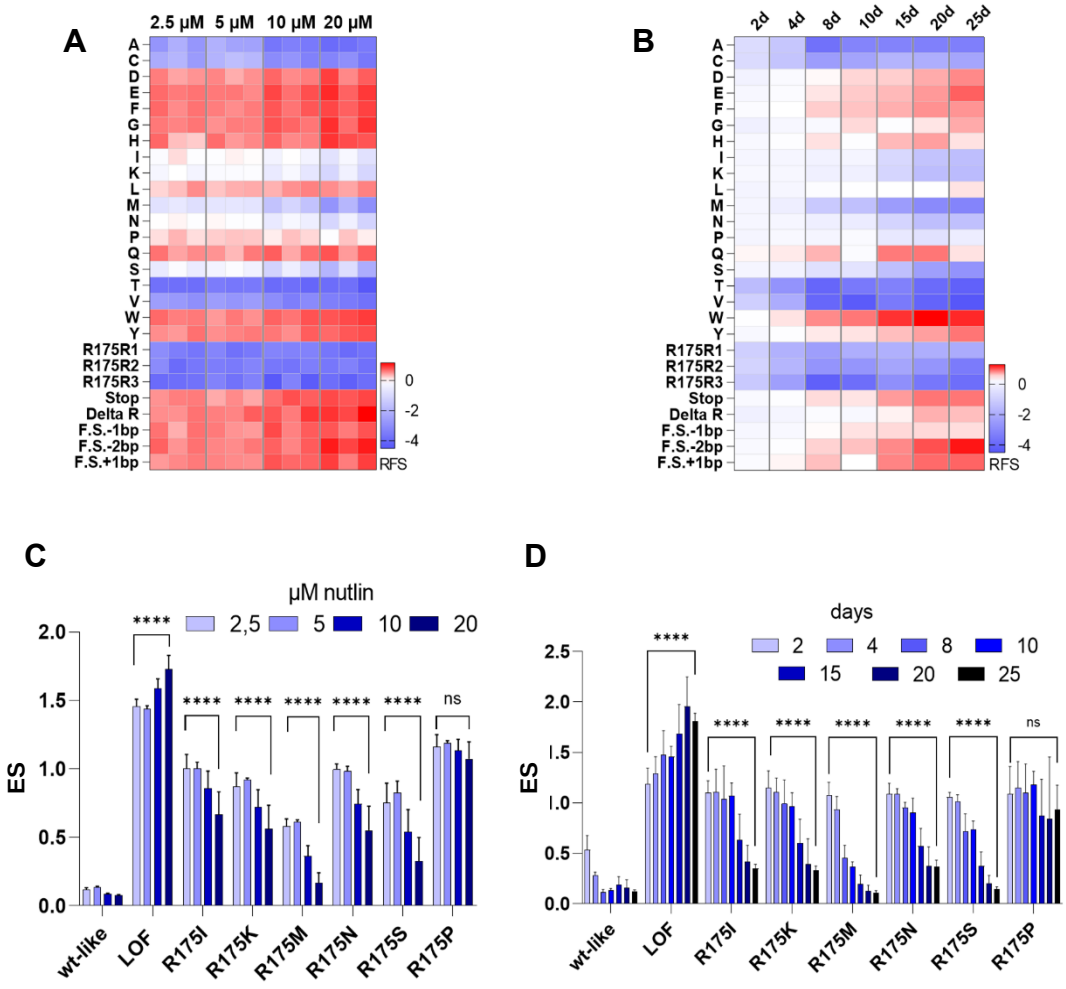

Figure 19. Dose- and time-dependent variations of the impact of mutations at the codon R175 on the response to MDM2 inhibitors

A. Cells were treated with 2.5 – 20 µM nutlin for 8 days. Heatmap shows RFS values for individual replicates. **B.** Mean enrichment score values for the selected R175 mutants from A. ns: p=0.29, ****p<0.0001, Two-way ANOVA with Sidak's test. **C.** Time course dynamics of variants in the R175 library (n=3) under nutlin treatment. Cells carrying R175 library were treated with 10 µM nutlin for 2 - 25 days as indicated on the heatmap. Mean RFS across triplicates are shown. **D.** Mean enrichment scores for the selected R175 mutants from C. ns: p=0.93, ****p<0.0001, Two-way ANOVA with Sidak's test.

been extensively studied. For example, mutants R175P, R181L, and E180R demonstrate a specific defect in apoptosis but retain the ability to arrest proliferation (Rowan et al. 1996; Ludwig et al. 1996; Liu et al. 2004; Timofeev et al. 2013). Furthermore, it is plausible that partially preserved functionality can be a widespread intrinsic property of non-hotspot tumor-associated mutations. Indeed, our analysis of the dataset “functionalAssessment” from the IARC database, which consists of manually curated information from almost 350 publications, identified 317 patient-derived variants that were reported to suppress cellular growth despite being apoptosis-deficient. Therefore, it was of considerable interest to examine if CSMS could identify mutants with selective defects in effector functions. Hence, we have designed experiments to explore the impact of mutants on apoptosis and cell cycle arrest.

In the first experiment, instead of continuously treating cells with MDM2-inhibitor, we have exposed them to nutlin for 4, 6, or 8 days. Afterward, nutlin was washed out, and surviving cells were further expanded and harvested eight days later. Control samples were either treated with nutlin for 16 days or left untreated (Fig. 20A). We assumed that cells harboring wild-type-like variants would be rapidly killed by apoptosis and strongly depleted from the population even after 4 days of treatment. Conversely, cells harboring LOF mutants will be markedly enriched in the population irrespective of the treatment duration. Partial-LOF mutants capable of arresting proliferation were expected to stay relatively abundant after short nutlin treatment due to resuming proliferation after drug withdrawal. Upon extended exposure to nutlin these mutants were anticipated to stay in cell cycle arrest and become progressively eliminated. In good agreement with our expectations, synonymous variants were strongly depleted already 4 days after the beginning of the treatment (mean ES=0.27±0.18), whereas nonsense and frameshift mutations, as well as hotspot R175H and other missense LOF variants, were enriched (mean ES=2.56±1.15) (Fig. 20B) in line with previous experiments (Fig. 19). Partial-LOF mutants identified in the experiment shown in Fig. 20B (R175I, K, M, N, S) and the extensively studied pLOF mutant R175P demonstrated an intermediate enrichment pattern. After four days of nutlin treatment, they were almost as abundant as LOF mutants (mean ES 1.00±0.17 versus 1.26±0.14), indicating that cells have resumed

proliferation. However, after 16 days of continuous MDM2 inhibition, partial-LOF mutants were eliminated (mean ES=0.39±0.28). Therefore, the pattern of enrichment and depletion of partial LOF mutants perfectly fits our expectations regarding protein variants with the selective defect in apoptosis and preserved ability to induce cell cycle arrest.

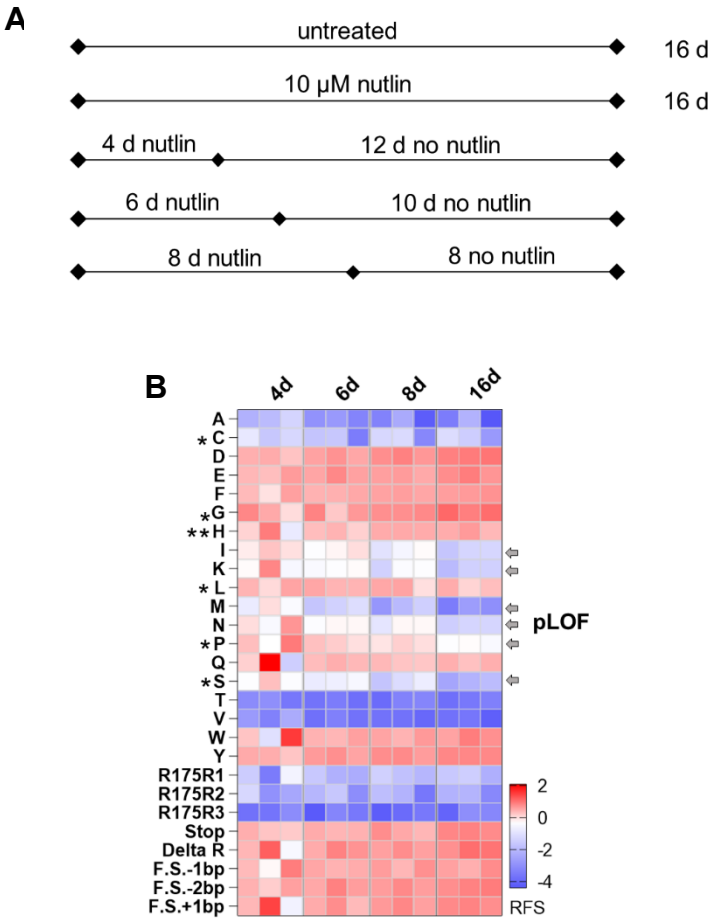

Figure 20. Annotation of the cell cycle arrest-proficient R175 mutants

A. Schematic of the experiment. Cells expressing the R175 library were treated with nutlin for 4, 6, 10, and 12 days. After 4-8 days drug was washed away, and cells were harvested on the 16th day from the beginning of the experiment for gDNA extraction. **B.** Heatmap shows RFS values for individual replicates calculated relative to untreated control. * -mutations annotated in the UMD database, ** - R175H. pLOF mutants are shown with arrowheads.

Next, we applied CSMS to demonstrate apoptosis deficiency of partial-LOF mutants directly. We have treated library-carrying cells with 10 μM nutlin and stained apoptotic cells after two and four days with annexin V-APC conjugate. Next, we

separated annexin V positive and negative populations using fluorescence-activated

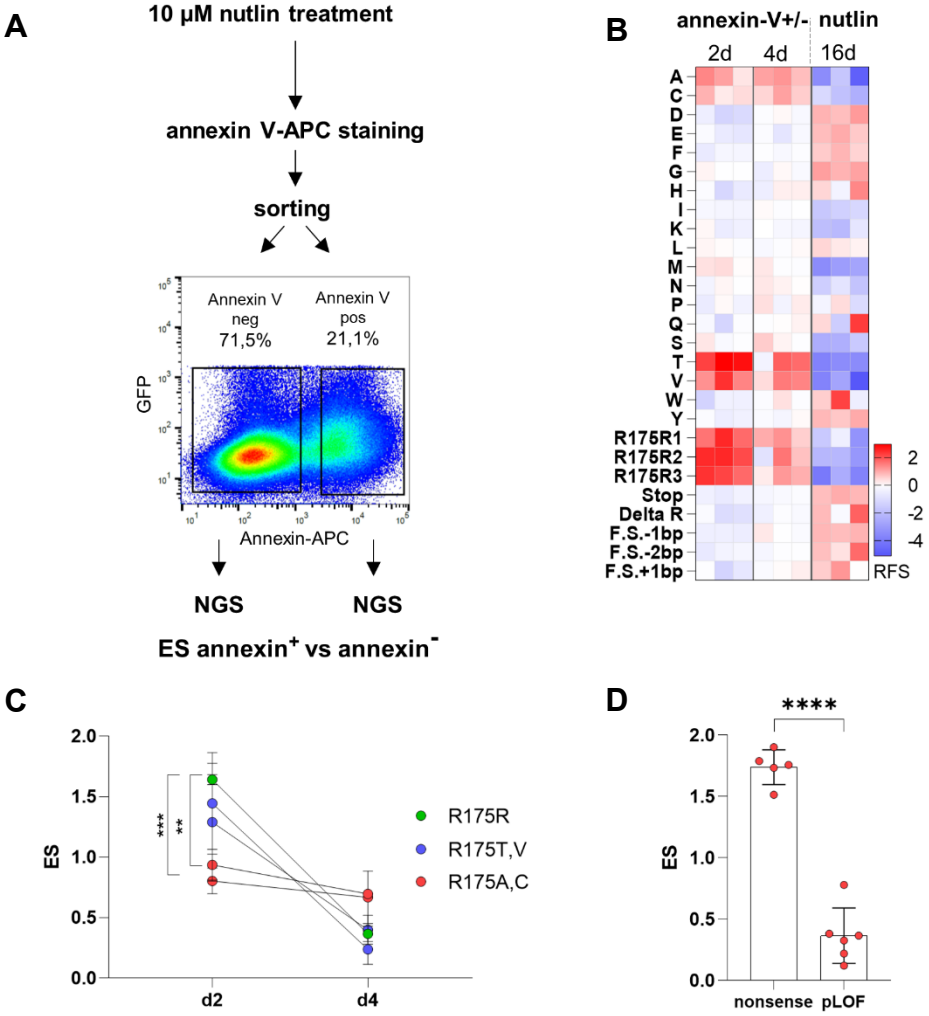

Figure 21. CSMS captures the apoptosis proficiency of R175 mutants

A. Schematic representation of the experiment. Cells carrying the R175 library were treated with 10 µM nutlin for 2 or 4 days and apoptotic cells were stained with annexin V-APC. Annexin V positive and negative fractions were separated using fluorescence-activated sorting and used for DNA isolation and library preparation. Representative FACS plot demonstrates the gating strategy. **B.** Heatmap demonstrates triplicate RFS values of each variant in the annexin V-positive population (RFS for each variant was calculated relative to the annexin V-negative population). Right 3 column: RFS of variants after 8 days of nutlin treatment (relative to untreated cells). **C.** Mean enrichment scores of apoptosis-proficient R175 mutants 2 and 4 days after p53 activation with nutlin. R175R – mean ES of 3 synonymous codons. **p=0.0048, ***p=0.0009, two-way ANOVA with Sidak's test. **D**. Enrichment scores of partial-LOF mutants (R175I, K, M, N, P, S) after 16 days of nutlin treatment compared with ES of nonsense variants. ****p<0.0001, t-test.

cell sorting. We have prepared amplicon libraries from both samples and sequenced them (Fig. 21A).

We have compared the fraction of reads corresponding to each sequence variant in annexin-positive and annexin-negative fractions and plotted the relative enrichment scores along with RFS for the library treated with nutlin for 16 days (Fig. 21B).

Concordant with their intact proapoptotic activity synonymous mutants were strongly enriched in annexin-positive fraction after two days of treatment (mean ES=1.64±0.23). Likewise, missense mutants characterized as wild-type-like in previous experiments (R175A, C, T, V) were also prevalent among the annexin-positive population after two and four days of treatment (Fig. 21B). Tumor-associated variant R175C revealed partially preserved apoptotic function in good agreement with our data and with previous reports (Ory et al. 1994). As expected, all apoptosis-proficient variants were depleted from the library after 16 days of continuous nutlin treatment (Fig. 21B). Interestingly, the abundance of synonymous variants, R175T and R175V, was strongly decreased after four days of treatment (mean ES at 4d 0.35±0.12), indicating rapid depletion of apoptotic cells. (Fig. 21C). At the same time, mutants R175A and C were significantly less abundant than wild-type among apoptotic cells at two days of treatment (ES=0.80 and 0.94, p=0.0048 and 0.0009, two-way ANOVA with Sidak's multiple comparison test, $p<0.005$) and were depleted from the annexin-positive fraction to a lesser extent at day 4 (mean ES 0.68±0.13). Distinct dynamics of the two groups of variants suggest partially compromised pro-apoptotic activity of R175A and R175C.

Loss-of-function mutants identified in the previous experiments (R175D, E, F, G, H, L, Q, W, Y) were expectedly unable to activate apoptosis, as evident from the depletion of these variants from the annexin-positive population (Fig. 21C).

Mutants categorized as partial-LOF (R175I, K, M, N, P, S) showed no enrichment in the annexin-positive fraction over nonsense variants (mean ES at 2 days 0.95±0.21 versus 0.82±0.31), highlighting their severe apoptosis deficiency (Fig. 21C). Nevertheless, they were depleted significantly more than stop codons after 16 days of nutlin treatment (mean ES=0.36±0.21 versus 1.74±0.13, unpaired t-test $p<0.0001$) (Fig. 21D). This observation further demonstrates that these apoptosis-deficient mutants retain the ability to induce cell cycle arrest.

In summary, our system accurately delineated p53 mutations with differential impact on effector mechanisms and identified several partial-LOF mutants in good agreement with previously published findings.

3.8.2 *CSMS measures the impact of p53 mutations on response to conventional chemo- and radiotherapy*

We have validated the CSMS as a sensitive tool for measuring the antiproliferative effects of p53 mutants in response to MDM2-inhibitors. MDM2-inhibitors act as direct non-genotoxic p53 activators. However, the therapy of many cancer entities still relies on the induction of DNA damage by genotoxic substances or irradiation. P53 integrates stress response signals to activate cell cycle arrest or cell death. Therefore, mutations in p53 enforce chemo- and radioresistance and are selected during therapy (Lee and Bernstein 1993; Sturm et al. 2003; Keshelava et al. 2001; Wong et al. 2015). Moreover, drug resistance can be further enhanced via neomorphic gain-of-function activities (Stiewe and Haran 2018; Blandino et al. 1999; Lavra et al. 2009; Wong et al. 2007). Therefore, the cataloging of p53 mutations causing resistance to DNA damaging agents would be of great value to advance personalized cancer treatment.

DNA-damaging agents induce extensive post-translational modifications of p53, which modulate p53-mediated responses. Therefore, p53 might show different activities upon treatment with DNA-damaging stimuli compared to nutlin. For example, treatment of cancer cells with nutlin or doxorubicin results in substantially different genome-wide binding patterns and transactivation outcomes (Tonelli et al. 2017; Menendez et al. 2006).

To examine how DNA damage response is affected by mutations in p53, we have treated cells expressing the R175-library with two genotoxic agents: X-rays and 5-fluorouracil (5-FU). Both modalities are used for the therapy of colorectal cancer and, therefore, are expected to produce clinically valuable estimates in our system based on the colorectal cancer cell line. Unlike MDM2-inhibitors, which specifically trigger apoptosis by stabilizing p53, DNA damage can result in both p53-dependent and p53-independent apoptosis (Clarke et al. 1993; Strasser et al. 1994; Lanni et al. 1997). Therefore, to minimize p53-independent effects and achieve maximal

resolution between wild-type, LOF, and partial LOF mutants, we have first optimized treatment conditions.

Preliminary experiments have demonstrated that X-ray irradiation with 6 Gy completely inhibited the growth of parental HCT-116 cells at clonogenic density (Fig. 22A). To determine the optimal treatment dose for cells growing in a dense culture, we have irradiated parental HCT-116 and HCT-116$^{\Delta/TP53E}$ (p53-null) cells with 8 Gy and evaluated the viability of cells by monitoring the confluence using the live-cell imaging system Incucyte S3. Relative viability was calculated by normalizing confluence at each timepoint to the confluence readings of untreated cells at the last time point (69 hours). As shown in Figure 22B, irradiation with 8 Gy resulted in a marked decrease in the viability of both cell lines. Parental p53 wt cells were more sensitive to irradiation, as evident from significantly lower relative viability (two-sided t-test, p<0.0001). Higher doses of irradiation resulted in the low viability of both cell

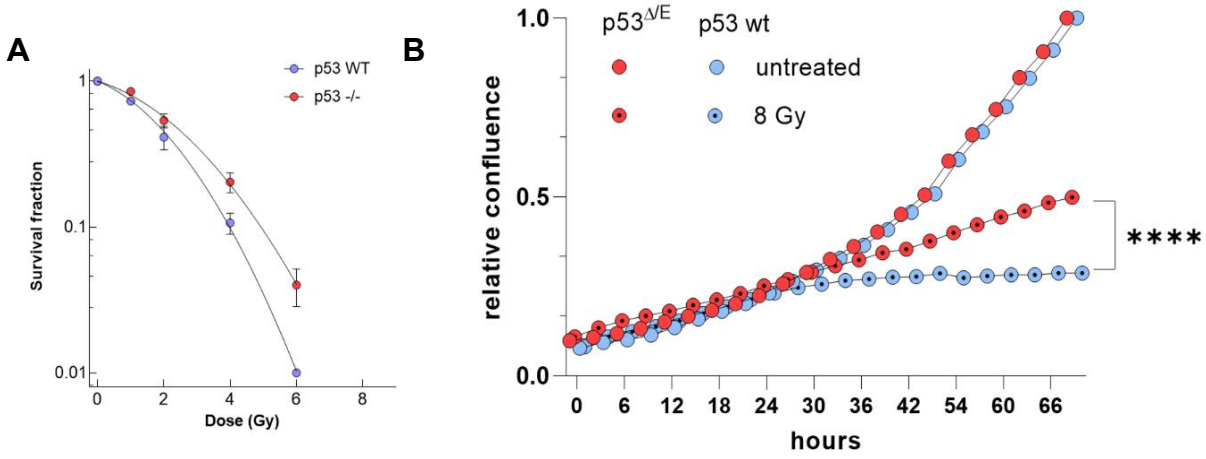

Figure 22. Establishment of the optimal irradiation regime for library-expressing cells

A. HCT-116 p53 wild-type and knockout cells were irradiated with 1-6 Gy and plated at clonogenic density. After 7 days of culture, colonies were counted. Survival fraction was calculated as a ratio of the number of colonies formed by treated versus untreated cells. Data courtesy of Bernadette Wezorke. **B.** Parental HCT-116 and HCT-116$^{\Delta/TP53E}$ cells were plated 3000 per well of 96 well plate. 18h after plating cells were irradiated with 8 Gy. Growth was monitored for 3 days by live-cell microscopy using the IncuCyte S3. Hour 0 is a time point after irradiation. All confluence values were normalized to the confluence of untreated cells at the end of the time course (69h) and shown as mean. ****p<0.0001, two-sided t-test.

lines (data not shown). We have irradiated library-expressing HCT-116Δ/TP53E cells with 4 doses ranging from 2 to 8 Gy based on these results.

Examination of changes in clonal abundance after X-ray irradiation revealed a characteristic pattern. Synonymous mutations, as well as wild-type-like mutations (R175A, C, M, T, V), were progressively depleted from the population with increasing irradiation dose, whereas nonsense and LOF variants (R175 D, E, F, G, H, L, Q, W, and Y) were markedly enriched (Fig. 23A). Mostly, functional effects of substitutions at the position R175 were correlated in irradiated and nutlin-treated cells (Rs=0.79

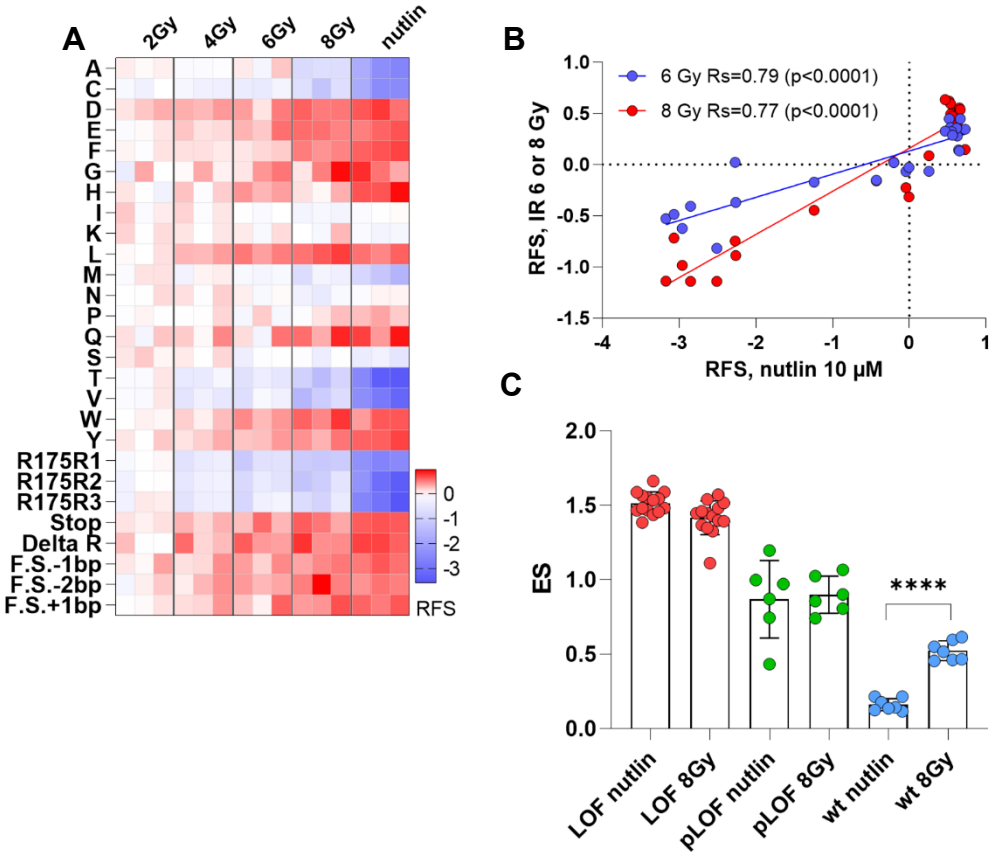

Figure 23. Annotation of R175 mutations conferring radioresistance

A. Cells harboring the R175 library were irradiated with X-rays with 2, 4, 6, and 8 Gy and harvested 8 days later. RFS values for irradiated cells relative to untreated cells are shown (n=3, four left columns). Right column: RFS values for cells treated for 8 days with nutlin. **B.** Correlation between RFS values of R175 mutants in nutlin- and X-ray-treated libraries. Rs: Spearman correlation coefficient. **C.** Comparison of ES between nutlin- and X-rays-treated libraries for 3 groups of mutants: LOF (red) wild type-like (blue) and partial-LOF (green). ****p<0.0001 mixed-effects analysis with Sidak's multiple comparison test.

and 0.77 for 6 Gy and 8 Gy versus nutlin) (Fig. 23B). More specifically, LOF and partially-LOF variants were similarly enriched after both treatments. Interestingly, synonymous and wild-type-like mutants demonstrated distinct behavior: all these variants were depleted by nutlin significantly stronger than by irradiation (mean ES for nutlin 0.16 ± 0.034, mean ES for 8Gy X-ray 0.52±0.06, $p<0.001$) (Fig 23C). This result points to the essential mechanistic difference in the cellular response to these stimuli. Moderate depletion of cells carrying wild-type-like p53 variants after irradiation suggests that this type of treatment induces both p53-dependent and p53-independent response, and thereby diminishes proliferation of all cells. By contrast, non-genotoxic activation of p53 with nutlin affects particularly wild-type cells and leaves cells with LOF mutants unaffected. Therefore, the difference between wild-type-like and LOF variants is stronger for nutlin than for the X-ray irradiation. Additionally, distinct depletion of wild-type variants can be explained by various stimuli duration. Transient p53 stabilization after irradiation results preferentially in cell cycle arrest and DNA repair leading to retention of funcitonal variants, whereas sustained p53 signaling under MDM2 inhibition triggers apoptosis and eliminates these mutants (Paek et al. 2016; Purvis et al. 2012). Examination of changes in clonal abundance after X-ray irradiation revealed a characteristic pattern. Synonymous mutations, as well as wild-type-like mutations (R175A, C, M, T, V), were progressively depleted from the population with increasing irradiation dose, whereas nonsense and LOF variants (R175 D, E, F, G, H, L, Q, W, and Y) were markedly enriched (Fig. 23A). Mostly, functional effects of substitutions at the position R175 were correlated in irradiated and nutlin-treated cells (Rs=0.79 and 0.77 for 6 Gy and 8 Gy versus nutlin) (Fig. 23B). More specifically, LOF and partially-LOF variants were similarly enriched after both treatments. Interestingly, synonymous and wild-type-like mutants demonstrated distinct behavior: all these variants were depleted by nutlin significantly stronger than by irradiation (mean ES for nutlin 0.16 ± 0.034, mean ES for 8Gy X-ray 0.52±0.06, $p<0.001$) (Fig 23C). This result points to the essential mechanistic difference in the cellular response to these stimuli. Moderate depletion of cells carrying wild-type-like p53 variants after irradiation suggests that X-ray irradiation induces both: p53-dependent and p53-independent response, and thereby diminishes proliferation of all cells. Since nutlin

affects particularly wild-type cells remaining LOF cells unaffected, the difference between wild-type-like and LOF is stronger for nutlin than for the X-ray irradiation. Besides, we measure enrichment relative to the population mean, ES values are more pronounced. they rather underwent cell cycle arrest than apoptosis. This difference can be explained by distinct stimuli duration: transient p53 stabilization after irradiation results preferentially in cell cycle arrest and DNA repair, whereas sustained p53 signaling under MDM2 inhibition triggers apoptosis (Paek et al. 2016; Purvis et al. 2012).

Next, we have treated library-expressing cells with 5-FU. To optimize 5-FU concentration, we have treated parental HCT-116 and HCT-116$^{\Delta/TP53E}$ cells with four concentrations of the compound (2.5-20 μM) and monitored culture confluence over one week using the Incucyte S3 (Fig. 24A, B). Nutlin treatment was used as a positive control. Treatment with 10 μM nutlin expectedly affected the growth of p53 wild-type cells and did not affect p53 knockout HCT-116$^{\Delta/TP53E}$. Treatment with the lowest dose of 5-FU (2.5 μM) did not influence the viability of both cell lines, whereas higher doses (10-20 μM) decreased proliferation below the level of nutlin-treated wild-type cells pointing at p53-independent toxicity. Cells treated with 5 μM 5-FU demonstrated an intermediate proliferation rate between nutlin-treated wild-type and HCT-116$^{\Delta/TP53E}$ cells. Moreover, p53-wt cells showed pronounced growth retardation 80h after treatment, whereas HCT-116$^{\Delta/TP53E}$ cells continued to proliferate (corresponding curves are labeled with arrowheads). We have reasoned that such treatment conditions would be the most suitable to measure the anti-proliferative effects accurately. Therefore, the library was treated with 5 μM 5-FU. To minimize the p53-independent effects of continuous treatment, we have exposed cells to 5-FU for 24 or 48h, washed the drug away, and harvested cells eight days after plating (Fig. 25A). Analysis of relative variant frequency revealed a high correlation with the nutlin dataset (Fig. 25B) (Rs=0.93 and 0.88 for 24 h and 48h, respectively).

Similar to the irradiation experiment, enrichment of most of the LOF variants was comparable to enrichment under nutlin treatment (Fig. 25C). However, by contrast to the nutlin-treated library, exposure to 5-FU produced more similar enrichment scores

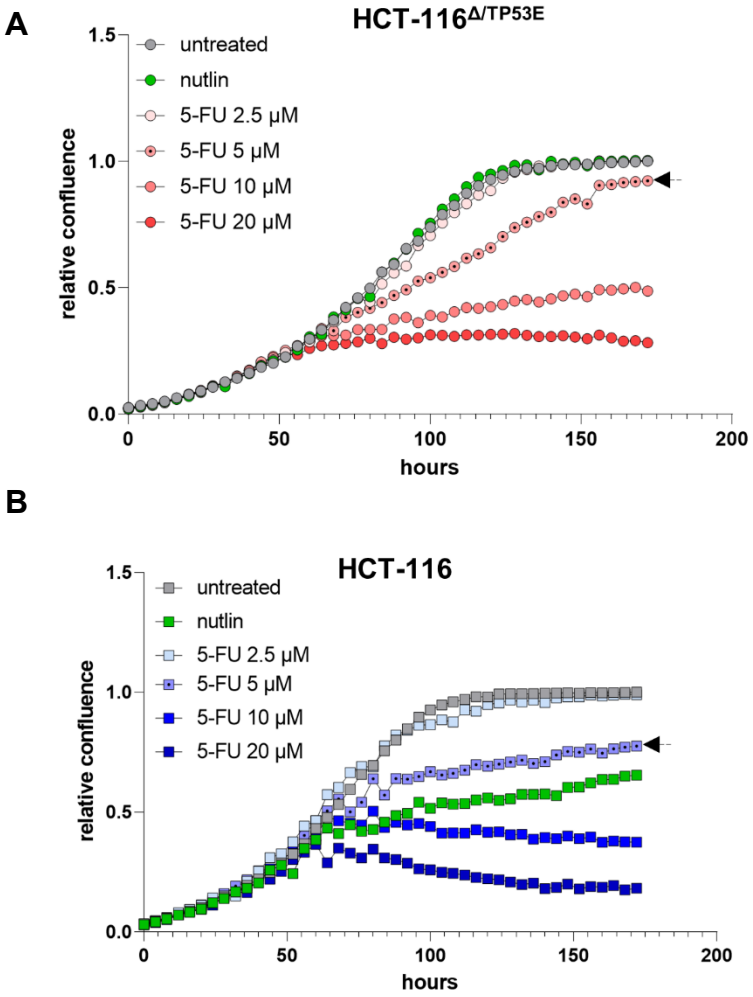

Figure 24 Estimation of the optimal concentration of 5-fluorouracil for the treatment of library-expressing cells

HCT-116$^{\Delta/TP53E}$ (A) and parental p53 wild-type (B) cells were treated with 2.5-20 µM of 5-FU. Growth was monitored for 7 days by live-cell microscopy using the IncuCyte S3. Hour 0 is the beginning of treatment. All confluence values were normalized to the confluence of untreated cells at the end of the time course (172 h) and shown as mean. Curves generated under the selected drug concentration are labeled with arrowheads.

for distinct mutant groups. For example, synonymous and wild-type-like mutants

were depleted by 5-FU markedly less than by nultin (mean ES=0.53 ± 0.09 versus 0.13±0.07) (Fig. 25C). Likewise, depletion of pLOF mutants was less prominent (mean ES for 5-FU 48h 0.92±0.15 versus 0.76±0.18 for nutlin). On the contrary,

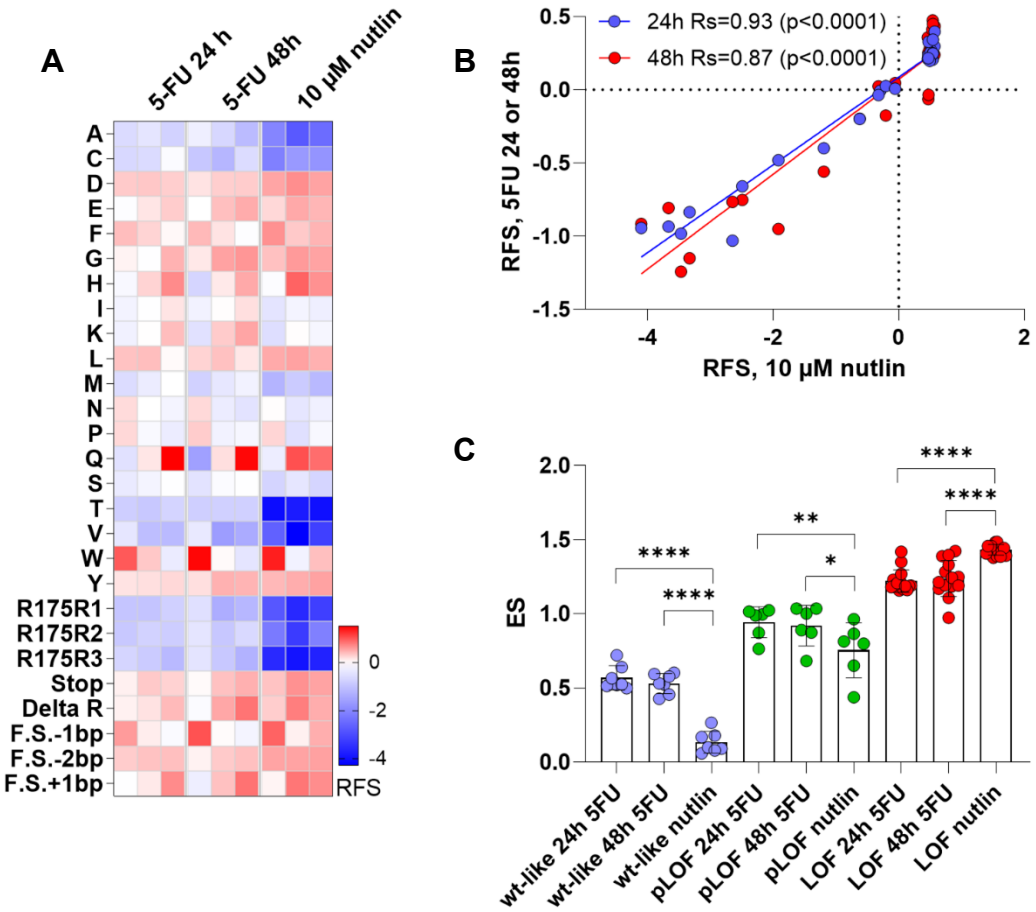

Figure 25. Impact of mutations at the codon R175 on the DNA damage response induced by 5-fluorouracil

A. Cells harboring the R175 library were treated with 5 µM 5-FU for 24 or 48h, washed with medium, and harvested 8 days after the beginning of treatment. RFS values for treated library triplicates are shown (two left columns). Right column: RFS values for cells treated for 8 days with nutlin. **B.** Correlation between enrichment scores of R175 mutants in nutlin- and 5-FU-treated libraries. Rs, Spearman correlation coefficient. C. Comparison of ES between nutlin- and 5-FU-treated libraries for 3 groups of mutants: LOF (red), wild-type-like (blue), and partial-LOF (green). Each dot represents one variant averaged across replicates. **** p<0.0001, ** p=0.004, * p=0.015. ANOVA with Sidak's multiple comparison test.

enrichment of LOF mutants was significantly lower under 5-FU treatment than under

nutlin (mean ES 5-FU 48h 1.24±0.27 versus 1.43±0.27 for nutlin Fig. 25C). Most likely, this was a result of distinct treatment duration. Under the short-term 5-FU treatment, some cells carrying wild-type-like mutants undergo cell cycle arrest and

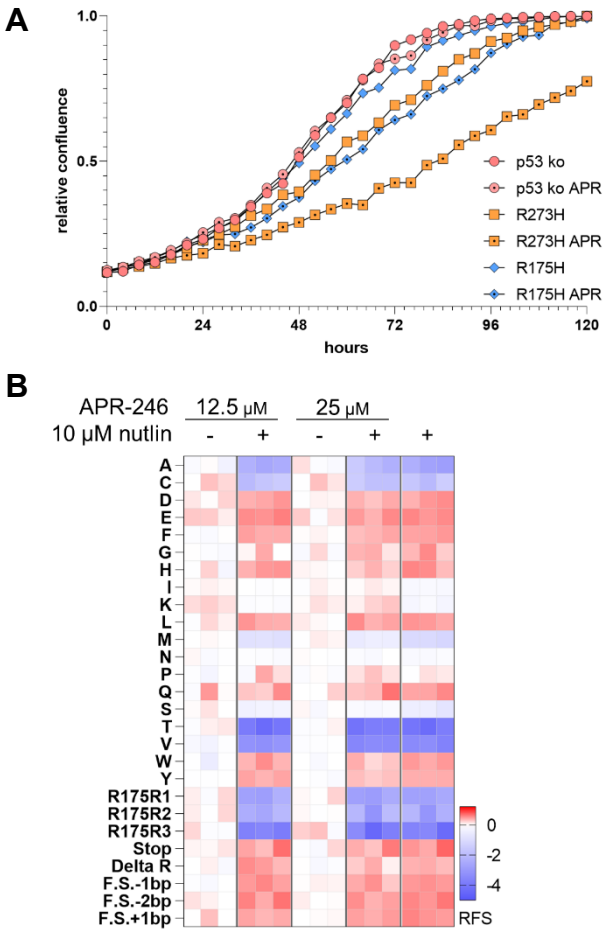

Figure 26. CSMS reveals no restoration mutants p53 functions by APR-246

A. Estimation of the optimal concentration of APR-246 for treatment of the library in H1299 cells expressing p53 mutants. Parental p53-negative H1299 cells and cells overexpressing R175H and R273H hot-spot mutants were treated with 25 µM APR-246. The growth of cells was monitored for 5 days by live-cell microscopy using the Incucyte S3. Hour 0 is the beginning of treatment. All confluence values were normalized to the confluence of untreated cells at the end of the time course (120 h) and shown as mean. **B.** Cells harboring the R175 library were treated with 12.5 and 25 µM of APR-246 for 8 days and harvested for DNA isolation. Additionally, cells were treated with a combination of APR-246 with 10 µM nutlin. RFS values for treated library triplicates are shown.

recover upon treatment withdrawal. Meanwhile, eight days long nutlin treatment

efficiently depletes wt-like and pLOF mutants either by apoptosis or by permanent cell cycle arrest. Furthermore, p53-independent action of genotoxic compound can also contribute to observed effects.

Our experiments have validated the CSMS as a versatile tool for predicting the response of mutant p53-expressing cells to various treatments: MDM2 inhibitors, irradiation, and 5-FU. Despite the substantial correlation between datasets, CSMS revealed a qualitative difference in response to these treatments. For example, prolonged exposure to nutlin strongly depleted synonymous variants indicating preferential induction of apoptosis. Conversely, single-dose irradiation or short-term (48h) treatment with 5-FU preferentially induced cell cycle arrest, exemplified by partial retention of wt-like mutants in the population. Our data argue that the CSMS captured an essential mechanistic difference between therapeutic agents and might be used to identify p53 mutations that confer drug resistance.

3.8.3 *CSMS reveals no reactivation of p53 mutants by APR-246*

Mutant p53 reactivation therapy aims at the pharmacological restoration of normal tumor-suppressive functions in missense mutants. Several p53 reactivators are currently investigated. Some compounds are active against single mutants: e.g., PK7088 and ZMC1 reactivate Y220C and R175H, respectively (Blanden et al. 2015; Bykov et al. 2018). Other molecules are targeting a broader spectrum of mutant proteins. However, most of the p53-reactivating compounds were only tested with a small number of exemplary hotspot mutations. Therefore, a comprehensive characterization of the response of non-hotspot mutants to p53 reactivators would give useful information for selecting patients for clinical trials. To this end, we have tested the response of cells expressing the R175 mutant library to APR-246, the most advanced compound in the class, which is currently under clinical studies (NCT03745716, NCT03931291, NCT03588078, NCT03072043, NCT00900614). The optimal concentration of the compound was determined by monitoring the growth of two isogenic H1299 cell lines expressing p53 hotspot mutants (R175H and R273H) in comparison to parental p53-null H1299 cells. 25 µM APR-246 delayed proliferation of both mutant-expressing cell lines but not parental p53-null cells. (Fig. 26A). We have treated cells expressing the R175 mutant library with two concentrations of APR-246 for eight days (12.5 and 25 mM). Since APR-246-

mediated restoration of p53 activity was shown to synergize with MDM2 inhibition (Izetti et al. 2014), we have additionally treated cells with the combination of APR-246 and nutlin to potentially amplify the effects of p53 reactivation by elevating the mutant protein levels.

We have expected that successful reactivation of mutant p53 with APR-246 would deplete some of the missense mutants (for example, R175H) from treated samples. Surprisingly, none of the mutants revealed any significant abundancy changes under treatment compared to untreated cells (Fig. 26B). Both sequencing datasets obtained from the APR-treated cells revealed almost absolute correlation with the dataset from untreated cells (Rs=0.989 and 0.993 for 12.5 and 25 µM respectively, p>0.0001). No changes in abundance of R175H mutant were observed as well. Combined treatment with APR-246 and nutlin revealed no APR-246-specific effects (correlations between nutlin-treated samples with or without APR-246: Rs=0.993 (12.5 µM) and 0.976 (25 µM), ANOVA p=0.88) (Fig. 26B). Again, no depletion of R175H variant hinting at p53 reactivation was evident upon combined treatment (ES=1.39 versus 1.37 and 1.21 for nutlin and nutlin-APR-246 combinations, respectively).

In summary, we were unable to reveal any p53-reactivating effects of APR-246 in the CSMS experiment with the HCT-116$^{\Delta/TP53E}$ cell line expressing the R175 mutant library.

3.9 CSMS probes the functional status of hundreds of H1 helix mutants

We have extensively validated the CSMS for accurate measurement of functional consequences of p53 mutations. To explore the applicability of the CSMS for high-content experiments, we have generated a library of HDR templates carrying 210 mutations representing all possible amino acid substitutions in the H1 helix of the p53 DNA-binding domain (positions C176-S185). H1 helix contains several residues essential for p53 function (e.g., C176, H179, E180, R181). Therefore, this small region was extensively studied, which makes it especially suitable for performance evaluation.

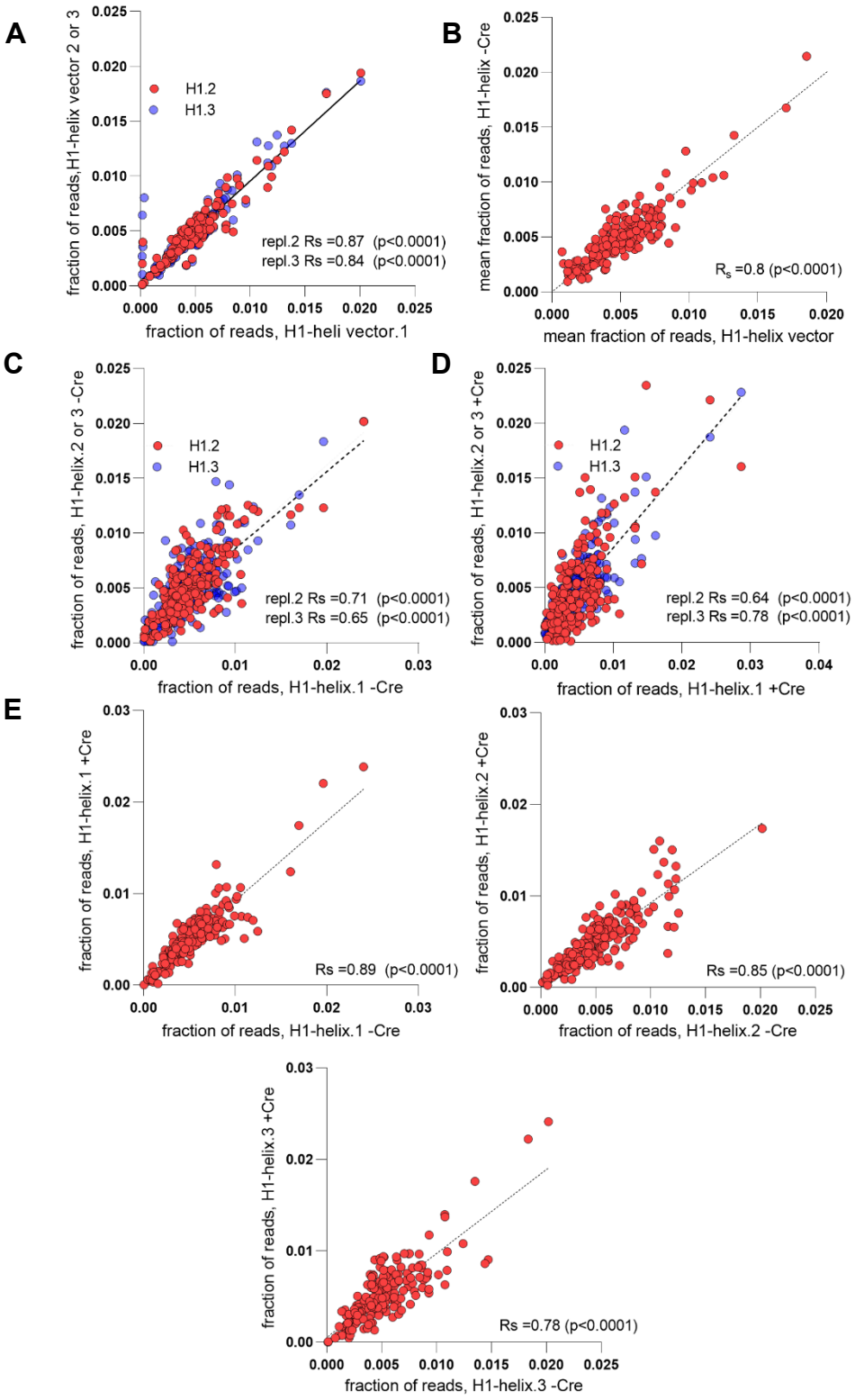

Figure 27. CRISPR-mediated homologous recombination reproducibly introduces the library of 210 H1 helix mutants into the endogenous *TP53* locus of the HCT-116$^{\Delta/TP53E}$ cells

To construct the library, 210 double-stranded 34 base pair-long oligonucleotides

Figure 27. Continued

Correlation between a fraction of reads for each variant in the library measured in the following samples:

A. Three independently prepared replicates of the HR-2-Golden-Gate plasmid pools carrying saturation mutagenesis library of the H1 helix (vector). **B.** Plasmid pools (library) and the transfected cell pools before infection with adeno-Cre (mean of 3 replicates). **C.** Three replicates of the transfected cell pools before adeno-Cre infection. **D.** Three replicates of the transfected cell pools after adeno-Cre infection. **E.** Three replicates of the transfected cell pools before and after adeno-Cre infection. Each figure shows one replicate.

On each figure fraction of reads for each mutant is shown (for individual samples or mean of 3 samples) together with corresponding values of Spearman correlation coefficients.

were cloned into the HR-2-Golden Gate vect**o**r and used together with a Cas9-encoding plasmid in a standard co-transfection procedure. To assess the reproducibility of the library production, we have first sequenced three independently prepared pools of targeting vectors (plasmid libraries) and found a high correlation between samples (Rs=0.87 and 0.84, p<0.0001 for comparison between triplicates) (Fig. 27A). Next, to evaluate the *TP53* targeting efficacy, we have sampled cells from three independently transfected pools before adeno-Cre infection and sequenced the H1 helix region. Reassuringly, the variant prevalence in the cellular libraries revealed a strong correlation with the targeting vector (Rs=0.8, p<0.0001), indicating that library complexity was preserved during mutagenesis (Fig. 27B). Moreover, high similarity between replicates of cellular libraries demonstrated reproducibility of the protocol (Rs=0.71 and 0.65, p<0.0001 before adeno-Cre infection, Rs=0.64 and 0.78, p<0.0001 after adeno-Cre infection) (Fig. 27C,D).

Analysis of libraries prepared from adeno-Cre-infected cells showed that the infection did not lead to global changes in variants abundancy since substantial correlation with libraries before the infection was evident (Rs=0.89, 0.85 and 0.78, p<0.0001) (Fig. 27E). Importantly, no mutations were lost from libraries at any step of the procedure, further demonstrating efficient targeting of the *TP53E* allele with a highly complex pool of mutants.

To assess the stability of the library, we have sampled three adeno-Cre-infected replicates after 4, 6, and 8 weeks of passaging. We have revealed significant global

changes in the abundance of variants after 6 and 8 weeks of library propagation (Friedman test, 2 weeks verses 4 and 8 weeks, p=0.0015 and 0.0007 respectively, Fig. 28A). Specifically, synonymous mutations were marginally depleted in 8 weeks

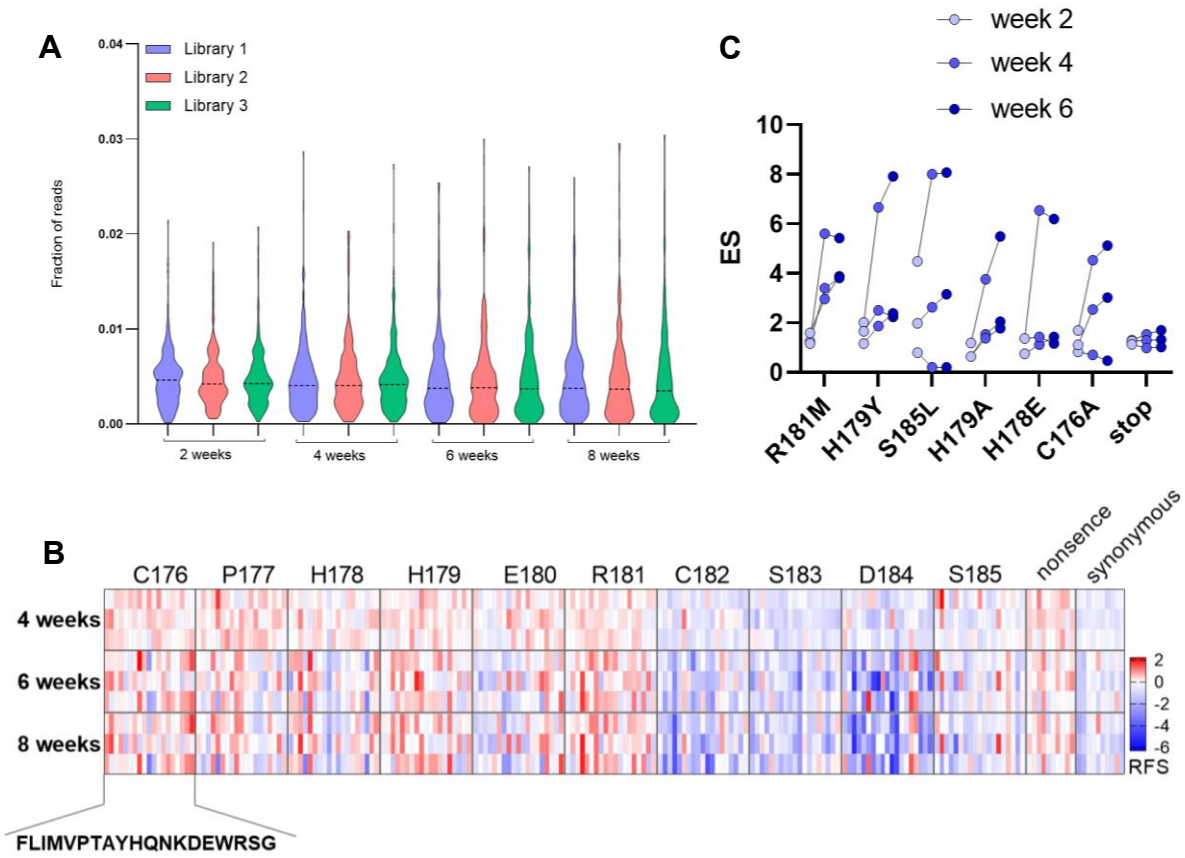

Figure 28. Time course dynamics of H1 helix sequence variants during 8 weeks of passaging of library-expressing cells

A. Cells carrying the H1 helix library were cultured for 2, 4, 6, and 8 weeks after infection with adeno-Cre. The violin plot illustrates the distribution of the fraction of reads for all variant in the library across biological replicates. Dashed lines indicate mean. Comparison of 4, 6 and 8 weeks to 2 weeks is non-significant (Kruskal-Wallis test, p>0,99, p=0,31, p=0,126 correspondingly). **B.** Heatmap illustrates the dynamics of individual protein variants along 8-week time course. RFS relative to the early timepoint sample (2 weeks) is shown for library triplicates. **C.** Dynamics of 6 variants with mean ES>(mean $ES_{stop\ codons}$)x2. R181M showed significant enrichment above the level of stop codons suggesting GOF effects.

(one-way ANOVA p=0.012), whereas nonsense mutations were slightly enriched (one-way ANOVA p=0.76, ns). Missense variants have shown a diverse pattern of enrichment and depletion.

Of note, repeated measurements at 4, 6, and 8 weeks revealed that some mutations were depleted from the population significantly stronger than synonymous variants, for example, D184 A, G, I, N, Q, R, T, V, and S (mean ES=0.16±0.08 versus 0.65±0.2 for synonymous variants at 8 weeks, Mann-Whitney test, $p<0.0001$) (Fig. 28B).

Interestingly, six mutations were enriched stronger than stop codons after 6-8 weeks of passaging (mean ES at 8 weeks exceeded more than two times mean ES of stop codons) (Fig. 28C). Such behavior likely pointed at GOF effect. However, enrichment of most of the variants was very inconsistent between library replicates, reaching statistical significance only for R181M (FDR q values 0.000284 and 0.000236 for 6 and 8 weeks respectively, multiple 2-sided t tests in combination with false discovery rates (FDRs). Growth-promoting GOF effects are likely more sensitive to culture conditions, cell density and stochastic fluctuations than potent cytotoxic effects of wild-type p53. Hence, experiments with a larger number of replicates will be needed to rigorously confirm these observations.

To gain insight into the functional diversity of H1 helix mutants, we have analyzed changes in clonal abundance upon treatment with MDM2 inhibitors. The outstanding reproducibility of the screening workflow was demonstrated by the uniform depletion of all synonymous mutations (mean ES=0.18±0.04), significant enrichment of all nonsense mutations (mean ES=1.7±0.5, $p=0.002$), and high correlation between replicates (average for all replicates $Rs=0.82$, $p<0.0001$). Similar to the R175 library, our analysis did not reveal any significant difference between the effects of five distinct MDM2 inhibitors (Rs for all inhibitors >0.95, $p<0.0001$).

Further analysis revealed a remarkably distinct sensitivity of H1 helix residues to mutagenesis. Residues 182-185 were highly resistant to alterations since most of the variants at these positions were depleted as strong as synonymous mutations (Fig. 29A). On the contrary, mutations at the positions C176-H179 most frequently lead to the loss of function, as evident from their strong enrichment. Variants at positions H178, E180, and R181 demonstrated the most variable pattern depletion and enrichment (Fig. 29B).

Interestingly, the cluster of amino acids resistant to mutagenesis (C182-S185) includes asparagine D184. This residue is conserved among 99 mammalian species,

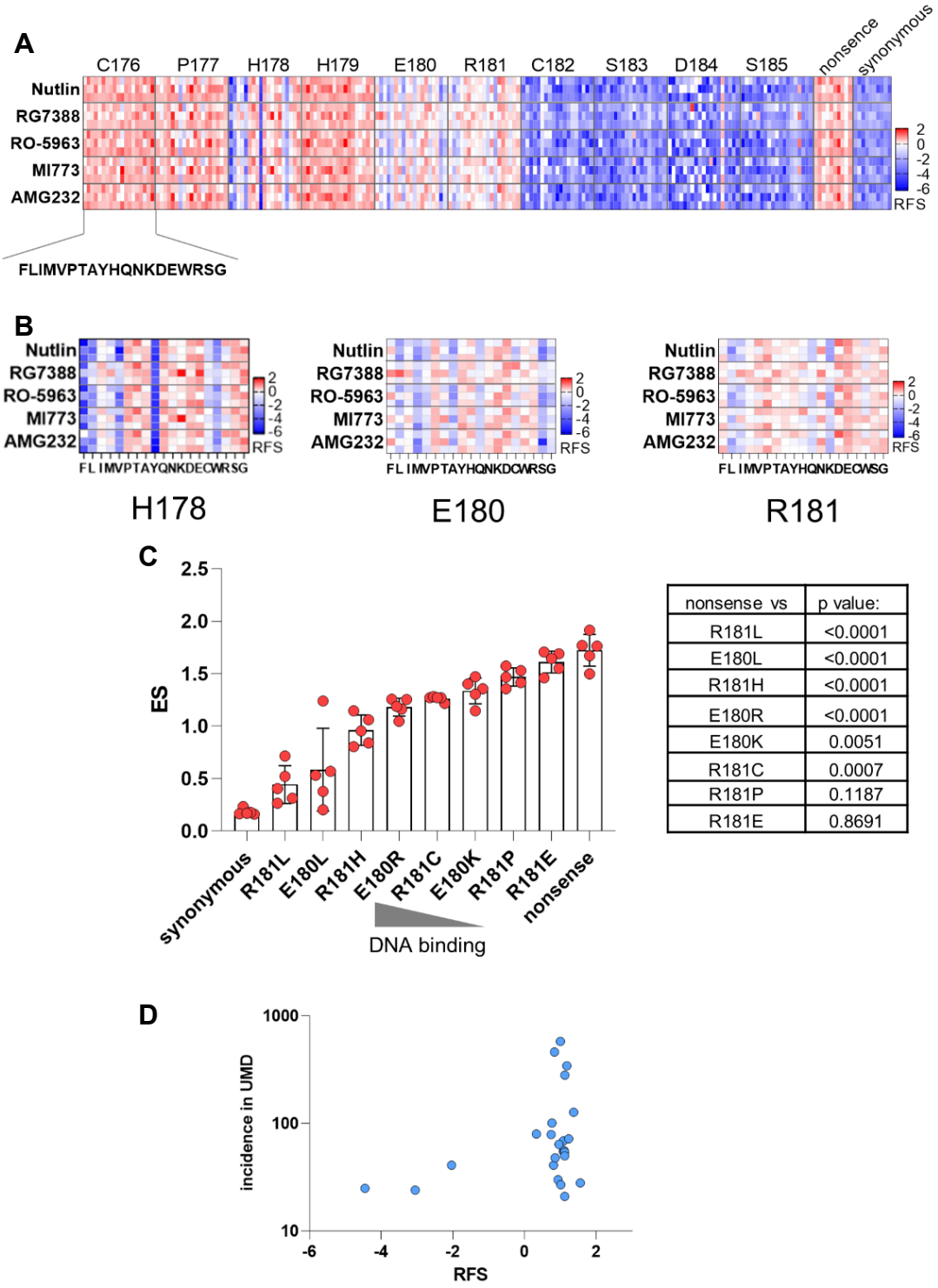

Figure 29. CSMS captures the functional consequences of H1 helix mutations

A. Cells expressing the library of H1 helix variants were treated 2 weeks after adeno-Cre infection with 5 mdm2-inhibitors at IC50 concentrations and harvested for gDNA extraction after 8 days. RFS values are shown (n=3). **B.** Same data as in (A) for mutations at positions H178, E180 and R181

suggesting its critical functional role (Sulak et al. 2016). Therefore, one could expect

Figure 29. Continued

C. Enrichment scores for selected mutants ordered according to their DNA binding ability *in vitro* as shown by Schlereth et al., 2010. Inverse correlation of ES and DNA binding is evident. Means of replicates for each mdm2-inhibitor are shown. Statistical significance was assessed by ANOVA with Dunnett's multiple comparison test. **D.** CSMS-derived RFS are plotted against the relative abundance of each mutant across human cancers (UMD database).

that mutations at this position would be damaging and highly prevalent in human cancers. In striking contrast, missense mutations of this amino acid are very rare (39 out of 80400 records in the UMD database). High conservation and low mutation rate collectively imply that most of the alterations at this position lead to the enhancement of the p53 activity, and therefore, such mutations are non-oncogenic in good agreement with CSMS-based classification.

Moreover, depletion of many D184 variants in our long-term culture experiment to the degree exceeding the depletion of wild-type variants also supports this notion (average mean ES for D184 A, G, I, N, R, S, Q, T, and V is 0.16±0.08 versus 0.65±0.23 for wild-type variants) (Fig. 28B). Much like mutations at D184, alteration of the serine 183 also did not lead to the loss of protein function and were depleted as strong as wild-type variants (mean ES for nutlin 0.16±0.09 versus 0.16±0.04) (Fig. 29A). Phosphorylation of the S183 by

Aurora B kinase promotes p53 degradation (Gully et al. 2012). Hence alterations at this site can lead to increased p53 stability rather than to the loss of function. In support of this, 140 of 159 annotated variants at this position are nonsense or frameshift (UMD database). Therefore, the depletion of most of the S183 variants from the screen is in line with the role of this residue in regulation of p53 stability. Unlike mutagenesis resistant residues C182-S185, mutations at positions C176-H179 had a strong damaging effect on p53 functionality (mean ES for all MDM2 inhibitors 1.28±1.33 respectively) (Fig. 29A). This observation was in good agreement with the known role of the H1 helix residues in maintaining the p53 structure. Cysteine 176 and histidine 179 are critical for coordinating a zinc ion that is essential for protein activity (Olivier et al. 2010). Accordingly, CSMS has scored all

mutations at these positions as damaging (mean ES_{C176}=1.77±0.43 and ES_{H179}=1.73±1.35) (Fig. 29A). Residues P177 and H178 are critical for forming a protein-protein interface between two p53 monomers bound to DNA (Brandt et al. 2009). In line with this, many mutations at these positions also impaired p53 function according to CSMS (mean ES_{P177}=1.73±0.67, ES_{H178}=1.08±0.33).

Residues E180 and R181 demonstrated intermediate sensitivity to mutagenesis (Fig. 29B). Our group and other investigators have identified these residues as essential for the cooperative binding of two p53 subunits to DNA. Oppositely charged arginine and glutamic acid of the two p53 monomers form reciprocal salt bridges that stabilize the DNA-bound p53 tetramer (Ma et al. 2007; Dehner et al. 2005; Liu et al. 2017; Olive et al. 2004). Missense mutations at the codons 180 and 181 alter the cooperative DNA binding to a different extent and are referred to as “cooperativity mutations.” Cooperativity mutants display distinct DNA binding affinity and, consequently, different transactivation capacities. For example, mutants E180L, E180R, and R181L have reduced DNA binding and demonstrate impaired apoptosis activation but can halt proliferation.

On the contrary, R181E is unable to transactivate any target genes and is deprived of both apoptotic and cell cycle arrest activities (Schlereth et al. 2010a). Notably, our screening could uncover functional differences between some cooperativity mutations in good agreement with published experimental data. As shown in Fig. 29C, R181L and E180L were depleted from the pool comparably to wild-type variants in line with their partially retained DNA binding and transactivation (mean ES for nutlin R181L 0.26±0.13, E180L 0.2±0.05, R181R 0.17±0.03, E180E 0.2±0.04) (Fig. 29B). Mutant R181H binds to DNA and transactivates target genes weaker than R181L (Schlereth et al. 2010a). Accordingly, this variant demonstrated intermediate enrichment in our dataset. Similarly, mutant E180R, which was extensively characterized as partial-LOF in vivo (Timofeev et al. 2013), also demonstrated significantly lower enrichment compared to nonsense variants (ANOVA with Dunnett’s test $p<.0001$) (Fig. 29C). Mutants with weaker residual DNA binding and transactivation (E180K and R181C) showed slightly lower enrichment than nonsense mutations, which was nevertheless statistically significant (ANOVA with Dunnett’s test p=0.0051 and 0.0007 respectively). Finally, mutants R181E and R181P were

described as entirely DNA binding- and transactivation-deficient (Schlereth et al. 2010a; Timofeev et al. 2019). They showed no significant difference from nonsense variants in our screening. Collectively, these observations further justify that CSMS can precisely capture even subtle functional differences between p53 variants.On the contrary, R181E is unable to transactivate any target genes and is deprived of both apoptotic and cell cycle arrest activities (Schlereth et al. 2010a). Notably, our screening could uncover functional differences between some cooperativity mutations in good agreement with published experimental data. Figure 29C depicts enrichment scores of 8 variants of R181 and E180. Mutants were ordered according to their *in vitro* DNA binding capacity measured in electrophoretic mobility shift assay with ^{32}P-labelled dsDNA fragment containing p53 concensus response element (data from Schlereth, 2010). As shown in Fig. 29C, R181L and E180L were depleted from the pool comparably to wild-type variants in line with their partially retained DNA binding and transactivation (mean ES for nutlin R181L 0.26±0.13, E180L 0.2±0.05, R181R 0.17±0.03, E180E 0.2±0.04) (Fig. 29B). Mutant R181H binds to DNA and transactivates target genes weaker than R181L (Schlereth et al. 2010a). Accordingly, this variant demonstrated intermediate enrichment in our dataset. Similarly, mutant E180R, which was extensively characterized as partial-LOF in vivo (Timofeev et al. 2013), also demonstrated significantly lower enrichment compared to nonsense variants (ANOVA with Dunnett's test $p<.0001$) (Fig. 29C). Mutants with weaker residual DNA binding and transactivation (E180K and R181C) showed slightly lower enrichment than nonsense mutations, which was nevertheless statistically significant (ANOVA with Dunnett's test $p=0.0051$ and 0.0007 respectively). Finally, mutants R181E and R181P were described as entirely DNA binding- and transactivation-deficient (Schlereth et al. 2010a; Timofeev et al. 2019). They showed no significant difference from nonsense variants in our screening. Collectively, these observations further justify that CSMS can precisely capture even subtle functional differences between p53 variants.

Next, we have analyzed how the loss of protein functionality in our screening correlates with the prevalence of mutations in cancer patients. Most variants found in more than ten cancer specimens had a positive RFS, indicating loss of tumor-suppressive activity (Fig. 29D). More specifically, mutagenesis-resistant residues

182-185 are rarely mutated in tumors (157 out of 58522 missense mutation records in the UMD *TP53* database, 39 mutations/codon). Thus, mutations at these positions do not impair protein functionality and do not give tumor cells a selective advantage.
By contrast, mutations of residues sensitive to mutagenesis (176-179) are found in tumors very frequently (2108 missense mutations in UMD *TP53* database, 527 mutations/codon) (Fig. 29A), and none of these variants are annotated in the UMD database as functional in respect of the transactivation, on the contrary to mutations in residues 182-185.

Mutations at residues E180 and R181 have demonstrated a variable pattern of functional p53 impairment in CSMS. They have an intermediate frequency in tumors (289 UMD *TP53* records, 144.5 mutations/codon).
Summarizing, our analysis identified many pathogenic mutations in the H1 helix in good agreement with known structure-function dependencies, previously published experimental and clinical data. This demonstrates that the CSMS is suitable for accurate functional classification of p53 mutations in a high-content manner.

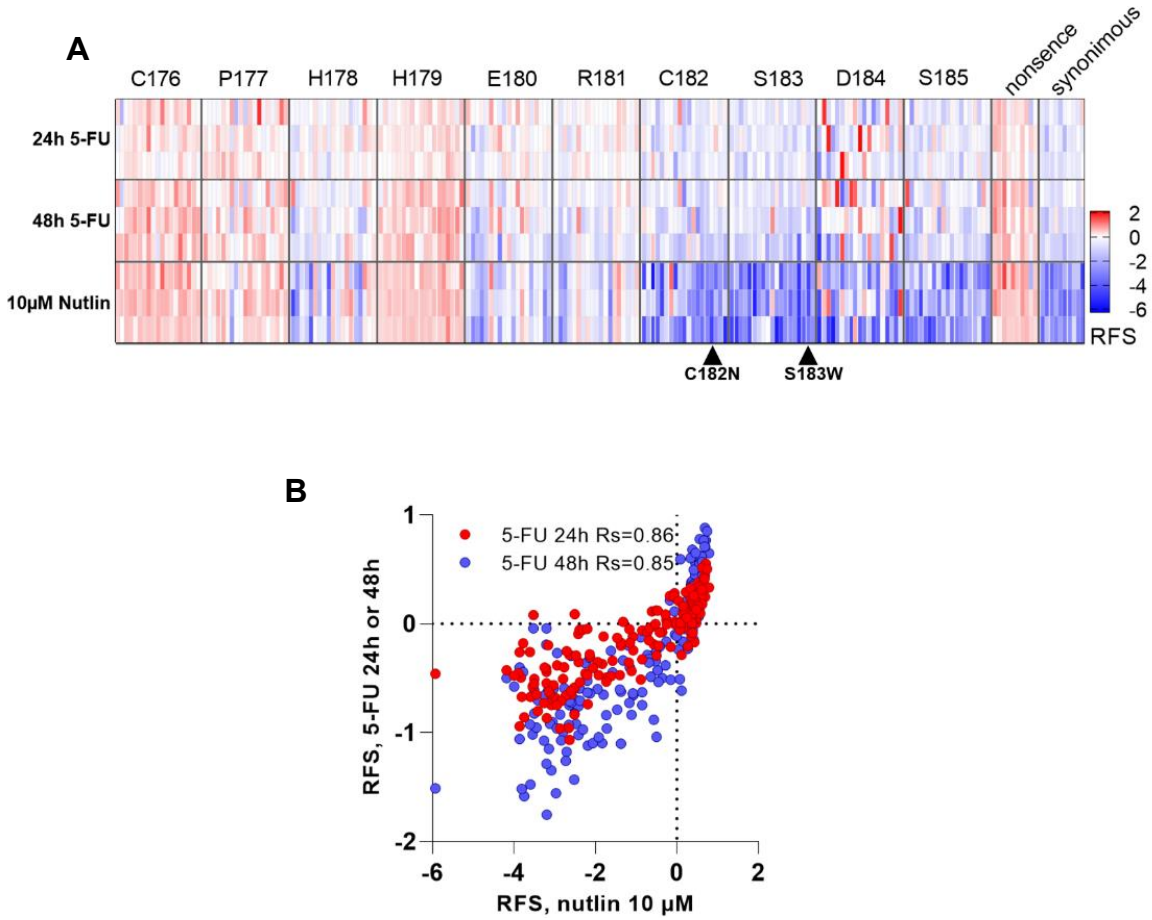

Figure 30. Impact of mutations in H1 helix on cellular fitness under treatment with 5-fluorouracil

A. Cells harboring the H1 helix library were treated with 5 µM 5-FU for 24 or 48h, washed with medium, and harvested 8 days after the beginning of treatment. Heatmap demonstrates RFS values for 5-FU and nutlin-treated cells (n=3). **B.** Correlation of RFS measured for cell libraries treated with nutlin or 5-FU. Rs, Spearman correlation coefficient.

In section 3.7.3 we have explored the effects of mutations in the codon R175 on cellular fitness under treatment with 5-FU and APR246. Although 5-FU has a distinct mechanism of action than nutlin, our screening revealed a very similar pattern (mean Rs=0.93 and 0.87 for 24 and 48h of treatment compared to nutlin (8 days). Surprisingly, the treatment of cells with APR-246 failed to identify any mutants that could be reactivated by the compound (Fig. 26B). This could be due to the small sample size (19 mutants). To confirm our validation experiment results with the larger panel of mutants, we have treated cells carrying the H1 helix library with 5-FU

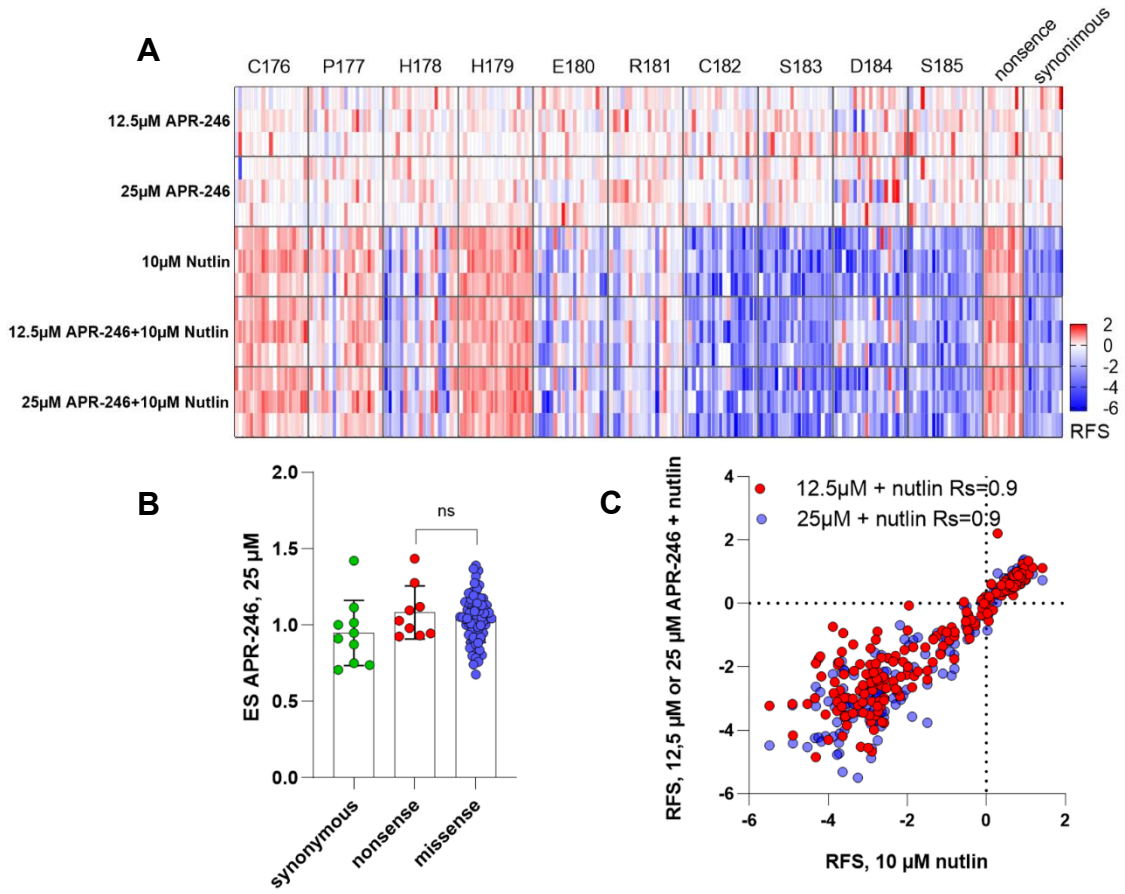

Figure 31. Lack of response of H1 helix mutants to the treatment with mutant p53 reactivating compound APR-246

A. Cells harboring the H1 helix library were treated with 12.5 and 25 μM of APR-246 alone or in combination with nutlin for 8 days and harvested for DNA isolation. RFS values are shown (n=3). **B.** ES measured after treatment of library-expressing cells with 25 μM APR-246 shown for 3 groups of mutants. p=0.54, unpaired t-test. **C.** Correlation of RFS measured for cell libraries treated with nutlin or with the combination of nutlin and APR-246. Rs, Spearman correlation coefficient.

and APR-246, as described previously (sections 3.7.2-3). Plotting of RFS computed for 5-FU and nutlin-treated libraries revealed a strong correlation (Rs=0.86 or 0.85 for 24 and 48h, p<0.0001) (Fig. 30A). Similar to the R175-library experiment, markedly lower depletion of mutants under 5-FU treatment compared to nutlin was noticed (compare X and Y axes on the Fig. 30B). Several variants were not depleted after 48 hours of 5-FU treatment, despite strong depletion after eight days of nutlin treatment (S183W, C182N), which may indicate preferential induction of cell cycle arrest by these mutants under 5-FU treatment. In summary, the experiment has

demonstrated that H1 helix p53 mutants reveal similar response patterns under treatment with MDM2- inhibitor nutlin and DNA damaging agent 5-fluorouracil.

Next, we have treated cells expressing the H1 helix library with APR-246. Rescue of tumor-suppressive functions of missense mutants would result in APR-246-dependent elimination of some of the variants enriched under nutlin treatment. Therefore, we have expected that such mutants would reveal significantly lower enrichment scores than both nonsense and wild-type-like variants (which should remain unaffected by APR-mediated p53 refolding). We did not observe any mutants demonstrating such behavior: all missense variants that were enriched under nutlin treatment (ES>1) showed an APR-246 response similar to nonsense and synonymous variants (mean ES=0.95, 1.0 and 1.0; range 0.7, 0.5, and 0.7 for synonymous, nonsense and missense variants respectively) (Fig. 31A, B). As noted before, APR-246-mediated restoration of p53 activity synergizes with MDM2 inhibition (Izetti et al. 2014). However, a comparison of RFS measurements from cells treated with nutlin or with the combination of two compounds demonstrated a high correlation, suggesting a lack of APR-specific effects. Not a single mutant conferring resistance to nutlin became depleted by combined treatment with APR-246 (Fig. 31C, lower right quadrant). In summary, our experiments again failed to demonstrate the rescue of mutant p53 functions by APR-246.

3.10 CSMS reveals mutations leading to nonsense-mediated mRNA decay of *TP53* transcript

Nonsense-mediated mRNA decay is a process used by eukaryotic cells to control the quality of mRNA. It detects and degrades mRNAs with nonsense mutations, for example, premature termination codons (Meyers et al. 1993; Mateo et al. 2020; Teng et al. 2017; Meisler 1975; Jones et al. 2008). In addition, the p53 missense mutation K120R leads to the formation of an aberrant splicing site which in turn generates a transcript variant with a frame-shifted premature termination codon. mRNA produced from this transcript is subjected to nonsense-mediated mRNA decay (Lee et al. 2019). Expression of p53 variants from the native locus in the CSMS system is expected to discover missense mutations leading to aberrant splicing. To explore this potential advantage of our protocol, we have isolated genomic DNA and RNA from cells expressing R175 and H1 helix libraries. After first-strand cDNA synthesis, PCR with a primer pair annealing at the 3'-end of the exon 5 and at the junction between exon 6 and exon 7 Nonsense-mediated mRNA decay is a process used by eukaryotic cells to control the quality of mRNA. It detects and degrades mRNAs with nonsense mutations, for example, premature termination codons (Meyers et al. 1993; Mateo et al. 2020; Teng et al. 2017; Meisler 1975; Jones et al. 2008). In addition, the p53 missense mutation K120R leads to the formation of an aberrant splicing site which in turn generates a transcript variant with a frame-shifted premature termination codon. mRNA produced from this transcript is subjected to nonsense-mediated mRNA decay (Lee et al. 2019). Thanks to the expression of p53 variants from the native locus the CSMS system is expected to discover missense mutations leading to aberrant splicing. To explore this potential advantage of our protocol, we have isolated genomic DNA and RNA from cells expressing R175 and H1 helix libraries. After first-strand cDNA synthesis, PCR with a primer pair annealing at the 3'-end of the exon 5 and at the junction between exon 6 and exon 7 was performed (primers #11 and #28 correspondingly). Such a design for the reverse primer was chosen to amplify exclusively cDNA and exclude amplification of genomic DNA. Genomic DNA was amplified as previously described (Fig. 32A).

Both amplicon libraries were sequenced, and the number of reads assigned to each mutation in cDNA and gDNA libraries were compared (Fig. 31A, B). Comparison of

read fractions (RF) measured in the R175 library revealed, that missense mutations were equally presented in gDNA and cDNA (mean RFgDNA=0.037±0.02, mean RFcDNA=0.043±0.025, Mann Whitney test p=0.216). Similar tendency was revealed in the H1 helix library: missense mutations were equally presented in genomic DNA and cDNA (mean RFgDNA=0.0046±0.0032, mean RFcDNA=0.005±0.003, Mann-Whitney test p=0.17, Fig. 32 A,B). Notably, nonsense variants and frameshifts demonstrated distinct behavior in both libraries. They were significantly less abundant in the cDNA as compared to gDNA (shown as red dots, R175 library: RFgDNA=0.037±0.008, RFcDNA=0.0021±0,0005, t-test p<0.0001; H1 helix library: RFgDNA=0.0072±0.0035, RFcDNA=0.00046±0,0004, Fig. 32A, B). These data imply that transcripts containing stop codons and frameshifts are subjected to nonsense-mediated decay. Importantly, the deletion of the codon 175, which disrupts protein functionality but does not influence mRNA stability, was equally abundant in gDNA and cDNA libraries (mean read fraction 0.020 versus 0.025, Delta R in Fig. 32A).

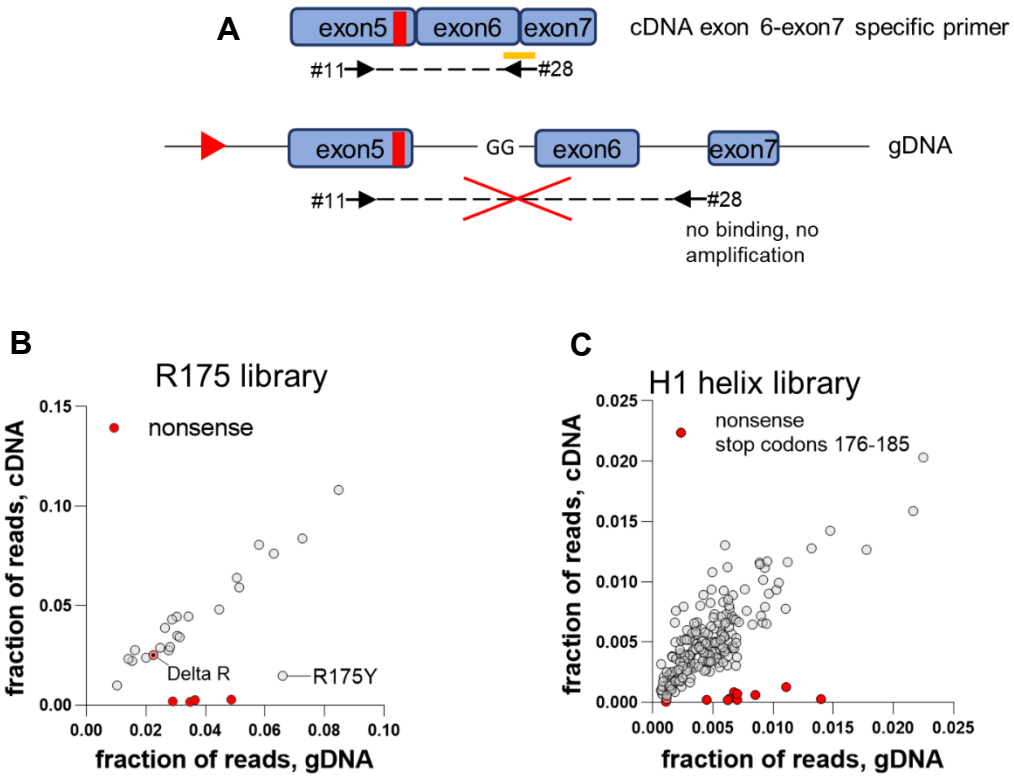

Figure 32. CSMS identifies mutations causing nonsense-mediated mRNA decay.

A. Schematic of the cDNA (above) encoded by the *TP53*^{E} allele (below). The junction between exons 6 and 7 in cDNA is indicated with the orange line. This junction is absent in the gDNA sequence and the fragment with primers #11 and #28 fails the amplification. **B,C.** Cells carrying R175 (B) and H1 helix libraries (C) were cultivated for 2 weeks after adeno-Cre infection and harvested for gDNA and mRNA extraction. gDNA and cDNA sequencing were performed to quantify the abundance of each variant in the population (gDNA) and abundance of variant-coding transcripts (cDNA). Shown are mean fraction of reads from gDNA and cDNA datasets (n=3). Nonsense mutations are labelled with red dots.

Interestingly, mutation R175Y was significantly less abundant in cDNA compared to all other missense variants (RFmissense=0.043±0,025, RFR175Y=0,015±0,002, Mann-Whitney test p=0.0082), suggesting that R175 CGC>TAC mutation might lead to mRNA degradation. R175Y was identified as LOF in CSMS and in earlier reports (Ryan and Vousden 1998; Kim et al. 2003). Although no data from the literature point on its influence on mRNA stability, our findings deserve further investigation.

Collectively, our observations show that CSMS can be used to discover mutations causing nonsense-mediated decay of *TP53* transcripts.

3.11 CSMS identifies pathogenic non-coding *TP53* mutations

We devised the CSMS as a system for analyzing *TP53* mutations in the context of the genomic locus with preserved regulatory elements (such as enhancers, introns, and promoters). Mutations at splice sites account for 2% of all detected *TP53* alterations (Fig. 33A) (Bouaoun et al. 2016; Leroy et al. 2014a). The pathogenic effects of such mutations cannot be studied using systems based on the expression of cDNAs. Consequently, none of the previous studies of the p53 mutome analyzed this class of mutations. On the contrary, our system enables capturing the complete diversity of alterations at the *TP53* locus, including mutations in non-coding regions.

To evaluate this potential advantage of the CSMS, we have assembled a saturating mutagenic library of the splice donor site (SDS) in the 5th intron. Mutations at this site were found in cancer patients (Smeby et al. 2019). Specifically, the SDS library comprised the following mutations at the junction between exon 5 and intron 5: synonymous mutations and stop codons (TAA, TAG, TGA) at positions D184, S185 and D186, all possible permutations of the last nucleotide (c.559) of exon 5 (forms the codon G187 with exon 6), and all possible permutations of the first 12 nucleotides of the intron 5. 54 double-stranded 26 base pair-long oligonucleotides were cloned into HR-2-Golden Gate vector and the resulting library was used in a standard co-transfection procedure. Cells carrying the SDS library cells were treated for eight days with nutlin and harvested for DNA isolation and sequencing. Strong enrichment of nonsense mutations and depletion of synonymous variants demonstrated the validity of the analysis (Fig. 33B). Remarkably, mutations at positions c. 559, +1, +2, and +5 turned out to impair p53 function, as evident from the enrichment of all sequence variants at these positions. These mutations likely disrupt splicing of the transcript, in line with stringent sequence requirements for positions +1, +2, and +5 in eukaryotic splice sites (G, T, and G respectively) (Burset et al. 2001; Shapiro and Senapathy 1987). Notably, mutation c.559+1G>A was described as a variant affecting splicing and leading to the production of the truncated polypeptide in individuals with the hereditary cancer-predisposing

syndrome (ClinVar record NM_001126112.2) (Surget et al. 2013; Lai et al. 1993).

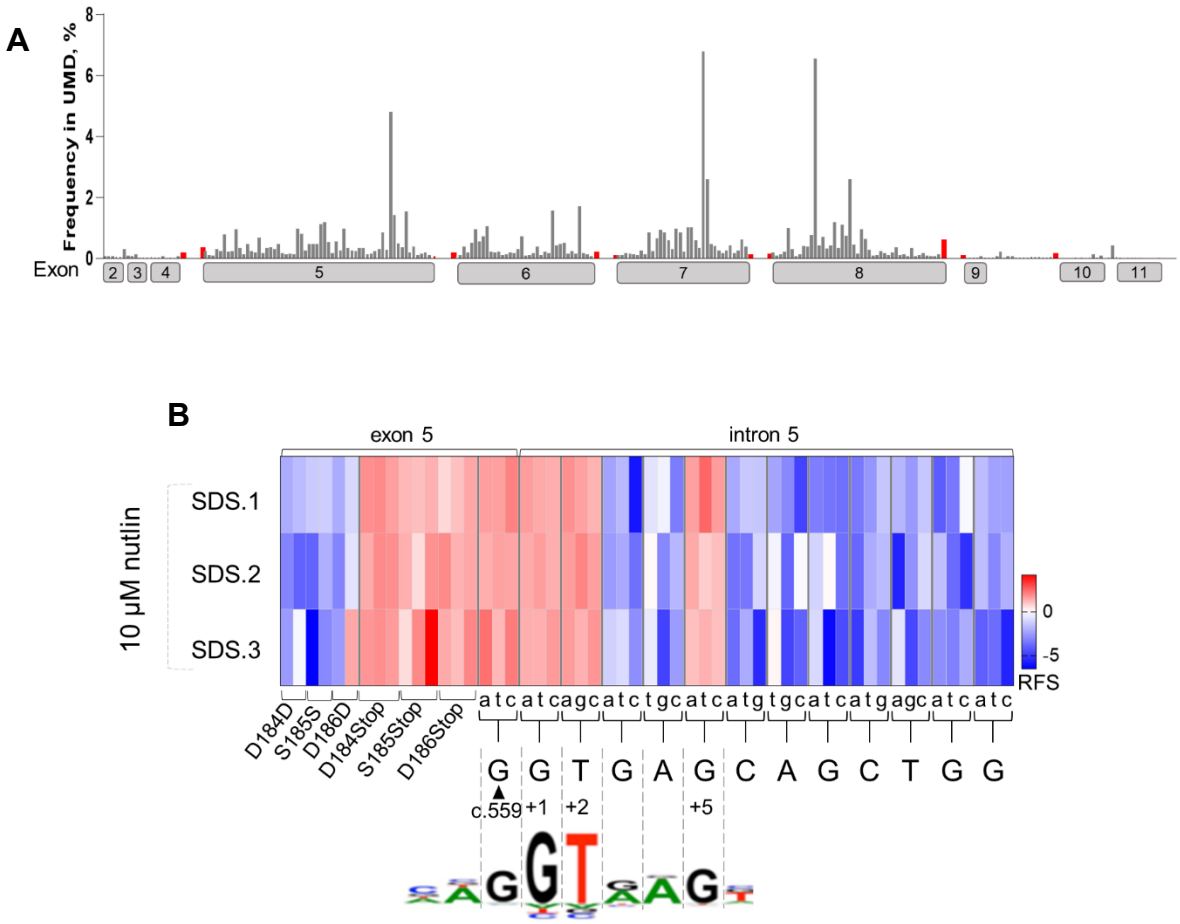

Figure 33. CSMS reveals non-coding pathogenic mutations of the splice donor site in the intron 5

A. Frequency and distribution of mutations in *TP53* splicing sites (red) and missense mutations (grey). Frequency of mutations at each codon or splice site in the UMD database is shown. Modified from Smeby et al. 2019
B. Heatmap depicts RFS of mutants in the SDS library measured in triplicate cultures of library-expressing cells treated with nutlin. The library was composed of 3 synonymous variants and 3 stop codons at positions D184, S185, and D186 as positive and negative controls and all possible permutations of the last nucleotide of the exon 5 and first 12 nucleotides of the intron 5. Wild-type sequence starting from the position c.559 is shown below. +1, +2, and +5 are positions in the splice donor site of the intron 5. Alignment of the wild-type sequence with the cocensus sequence of the donor splice site is shown (modified from Desmet F., Hamroun Dalil, Collod-Béroud, Gwenaëlle, Claustres, M., Beroud, Christophe, 2010).

These results showcase the extended capabilities of the CSMS platform in the

characterization of. Mutations at this site were found in cancer patients (Smeby et al. 2019).

Donor splice sites are very conserved across eukaryotes (Shapiro and Senapathy 1987). The concensus sequence of 5'-donor splice sites is AGGTA/GAGT. The donor splice site in the 5th intron of *TP53* is almost identical to the concensus (AGGTGAC). We have included the following mutations at the junction between exon 5 and intron 5 into the SDS library: synonymous mutations and stop codons (TAA, TAG, TGA) at positions D184, S185 and D186, all possible permutations of the last nucleotide (c.559) of exon 5 (forms the codon G187 with exon 6), and all possible permutations of the first 12 nucleotides of the intron 5. 54 double-stranded 26 base pair-long oligonucleotides were cloned into HR-2-Golden Gate vector and the resulting library was used in a standard co-transfection procedure. Cells carrying the SDS library cells were treated for eight days with nutlin and harvested for DNA isolation and sequencing. Strong enrichment of nonsense mutations and depletion of synonymous variants demonstrated the validity of the analysis (Fig. 33B). Remarkably, mutations at positions c. 559, +1, +2, and +5 turned out to impair p53 function, as evident from the enrichment of all sequence variants at these positions. These mutations likely disrupt splicing of the transcript, in line with stringent sequence requirements for positions +1, +2, and +5 in eukaryotic splice sites (G, T, and G respectively) (Burset et al. 2001; Shapiro and Senapathy 1987). Notably, mutation c.559+1G>A was described as a variant affecting splicing and leading to the production of the truncated polypeptide in individuals with the hereditary cancer-predisposing syndrome (ClinVar record NM_001126112.2) (Surget et al. 2013; Lai et al. 1993). These results showcase the extended capabilities of the CSMS platform in the characterization of non-coding *TP53* alterations.

3.12 CSMS-based functional classification of >1200 p53 protein variants

To further evaluate the performance and scalability of the CSMS system, we have designed a saturation mutagenesis library encoding 3843 *TP53* nucleotide variants. Specifically, the library encoded the pool of sequence variants representing all possible permutations at each position from Y126 until S186 (encoded by the 5th exon).

To prepare the HDR template library, a pool of 3843 single-stranded oligonucleotides (230 bp) was manufactured by Agilent using array-based synthesis. Each oligonucleotide was spanning the genomic region Chr. 17: 7.675.045 – 7.675.261 (assembly GRCh38) and contained a single codon substitution. To make the HR-2 Golden Gate vector compatible with 230 bp-long oligonucleotides, the BbsI recognition sequences were located at the beginning and at the end of exon 5. The pool of single-stranded oligonucleotides was converted into double-stranded using PCR with primers #26 and #27 containing BbsI recognition sequences at 5'-ends. The resulting PCR fragments were cloned into the modified HR-2 Golden Gate cloning vector (Fig. 8) using Golden Gate protocol. The plasmid library was purified using procedures described in the Materials and methods section. Library quality was verified using NGS.

The pool of library-encoding plasmids was transfected into 100 million HCT-116$^{\Delta/TP53E}$ cells. For adeno-Cre infection and nutlin treatment, the same number of transfected cells was used, and the splitting ratio was maintained at 1:2 to retain library complexity. Triplicate cultures were treated for eight days with nutlin and harvested simultaneously with untreated samples. It is essential to highlight the fact that Cre-mediated recombination is not 100% efficient. Therefore, cellular libraries always contain non-recombined cells expressing no p53. This results in the background from unrecombined (GFP-positive) cells, which does not affect sequencing results for the low complex R175 and H1 helix libraries, but becomes an important factor in the case of the highly complex exon 5 library. To enrich the cellular library for GFP-negative cells which have undergone Cre-mediated recombination, we have used FACS sorting. Genomic DNA was isolated from 15 million cells per replicate. To improve the sequencing coverage, the amount of

genomic DNA and the number of PCR reactions was increased as described in Materials and methods in section 2.2.10. Next-generation sequencing of the *TP53* locus was conducted as described above.

The sequencing of the targeting vector revealed that all 3843 nucleotide variants were retained in the plasmid preparation. This demonstrated that the large-scale oligonucleotide synthesis and cloning procedures were successfully implemented (read counts: minimum 45, maximum: 42111, mean: 917). Comparison of sequencing data derived from the vector and the cellular library revealed a substantial abundance decrease for many mutants: the frequency of the least abundant variant in the Cre-infected cell library was 0.0000008 compared to 0.000013 in the vector (16-fold change, Wilcoxon test $p<0.0001$ (Fig. 34A) This indicates that transfection and subsequent propagation of the library introduced substantial bias. Nevertheless, further analysis of the dataset confirmed the validity of the experiment.

Analysis of sequencing data from untreated cells revealed that variant frequencies were highly correlated between three library replicates, demonstrating good reproducibility of the mutagenesis procedure ($Rs=0.9$ and 0.86 for library 1 versus 2 and 3 respectively, $p<0.0001$) (Fig. 34B). Libraries prepared from adeno-Cre-infected and sorted GFP-negative cells yielded 99.79% variant coverage, demonstrating preserved library complexity. As shown in Fig. 33C, in two library replicates only 6% of nucleotide variants were covered by less than 50 reads, approximately 20% were covered by less than 500 reads, and the majority of mutants was covered by more than 500 reads (Fig. 34C). The third replicate revealed lower sequencing depth, which could be caused by poor DNA quality or some error during library preparation.

Considering the high coverage of most of the variants in the library and high reproducibility of the mutagenesis procedure, we have considered our data to have sufficient quality for further analysis, despite some obvious technical issues (Fig. 34B, C).

Next, we have assessed the measurement precision by calculating the coefficient of variation (CV) for each variant as a ratio of the standard deviation to the mean read count across replicates. Comparison of CVs revealed a substantial difference between untreated and nutlin-treated libraries. In the untreated dataset, 644 variants

had CV >0.25, whereas in the nutlin dataset, only 128 (Fig. 35A). These data imply that in the untreated cellular library, variant frequencies are subjected to stronger fluctuations than in the nutlin-treated library. To reduce measurement noise, we have selected an arbitrary threshold based on CV values. All variants with $CV_{untreated}$<0.45 and CV_{nutlin}<0.3 were retained for further analysis, whereas variants with

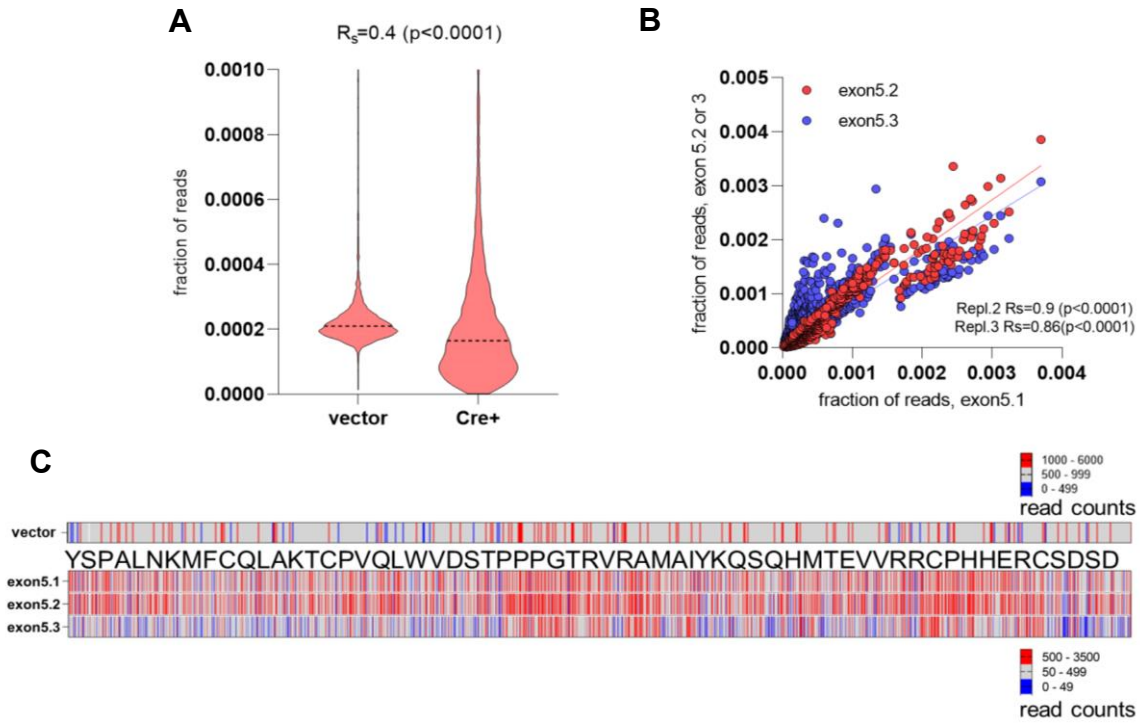

Figure 34. CSMS protocol enables introduction of a highly complex library of 3646 variants in the *TP53* locus

A. Comparison of read fractions for each of 3646 nucleotide variants in the plasmid library (vector) and in the transfected cell pool after infection with adeno-Cre. **B.** Correlation of read fractions for all variants across 3 library-expressing replicates. Rs, Spearman correlation coefficient. **C.** Heatmap depicts variant coverage in the vector and triplicate cultures of library-expressing cells. Number of reads assigned to each variant is shown aligned to the sequence of exon 5 according to the color scale.

$CV_{untreated}$>0.45 or CV_{nutlin}>0.3 were discarded (Fig. 35B). Application of the threshold enabled us to remove the most inconsistently measured mutants without compromising the global complexity of the dataset.

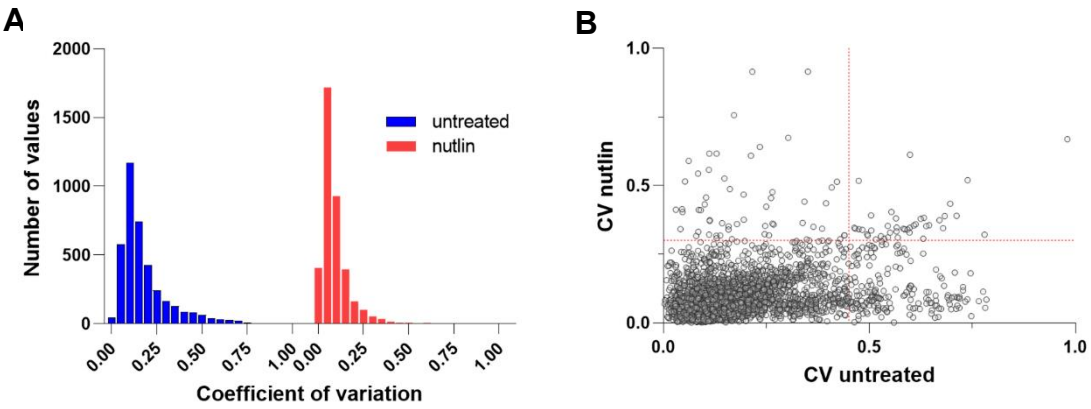

Figure 35. Comparison of variance in sequencing data of untreated and nutlin-treated cell libraries

A. Frequency distribution of the coefficient of variation (CV) calculated for each variant across triplicates in the untreated and nutlin-treated cell libraries. CV was calculated as a ratio of the standard deviation to the mean normalized reads. Smaller variance in the nutlin dataset is evident. **B.** CVs for each variant from untreated and nutlin-treated libraries were plotted and used to select the threshold: all sequence variants outside the lower-left quadrant were excluded from the analysis to reduce measurement noise. CV calculation was performed with the help of Boris Klimovich.

Next, we have summarized filtered read counts for all mutations encoding the same amino acid substitution in each replicate and computed normalized read counts for protein variants. Application of the threshold resulted in a loss of just 21 protein variants from the dataset, 1249 protein variants (98%) were retained in the processed dataset.

The relative abundance of variants upon nutlin treatment revealed expected dynamics: all synonymous variants were depleted from the population (mean ES=0.6±0.27), whereas missense and nonsense mutations were enriched (mean ES=1.26±0.9 and 1.62 ±0.95 respectively) (Fig. 36A).

To assess the accuracy of the CSMS in a high-content format, we have compared results with R175 and H1 helix and libraries as validation datasets since mutations present in the two smaller libraries were also contained in the larger exon 5 library.

Reassuringly, both comparisons revealed a significant positive correlation ($Rs_{(R175)}$=0.63, p=0.002, and $Rs_{(H1\ helix)}$=0.72, p<0.0001), demonstrating that high-content screening mainly reproduces the classification made in the low-throughput experiments (Fig.36 B, C). Nevertheless, some variants were classified discordantly in two experiments (located in the upper left and lower right quadrants in Fig. 36B and 36C). To find the reason for discordant classification, we have compared enrichment scores for all variants present in both H1 helix and exon 5 datasets (Fig. 36D). The comparison revealed a remarkably distinct distribution of RFS values. Despite having similar median RFS (-0.15 and 0.07), the H1 helix dataset demonstrated significantly larger data spread, exemplified by the higher range and interquartile range values (5.42 versus 3.08 and 1.43 versus 0.74 respectively). Data presented in Fig. 36 clearly demonstrate that the primary source of higher variance in the H1 helix dataset is more substantial depletion of variants compared to the exon 5 dataset. Therefore, scaling up the CSMS protocol resulted in decreased resolution between LOF and wild-type-like mutants due to reduced depletion of mutants from cellular pools.

To further examine the ability of high-throughput CSMS to capture the functionality of p53 variants, we have calculated an evolutionary conservation score (ECS). ECS was previously used as an indicator of the vulnerability of p53 residues to functional alteration. The most conservative amino acids were identified as highly susceptible to mutations, whereas less conservative were resilient to mutations (Kotler et al. 2018). ECS was computed for each of the 50 residues based on the alignment of 1498 p53 protein sequences using ConSurf2016 (Ashkenazy et al. 2016). Negative scores indicate high evolutionary conservation. Comparison of the ECS with mean enrichment score values for each amino acid position revealed significant negative correlation (Rs=-0.54, p<0.0001): evolutionary conserved residues with low ECS demonstrated higher mean ES in our screening, indicating intolerance to mutagenesis (Fig. 37A). Therefore, our experiment performed the classification of p53 variants in good agreement with functionality prediction inferred from evolutionary conservation.

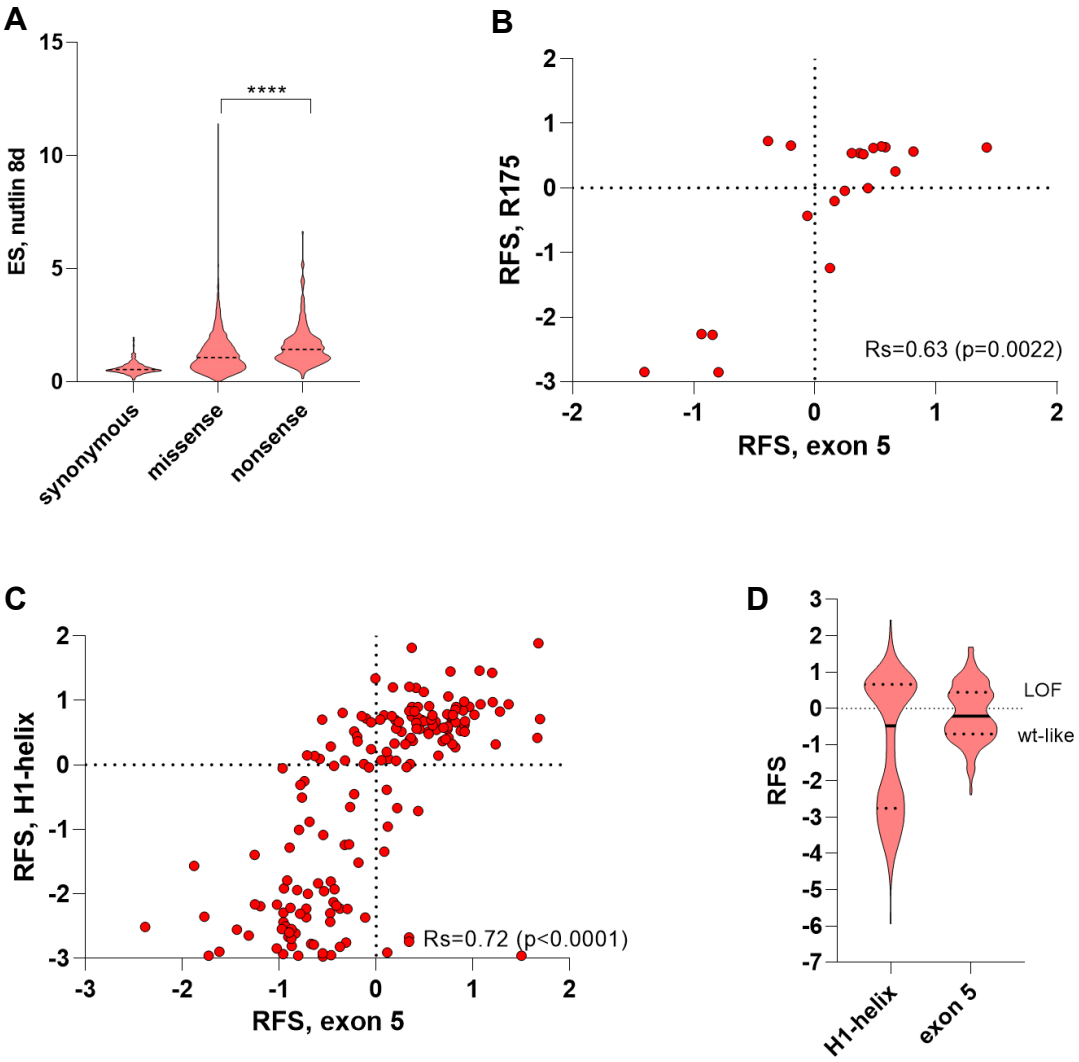

Figure 36. Comparison of the relative fitness scores measured for R175 and H1 helix variants by low- and high-content CSMS protocols

A. ES values measured in the nutlin-treated libraries for 3 groups of variants. Synonymous variants are significantly depleted, nonsense variants are strongly enriched, enrichment pattern of missense mutations is highly variable n=3. **** p<0.0001, unpaired t-test with Welch's correction. **B.** RFS values derived from the exon 5 dataset are plotted against corresponding RFS values from the R175 dataset. Rs, Spearman correlation coefficient. **C.** RFS values derived from the exon 5 dataset are plotted against corresponding RFS values from the H1 helix dataset. Rs, Spearman correlation coefficient. **D.** Comparison of RFS values computed for all missense variants from H1 helix and exon 5 datasets. Bold line: median, dotted lines: quartiles.

Next, we have analyzed if our functional measurements correlated with the transactivating capacity of the mutants. As in Section 3.7, Fig. 18D, we have utilized the data capturing transactivation of 8 response elements by p53 mutants derived from the yeast reporter assay (Kato S. et al. 2003). We have extracted the reporter activity values for 352 variants encoded by the 5^{th} exon and performed principal component analysis using ClustVisto to separate mutants with mostly dissimilar transactivating patterns (Metsalu and Vilo 2015). Then we have plotted relative fitness scores derived from the nutlin treatment experiment versus values of principal component 1 (PC1), which explains 79.1% of the variance in the transcriptional activity dataset (Fig. 37B). The comparison revealed a significant correlation between relative fitness score and transactivating properties of mutants represented by PC1 values ($Rs=-0.68$, $p<0.0001$). This implies that the high-content CSMS captures the global difference in the transactivation capacity of hundreds of mutants.

We next analyzed whether the functional consequences of mutations in exon 5 measured by CSMS correlate with mutational prevalence in human tumors. To this end, we have selected all exon 5 variants reported in more than 10 patients' samples and plotted their frequency in the UMD database against mean relative fitness scores. This comparison revealed a weak but significant correlation between ES and mutation prevalence in tumors ($Rs=0.33$, $p<0.0001$). The most frequent cancer-associated hotspot mutant R175H was enriched markedly weaker than many other less frequent mutants (Fig. 37C). This fact further highlighted the low resolution of the high-content CSMS because, in the experiment with the R175 library, this mutant had markedly higher enrichment (1.66 versus 0.83).

Interestingly, many rare tumor-associated mutations were highly enriched in the dataset, supporting earlier observations (Fig. 37C) (Kotler et al. 2018; Ory et al. 1994). Therefore, the loss of functionality and clinical significance cannot be deduced solely from mutation prevalence in patients and highlights the importance of functional measurements.

Plotting individual RFS for each protein variant revealed a diverse pattern of sensitivity to alterations (Fig. 38). Anti-proliferative capacity remained almost unaffected by mutations at specific positions (for example, 165-170 and 182-186). However, p53 functionality was strongly impaired by almost every substitution of

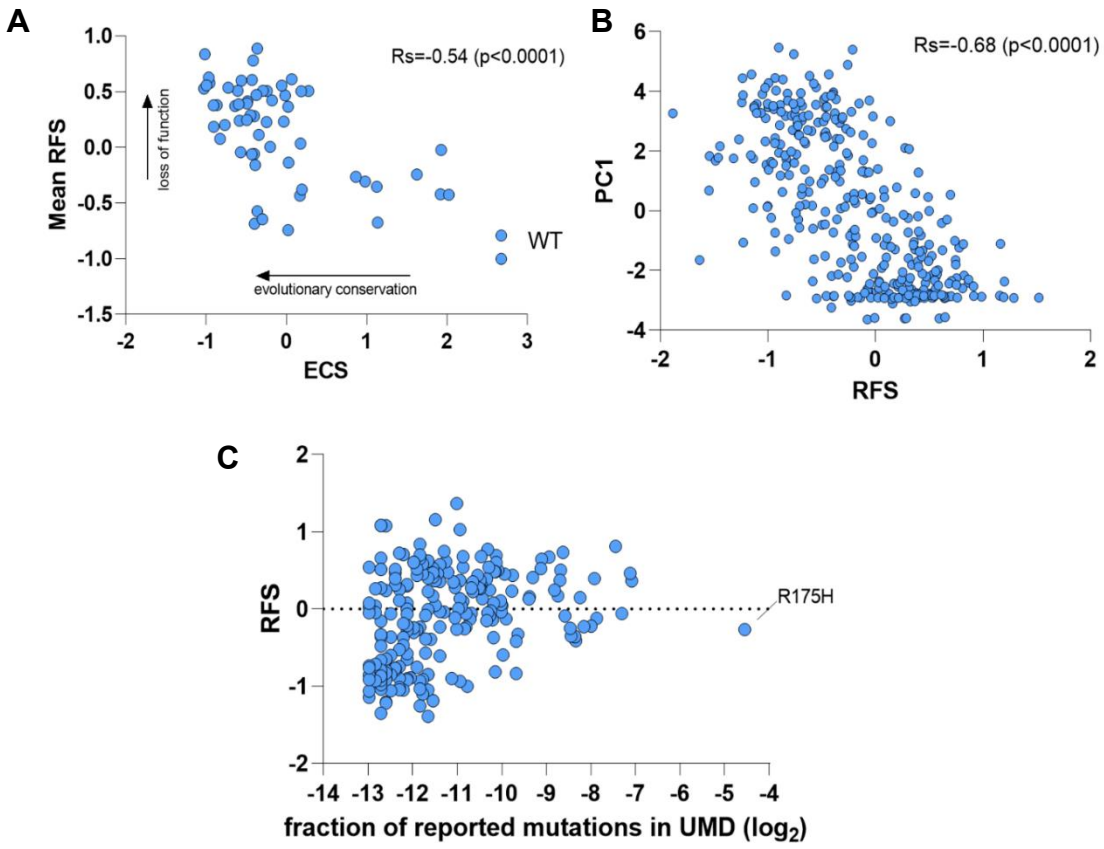

Figure 37. Functional effects measured by CSMS correlate with evolutionary conservation, transactivation capacity, and occurrence in cancer patients

A. Evolutionary conservation score (ECS) was computed for every residue encoded by the 5th exon using ConSurf 2016 and plotted against corresponding mean RFS values (calculated for each amino acid position across all missense mutations). Rs, Spearman correlation coefficient. Analysis performed by Boris Klimovich. **B.** Data on transactivation of p53 response elements in yeast reporter system were extracted from the study of Kato (Kato et al., 2002) and subjected to the principal component analysis using ClustVis. The resulting PC1 values were plotted against RFS. Rs, Spearman correlation coefficient. Analysis performed by Boris Klimovich. **C.** RFS values for exon 5 mutants are plotted against their relative abundance in human tumor specimens (from the UMD database, Log2-transformed).

some residues (e.g., 162-163, 173, 179). Importantly, the cluster of mutagenesis-tolerant residues (C182-S185), as well as mutagenesis-sensitive Zn-coordinating residues C176 and H179, were already revealed in the experiment with the H1 helix library. Therefore, our high-content assay displayed a similar phenotypic response to mutagenesis compared to low-content validation experiments.

Importantly, clusters of mutagenesis-sensitive residues contained the positions most frequently mutated in cancers (orange bars, Fig. 38). Taken together, analysis of the exon 5 dataset demonstrated that the CSMS platform allows the fast and simple generation of large libraries of p53 mutants. We were able to measure the functional consequences of more than 1000 protein variants in a single high-content screening experiment. We have revealed strong associations between our functional classification, evolutionary conservation, transactivating properties, mutation prevalence in human tumors, and results of our validation experiments. Despite remarkable results achieved in this experiment, further improvements are needed to increase the classification accuracy of the high-content CSMS protocol.

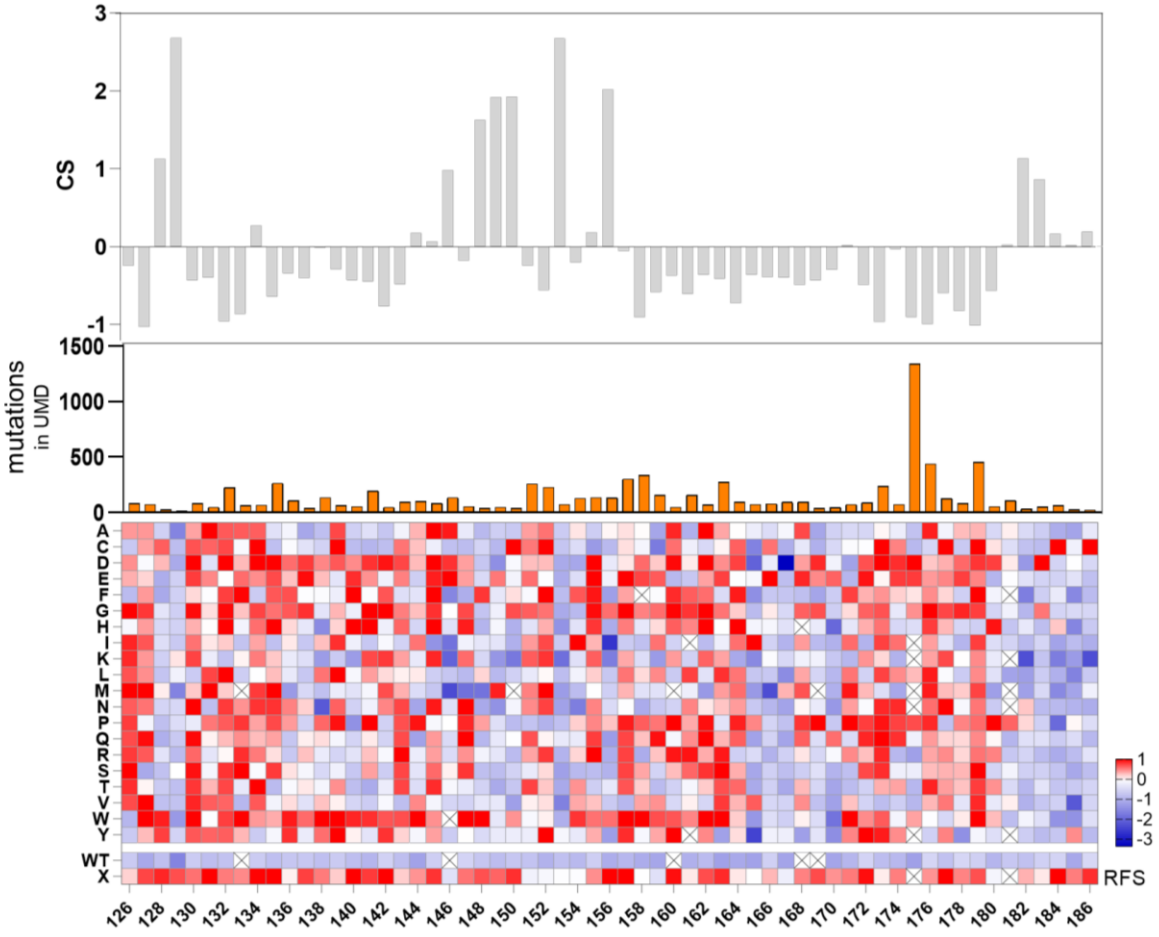

Figure 38. CSMS captures the impact of 3646 mutations on the anti-proliferative capacity of p53

Triplicate cultures of adeno-Cre-infected cell libraries were treated with nutlin for 8 days. Heatmap depicts RFS for each protein variant. Grey bars on top show conservation score (CS) at each position across all tumor types (data from ConSurf). Orange bars below show the prevalence of mutations at each position across all tumor types (data from UMD). Synonymous and nonsense variants are shown separately, missing data points are labeled with X.

3.13 Comparison of functional classification of exon 5 mutations derived from CRISPR- and cDNA-based screening experiments

3.13.1 *CSMS outperforms the cDNA-based method in the classification of rare patient-derived mutations of H1 helix*

To better understand the ability of CSMS to predict the tumorigenic potential of *TP53* mutations, we have compared CSMS-derived classification patterns of p53 mutations with the recently published dataset from the study of Kotler et al. The authors established the cDNA library encoding >10 000 of p53 variants. They delivered it into p53-negative H1299 cells using lentiviral infection and cultured cells for two weeks. Afterward, the relative abundance of each mutation was quantified using deep sequencing. The depletion or enrichment of variants after two weeks of cultivation was used as a measure of antiproliferative capacity. On the contrary to our experiments, no treatment with MDM2-inhibitors or other compounds was performed. We have extracted corresponding enrichment scores for all protein variants present in our dataset and plotted them against CSMS-derived RFS values (Table S3 from Kotler et al, 2019).

First, we have compared enrichment scores for all mutations at position 175. Noteworthy, both methods yielded a very similar pattern of enrichment and depletion: synonymous variants were strongly depleted in both datasets, whereas nonsense variants and the most frequent cancer-derived variant R175H were enriched. Interestingly, the cDNA-based screen scored several variants as wild-type-like, whereas in CSMS these variants were enriched as strong as LOF mutants. Such discordant classification raised the question, which estimation is correct. Importantly, among these mutations (shown in the lower right quadrant on Fig. 39A), two were repeatedly recovered from tumor samples: R175P and R175L (12 and 74 records in the UMD database, respectively). R175L was described as a germline mutation associated with adrenal cortical carcinoma (West et al. 2006). R175P is a partial-LOF variant (Crook et al., 1994; Ludwig et al., 1996; Rowan et al., 1996), whose mouse analog (R172P) was reported as tumorigenic in a knock-in model (Liu et al. 2004). Hence, CSMS correctly identified these two variants as pathogenic, whereas the cDNA-based system misclassified them as benign.

Next, we have expanded our analysis to the H1 helix dataset. We have listed all missense mutations from H1 helix found in human tumors and compared the classification of these mutations made by CSMS and cDNA-based screening (Fig.

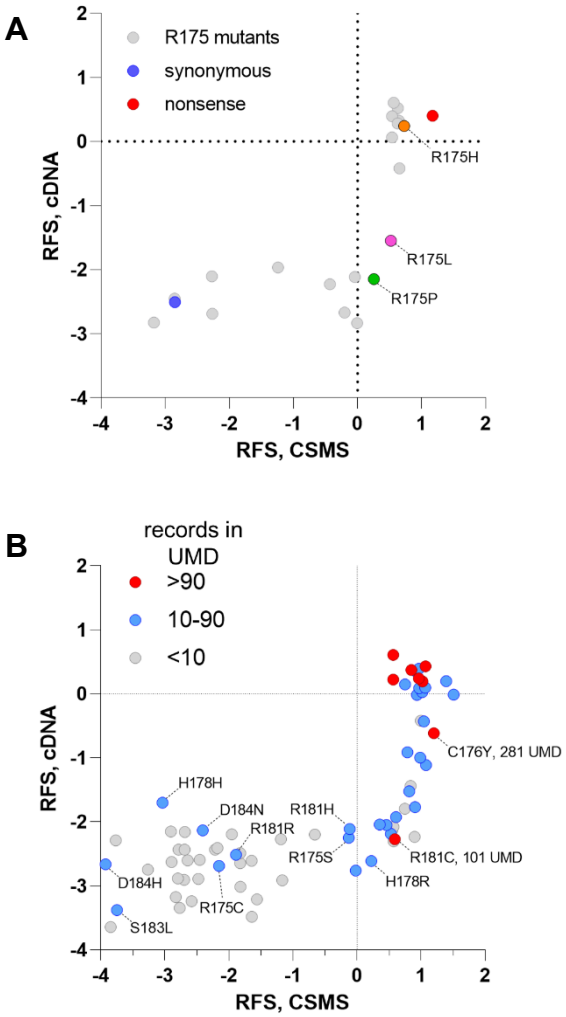

Figure 39. CSMS outperforms cDNA-based screening in classification of the pathogenic mutations in the H1 helix

A, B. CSMS-derived RFS values form the R175 (A) and H1 helix (B) datasets are plotted against corresponding RFS values extracted from the cDNA-based study (Kotler et al., 2019). **A.** Synonymous and nonsense mutations are presented as mean RFS values of all corresponding variants (10 synonymous and 10 nonsense). R175P (green) and R175L (violet) are two mutations with documented residual activities. **B.** H1 helix mutations are color-coded according to their prevalence in cancer patients (from the UMD database). Individual mutations discussed in the text are labeled.

39B). All variants retrieved from more than 90 tumor samples and therefore being undoubtedly cancer-predisposing, were classified as loss of function by CSMS

(enrichment score >0, red dots). However, the cDNA-based analysis failed to predict loss of functionality for two *bona fide* cancer-driving mutations (C176Y and R181C (281 and 101 UMD records respectively, the pathogenicity of the R181C was recently confirmed in a mouse model (Kang et al. 2020). Less frequent H1 helix mutations found in 10-90 patients still can be considered as likely cancer-predisposing. In good agreement with this, 71% of them were classified as loss of function by CSMS (blue dots). In contrast, just 8 of them (26%) were scored as LOF in the study of Kotler. Data from the literature imply that the scoring of the rest 29% of intermediate-frequency variants as wild-type-like is also correct. For example, mutation R181H is relatively abundant in patients (80 UMD records), lies in the “grey zone” in the CSMS dataset, but is scored as wild-type-like in the cDNA screen. This is a temperature-sensitive mutant, which exhibits normal properties at 30ºC and, therefore, can exhibit residual activity but is nevertheless tumor-promoting (Soussi et al. 2005). Relatively abundant variant D184N (41 UMD *TP53* records) is a known natural benign SNP (Wang et al. 2013). Two variants: D184H and S183L, were shown to retain 60-100% of transactivation of most of the promoters in the study of Kato et al. (Kato S. et al. 2003) and are classified by both screenings as more active than two synonymous variants annotated in the UMD database (H178H and P177P), being most obviously passenger variants or sequencing artifacts. Most variants found in less than ten tumor samples, being more likely neutral passenger mutations or sequencing errors (grey circles), are consistently classified by both studies as wild-type-like, demonstrating that the CSMS system does not over-estimate LOF properties of mutants. Finally, we have compared the classification of 532 cancer-associated variants inferred from our exon 5 CSMS dataset with the cDNA-based screening outcome (Fig. 40). As expected, both systems classified most of the very rare variants (<10 UMD records, grey dots) as wild-type-like (227 variants), and only 25 of them were classified by both screenings as LOF, suggesting that most of these mutations are either sequencing errors or neutral passenger mutations. 39 variants were scored by two systems discordantly: 29 variants were classified as LOF only by the CSMS, and 10 only by the cDNA screen. Thus, the high-throughput CSMS could overrate LOF properties of mutants compared to the cDNA-based system. Among protein variants with the intermediate frequency (11-90 UMD records (potentially

tumorigenic) both systems classified 40% as functional and 23% as non-functional (72 and 43 variants, respectively). Amid discordantly classified mutations, 43 were scored as LOF only by CSMS and 22 only by cDNA-based analysis.

Out of 32 *bona fide* cancer-driving mutations (>90 UMD records), 13 were consistently classified by both methods as LOF. For other variants, two experiments provided contradictory classification. As noted in section 3.9, the most frequent hotspot mutant R175H was unexpectedly depleted in the CSMS (RFS=-0.26). Seven other variants were scored by the CSMS as functional (depleted), while cDNA-screen scored them as LOF (Y163C, H179Y, V173M, P151S, C135Y, K132R, Y126C). 7 of these mutants had CSMS-derived RFS values markedly higher than synonymous variants (-0.22±0.12 versus -0.89±0.2), demonstrating moderate depletion. One mutant (Y126C, 98 UMD records) was depleted in CSMS to a degree comparable to synonymous variants (mean RFS -0.83 versus -0.88). This mutation was characterized in several studies as LOF (Kato et al. 2003; Monti et al. 2011; Shi

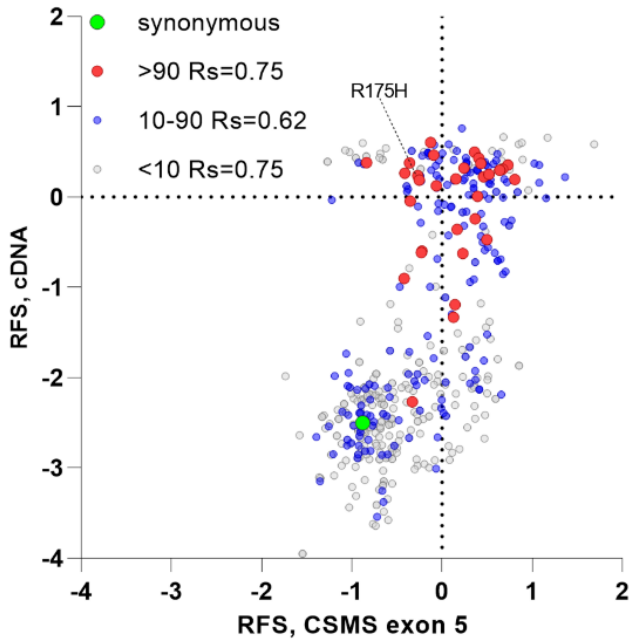

Figure 40. Comparison of CSMS- and cDNA-based classification of exon 5 mutants

CSMS-derived RFS values are plotted against corresponding RFS values extracted from Kotler et al., 2019 Mutations are color-coded according to their prevalence in cancer patients (from the UMD database). Green dot – mean RFS value of all synonymous variants. Rs, Spearman correlation coefficient.

et al. 2002; Grochova et al. 2008) and therefore is falsely classified as functional by the CSMS.

The opposite classification (LOF in CSMS and wild-type-like in the cDNA screen) was derived for six mutants (G154V, C135F, A161T, V143M, P152L, and R156P).arge

Interestingly, both screenings have classified five variants frequently found in tumors as partially functional: R158H, C176Y, C141Y, R181C, P151H (315, 281, 230 101, and 98 UMD records, respectively). RFS values for these mutants (red dots in the lower right quadrant in Fig. 40) were higher than of synonymous variants but below zero in both screenings. According to the ClinVar database, all these variants were recovered from patients with hereditary cancer predisposition, attesting them as cancer-driving. However, several of them were shown to retain residual functions. For example, R158H demonstrated transactivating capacity and growth-suppressing activity (Campomenosi et al. 2001; Wasserman et al. 2015; Monti et al. 2011). R181C has been described as a cancer-predisposing variant in the mouse model; however, the phenotype conferred by this mutation was mild compared to the p53-null allele (30% reduction of median survival, 25% increase in cancer incidence) (Kang et al. 2020). Therefore, the classification of these two mutants as partially functional seems plausible. Importantly, R181C was undoubtedly scored as LOF in our H1 helix dataset (Fig. 29C), as well as the other clearly tumorigenic variant from the group: C176Y.

Taken together, our comparison of the exon 5-CSMS dataset with the study of Kotler demonstrates that both systems classify many p53 variants in good agreement with their incidence in cancer patients. Both approaches generated discrepant classification of many mutants abundant in tumor samples. Notably, several of these mutants were classified in the low-content H1 helix dataset as tumorigenic, whereas cDNA-based screening scored them as benign. This implies that CSMS is potentially more accurate in classifying p53 mutants and calls for further optimization of the high-content screening protocol.

3.13.2 *CSMS outperforms in silico prediction tools in categorizing of pathogenic p53 variants*

The introduction of multi-gene panel testing led to the identification of rare *TP53* variants of uncertain clinical significance. Bioinformatic predictors are valuable tools for estimating pathogenicity of mutations that were neither reported in families with Li-Fraumeni syndrome nor tested experimentally. The IARC *TP53* and UMD *TP53* databases contain predictions made by seven tools: SIFT, Polyphen2, REVEL, BayesDel, Mutassessor, Provean, and Align-GVGD. SIFT and Mutassessor use evolutionary conservation to predict mutations affecting protein functions. Align-GVGD and Polyphen2 utilize a combination of evolutionary conservation with biochemical and structural information. REVEL and BayesDel combine multiple algorithms (SIFT, REVEL, Polyphen, and others) for predictions (Leroy et al. 2013; Hicks et al. 2011; Adzhubei et al. 2010; Ramensky et al. 2002; Sunyaev et al. 1999; Vaser et al. 2016; Sim et al. 2012; Ioannidis et al. 2016; Choi 2012; Choi et al. 2012; Reva et al. 2007, 2011).

Although instrumental, such tools have important limitations: they do not include functional test results and do not predict the response of mutation-carrying cancer cells to therapy. To our knowledge, no systematical comparison of the performance of the *in silico* predictors with high-content cell-based functional assays has been made.

We, therefore, assessed how the effects of mutations measured *in vitro* by CSMS correlate with *in silico*-predicted impact.

First, we have extracted values computed by three *in silico* predictors (SIFT, Provean, and Mutassessor) from the UMD database and plotted them against RFS scores from the H1 helix CSMS dataset (we did not use the Polyphen2 scoring because it separates variants in just three classes) (Fig. 40A). This comparison revealed that most of the H1 helix mutations enriched in the CSMS dataset (RFS>0) were accordingly classified as damaging by all three tools tested (lower right quadrant on each diagram). However, partial-LOF and wild-type-like variants that were depleted in the CSMS screening have demonstrated inconsistent classification by algorithms: approximately half of these variants were scored as tolerated and half as damaging. Mutassessor predicted 4 neutral mutations, SIFT and Provean 13,

whereas CSMS discovered 21 mutations with no apparent impact on protein function (RFS below mean score of synonymous mutants (<-2,5).

Next, we have extended our analysis to the complete exon 5 dataset. As shown in Fig. 41B, CSMS and all algorithms tested agreed on the classification of the substantial number of mutants as LOF (lower right quadrant). Similar to the H1 helix dataset, half of the variants with negative RFS (tolerated) were classified by all algorithms as deleterious. Therefore, our comparison revealed a substantial discrepancy: all three predictive algorithms significantly overrated the number of deleterious variants by contrast to the functional test**.**

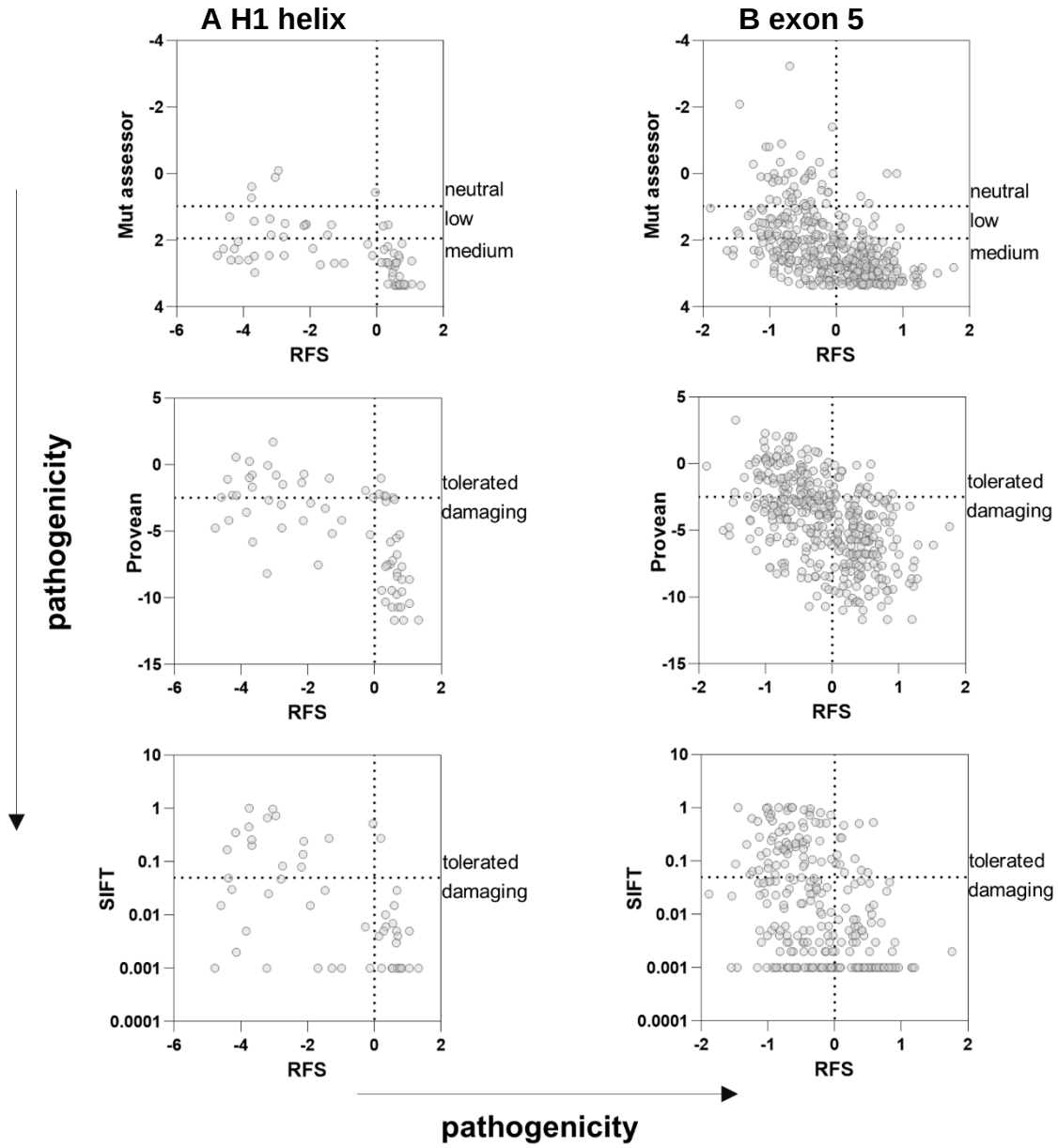

Figure 41. Comparison of the CSMS-based classification of H1 helix (A) and exon 5 (B) variants with pathogenicity estimations made by 3 in silico predictors (Mutassessor, Provean, and SIFT)

RFS values are plotted against corresponding scores. Dotted lines show specific threshold values for each of the methods: Mutassessor: <0.8 – neutral mutation, 0.98-1.935 – low probability of pathogenicity, >1.95 – the medium probability of pathogenicity. Provean: <-2.5 – deleterious mutation, >-2.5 – neutral mutation. SIFT: >0.05 – tolerated mutation, <0.05 – damaging mutation- CSMS: <0 – depleted, >0 – enriched. Analysis by courtesy of Boris Klimovich.

Next, we have compared CSMS-derived RFS values with the estimates made by two

pathogenicity predictors: Align GVGD and BayesDel. A combination of these scoring algorithms was shown to be the most accurate method for in silico categorization (Fortuno et al. 2018). Align GVGD assigns a class value to each mutation (from 0 to 65, where 0 is the strongest evidence for benign impact, and 65 is the strongest evidence for pathogenic impact). Fortuno and colleagues defined optimal cut-off parameters: Align GVGD class >15 and BayesDel score >0,16. We have extracted both values for each mutant from the IARC database (geneVariationIARC *TP53* dataset), filtered all mutations with BayesDel score >0,16, and plotted 208 variants against corresponding RFS values extracted from the CSMS exon 5 dataset. Additionally, we have plotted corresponding RFS values from our most rigorously validated H1 helix dataset (Fig. 42). The resulting plot depicts all variants from exon 5 having moderate to strong evidence of pathogenicity (Align GVGD class >15, BayesDel >0,16) and their corresponding RFS from the two CSMS experiments.

Values from the exon 5 dataset were scattered around RFS=0 (red dots), demonstrating no consistent pattern. Although CSMS and Align GVGD coherently classified many variants as LOF (class >15, RFS>0), a substantial number of variants with the highest probability of loss-of-function (class 65) were scored as benign by CSMS (RFS<0, 39 of 116 mutants). When we overlaid values from the H1 helix dataset on the Align GVGD-BayesDel classification (blue dots) we revealed that 20% of mutants (6 out of 27) belonging to class 65 were scored by the CSMS as functional. Among them, the H178Y was depleted below the average level of synonymous variants (-4.8 versus -2.5) and is most probably benign (2 UMD records), whereas the other five variants had intermediate depletion (from -0.8 to -2.1). Additionally, among other possibly pathogenic variants (class 25-55) 4 were classified in the CSMS-H1 helix dataset as wild-type-like, 2 as intermediate (RFS≈0), and only 2 as LOF. Finally, two mutations falling into class 15 (uncertain pathogenicity) were classified by the CSMS as LOF and were in
deed recurrently found in cancer patients (H179Q: RFS 0.7, 91 UMD records, H178Q: RFS 0.6, 18 UMD records).

Therefore, the most advanced predictive approach failed to identify two likely pathogenic variants and simultaneously erroneously classified many benign mutations as damaging. Summarizing, our observations very clearly demonstrate

that the CSMS provides more accurate estimates of pathogenicity of *TP53* mutations than any of the existing in silico prediction tools.

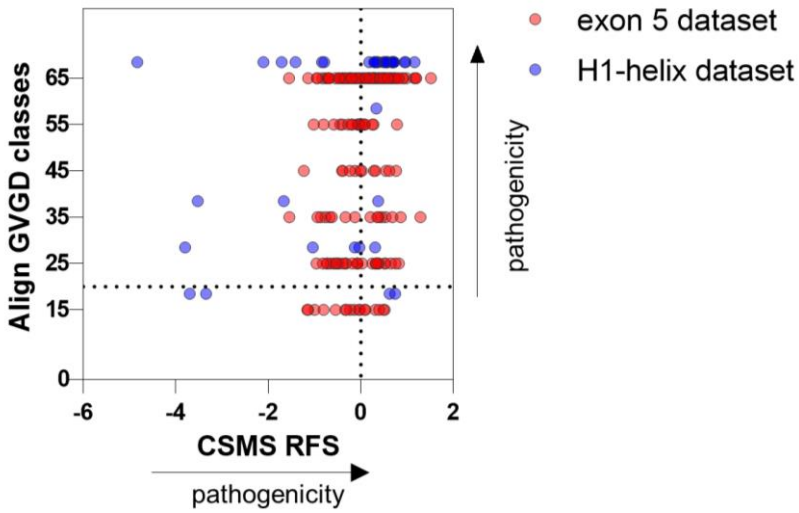

Figure 42. Comparison of the CSMS-based classification of exon 5 variants with pathogenicity prediction made by the combined Aligh GVGD-BayesDel algorithm (Fortuno et al., 2018)

The plot depicts all variants from the exon 5 dataset having moderate to strong evidence of pathogenicity (red dots) (Align GVGD class >15, BayesDel >0,16) (located above the dotted line). X-axis – CSMS-RFS, Y-axis – Align GVGD classes. The higher is the class – the stronger is the evidence for pathogenicity. Additionally, all variants from the H1 helix dataset are plotted (blue dots). Analysis by courtesy of Boris Klimovich.

Note that many H1 helix mutants undoubtedly classified as benign by the CSMS, have the highest Align GVGD class.

4. Discussion

Comprehensive functional classification of recurrent cancer-associated *TP53* alterations can improve clinical decision-making (Sabapathy and Lane 2018; Cheok and Lane 2017). Compelling evidence suggests that information about individual *TP53* mutations can be useful for predicting the disease course, chemo- and radiotherapy response, and ultimately patient survival (Campling and El-Deiry 2003; Schon and Tischkowitz 2018; Richter-Pechańska et al. 2017; Murakami et al. 2000; Hamelin et al. 1994; Zhu et al. 2020). The development of numerous p53-targeting therapeutics further increases the value of the detailed characterization of *TP53* mutations (Mantovani et al. 2017; Di Agostino et al. 2019). For example, *TP53* status is the main eligibility criteria for clinical trials of MDM2 inhibitors (Jiang and Zawacka-Pankau 2020). The inclusion of mutant p53 in the list of actionable targets requires precise characterization of the full spectrum of p53 variants beyond the most frequent hotspot mutations.

Two recent studies have performed a thorough investigation of the p53 mutome and substantially updated the catalog of p53 variants (Kotler et al. 2018; Giacomelli et al. 2018). One severe limitation of these studies is the employment of lentiviral cDNA libraries to express p53 protein variants. Expression of the transgene from heterologous promoters may result in non-physiological protein levels and, consequently, in biased classification. Moreover, such an experimental setting excludes many other variables from the analysis, such as mutations in non-coding regions and splicing sites, p53 isoforms and miRNA-dependent regulation of the transcript stability (Feng et al. 2011).

We aimed to create an improved phenotypic screening system that probes the effects of multiple *TP53* mutations in the native genomic context. As a result, we have developed the CRISPR-based saturated mutagenesis screening, a high-throughput protocol that enables precise functional characterization of thousands of p53 variants.

4.1 CSMS: a novel system for high-content functional classification of *TP53* mutations

We have envisioned a screening system where p53 mutations are targeted into the *TP53* locus using CRISPR-Cas9-induced homology-directed repair. Although numerous attempts to improve HDR-driven genome editing were undertaken, its inherently low frequency remains a major obstacle for high-content applications (Lin et al. 2014). To overcome this limitation, we have engineered the original cell line (HCT-116$^{\Delta/TP53E}$) to achieve the highest possible gene editing efficiency. The resulting cell line became a cornerstone of the CSMS platform and had several important features. It enables editing of the single *TP53* locus in each cell by using an allele-specific CRISPR-nuclease. During the editing process, the allele is inactive, which ensures the editing in the absence of the efficiency-limiting p53-induced DNA damage response (Bowden et al. 2020; Haapaniemi et al. 2018; Ihry et al. 2018).

Multiple approaches were attempted to enhance HDR-mediated gene editing efficiency, for example, chemical or genetic modulation of mediators of DNA repair, usage of mutant Cas9 variants, and conjugation of Cas9 nuclease with oligonucleotides (Liu et al. 2018; Nambiar et al. 2019). Most of these improvements lead to several-fold increased HDR frequency (up to roughly 30%, reviewed in (Ling et al. 2020; Liu et al. 2018). Our protocol achieved a very high editing rate (80%, Fig. 10A). The simplicity of the protocol and the underlying mechanism (p53 inactivation and selection of recombined cells with puromycin) suggests that this approach can be easily adapted for other cell lines.

We have demonstrated the efficient generation of cell lines carrying multiple individual p53 variants (Fig. 11), implying that our protocol can be used to generate large panels of isogenic cell lines rapidly. CRISPR-Cas9 technology was previously used to perform saturation mutagenesis of tumor suppressor genes (BRCA1) (Findlay et al. 2018; Kweon et al. 2020) and oncogenes (BCR-ABL) (Ma et al. 2017) and to introduce single point mutations into the *TP53* locus (Boettcher et al. 2019). To our knowledge, the present work is the first successful attempt of CRISPR-mediated saturation mutagenesis of the endogenous *TP53* locus.

Editing of the single *TP53* allele in the HCT-116$^{\Delta/TP53E}$ cell line ensured unambiguous genotype-phenotype correlation. The drawback of this approach is a reduced level of p53 expression evident in Fig. 7. P53 is the haploinsufficient tumor suppressor: lack of one gene copy reduces transcript levels up to 4-fold, decreases protein levels, and impairs DNA damage response (Lynch and Milner 2006; Teoh et al. 2014). Reduction of gene dosage was shown to accelerate carcinogen-induced tumor formation (Venkatachalam et al. 2001). Consequently, decreased basal expression levels in the HCT-116$^{\Delta/TP53E}$ cells compared to the parental line could reduce functionality, blunted transactivation, and apoptosis resistance. This, in turn, could lead to the misclassification of wild type-like variants as LOF or pLOF. However, our analysis has clearly demonstrated that wild-type variants were markedly depleted from cellular libraries even without additional stabilization with nutlin (Fig. 17A, 27B), suggesting adequate expression levels. Data shown in Fig. 39 demonstrate that most of the rare tumor-associated variants (found in less than 10 samples) are classified by CSMS as wild-type (28 out of 35) in good agreement with the cDNA-based screening (Kotler, 2019). This further substantiates that the p53 expression level in the cell line is sufficient to drive a full-blown p53-mediated response and that the CSMS does not overestimate the pathogenicity of neutral variants.

We have performed a comprehensive evaluation of the performance of the CSMS protocol by conducting saturation mutagenesis of codon R175 and, subsequently, of the H1-helix. Encouragingly, we have confirmed the reproducible introduction of both libraries into the *TP53* locus (Fig. 14, 27). Analysis of variant dynamics in the cell population after treatment with a panel of MDM2 inhibitors revealed the excellent performance of the screening system. All variants with an expected loss of function (nonsense, R175 codon deletion, as well as the most frequent cancer-associated variant R175H) were strongly enriched after treatment, whereas synonymous mutations were eliminated, supporting the robustness of measurements (Fig. 12). The comparison of the CSMS results with the prevalence of mutations in human tumors further confirmed the outstanding ability of the workflow to identify pathogenic mutants: most of the cancer-associated H1-helix variants were scored as LOF (Fig. 29D).

4.2 CSMS grasps the complexity of the TP53 mutome: classification of rare pLOF and wt-like variants

Correct estimation of LOF phenotype by the CSMS would not be sufficient for reliable categorization of the plethora of p53 variants. To produce clinically-relevant predictions, the system should capture the complex of natural phenotypic diversity of the p53 mutome and provide sufficient resolution to separate mutants with partially-retained functionality form truly LOF and fully functional variants. Reassuringly, in all our experiments, synonymous (fully functional) variants were reproducibly depleted form the library to a much higher degree than missense mutants concordant with their fully preserved anti-proliferative functions (Fig. 17C, 29A, 36A). This underlines the reliable identification of neutral mutations, which is critical for distinguishing between non-damaging passenger variants and genuine driver mutations. Discriminating driver and passenger mutations is a considerable challenge for cancer genomics. Driver mutations affect critical positions in tumor suppressor genes or oncogenes, support transformation, and confer growth advantage, whereas passenger mutations are randomly scattered across the genome and confer no malignant traits. A good demonstration of the power of the CSMS in identifying passenger mutations is the R175C variant. Despite being a clear cancer-associated mutant (71 UMD records), it was classified as wt-like by the CSMS (Fig. 17C). Further analysis of published data confirmed the intact functionality of the variant (Fig. 18) (Ryan and Vousden 1998; Flaman et al. 1998; Blagosklonny 1997; Ory et al. 1994; Blagosklonny 2002). Several other lines of evidence further support that the R175C is a neutral passenger variant. First, 30% of tumors with this mutation have other *TP53* alterations. Second, this variant has never been described as a germline mutation (Leroy et al. 2014a). Third, mutation R175C originates from C>T transition at the methylated CpG site, which is the most frequent mutation signature of *TP53* (Giacomelli et al. 2018). The other transition type, G>A, happens at a similar rate. Therefore, mutations generated by these two transition types are expected to arise with equal probability. This holds true for hotspot codons 248 and 273. Variant pairs R248Q-R248W and R273H-R273C have similar frequencies and share LOF phenotype (2562, 2003, 2361, and 2214 UMD records, respectively). However, R175H mutation originating from G>A transition is 50 times more frequent than the

R175C. Therefore, R175C mutation is not selected during neoplastic transformation and is a neutral passenger variant. Notably, the benign phenotype of R175C could not be deduced from the variant occurrence in cancer patients or from *in silico* predictors (Fig. 18A). Conversely, direct functional measurement inferred from the CSMS unambiguously identified the mutant as benign, again underscoring the utility of the system.

Detailed analysis of the H1-helix dataset further showcased the excellent ability of the CSMS to explore the complex mutational landscape of *TP53*.

CSMS revealed a mutagenesis-resistant region in H1-helix (C182-S185): almost all substitutions at these positions were classified as non-damaging (Fig. 29A). Among these residues, two are highly conserved: S183 is found in all mammals, whereas D184 is almost invariant among 99 animal species (Sulak et al). Highly conservative residues in p53 are frequently mutated in tumors in line with their functional importance (Baugh et al. 2018). The p53 protein contains 64 amino acid residues that are conserved in all vertebrates. Most of these residues are frequently mutated in cancers (between 25 and >2,000 UMD records) (Soussi 2014). However, missense mutations F19 and W23 have never been reported in cancer. These residues are essential for the binding of MDM2 to p53; therefore, any substitutions at these positions would be lethal for the cell due to uncontrolled p53 stabilization (Kussie et al. 1996). Likewise, missense mutations at conserved positions D184 and S183 are strikingly rare. The UMD database contains only 73 mutations at D184 and 19 at S183 (the mean frequency of missense mutations in DBD is 287 per residue). Collectively this indicates that alterations at position 184 do not give a fitness advantage and do not lead to enhanced tumorigenesis. Similar to D184, missense mutations of the conserved residue S183 were eliminated from the cell library in the screening, as well as mutations at S185. Phosphorylation of the S183 by Aurora B kinase was shown to stimulate p53 degradation (Gully et al. 2012). The recent report from our group further supported the data on the inhibitory role of phosphorylation of S183/S185. Timofeev and colleagues reported on the mouse knock-in model of the phosphorylation-deficient mutant p53 S180A (unlike a human, mice have one serine residue in H1 helix). Cells expressing S180A demonstrated enforced DNA binding and increased transactivation of target genes. Elevated p53 activity translated into a

reduced incidence of spontaneous and oncogene-induced cancer. Interestingly, despite lower susceptibility to cancer, S180A mice demonstrated shortened lifespan due to accelerated aging (Timofeev et al. 2020). These results were also confirmed in human HCT-116 cells. Isogenic cell lines expressing the double phospho-deficient mutant (S183A, S185A) were generated by the author using the procedure described in section 3.5. HCT-116$^{\Delta/TP53S183A,\ S185A}$ cells demonstrated enhanced target gene expression and apoptosis in response to DNA damage. Taken together, these results strongly suggest that phosphorylation of S183 and S185 have inhibitory effects on p53 function; therefore, alterations at these positions are expected to be benign in good agreement with CSMS predictions, which explains their low frequency in human tumors.

Finally, alterations at C182 were previously shown to have a minor effect on p53 functionality, in good agreement with our data (Stoner et al. 2009; Eldar et al. 2013; Kaar et al. 2010). In summary, the discovery of the mutagenesis-resistant region (C182-S185) in the H1-helix made by CSMS is supported by several lines of evidence, including the cDNA-based screening (Kotler et al.), functional data from animal models, and clinical observations. This further demonstrates that the CSMS protocol correctly classifies neutral *TP53* variants. Reliable identification of benign mutations has an important medical implication. Although rarely, such mutations are found in human tumors. For example, the UMD database contains 157 cases with missense mutations at mutagenesis-resistant positions C182-S185.

Moreover, the UMD database contains 187 cases with mutations in H1-helix classified by the CSMS as neutral. Such mutations must be considered wild-type, and patients carrying them can profit from therapy with MDM2 inhibitors and should be included in clinical trials. Furthermore, detection of such benign p53 variant in the germline of a cancer patient would indicate a lack of inherited cancer predisposition (if no other predisposing mutations (e.g., in *BRCA1/2*) are also not found). Therefore, family members of such individuals do not have an elevated risk of developing cancer, do not need to be screened for this variant, and can evade unnecessary screening procedures and preventive measures (e.g., prophylactic mastectomy).

Closer examination of the mutational effects within positions E180 and R181 underlined the exquisite ability of the CSMS to detect partially-functional p53 variants. Residues E180 and R181 form a salt bridge between two adjacent monomers in the DNA-bound tetramer (Ma and Levine 2007; Dehner et al. 2005). Alterations at these positions modulate DNA binding cooperativity and were extensively studied by our group and others (Madhumalar et al. 2009; Schlereth et al. 2010a; Timofeev et al. 2013). Therefore, these positions are especially suited for the characterization of partially-active mutants because comprehensive data on DNA binding for multiple variants are available. The fitness advantage conferred by eight distinct mutations revealed a striking correlation with DNA binding strength inferred from biochemical studies (Fig. 29C) (Schlereth et al. 2010a). Among 8 mutants, the R181L showed antiproliferative capacity mostly similar to the wild-type. This is a well-characterized tumor-associated apoptosis-deficient partial-LOF mutant with preserved transactivation of certain target genes (*CDKN1A*, *MDM2*) and the ability to activate cell cycle arrest (Ludwig et al. 1996; Schlereth et al. 2010a). The other well-characterized pLOF mutant in H1-helix is E180R. It also demonstrated a selective apoptotic defect and retained the cell cycle arrest (Timofeev et al. 2013; Klimovich et al. 2019). Importantly, its DNA binding was weaker than of R181L (Schlereth et al. 2010a; Schlereth et al. 2010b). In good agreement with weaker DNA binding, E180R was depleted from the library significantly weaker than the R181L.

In the work of Schlereth and coauthors, tumor-suppressive properties of other H1 helix mutants inferred from DNA binding strength, transactivation of p53 response elements, and proapoptotic activity declined in the order WT > R181L > R181H > R181C > E180K > R181P. Strikingly, the CSMS-derived measurement of the activity of protein variants reproduced precisely the same pattern, justifying the single CSMS screening ability to replace a multitude of functional assays to decipher the complex landscape of p53 mutants.

4.3 High-content CSMS protocol: advantages and limitations

Successful validation of the CSMS performance using the R175 and H1-helix datasets prompted us to establish the high-throughput CSMS workflow to perform a comprehensive analysis of thousands of p53 variants. The CSMS design enabled a

relatively simple scale-up of the procedure. We have engineered a novel targeting vector to accommodate large 230-bp long oligonucleotides spanning the whole 5th exon and increased the number of cultured cells and input DNA used for the sequencing library construction to compensate for the increase in library complexity. Importantly, the same system can be easily employed for extended analysis to the complete DNA binding domain encoded by a relatively short region (exons 5-8 span 1,5 kb). For this purpose, one would need to design a set of targeting vectors with extended homology arms spanning the region between intron 4 and intron 9. Because the maximum size of synthetic oligonucleotides slightly exceeds 200 nucleotides, each exon will be targeted by a separate vector. Therefore, each of the 3 vectors needs two recognition sites for type IIs restriction enzymes flanking corresponding exons for cloning oligonucleotides using the Golden Gate protocol. Since the probability of homologous recombination significantly decreases with the distance from the double-strand break, additional modification of HCT-116$^{\Delta/TP53E}$ cell line might be needed to ensure efficient editing. Specifically, the generation of a novel recognition site for the allele-specific CRISPR-nuclease could be required to shift the location of the double-strand break closer to the region of interest. This can be achieved by transfecting HCT-116$^{\Delta/TP53E}$ cells with a CRISPR-nuclease specific to intron 7 or 8. Random nucleotide polymorphisms in the *TP53E* allele generated by non-homologous end joining can be used as a target for the allele-specific nuclease, as it is shown in Fig. 7 for exon 5. Finally, minor modifications of PCR protocols and bioinformatics pipeline will make the CSMS platform suitable for analysis of >90% of the complexity of the p53 mutome.

Analysis of the exon 5 dataset revealed that despite strongly increased library complexity, 99.79% of mutants were successfully integrated into the *TP53* locus, supporting the applicability of our methodology for high-content mutagenesis. However, a comparison of the scorings retrieved from the exon 5 dataset with the measurements made in the validation experiments (R175 and H1 helix libraries) showed substantial inconsistency between low- and high-throughput protocols (Fig. 36 B,D). We have observed markedly lower depletion of variants as a major source of these discrepancies and concluded that applying the high-content protocol resulted in decreased resolution between LOF and wild-type-like mutants (Fig. 36 C).

Most probably, this issue was a result of the suboptimal passaging schedule used during nutlin treatment. During two weeks of nutlin treatment, library-expressing cells were passaged with a low split ratio (1:2) to avoid accidental loss of rare mutations and maintain the complexity of the library. Passaging at high density can result in a decreased effective concentration of nutlin, ineffective killing of nutlin-sensitive cells, and consequently reduced depletion of wild-type-like variants. At the same time, the exponential outgrowth of resistant cells can be limited by high culture density. Both factors will reduce the dynamic range of the system.

Despite this technical issue, the relative fitness landscape derived from the high-throughput CSMS experiment was highly correlated with the study of Kotler and with the distribution of mutants in human tumor specimens (Fig. 39 and 40). This implies that we have successfully captured a large portion of phenotypic diversity in our cellular library.

We are convinced that simple measures can further improve the performance of the high-throughput protocol. Reducing cell density and prolonging the expansion of the population would enhance the separation of wild-type and LOF variants. Increasing the cell number and adding more replicates would reduce the drop out of mutations from the pool. Therefore, despite the need for minor protocol improvements, the CSMS has fully demonstrated its utility as a high-throughput phenotypic screening platform.

4.4 CSMS dissects distinct p53-dependent tumor-suppressive programs

Previously reported screening systems employed the antiproliferative activity as a single measure of p53 functionality (Giacomelli et al. 2018; Kotler et al. 2018). To demonstrate the value of CSMS for in-depth characterization of the p53 mutome, we have employed our system to dissect two p53-mediated programs, apoptosis and cell cycle arrest, in the context of the R175-variant library. To this end, we have performed two experiments described in section 3.8.1. In the first experiment, we have compared populations of cells treated with nutlin for a short or prolonged time and identified mutants, which were able to arrest proliferation temporarily but could

not kill cells by apoptosis (Fig. 20). In the second experiment, we have compared mutations prevalent among annexin V positive and negative library fractions after nutlin treatment to directly reveal apoptosis proficient and deficient mutants (Fig. 13 A,B). These experiments gave several interesting insights into the functional impact of R175 mutations. For example, the non-damaging tumor-associated variant R175C has demonstrated preserved proapoptotic activity in good agreement with published data, further confirming its benign properties (Xu-Monette et al. 2012; Ory et al. 1994). Interestingly, mutants R175C and R175S exhibited very similar transcriptional profiles in the study of Kato et al. (Fig. 18C,D) (Kato S. et al. 2003). However, they demonstrated distinct features in the annexin-V experiment. Apoptosis-proficient R175C was depleted to the level of wild-type, whereas R175S was apoptosis-deficient (Fig. 21B). This example clearly shows the advantage of phenotypical functional measurements.

Several apoptosis-deficient mutants recovered from the annexin-negative fraction (Fig. 21B, R175I/K/N/P/S) demonstrated remarkable behavior in the other experiment: they were moderately enriched after short nutlin treatment but progressively depleted upon more prolonged exposure, suggesting their ability to induce cell cycle arrest (Fig. 20B). Strikingly, all these mutants were previously shown to provoke cell cycle arrest when separately expressed in p53-negative Saos cells (Ryan and Vousden 1998). Moreover, the murine analog of R175P, R172P revealed similar properties in a mouse model (Liu 2004). These findings have further strengthened our confidence that CSMS is a powerful tool for the elaborate functional characterization of p53 variants. Two simple experiments allowed us to dissect between mutants proficient in the induction of cell cycle arrest or apoptosis in exceptional agreement with previous experimental observations.

Sorting of library-expressing cells according to the expression of a particular marker (as we did with annexin) is a simple and elegant approach to decipher complex genotype-phenotype correlations. The array of markers can be easily extended to quantify proliferation (EdU), DNA repair (γH2AX), the activity of certain promoters (using reporter genes), or even phosphorylation states (using phospho-specific antibodies) or metabolic conditions.

4.5 CSMS quantifies the impact of p53 mutations on cellular response to therapeutic agents

p53 plays a central role in apoptosis induction in response to DNA damage. Therefore, mutations in *TP53* confer resistance to chemo- and radiotherapy, which rely on DNA damage induction(Stiewe and Haran 2018; Hientz et al. 2017; Zhou et al. 2019). Besides reduced sensitivity to apoptosis, various GOF mechanisms have been implicated in protecting cancer cells from chemotherapy-induced death (He et al. 2017; Blandino et al. 1999; Keshelava et al. 2000; Zhang et al. 2020). However, little is known about the impact of non-hotspot mutations on therapy resistance. Considering the complexity of the p53 mutome and the multitude of mutant p53 protein interactions with binding partners and the genome, a systematic characterization of the drug resistance phenotype conferred by multiple p53 mutations has an important clinical implication.

p53-reactivating compounds can potentially tackle mutant p53-induced drug resistance. Some p53 reactivators are directed against specific mutants (for example, PK083 and NSC319726 target Y220C and R175H, respectively), whereas other molecules affect a broader spectrum of variants (for example, APR-246) (Bykov and Wiman 2014). All emerging mutant p53-targeting therapeutics have been tested on several exemplary hotspot mutants, and none of them was systematically assayed with multiple protein variants in an isogenic context.

Previous functional studies of the p53 mutome did not address the issue of drug resistance. In the work of Kotler and colleagues, the proliferation of untreated cells was used as a readout. In the Giacomelli study, cells were treated with nutlin or etoposide; however, etoposide treatment was used solely to identify wild-type-like variants. Therefore, we have utilized the CSMS to investigate the influence of p53 mutations on the response to therapeutic agents. Besides treating the library with the non-genotoxic p53 activator nutlin, we have subjected cells to irradiation and treatments with the chemotherapeutic 5-fluorouracil and the p53 reactivator APR-246. Our analysis revealed significant similarity in response of mutant-expressing cells to treatment with nutlin, irradiation, and 5-FU (Fig. 23B and 25B). However, one mutant group demonstrated a substantial difference in enrichment pattern: wild-type-

like mutants were depleted significantly stronger under nutlin treatment than under treatment with DNA-damaging agents, demonstrating preferential induction of cell cycle arrest by wild-type like mutants under tested conditions as compared to nutlin. Although all three stimuli activate apoptosis in HCT-116 cells, distinct dynamics of the p53 activation play a significant role in controlling p53 response outcome. Irradiation induces rapid activation of p53 followed by pulsing p53 protein levels of decreasing amplitude (Hafner et al. 2017; Lev Bar-Or et al. 2000), leading to preferential activation of arrest-inducing genes and recovery from DNA damage. Conversely, continuous treatment with MDM2 inhibitors results in sustained p53 activation expression of proapoptotic target genes and cell death (Paek et al. 2016; Purvis et al. 2012). Distinct behavior of the group of synonymous and wild-type-like mutants under distinct stimuli likely reflects the influence of p53 signaling dynamics on cell fate.

We did not reveal any other mutants which dynamics were significantly distinct under non-genotoxic p53 activation with nutlin and after exposure to genotoxic agents. This suggests that resistance to apoptosis is the most important determinant of therapy resistance in our system.

Besides genotoxic agents, we have treated library-expressing HCT-116 cells with the p53-reactivating compound APR-246. It is the most advanced p53 reactivator and currently undergoes clinical testing (12 studies listed at clinicaltrials.gov). A successful rescue of functions of mutant p53 would result in depletion of selected missense LOF mutants from the library compared to nonsense and synonymous mutations. Surprisingly, our analysis did not reveal any mutant-specific effects (Fig. 26 and 31). Neither the R175H mutants shown previously to be refolded with APR-246 nor other missense mutants showed any depletion below the basal level (Zhang et al. 2018; Ceder et al. 2020; Bykov et al. 2016; Bykov et al. 2002).

Mutant p53 is constitutively stabilized in cancer cells. Refolding of the mutant protein with a reactivating compound leads to rapid accumulation of active p53 and cytotoxicity. However, mutant p53 stabilization is not an immediate consequence of p53 mutation but rather an acquired hallmark of the cancer cell (Schulz-Heddergott and Moll 2018; Yamamoto and Iwakuma 2018). HCT-116 cells express wild-type p53 and therefore likely lack alterations essential for p53 stabilization. Consequently, the

introduction of the mutant allele into HCT-116$^{\Delta/TP53E}$ cells did not result in the accumulation of the mutant protein: expression levels of missense mutants were comparable to the wild-type (Fig. 11C). Treatment of mutant-expressing cells with nutlin increased p53 levels (Fig. 11C). The synergy between nutlin and APR-246 has been shown before (Izetti et al. 2014). However, our experiments did not reveal any APR-246-specific cytotoxicity under combined treatment with nutlin and APR-246 (Fig. 31). Nutlin induced a moderate increase of p53 levels in mutant-expressing HCT-116$^{\Delta/TP53E}$ cells (Fig. 11C). By contrast, mutant p53-expressing cell lines usually demonstrate massive protein accumulation (Zandi et al. 2011). Therefore, the most likely explanation for the failure to observe any effects of APR-246 in our system is insufficient expression levels of mutant proteins. Presumably, using a mutant p53-expressing cell line with a high basal level of mutant protein would enable us to explore the p53 mutome in the context of continuous p53 stabilization. However, gene editing in p53-mutated cell lines presents a substantial challenge due to genomic instability and frequent copy number alterations of the *TP53* locus (Donehower et al. 2019).

In conclusion, our work is the first study that has attempted to assess the impact of p53 mutants on the response to therapeutic regimens. The simplicity of our system enables rapid and cost-effective testing of multiple compounds to gain insight into mutant p53-mediated drug resistance and expand the knowledge about the selectivity of mutant p53 targeting compounds.

4.6 GOF of mutant p53 in CSMS

Numerous p53 mutations confer neomorphic GOF activities to the protein. These activities foster cancer cell proliferation, enhance invasion and metastasis and promote chemoresistance (Walerych et al. 2012; Walerych et al. 2015; Mantovani et al. 2019). GOF effects are mutant- and context-specific. Therefore, high-content profiling of GOF properties of multiple p53 mutant variants would significantly impact personalized cancer treatment.

We have identified several mutants that displayed higher enrichment than nonsense variants upon prolonged cultivation of the untreated H1-helix library, suggesting that these mutants stimulate proliferation (Fig. 28 C). However, the detected proliferative

advantage was statistically significant only for a single mutant (R181M, not found in tumors). Interestingly, variant H179Y, which demonstrated strong enrichment in one of three library replicates but failed to reach a statistically significant difference with nonsense mutants, was reported to promote the proliferation of embryonic lung fibroblasts (Di Yang et al. 2007). Enrichment of mutants with suggested GOF activity showed substantial variance between replicate libraries (Fig. 28C). Therefore, to discriminate between true neomorphic activities and stochastic fluctuations of variant frequency in the complex library, experiments with an increased number of replicates might be needed.

Besides fueling proliferation, GOF mutants can promote radio- and chemoresistance (Valenti et al. 2011; Lisek et al. 2018; He et al. 2017; Yue et al. 2017). Therefore, we have analyzed data from nutlin-, 5-FU and X-ray treatment experiments to identify mutants with GOF properties. However, we did not detect any variants with enrichment significantly exceeding nonsense mutations. For example, in the library treated with MDM2 inhibitors, ES of 98% of missense mutants lies within 3 standard deviations of the mean ES of nonsense variants. The only mutant with enrichment exceeding this level in all 5 libraries is P177D, but its high enrichment is due to the extremely low amount of reads in one of the untreated library replicates (8 reads, obvious outlier) (Supplementary Fig. 1). Similarly, we found no evidence of more extensive enrichment for any of the missense mutants under 5-FU treatment or after irradiation. Therefore, our analysis suggests that most p53 mutants exhibit no GOF phenotype in the CSMS system.

The stabilization of mutant p53 is a prerequisite for its tumor-promoting GOF (Alexandrova et al. 2017a; Hingorani et al. 2005; Terzian et al. 2008; Schulz-Heddergott and Moll 2018). Tumor dependence on sustained elevated levels of mutant p53 has been demonstrated in elegant animal models: ablation of mutant p53 expression results in tumor regression, decreased metastasis, and improved survival (Muller and Vousden 2014; Weissmueller et al. 2014; Vogiatzi et al. 2016). Therefore, mechanisms driving mutant p53 stabilization are attractive therapeutic targets (Alexandrova et al. 2015; Schulz-Heddergott and Moll 2018; Yue et al. 2017; Yue et al. 2015). As already noted, none of the missense mutants showed expression levels exceeding the wild-type protein when expressed in HCT-116$^{\Delta/TP53}$

(Fig. 11), despite some of these mutants showing prominent stabilization in tumor samples (e.g., R175H and mouse equivalent of E180R) (Timofeev et al. 2013; Hwang et al. 2018). The lack of clearly detectable GOF properties in our screening is in line with previous observations. Both comprehensive high-throughput mutagenesis screens failed to identify any GOF properties in *in vitro* experiments (Kotler et al. 2018; Boettcher et al. 2019). However, clear predominant expansion of cells carrying hotspot mutants with proven GOF properties was demonstrated in tumor xenografts grown in nude mice in the study of Kotler. This exceptionally interesting observation highlights the difference between selective forces operating *in vitro* and *in vivo*. Although HCT-116 cells used in the CSMS do not show stabilization of mutp53 in vitro and reveal no addiction to the mutant protein, adaptation of the cellular library to the growth in a complex *in vivo* setting could result in a selection of subclones with stabilized mutp53 with neomorphic activities conferring the selective advantage. Therefore, optimization of the CSMS procedure for *in vivo* experiments could enable the identification of mutants with GOF and further improve the clinical value of our work.

Two recent studies attested DNE as a universal feature of p53 mutants (Boettcher et al. 2019; Giacomelli et al. 2018). Unfortunately, the CSMS is unable to capture the DNE because it utilizes a cell line with a single *TP53* allele. However, minor modifications would enable us to do this. Specifically, one needs to establish a cell line with an editable *TP53* allele and preserved second wild-type allele. The generation of such cell lines is currently underway in our group.

4.7 CSMS identifies pathogenic mutations in non-coding regions

CSMS has demonstrated its outstanding performance in measuring the functional impact of missense p53 mutations. However, all these experiments could also be performed in cDNA-based screening systems with comparable results. The unquestionable advantage of the CSMS approach is its ability to assess the consequences of mutations in non-coding regions of the endogenous locus. Our experiments showcased this advantage of the CSMS by identifying the known pathogenic variant of the splice site in the 5th intron (c.559+1 G>A) (ClinVar record NM_001126112.2) (Surget et al. 2013; Lai et al. 1993; Smeby et al. 2019) (Fig. 33).

Mutations in non-coding regions are rarely found in cancer patients (156 splice site mutations are listed in the UMD *TP53* database). However, their actual frequency in cancers may be underestimated since mutational analysis is mainly restricted to protein-coding regions. They are frequently mutually exclusive with exonic variants, highlighting their pathogenicity (Li et al. 2018). Identification of intronic pathogenic variants in *TP53* outside splice sites suggests that non-coding tumor-predisposing *TP53* variants are more frequent than previously considered (Peller et al. 1995; Avigad et al. 1997; Sailaja et al. 2012; Barel et al. 1998).
Interestingly, several synonymous SNVs (sSNV) in the coding TP53 sequence were identified as pathogenic. For example, two sSNV at codon 125 (c.375G>A or c.375C>T) at the end of exon 4 are adjacent to the donor site in intron 4 and impair *TP53* splicing) (54 UMD records) (Varley et al. 1998). Similarly, sSNV c.672G>A (encodes E224) is likely to disturb splicing (Leroy et al. 2014a). cDNA-based methods would undoubtedly characterize these rare mutations as benign but likely scored correctly as pathogenic by the CSMS.

Summarizing, we believe that the CSMS is a powerful novel platform for discovering novel pathogenic variants in non-coding regions of p53. Identification of intronic pathogenic variants in *TP53* outside splice sites suggests that non-coding tumor-predisposing *TP53* variants are more frequent than previously considered (Peller et al. 1995; Avigad et al. 1997; Sailaja et al. 2012; Barel et al. 1998). This further emphasizes the advantage of the CSMS over cDNA-based screening protocols for the comprehensive classification of rare *TP53* variants.

4.8 CSMS outperforms cDNA-based methods in the classification of pathogenic variants

Comparing the CSMS-derived measurements with the cDNA-based screening results revealed a clear correlation between the two datasets (Fig. 39 and 40) (Kotler et al. 2018). However, the classification was discrepant for some variants. Notably, several of these variants are experimentally confirmed LOF (R175P, R175L, R181C) (Kang et al. 2020). Moreover, another mutant (C176Y) is also definitely pathogenic (it was frequently found in ovarian and other cancers, 281 UMD records) (Kang et al.

2013; Mullany et al. 2015). These four mutants were erroneously classified in the cDNA-based screen as functional but correctly scored by the CSMS as non-functional.

Furthermore, CSMS scored several potentially tumorigenic H1 helix mutants with intermediate occurrence in tumor samples (10-90 records) as LOF. Again, the cDNA-based screen failed to assign these variants to the pathogenic category (Fig. 39). At the same time, our screening did not overestimate the pathogenicity of mutation since most of the mutations found in less than 10 patient samples were classified as benign. Therefore, CSMS demonstrated a more accurate classification of H1-helix variants compared to the cDNA study. Unfortunately, the low dynamic range of the exon 5 dataset resulted in imprecise classification (as illustrated by low RFS values of the R175H mutant). However, we expect that minor modifications of screening conditions would be sufficient to confirm the superior performance of the CSMS over cDNA-based methods.

We did not include the other similar study in the analysis because it quantified wild-type and LOF effects in two separate experiments, making the direct juxtaposition of data cumbersome (Giacomelli et al. 2018). Direct comparison between studies of Kotler and Giacomelly was performed recently and found their excellent agreement (Carbonnier et al. 2020). Therefore, we can anticipate that our conclusions would be valid for the second study as well. Finally, most of the very rare variants (<10 UMD records, being likely sequencing artifacts or neutral bystander mutations) are unequivocally classified by both systems as functionally normal, suggesting that our protocol does not overestimate the amount of LOF mutations. Summarizing, a detailed comparison of our data with the dataset of Kotler et al. provides compelling evidence that the procedure established in our study is significantly more accurate in the categorization of pathogenic *TP53* mutations, especially mutations with residual functions.

4.9 Method limitations

CSMS demonstrated impressive performance in our hands. However, we ought to address some limitations of our approach. Our aim, among others, was to improve the catalog of p53 mutations used for testing patients with increased cancer

susceptibility. From this perspective, the important limitation is the employed readout. We assessed the tumor-suppressive properties of mutants by quantifying the antiproliferative capacity of p53 mutants under treatment with mdm2 inhibitors. However, the ability of a p53 variant to kill cancer cells upon mdm2 inhibition is not a direct measure of “tumor suppression,” the ability of a protein to prevent initiation and progression of cancer *in vivo*. Two observations can exemplify this notion.

On the one hand, therapeutic response to nutlin in murine Eμ-Myc lymphoma solely relies on Puma-mediated apoptosis (Valente et al. 2016b). At the same time, neither loss of Puma alone nor in combination with the other critical proapoptotic factor Noxa does not accelerate tumorigenesis to the same extent as p53 loss (Valente et al. 2016a). Even more strikingly, p53 efficiently suppresses spontaneous tumorigenesis in mice deficient for *p21*, *puma,* and *noxa* in the absence of its three main programs: apoptosis, cell cycle arrest, and senescence (Valente et al. 2013). These observations clearly demonstrate that classical p53 functions assessed by mutagenesis screens, including CSMS, are dispensable for tumor suppression. Other activities, such as maintaining genomic stability, can be more crucial but are difficult to assess *in vitro* in a high-content manner (Eischen 2016; Hanel and Moll 2012; Liu et al. 2004). Therefore, caution is needed when applying data on sensitivity to mdm2 inhibitors to identify cancer-predisposing mutants.

The other limitation of our method stems from the usage of the isogenic setting: all mutants are expressed in the same cell line. Despite obvious advantages, this approach dramatically simplifies the cellular context and limits the findings to the single colorectal cell line. However, p53-mediated effects and their importance for tumor suppression are considerably distinct between tissue types. For example, p53-null mice predominantly develop T-cell lymphomas and soft tissue sarcomas, whereas other cancer types are much rarer, pointing at the paramount importance of p53 for tumor suppression in the hematopoietic compartment in mice. In humans, the most frequent tumor type among carriers of germline *TP53* mutations is breast cancer (Donehower et al. 1992; Bouaoun et al. 2016). *TP53* mutational spectrum varies significantly between cancer types (Kastenhuber and Lowe 2017). To a large extent, this variation can be explained by specific mutagenic processes operating in different tissues (Alexandrov et al. 2016; Giacomelli et al. 2018). However, tissue-

specific oncogenic GOF might also shape the mutational landscape (Barta and McMahon 2019). Collectively this suggests that the prognostic value of a mutant determined in colorectal cancer cell line can be distinct in the other tumor types. This can be especially relevant for low penetrant cancer-predisposing mutants acting in a tissue-specific manner, such as R337H. This inherited p53 variant is found in the Brazilian population and predisposes to developing adrenal cortical tumors and lung adenocarcinomas (Ribeiro et al. 2001; Vieira et al. 2021). Importantly, R337H is a pLOF mutant with preserved proapoptotic capacity. Therefore, its tissue-specific tumorigenic effects would presumably be difficult to capture in experimental systems based on cancer cells of distinct tissue origin.

Tissue specificity of p53-driven response has an important implication for therapeutic response: the outcome of p53 activation can be very heterogeneous in different tissues. For example, in normal tissues, irradiation-induced p53 activation damages hematopoietic tissues and hair follicles due to apoptosis induction but exerts protective effects due to activation of cell cycle arrest and DNA repair in small intestine (Gudkov and Komarova 2010). Diverse p53-mediated responses are dictated by tissue-specific activation of p53 targets and distinct dynamics of p53 levels (Fei et al. 2002; Tanikawa et al. 2017; Stewart-Ornstein et al. 2021). A paradoxical example of tissue-specific action of p53 in the context of cancer therapy is the tumor-protective action of wild-type p53 in breast cancer. Contrary to a textbook view, wild-type p53 was shown to mediate poor chemotherapy response in murine MMTV-Wnt1 mammary tumors compared to the mutant. Mechanistically, p53 activated cell cycle arrest and senescence, which protected cancer cells from doxorubicin-induced DNA damage.

Conversely, mutant p53 was unable to halt proliferation which leads to cell death via mitotic catastrophe (Jackson et al. 2012; Tonnessen-Murray et al. 2018). A similar protective action of p53 was revealed in melanoma (Webster et al. 2020). These observations underscore the importance of tissue context when assessing the response of cancer cells to chemotherapy and translation of results of high-content screenings.

The application of isogenic background in our screening has another important implication. *TP53* mutations never act as the sole driver of malignant growth. Conversely, in many tumors, p53 loss is a late genetic event, which cooperates with multiple preexisting oncogenic alterations to fuel aggressive cancer growth (Fearon and Vogelstein 1990). Every tumor carries a unique combination of genetic alterations, which collectively determines its properties, including the behavior of wild-type or mutant p53. Cooperating oncogene may dramatically change the effect of p53 mutations on tumor development and therapy response. For example, murine leukemia arising from progenitors expressing AML1/ETO fusion protein demonstrates strongly increased aggressiveness and therapy resistance upon loss of p53.

Conversely, leukemias initiated by the MLL/ENL fusion protein are highly aggressive and resistant to chemotherapy independently of p53 status (Zuber et al. 2009). This example underscores that functional screens based on a single cell line are confined to a unique combination of mutations. The importance of genetic background is further exemplified by the fact that even p53-wild-type cell lines demonstrate a fairly distinct response to mdm2 inhibitors, determined by additional genetic alterations (e.g., MDM2 amplification) (Ishizawa et al. 2018; Saiki et al. 2015). Accordingly, phenotypic effects of p53 mutations are partially determined by the cooperating mutations. Colorectal cancer cell line HCT-116 harbors activating mutations in b-catenin and KRas (G13D) (Sekine et al. 2002; Steckel et al. 2012). Additionally, it contains a mutation of the *CDKN2A* locus encoding p14ARF protein. p14ARF acts as an mdm2 inhibitor and activates p53 in response to oncogenic signaling. Therefore, the *CDKN2A* mutation enables cells to maintain high levels of Ras-driven MAPK signaling and evade activation of the wild-type p53. Importantly, the introduction of p53 mutants into HCT-116 cells creates a genetic configuration that rarely exists in tumors: *TP53* and *CDNKN2a* mutations are mutually exclusive (Donehower et al. 2019). Assaying the effects of mutant p53 in such context have important consequences. In a typical mutant p53-expressing cell with wild-type *CDKN2A,* constitutively active KRas drives p14ARF-dependent stabilization and accumulation of mutant p53. P53 stabilization is a prerequisite for oncogenic GOF (Suh et al. 2011). Lack of ARF in HCT-116 cells prevents stabilization of mutant

variants. This might explain the lack of detectable GOF effects in our system and emphasize the necessity to perform screenings in multiple cell lines. Another important consequence of the usage of ARF-mutant cell line concerns the testing p53 reactivating compounds. Cells harboring p53 mutations are not responding to the restoration of wild-type p53 equally well. Conversely, p53 reactivation successfully eliminates only those tumors where upregulated oncogenic signaling is translated into ARF-dependent stabilization of mutant p53 (Junttila et al. 2010; Feldser et al. 2010). Accordingly, screening in ARF-deficient HCT-116 cells will likely keep effects of p53-reactivating compounds such as APR-246 obscured.

In summary, the aforementioned limitations need to be considered when interpreting and generalizing data of our study. We are convinced that CSMS-based classification of most LOF and wild type-like variants could be applied to a broad spectrum of cancer entities. In support of this, the CSMS dataset obtained from colorectal cancer cells revealed a reassuringly high correlation with the study of Kotler and colleagues performed in the H1299 cell line (expresses oncogenic NRas and wild-type p14ARF). Furthermore, a recent report revealed an excellent correlation between the study of Kotler and another cDNA-based screening performed in A549 cells (Carbonnier et al. 2020). However, our estimates regarding pLOF mutants could be affected by cell line-specific traits (e.g., tissue-specific p53-dependent transcriptome, cooperating mutations) and can therefore be confined to a particular cancer subtype. Likewise, CSMS-based predictions regarding GOF and the impact of mutations on response to chemotherapy or p53-reactivating compounds can be predetermined by choice of the host cell line and need to be interpreted with caution.

4.10 Conclusion

TP53 is mutated in up to 80% of human cancers (Donehower et al. 2019; Leroy et al. 2014a), and the proper systematization of p53 mutants is in high demand. Our study provides the foundation of the first catalog of functional consequences of p53 variants encoded by the native *TP53* locus in an isogenic genetic background.

At present development of the system in our group progresses further. For instance, the editing of the *TP53* locus in the HCT-116$^{\Delta/TP53}$ cell line was implemented in exons 6, 7, and 8, and reassuring preliminary data were obtained. Furthermore, the CSMS toolkit was expanded with a lung cancer cell line. *TP53* mutations are very abundant in lung cancer patients; therefore, the addition of non-small cell lung cancer cell line to the screening will provide valuable information and broaden the clinical relevance of generated data.

Over the decades, studies of p53 mutations were mainly focused on *bona fide* cancer-driving hotspot variants. Pathogenicity of rare non-hotspot alterations remained ambiguous due to the small number of reported patients and lack of experimental evidence (e.g., cell lines or mouse models). Clinical interpretation of rare variants was greatly empowered by bioinformatic tools such as SIFT, PolyPhen, REVEL, and others (Ng and Henikoff 2003; Adzhubei et al. 2013; Ioannidis et al. 2016). Nowadays rapid development of gene editing technologies and next-generation sequencing offered the exciting possibility to directly test phenotypic effects of hundreds of mutants in parallel in a time- and cost-effective manner. We have demonstrated that the CSMS-based classification is significantly more precise than existing bioinformatic predictors (Fig. 41). Moreover, CSMS has showcased its outstanding ability to predict the impact of mutations on therapy response, whereas none of the currently available algorithms are able to do this.

Although several earlier studies have already reported high content characterization of the p53 mutome, the CSMS approach has several unique advantages and is likely more accurate. Therefore, we are convinced that the findings of the present work will serve as a substantial contribution to the further development of public p53-focused resources for researchers and clinicians.

Publication bibliography

Achatz, Maria Isabel; Zambetti, Gerard P. (2016): The Inherited p53 Mutation in the Brazilian Population. In *Cold Spring Harbor perspectives in medicine* 6 (12). DOI: 10.1101/cshperspect.a026195.

Adzhubei, Ivan; Jordan, Daniel M.; Sunyaev, Shamil R. (2013): Predicting functional effect of human missense mutations using PolyPhen-2. In *Current protocols in human genetics* Chapter 7, Unit7.20. DOI: 10.1002/0471142905.hg0720s76.

Adzhubei, Ivan A.; Schmidt, Steffen; Peshkin, Leonid; Ramensky, Vasily E.; Gerasimova, Anna; Bork, Peer et al. (2010): A method and server for predicting damaging missense mutations. In *Nature methods* 7 (4), pp. 248–249. DOI: 10.1038/nmeth0410-248.

Alexandrov, Ludmil B.; Ju, Young Seok; Haase, Kerstin; van Loo, Peter; Martincorena, Iñigo; Nik-Zainal, Serena et al. (2016): Mutational signatures associated with tobacco smoking in human cancer. In *Science (New York, N.Y.)* 354 (6312), pp. 618–622. DOI: 10.1126/science.aag0299.

Alexandrova, E. M.; Yallowitz, A. R.; Li, D.; Xu, S.; Schulz, R.; Proia, D. A. et al. (2015): Improving survival by exploiting tumour dependence on stabilized mutant p53 for treatment. In *Nature* 523 (7560), pp. 352–356. DOI: 10.1038/nature14430.

Alexandrova, Evguenia M.; Mirza, Safia A.; Xu, Sulan; Schulz-Heddergott, Ramona; Marchenko, Natalia D.; Moll, Ute M. (2017a): p53 loss-of-heterozygosity is a necessary prerequisite for mutant p53 stabilization and gain-of-function in vivo. In *Cell death & disease* 8 (3), e2661. DOI: 10.1038/cddis.2017.80.

Alexandrova, Evguenia M.; Xu, Sulan; Moll, Ute M. (2017b): Ganetespib synergizes with cyclophosphamide to improve survival of mice with autochthonous tumors in a mutant p53-dependent manner. In *Cell death & disease* 8 (3), e2683. DOI: 10.1038/cddis.2017.108.

Andreeff, Michael; Kelly, Kevin R.; Yee, Karen; Assouline, Sarit; Strair, Roger; Popplewell, Leslie et al. (2016): Results of the Phase I Trial of RG7112, a Small-Molecule MDM2 Antagonist in Leukemia. In *Clinical cancer research : an official*

journal of the American Association for Cancer Research 22 (4), pp. 868–876. DOI: 10.1158/1078-0432.CCR-15-0481.

Ang, Hwee Ching; Joerger, Andreas C.; Mayer, Sebastian; Fersht, Alan R. (2006): Effects of common cancer mutations on stability and DNA binding of full-length p53 compared with isolated core domains. In *The Journal of biological chemistry* 281 (31), pp. 21934–21941. DOI: 10.1074/jbc.M604209200.

Aschauer, Lydia; Muller, Patricia A. J. (2016): Novel targets and interaction partners of mutant p53 Gain-Of-Function. In *Biochemical Society transactions* 44 (2), pp. 460–466. DOI: 10.1042/BST20150261.

Ashkenazy, Haim; Abadi, Shiran; Martz, Eric; Chay, Ofer; Mayrose, Itay; Pupko, Tal; Ben-Tal, Nir (2016): ConSurf 2016: an improved methodology to estimate and visualize evolutionary conservation in macromolecules. In *Nucleic acids research* 44 (W1), W344-50. DOI: 10.1093/nar/gkw408.

Aubrey, Brandon J.; Janic, Ana; Chen, Yunshun; Chang, Catherine; Lieschke, Elizabeth C.; Diepstraten, Sarah T. et al. (2018a): Mutant TRP53 exerts a target gene-selective dominant-negative effect to drive tumor development. In *Genes & development* 32 (21-22), pp. 1420–1429. DOI: 10.1101/gad.314286.118.

Aubrey, Brandon J.; Kelly, Gemma L.; Janic, Ana; Herold, Marco J.; Strasser, Andreas (2018b): How does p53 induce apoptosis and how does this relate to p53-mediated tumour suppression? In *Cell death and differentiation* 25 (1), pp. 104–113. DOI: 10.1038/cdd.2017.169.

Avigad, S.; Barel, D.; Blau, O.; Malka, A.; Zoldan, M.; Mor, C. et al. (1997): A novel germ line p53 mutation in intron 6 in diverse childhood malignancies. In *Oncogene* 14 (13), pp. 1541–1545. DOI: 10.1038/sj.onc.1200990.

Bao, Junjie; Nanding, Abiyasi; Song, Haibin; Xu, Rui; Qu, Guofan; Xue, Yingwei (2016): The overexpression of MDM4: an effective and novel predictor of gastric adenocarcinoma lymph node metastasis. In *Oncotarget* 7 (41), pp. 67212–67222. DOI: 10.18632/oncotarget.11971.

Baptiste, Nicole; Friedlander, Philip; Chen, Xinbin; Prives, Carol (2002): The proline-rich domain of p53 is required for cooperation with anti-neoplastic agents to promote

apoptosis of tumor cells. In *Oncogene* 21 (1), pp. 9–21. DOI: 10.1038/sj.onc.1205015.

Barboza, Juan A.; Liu, Geng; Ju, Zhenlin; El-Naggar, Adel K.; Lozano, Guillermina (2006): p21 delays tumor onset by preservation of chromosomal stability. In *Proceedings of the National Academy of Sciences of the United States of America* 103 (52), pp. 19842–19847. DOI: 10.1073/pnas.0606343104.

Barel, D.; Avigad, S.; Mor, C.; Fogel, M.; Cohen, I. J.; Zaizov, R. (1998): A novel germ-line mutation in the noncoding region of the p53 gene in a Li-Fraumeni family. In *Cancer genetics and cytogenetics* 103 (1), pp. 1–6. DOI: 10.1016/s0165-4608(97)00258-6.

Barrangou, Rodolphe (2015): The roles of CRISPR-Cas systems in adaptive immunity and beyond. In *Current opinion in immunology* 32, pp. 36–41. DOI: 10.1016/j.coi.2014.12.008.

Barta, Julie A.; McMahon, Steven B. (2019): Lung-Enriched Mutations in the p53 Tumor Suppressor: A Paradigm for Tissue-Specific Gain of Oncogenic Function. In *Molecular cancer research : MCR* 17 (1), pp. 3–9. DOI: 10.1158/1541-7786.MCR-18-0357.

Bartek, J.; Iggo, R.; Gannon, J.; Lane, D. P. (1990): Genetic and immunochemical analysis of mutant p53 in human breast cancer cell lines. In *Oncogene* 5 (6), pp. 893–899.

Basu, Subhasree; Gnanapradeepan, Keerthana; Barnoud, Thibaut; Kung, Che-Pei; Tavecchio, Michele; Scott, Jeremy et al. (2018): Mutant p53 controls tumor metabolism and metastasis by regulating PGC-1α. In *Genes & development* 32 (3-4), pp. 230–243. DOI: 10.1101/gad.309062.117.

Baugh, Evan H.; Ke, Hua; Levine, Arnold J.; Bonneau, Richard A.; Chan, Chang S. (2018): Why are there hotspot mutations in the TP53 gene in human cancers? In *Cell death and differentiation* 25 (1), pp. 154–160. DOI: 10.1038/cdd.2017.180.

Baumann, Kim (2012): Cell death: multitasking p53 promotes necrosis. In *Nature reviews. Molecular cell biology* 13 (8), pp. 480–481. DOI: 10.1038/nrm3401.

Bernal, Federico; Wade, Mark; Godes, Marina; Davis, Tina N.; Whitehead, David G.; Kung, Andrew L. et al. (2010): A stapled p53 helix overcomes HDMX-mediated suppression of p53. In *Cancer cell* 18 (5), pp. 411–422. DOI: 10.1016/j.ccr.2010.10.024.

Bieging, Kathryn T.; Attardi, Laura D. (2012): Deconstructing p53 transcriptional networks in tumor suppression. In *Trends in cell biology* 22 (2), pp. 97–106. DOI: 10.1016/j.tcb.2011.10.006.

Billant, Olivier; Blondel, Marc; Voisset, Cécile (2017): p53, p63 and p73 in the wonderland of S. cerevisiae. In *Oncotarget* 8 (34), pp. 57855–57869. DOI: 10.18632/oncotarget.18506.

Blagosklonny, M. (1997): Loss of function and p53 protein stabilization. In *Oncogene* (15), pp. 1889–1893.

Blagosklonny, M. V.; Toretsky, J.; Bohen, S.; Neckers, L. (1996): Mutant conformation of p53 translated in vitro or in vivo requires functional HSP90. In *Proceedings of the National Academy of Sciences of the United States of America* 93 (16), pp. 8379–8383. DOI: 10.1073/pnas.93.16.8379.

Blagosklonny, Mikhail V. (2002): P53: an ubiquitous target of anticancer drugs. In *International journal of cancer* 98 (2), pp. 161–166. DOI: 10.1002/ijc.10158.

Blanden, Adam R.; Yu, Xin; Loh, Stewart N.; Levine, Arnold J.; Carpizo, Darren R. (2015): Reactivating mutant p53 using small molecules as zinc metallochaperones: awakening a sleeping giant in cancer. In *Drug discovery today* 20 (11), pp. 1391–1397. DOI: 10.1016/j.drudis.2015.07.006.

Blandino, G.; Levine, A. J.; Oren, M. (1999): Mutant p53 gain of function: differential effects of different p53 mutants on resistance of cultured cells to chemotherapy. In *Oncogene* 18 (2), pp. 477–485. DOI: 10.1038/sj.onc.1202314.

Blandino, Giovanni; Di Agostino, Silvia (2018): New therapeutic strategies to treat human cancers expressing mutant p53 proteins. In *Journal of experimental & clinical cancer research : CR* 37 (1), p. 30. DOI: 10.1186/s13046-018-0705-7.

Boeckler, Frank M.; Joerger, Andreas C.; Jaggi, Gaurav; Rutherford, Trevor J.; Veprintsev, Dmitry B.; Fersht, Alan R. (2008): Targeted rescue of a destabilized

mutant of p53 by an in silico screened drug. In *Proceedings of the National Academy of Sciences of the United States of America* 105 (30), pp. 10360–10365. DOI: 10.1073/pnas.0805326105.

Boehme, Karen A.; Blattner, Christine (2009): Regulation of p53--insights into a complex process. In *Critical reviews in biochemistry and molecular biology* 44 (6), pp. 367–392. DOI: 10.3109/10409230903401507.

Boettcher, S.; Miller, P.; Sharma, R.; McConkey, M.; Leventhal M; KrivtsovA et al. (2019): A dominant-negative effect drives selection of TP53 missense mutations in myeloid malignancies. ,. In *Science (New York, N.Y.)* 365 (6453), pp. 599–604. DOI: 10.1126/science.aax3649.

Bottini, Silvia; Hamouda-Tekaya, Nedra; Mategot, Raphael; Zaragosi, Laure-Emmanuelle; Audebert, Stephane; Pisano, Sabrina et al. (2017): Post-transcriptional gene silencing mediated by microRNAs is controlled by nucleoplasmic Sfpq. In *Nature communications* 8 (1), p. 1189. DOI: 10.1038/s41467-017-01126-x.

Bouaoun, Liacine; Sonkin, Dmitriy; Ardin, Maude; Hollstein, Monica; Byrnes, Graham; Zavadil, Jiri; Olivier, Magali (2016): TP53 Variations in Human Cancers: New Lessons from the IARC TP53 Database and Genomics Data. In *Human mutation* 37 (9), pp. 865–876. DOI: 10.1002/humu.23035.

Bowden, Anne Ramsay; Morales-Juarez, David A.; Sczaniecka-Clift, Matylda; Agudo, Maria Martin; Lukashchuk, Natalia; Thomas, John Christopher; Jackson, Stephen P. (2020): Parallel CRISPR-Cas9 screens clarify impacts of p53 on screen performance. In *eLife*. DOI: 10.7554/eLife.55325.

Brandt, Tobias; Petrovich, Miriana; Joerger, Andreas C.; Veprintsev, Dmitry B. (2009): Conservation of DNA-binding specificity and oligomerisation properties within the p53 family. In *BMC genomics* 10, p. 628. DOI: 10.1186/1471-2164-10-628.

Brendel, C.; Müller-Kuller, U.; Schultze-Strasser, S.; Stein, S.; Chen-Wichmann, L.; Krattenmacher, A. et al. (2012): Physiological regulation of transgene expression by a lentiviral vector containing the A2UCOE linked to a myeloid promoter. In *Gene therapy* 19 (10), pp. 1018–1029. DOI: 10.1038/gt.2011.167.

Bromidge, T.; Lowe, C.; Prentice, A.; Johnson, S. (2000): p53 intronic point mutation, aberrant splicing and telomeric associations in a case of B-chronic lymphocytic leukaemia. In *British journal of haematology* 111 (1), pp. 223–229. DOI: 10.1046/j.1365-2141.2000.02335.x.

Brosh, Ran; Rotter, Varda (2009): When mutants gain new powers: news from the mutant p53 field. In *Nature Reviews Cancer* 9 (10), pp. 701–713. DOI: 10.1038/nrc2693.

Buganim, Yosef; Kalo, Eyal; Brosh, Ran; Besserglick, Hila; Nachmany, Ido; Rais, Yoach et al. (2006): Mutant p53 protects cells from 12-O-tetradecanoylphorbol-13-acetate-induced death by attenuating activating transcription factor 3 induction. In *Cancer research* 66 (22), pp. 10750–10759. DOI: 10.1158/0008-5472.CAN-06-0916.

Bullock, A. N.; Fersht, A. R. (2001): Rescuing the function of mutant p53. In *Nature reviews. Cancer* 1 (1), pp. 68–76. DOI: 10.1038/35094077.

Burset, M.; Seledtsov, I. A.; Solovyev, V. V. (2001): SpliceDB: database of canonical and non-canonical mammalian splice sites. In *Nucleic acids research* 29 (1), pp. 255–259. DOI: 10.1093/nar/29.1.255.

Butler, James S.; Loh, Stewart N. (2003): Structure, function, and aggregation of the zinc-free form of the p53 DNA binding domain. In *Biochemistry* 42 (8), pp. 2396–2403. DOI: 10.1021/bi026635n.

Butler, James S.; Loh, Stewart N. (2007): Zn(2+)-dependent misfolding of the p53 DNA binding domain. In *Biochemistry* 46 (10), pp. 2630–2639. DOI: 10.1021/bi062106y.

Bykov, Vladimir J. N.; Eriksson, Sofi E.; Bianchi, Julie; Wiman, Klas G. (2018): Targeting mutant p53 for efficient cancer therapy. In *Nature reviews. Cancer* 18 (2), pp. 89–102. DOI: 10.1038/nrc.2017.109.

Bykov, Vladimir J. N.; Issaeva, Natalia; Shilov, Alexandre; Hultcrantz, Monica; Pugacheva, Elena; Chumakov, Peter et al. (2002): Restoration of the tumor suppressor function to mutant p53 by a low-molecular-weight compound. In *Nature medicine* 8 (3), pp. 282–288. DOI: 10.1038/nm0302-282.

Bykov, Vladimir J. N.; Issaeva, Natalia; Zache, Nicole; Shilov, Alexandre; Hultcrantz, Monica; Bergman, Jan et al. (2017): Reactivation of mutant p53 and induction of apoptosis in human tumor cells by maleimide analogs. In *The Journal of biological chemistry* 292 (48), p. 19607. DOI: 10.1074/jbc.AAC117.000815.

Bykov, Vladimir J. N.; Wiman, Klas G. (2014): Mutant p53 reactivation by small molecules makes its way to the clinic. In *FEBS letters* 588 (16), pp. 2622–2627. DOI: 10.1016/j.febslet.2014.04.017.

Bykov, Vladimir J. N.; Zache, Nicole; Stridh, Helene; Westman, Jacob; Bergman, Jan; Selivanova, Galina; Wiman, Klas G. (2005): PRIMA-1(MET) synergizes with cisplatin to induce tumor cell apoptosis. In *Oncogene* 24 (21), pp. 3484–3491. DOI: 10.1038/sj.onc.1208419.

Bykov, Vladimir J. N.; Zhang, Qiang; Zhang, Meiqiongzi; Ceder, Sophia; Abrahmsen, Lars; Wiman, Klas G. (2016): Targeting of Mutant p53 and the Cellular Redox Balance by APR-246 as a Strategy for Efficient Cancer Therapy. In *Frontiers in oncology* 6, p. 21. DOI: 10.3389/fonc.2016.00021.

Campling, Barbara G.; El-Deiry, Wafik S. (2003): Clinical implications of p53 mutations in lung cancer. In *Methods in molecular medicine* 75, pp. 53–77. DOI: 10.1385/1-59259-324-0:53.

Campomenosi, P.; Monti, P.; Aprile, A.; Abbondandolo, A.; Frebourg, T.; Gold, B. et al. (2001): p53 mutants can often transactivate promoters containing a p21 but not Bax or PIG3 responsive elements. In *Oncogene* 20 (27), pp. 3573–3579. DOI: 10.1038/sj.onc.1204468.

Canver, Matthew C.; Tripathi, Pratibha; Bullen, Michael J.; Olshansky, Moshe; Kumar, Yogesh; Wong, Lee H. et al. (2020): A saturating mutagenesis CRISPR-Cas9-mediated functional genomic screen identifies cis- and trans-regulatory elements of Oct4 in murine ESCs. In *The Journal of biological chemistry* 295 (47), pp. 15797–15809. DOI: 10.1074/jbc.RA120.013772.

Carbonnier, Vincent; Leroy, Bernard; Rosenberg, Shai; Soussi, Thierry (2020): Comprehensive assessment of TP53 loss of function using multiple combinatorial

mutagenesis libraries. In *Scientific reports* 10 (1), p. 20368. DOI: 10.1038/s41598-020-74892-2.

Cariello, N. F.; Beroud, C.; Soussi, T. (1994): Database and software for the analysis of mutations at the human p53 gene. In *Nucleic acids research* 22 (17), pp. 3549–3550.

Ceder, Sophia; Eriksson, Sofi E.; Cheteh, Emarndeena H.; Dawar, Swati; Corrales Benitez, Mariana; Bykov, Vladimir J. N. et al. (2020): A thiol-bound drug reservoir enhances APR-246-induced mutant p53 tumor cell death. In *EMBO molecular medicine*, e10852. DOI: 10.15252/emmm.201910852.

Chae, Young Kwang; Yousaf, Muhammad; Malecek, Mary-Kate; Carneiro, Benedito; Chandra, Sunandana; Kaplan, Jason et al. (2015): Statins as anti-cancer therapy; Can we translate preclinical and epidemiologic data into clinical benefit? In *Discovery medicine* 20 (112), pp. 413–427.

Chakrabarti, Anob M.; Henser-Brownhill, Tristan; Monserrat, Josep; Poetsch, Anna R.; Luscombe, Nicholas M.; Scaffidi, Paola (2019): Target-Specific Precision of CRISPR-Mediated Genome Editing. In *Molecular cell* 73 (4), 699-713.e6. DOI: 10.1016/j.molcel.2018.11.031.

Chang, Yong S.; Graves, Bradford; Guerlavais, Vincent; Tovar, Christian; Packman, Kathryn; To, Kwong-Him et al. (2013): Stapled α-helical peptide drug development: a potent dual inhibitor of MDM2 and MDMX for p53-dependent cancer therapy. In *Proceedings of the National Academy of Sciences of the United States of America* 110 (36), E3445-54. DOI: 10.1073/pnas.1303002110.

Chen, Si; Li, Xiang; Yuan, Weirong; Zou, Yan; Guo, Zhongwu; Chai, Yifeng; Lu, Wuyuan (2017): Rapid identification of dual p53-MDM2/MDMX interaction inhibitors through virtual screening and hit-based substructure search. In *RSC Adv.* 7 (16), pp. 9989–9997. DOI: 10.1039/C7RA00473G.

Chen, Xiang; Bahrami, Armita; Pappo, Alberto; Easton, John; Dalton, James; Hedlund, Erin et al. (2014): Recurrent somatic structural variations contribute to tumorigenesis in pediatric osteosarcoma. In *Cell reports* 7 (1), pp. 104–112. DOI: 10.1016/j.celrep.2014.03.003.

Cheok, Chit Fang; Lane, David Philip (2017): Exploiting the p53 Pathway for Therapy. In *Cold Spring Harbor perspectives in medicine* 7 (3). DOI: 10.1101/cshperspect.a026310.

Chin, K. V.; Ueda, K.; Pastan, I.; Gottesman, M. M. (1992): Modulation of activity of the promoter of the human MDR1 gene by Ras and p53. In *Science (New York, N.Y.)* 255 (5043), pp. 459–462. DOI: 10.1126/science.1346476.

Chipuk, Jerry E.; Kuwana, Tomomi; Bouchier-Hayes, Lisa; Droin, Nathalie M.; Newmeyer, Donald D.; Schuler, Martin; Green, Douglas R. (2004): Direct activation of Bax by p53 mediates mitochondrial membrane permeabilization and apoptosis. In *Science (New York, N.Y.)* 303 (5660), pp. 1010–1014. DOI: 10.1126/science.1092734.

Cho, Y.; Gorina, S.; Jeffrey, P. D.; Pavletich, N. P. (1994): Crystal structure of a p53 tumor suppressor-DNA complex: understanding tumorigenic mutations. In *Science (New York, N.Y.)* 265 (5170), pp. 346–355. DOI: 10.1126/science.8023157.

Choi, Yongwook (2012): A fast computation of pairwise sequence alignment scores between a protein and a set of single-locus variants of another protein. In Sanjay Ranka, Tamer Kahveci, Mona Singh (Eds.): Proceedings of the ACM Conference on Bioinformatics, Computational Biology and Biomedicine - BCB '12. the ACM Conference. Orlando, Florida, 10/7/2012 - 10/10/2012. New York, New York, USA: ACM Press, pp. 414–417.

Choi, Yongwook; Sims, Gregory E.; Murphy, Sean; Miller, Jason R.; Chan, Agnes P. (2012): Predicting the functional effect of amino acid substitutions and indels. In *PloS one* 7 (10), e46688. DOI: 10.1371/journal.pone.0046688.

Chou, Cheng-Wei; Lin, Ching-Heng; Hsiao, Tzu-Hung; Lo, Chia-Chien; Hsieh, Chih-Ying; Huang, Cheng-Chung; Sher, Yuh-Pyng (2019): Therapeutic effects of statins against lung adenocarcinoma via p53 mutant-mediated apoptosis. In *Scientific reports* 9 (1), p. 20403. DOI: 10.1038/s41598-019-56532-6.

Clarke, A. R.; Purdie, C. A.; Harrison, D. J.; Morris, R. G.; Bird, C. C.; Hooper, M. L.; Wyllie, A. H. (1993): Thymocyte apoptosis induced by p53-dependent and independent pathways. In *Nature* 362 (6423), pp. 849–852. DOI: 10.1038/362849a0.

Cluzeau, Thomas; Sebert, Marie; Rahmé, Ramy; Cuzzubbo, Stefania; Walter-petrich, Anouk; Lehmann che, Jacqueline et al. (2019): APR-246 Combined with Azacitidine (AZA) in TP53 Mutated Myelodysplastic Syndrome (MDS) and Acute Myeloid Leukemia (AML). a Phase 2 Study By the Groupe Francophone Des Myélodysplasies (GFM). In *Blood* 134 (Supplement_1), p. 677. DOI: 10.1182/blood-2019-125579.

Cooks, Tomer; Harris, Curtis C.; Oren, Moshe (2014): Caught in the cross fire: p53 in inflammation. In *Carcinogenesis* 35 (8), pp. 1680–1690. DOI: 10.1093/carcin/bgu134.

Danovi, Davide; Meulmeester, Erik; Pasini, Diego; Migliorini, Domenico; Capra, Maria; Frenk, Ruth et al. (2004): Amplification of Mdmx (or Mdm4) directly contributes to tumor formation by inhibiting p53 tumor suppressor activity. In *Molecular and cellular biology* 24 (13), pp. 5835–5843. DOI: 10.1128/MCB.24.13.5835-5843.2004.

Dehner, Alexander; Klein, Christian; Hansen, Silke; Müller, Lin; Buchner, Johannes; Schwaiger, Manfred; Kessler, Horst (2005): Cooperative binding of p53 to DNA: regulation by protein-protein interactions through a double salt bridge. In *Angewandte Chemie (International ed. in English)* 44 (33), pp. 5247–5251. DOI: 10.1002/anie.200501887.

Deltcheva, Elitza; Chylinski, Krzysztof; Sharma, Cynthia M.; Gonzales, Karine; Chao, Yanjie; Pirzada, Zaid A. et al. (2011): CRISPR RNA maturation by trans-encoded small RNA and host factor RNase III. In *Nature* 471 (7340), pp. 602–607. DOI: 10.1038/nature09886.

Di Agostino, Silvia; Fontemaggi, Giulia; Strano, Sabrina; Blandino, Giovanni; D'Orazi, Gabriella (2019): Targeting mutant p53 in cancer: the latest insights. In *Journal of experimental & clinical cancer research : CR* 38 (1), p. 290. DOI: 10.1186/s13046-019-1302-0.

Di Yang; Qi, Yitao; Chen, Qian; Wang, Zhiqin; Jin, Xi; Gao, Jie et al. (2007): The over-expression of p53 H179Y residue mutation causes the increase of cyclin A1 and Cdk4 expression in HELF cells. In *Molecular and cellular biochemistry* 304 (1-2), pp. 219–226. DOI: 10.1007/s11010-007-9503-9.

DiGiammarino, Enrico L.; Lee, Amanda S.; Cadwell, Craig; Zhang, Weixing; Bothner, Brian; Ribeiro, Raul C. et al. (2002): A novel mechanism of tumorigenesis involving pH-dependent destabilization of a mutant p53 tetramer. In *Nature structural biology* 9 (1), pp. 12–16. DOI: 10.1038/nsb730.

Ding, Qingjie; Zhang, Zhuming; Liu, Jin-Jun; Jiang, Nan; Zhang, Jing; Ross, Tina M. et al. (2013): Discovery of RG7388, a potent and selective p53-MDM2 inhibitor in clinical development. In *Journal of medicinal chemistry* 56 (14), pp. 5979–5983. DOI: 10.1021/jm400487c.

Dittmer, D.; Pati, S.; Zambetti, G.; Chu, S.; Teresky, A. K.; Moore, M. et al. (1993): Gain of function mutations in p53. In *Nature genetics* 4 (1), pp. 42–46. DOI: 10.1038/ng0593-42.

Do, Phi M.; Varanasi, Lakshman; Fan, Songqing; Li, Chunyang; Kubacka, Iwona; Newman, Virginia et al. (2012): Mutant p53 cooperates with ETS2 to promote etoposide resistance. In *Genes & development* 26 (8), pp. 830–845. DOI: 10.1101/gad.181685.111.

Donehower, L. A.; Harvey, M.; Slagle, B. L.; McArthur, M. J.; Montgomery, C. A.; Butel, J. S.; Bradley, A. (1992): Mice deficient for p53 are developmentally normal but susceptible to spontaneous tumours. In *Nature* 356 (6366), pp. 215–221. DOI: 10.1038/356215a0.

Donehower, Lawrence A.; Soussi, Thierry; Korkut, Anil; Liu, Yuexin; Schultz, Andre; Cardenas, Maria et al. (2019): Integrated Analysis of TP53 Gene and Pathway Alterations in The Cancer Genome Atlas. In *Cell reports* 28 (5), 1370-1384.e5. DOI: 10.1016/j.celrep.2019.07.001.

Eischen, Christine M. (2016): Genome Stability Requires p53. In *Cold Spring Harbor perspectives in medicine* 6 (6). DOI: 10.1101/cshperspect.a026096.

Eldar, Amir; Rozenberg, Haim; Diskin-Posner, Yael; Rohs, Remo; Shakked, Zippora (2013): Structural studies of p53 inactivation by DNA-contact mutations and its rescue by suppressor mutations via alternative protein-DNA interactions. In *Nucleic acids research*, pp. 8748–8759. DOI: 10.1093/nar/gkt630.

Elliott, B.; Richardson, C.; Winderbaum, J.; Nickoloff, J. A.; Jasin, M. (1998): Gene conversion tracts from double-strand break repair in mammalian cells. In *Molecular and cellular biology* 18 (1), pp. 93–101. DOI: 10.1128/mcb.18.1.93.

Enache, Oana M.; Rendo, Veronica; Abdusamad, Mai; Lam, Daniel; Davison, Desiree; Pal, Sangita et al. (2020): Cas9 activates the p53 pathway and selects for p53-inactivating mutations. In *Nature genetics* 52 (7), pp. 662–668. DOI: 10.1038/s41588-020-0623-4.

Engler, Carola; Kandzia, Romy; Marillonnet, Sylvestre (2008): A one pot, one step, precision cloning method with high throughput capability. In *PloS one* 3 (11), e3647. DOI: 10.1371/journal.pone.0003647.

Fearon, E. R.; Vogelstein, B. (1990): A genetic model for colorectal tumorigenesis. In *Cell* 61 (5), pp. 759–767. DOI: 10.1016/0092-8674(90)90186-i.

Fei, Peiwen; Bernhard, Eric J.; El-Deiry, Wafik S. (2002): Tissue-specific induction of p53 targets in vivo. In *Cancer research* 62 (24), pp. 7316–7327.

Feldser, David M.; Kostova, Kamena K.; Winslow, Monte M.; Taylor, Sarah E.; Cashman, Chris; Whittaker, Charles A. et al. (2010): Stage-specific sensitivity to p53 restoration during lung cancer progression. In *Nature* 468 (7323), pp. 572–575. DOI: 10.1038/nature09535.

Feng, Zhaohui; Zhang, Cen; Wu, Rui; Hu, Wenwei (2011): Tumor suppressor p53 meets microRNAs. In *Journal of molecular cell biology* 3 (1), pp. 44–50. DOI: 10.1093/jmcb/mjq040.

Findlay, Gregory M.; Boyle, Evan A.; Hause, Ronald J.; Klein, Jason C.; Shendure, Jay (2014): Saturation editing of genomic regions by multiplex homology-directed repair. In *Nature* 513 (7516), pp. 120–123. DOI: 10.1038/nature13695.

Findlay, Gregory M.; Daza, Riza M.; Martin, Beth; Zhang, Melissa D.; Leith, Anh P.; Gasperini, Molly et al. (2018): Accurate classification of BRCA1 variants with saturation genome editing. In *Nature*, pp. 217–222. DOI: 10.1038/s41586-018-0461-z.

Flaman, J. M.; Robert, V.; Lenglet, S.; Moreau, V.; Iggo, R.; Frebourg, T. (1998): Identification of human p53 mutations with differential effects on the bax and p21

promoters using functional assays in yeast. In *Oncogene* 16 (10), pp. 1369–1372. DOI: 10.1038/sj.onc.1201889.

Fortuno, Cristina; James, Paul A.; Young, Erin L.; Feng, Bing; Olivier, Magali; Pesaran, Tina et al. (2018): Improved, ACMG-compliant, in silico prediction of pathogenicity for missense substitutions encoded by TP53 variants. In *Human mutation* 39 (8), pp. 1061–1069. DOI: 10.1002/humu.23553.

Frazier, M. W.; He, X.; Wang, J.; Gu, Z.; Cleveland, J. L.; Zambetti, G. P. (1998): Activation of c-myc gene expression by tumor-derived p53 mutants requires a discrete C-terminal domain. In *Molecular and cellular biology* 18 (7), pp. 3735–3743. DOI: 10.1128/mcb.18.7.3735.

Freed-Pastor, William A.; Mizuno, Hideaki; Zhao, Xi; Langerød, Anita; Moon, Sung-Hwan; Rodriguez-Barrueco, Ruth et al. (2012): Mutant p53 disrupts mammary tissue architecture via the mevalonate pathway. In *Cell* 148 (1-2), pp. 244–258. DOI: 10.1016/j.cell.2011.12.017.

Freed-Pastor, William A.; Prives, Carol (2012): Mutant p53: one name, many proteins. In *Genes & development* 26 (12), pp. 1268–1286. DOI: 10.1101/gad.190678.112.

Friedlander, P.; Legros, Y.; Soussi, T.; Prives, C. (1996): Regulation of mutant p53 temperature-sensitive DNA binding. In *The Journal of biological chemistry* 271 (41), pp. 25468–25478. DOI: 10.1074/jbc.271.41.25468.

Frum R.A., Grossman S.R. (Ed.) (2014): Mechanisms of Mutant p53 Stabilization in Cancer. Deb S., Deb S. (eds) Mutant p53 and MDM2 in Cancer. Subcellular Biochemistry: Springer, Dordrecht (85). Available online at 978-94-017-9211-0.

Geng Liu, Timothy J.; McDonnell; Roberto Montes de Oca Lun; Mini Kapoor; Betsy Mims; Adel K. El-Naggar; Guillermina Lozano (2000): High metastatic potential in mice inheriting a targeted p53 missense mutation. In *PNAS* 97 (8), pp. 4174–4179.

Ghosh, Abhijit; Chen, Tina Chunyuan; Kapila, Yvonne L. (2010): Anoikis triggers Mdm2-dependent p53 degradation. In *Molecular and cellular biochemistry* 343 (1-2), pp. 201–209. DOI: 10.1007/s11010-010-0514-6.

Giacomelli, Andrew O.; Yang, Xiaoping; Lintner, Robert E.; McFarland, James M.; Duby, Marc; Kim, Jaegil et al. (2018): Mutational processes shape the landscape of TP53 mutations in human cancer. In *Nature genetics* 50 (10), pp. 1381–1387. DOI: 10.1038/s41588-018-0204-y.

Goh, Amanda M.; Coffill, Cynthia R.; Lane, David P. (2011): The role of mutant p53 in human cancer. In *The Journal of pathology* 223 (2), pp. 116–126. DOI: 10.1002/path.2784.

Gonzalez, Kelly D.; Noltner, Katie A.; Buzin, Carolyn H.; Gu, Dongqing; Wen-Fong, Cindy Y.; Nguyen, Vu Q. et al. (2009): Beyond Li Fraumeni Syndrome: clinical characteristics of families with p53 germline mutations. In *Journal of clinical oncology : official journal of the American Society of Clinical Oncology* 27 (8), pp. 1250–1256. DOI: 10.1200/JCO.2008.16.6959.

Gorlov, Ivan P.; Gorlova, Olga Y.; Frazier, Marsha L.; Amos, Christopher I. (2004): Missense mutations in cancer suppressor gene TP53 are colocalized with exonic splicing enhancers (ESEs). In *Mutation research* 554 (1-2), pp. 175–183. DOI: 10.1016/j.mrfmmm.2004.04.014.

Graupner, Vilma; Schulze-Osthoff, Klaus; Essmann, Frank; Jänicke, Reiner U. (2009): Functional characterization of p53beta and p53gamma, two isoforms of the tumor suppressor p53. In *Cell cycle (Georgetown, Tex.)* 8 (8), pp. 1238–1248. DOI: 10.4161/cc.8.8.8251.

Graves, Bradford; Thompson, Thelma; Xia, Mingxuan; Janson, Cheryl; Lukacs, Christine; Deo, Dayanand et al. (2012): Activation of the p53 pathway by small-molecule-induced MDM2 and MDMX dimerization. In *Proceedings of the National Academy of Sciences of the United States of America* 109 (29), pp. 11788–11793. DOI: 10.1073/pnas.1203789109.

Gregory M. Findlay; Riza M. Daza; Beth Martin; Melissa D. Zhang; Anh P. Leith; Molly Gasperini et al. (2018): Accurate classification of BRCA1 variants with saturation genome editing. In *Nature* 562.

Grochova, D.; Vankova, J.; Damborsky, J.; Ravcukova, B.; Smarda, J.; Vojtesek, B.; Smardova, J. (2008): Analysis of transactivation capability and conformation of p53

temperature-dependent mutants and their reactivation by amifostine in yeast. In *Oncogene* 27 (9), pp. 1243–1252. DOI: 10.1038/sj.onc.1210748.

Gu, Bo; Zhu, Wei-Guo (2012): Surf the post-translational modification network of p53 regulation. In *International journal of biological sciences* 8 (5), pp. 672–684. DOI: 10.7150/ijbs.4283.

Gudkov, Andrei V.; Komarova, Elena A. (2010): Pathologies associated with the p53 response. In *Cold Spring Harbor perspectives in biology* 2 (7), a001180. DOI: 10.1101/cshperspect.a001180.

Guha, Tanya; Malkin, David (2017): Inherited TP53 Mutations and the Li-Fraumeni Syndrome. In *Cold Spring Harbor perspectives in medicine* 7 (4). DOI: 10.1101/cshperspect.a026187.

Gully, Chris P.; Velazquez-Torres, Guermarie; Shin, Ji-Hyun; Fuentes-Mattei, Enrique; Wang, Edward; Carlock, Colin et al. (2012): Aurora B kinase phosphorylates and instigates degradation of p53. In *Proceedings of the National Academy of Sciences of the United States of America* 109 (24), E1513-22. DOI: 10.1073/pnas.1110287109.

Haapaniemi, Emma; Botla, Sandeep; Persson, Jenna; Schmierer, Bernhard; Taipale, Jussi (2018): CRISPR-Cas9 genome editing induces a p53-mediated DNA damage response. In *Nature medicine* 24 (7), pp. 927–930. DOI: 10.1038/s41591-018-0049-z.

Hafner, Antonina; Stewart-Ornstein, Jacob; Purvis, Jeremy E.; Forrester, William C.; Bulyk, Martha L.; Lahav, Galit (2017): p53 pulses lead to distinct patterns of gene expression albeit similar DNA-binding dynamics. In *Nature structural & molecular biology* 24 (10), pp. 840–847. DOI: 10.1038/nsmb.3452.

Hainaut, P.; Milner, J. (1993): A structural role for metal ions in the "wild-type" conformation of the tumor suppressor protein p53. In *Cancer research* 53 (8), pp. 1739–1742.

Hall, Callum; Muller, Patricia A. J. (2019): The Diverse Functions of Mutant 53, Its Family Members and Isoforms in Cancer. In *International journal of molecular sciences* 20 (24). DOI: 10.3390/ijms20246188.

Hamelin, Richard; Laurent-Puig, Pierre; Olschwang, Sylviane; Jego, Nathalie; Asselain, Bernard; Remvikos, Yorghos et al. (1994): Association of p53 mutations with short survival in colorectal cancer. In *Gastroenterology* 106 (1), pp. 42–48. DOI: 10.1016/S0016-5085(94)94217-X.

Hanel, W.; Marchenko, N.; Xu, S.; Yu, S. Xiaofeng; Weng, W.; Moll, U. (2013): Two hot spot mutant p53 mouse models display differential gain of function in tumorigenesis. In *Cell death and differentiation* 20 (7), pp. 898–909. DOI: 10.1038/cdd.2013.17.

Hanel, Walter; Moll, Ute M. (2012): Links between mutant p53 and genomic instability. In *Journal of cellular biochemistry* 113 (2), pp. 433–439. DOI: 10.1002/jcb.23400.

Haupt, Susan; Berger, Michael; Goldberg, Zehavit; Haupt, Ygal (2003): Apoptosis - the p53 network. In *Journal of cell science* 116 (Pt 20), pp. 4077–4085. DOI: 10.1242/jcs.00739.

Haupt, Y.; Maya, R.; Kazaz, A.; Oren, M. (1997): Mdm2 promotes the rapid degradation of p53. In *Nature* 387 (6630), pp. 296–299. DOI: 10.1038/387296a0.

He, Chao; Li, Lun; Guan, Xuan; Xiong, Li; Miao, Xiongying (2017): Mutant p53 Gain of Function and Chemoresistance: The Role of Mutant p53 in Response to Clinical Chemotherapy. In *Chemotherapy* 62 (1), pp. 43–53. DOI: 10.1159/000446361.

Hepburn, Allan (2007): Troubled legacies. Narrative and inheritance. Toronto, Buffalo: University of Toronto Press.

Hernandez-Boussard, T.; Rodriguez-Tome, P.; Montesano, R.; Hainaut, P. (1999): IARC p53 mutation database: a relational database to compile and analyze p53 mutations in human tumors and cell lines. International Agency for Research on Cancer. In *Human mutation* 14 (1), pp. 1–8. DOI: 10.1002/(SICI)1098-1004(1999)14:1<1::AID-HUMU1>3.0.CO;2-H.

Hicks, Stephanie; Wheeler, David A.; Plon, Sharon E.; Kimmel, Marek (2011): Prediction of missense mutation functionality depends on both the algorithm and sequence alignment employed. In *Human mutation* 32 (6), pp. 661–668. DOI: 10.1002/humu.21490.

Hientz, Karin; Mohr, André; Bhakta-Guha, Dipita; Efferth, Thomas (2017): The role of p53 in cancer drug resistance and targeted chemotherapy. In *Oncotarget* 8 (5), pp. 8921–8946. DOI: 10.18632/oncotarget.13475.

Hingorani, Sunil R.; Wang, Lifu; Multani, Asha S.; Combs, Chelsea; Deramaudt, Therese B.; Hruban, Ralph H. et al. (2005): Trp53R172H and KrasG12D cooperate to promote chromosomal instability and widely metastatic pancreatic ductal adenocarcinoma in mice. In *Cancer cell* 7 (5), pp. 469–483. DOI: 10.1016/j.ccr.2005.04.023.

Ho, Cheng-Jung; Lin, Ru-Wei; Zhu, Wei-Hua; Wen, Tsung-Kai; Hu, Chieh-Ju; Lee, Yi-Lin et al. (2019): Transcription-independent and -dependent p53-mediated apoptosis in response to genotoxic and non-genotoxic stress. In *Cell death discovery* 5, p. 131. DOI: 10.1038/s41420-019-0211-5.

Hollstein, M.; Rice, K.; Greenblatt, M. S.; Soussi, T.; Fuchs, R.; Sørlie, T. et al. (1994): Database of p53 gene somatic mutations in human tumors and cell lines. In *Nucleic acids research* 22 (17), pp. 3551–3555.

Holmila, R.; Fouquet, C.; Cadranel, J.; Zalcman, G.; Soussi, T. (2003): Splice mutations in the p53 gene: case report and review of the literature. In *Human mutation* 21 (1), pp. 101–102. DOI: 10.1002/humu.9104.

Hong, Bo; Prabhu, Varun V.; Zhang, Shengliang; van den Heuvel, A. Pieter J.; Dicker, David T.; Kopelovich, Levy; El-Deiry, Wafik S. (2014): Prodigiosin rescues deficient p53 signaling and antitumor effects via upregulating p73 and disrupting its interaction with mutant p53. In *Cancer research* 74 (4), pp. 1153–1165. DOI: 10.1158/0008-5472.CAN-13-0955.

Hunter, Anthony M.; Sallman, David A. (2019): Current status and new treatment approaches in TP53 mutated AML. In *Best practice & research. Clinical haematology* 32 (2), pp. 134–144. DOI: 10.1016/j.beha.2019.05.004.

Hwang, Le-Ann; Phang, Beng Hooi; Liew, Oi Wah; Iqbal, Jabed; Koh, Xiao Hui; Koh, Xin Yu et al. (2018): Monoclonal Antibodies against Specific p53 Hotspot Mutants as Potential Tools for Precision Medicine. In *Cell reports* 22 (1), pp. 299–312. DOI: 10.1016/j.celrep.2017.11.112.

Ihry, Robert J.; Worringer, Kathleen A.; Salick, Max R.; Frias, Elizabeth; Ho, Daniel; Theriault, Kraig et al. (2018): p53 inhibits CRISPR-Cas9 engineering in human pluripotent stem cells. In *Nature medicine* 24 (7), pp. 939–946. DOI: 10.1038/s41591-018-0050-6.

Ingallina, Eleonora; Sorrentino, Giovanni; Bertolio, Rebecca; Lisek, Kamil; Zannini, Alessandro; Azzolin, Luca et al. (2017): Mechanical cues control mutant p53 stability through a Mevalonate/RhoA axis. In *Nature cell biology* 20 (1), pp. 28–35. DOI: 10.1038/s41556-017-0009-8.

Ioannidis, Nilah M.; Rothstein, Joseph H.; Pejaver, Vikas; Middha, Sumit; McDonnell, Shannon K.; Baheti, Saurabh et al. (2016): REVEL: An Ensemble Method for Predicting the Pathogenicity of Rare Missense Variants. In *American journal of human genetics* 99 (4), pp. 877–885. DOI: 10.1016/j.ajhg.2016.08.016.

Ishizawa, Jo; Nakamaru, Kenji; Seki, Takahiko; Tazaki, Koichi; Kojima, Kensuke; Chachad, Dhruv et al. (2018): Predictive Gene Signatures Determine Tumor Sensitivity to MDM2 Inhibition. In *Cancer research* 78 (10), pp. 2721–2731. DOI: 10.1158/0008-5472.CAN-17-0949.

Izetti, Patricia; Hautefeuille, Agnes; Abujamra, Ana Lucia; Farias, Caroline Brunetto de; Giacomazzi, Juliana; Alemar, Bárbara et al. (2014): PRIMA-1, a mutant p53 reactivator, induces apoptosis and enhances chemotherapeutic cytotoxicity in pancreatic cancer cell lines. In *Investigational new drugs* 32 (5), pp. 783–794. DOI: 10.1007/s10637-014-0090-9.

Jackson, James G.; Pant, Vinod; Li, Qin; Chang, Leslie L.; Quintás-Cardama, Alfonso; Garza, Daniel et al. (2012): p53-mediated senescence impairs the apoptotic response to chemotherapy and clinical outcome in breast cancer. In *Cancer cell* 21 (6), pp. 793–806. DOI: 10.1016/j.ccr.2012.04.027.

Jacob, Aishwarya G.; O'Brien, Dennis; Singh, Ravi K.; Comiskey, Daniel F.; Littleton, Robert M.; Mohammad, Fuad et al. (2013): Stress-induced isoforms of MDM2 and MDM4 correlate with high-grade disease and an altered splicing network in pediatric rhabdomyosarcoma. In *Neoplasia (New York, N.Y.)* 15 (9), pp. 1049–1063. DOI: 10.1593/neo.13286.

Jayasinghe, Reyka G.; Cao, Song; Gao, Qingsong; Wendl, Michael C.; Vo, Nam Sy; Reynolds, Sheila M. et al. (2018): Systematic Analysis of Splice-Site-Creating Mutations in Cancer. In *Cell reports* 23 (1), 270-281.e3. DOI: 10.1016/j.celrep.2018.03.052.

Jiang, Liren; Zawacka-Pankau, Joanna (2020): The p53/MDM2/MDMX-targeted therapies-a clinical synopsis. In *Cell death & disease* 11 (4), p. 237. DOI: 10.1038/s41419-020-2445-9.

Jiaxiong Lu; Guan Shan; Zhao Yanling; Yu Yang; Wang Yongfeng; Shi Yonghua et al. (2016): Novel MDM2 inhibitor SAR405838 (MI-773) induces p53-mediated apoptosis in neuroblastoma (7), 82757-82769. Available online at https://doi.org/10.18632/oncotarget.12634.

Jillian M Birch; Valerie Blair; Anna M Kelsey; D Gareth Evans; Martin Harris; Karen J Tricker; Jennifer M Varley. (1998): Cancer phenotype correlates with constitutional TP53 genotype in families with the Li-Fraumeni syndrome. In *Oncogene* (17), pp. 1061–1068.

Jinek, Martin; Chylinski, Krzysztof; Fonfara, Ines; Hauer, Michael; Doudna, Jennifer A.; Charpentier, Emmanuelle (2012): A programmable dual-RNA-guided DNA endonuclease in adaptive bacterial immunity. In *Science (New York, N.Y.)* 337 (6096), pp. 816–821. DOI: 10.1126/science.1225829.

Joerger, A. C.; Fersht, A. R. (2007): Structure-function-rescue: the diverse nature of common p53 cancer mutants. In *Oncogene* 26 (15), pp. 2226–2242. DOI: 10.1038/sj.onc.1210291.

Joerger, Andreas C.; Ang, Hwee Ching; Fersht, Alan R. (2006): Structural basis for understanding oncogenic p53 mutations and designing rescue drugs. In *Proceedings of the National Academy of Sciences of the United States of America* 103 (41), pp. 15056–15061. DOI: 10.1073/pnas.0607286103.

Jones, Siân; Zhang, Xiaosong; Parsons, D. Williams; Lin, Jimmy Cheng-Ho; Leary, Rebecca J.; Angenendt, Philipp et al. (2008): Core signaling pathways in human pancreatic cancers revealed by global genomic analyses. In *Science (New York, N.Y.)* 321 (5897), pp. 1801–1806. DOI: 10.1126/science.1164368.

Jordan, Jennifer J.; Inga, Alberto; Conway, Kathleen; Edmiston, Sharon; Carey, Lisa A.; Wu, Lin; Resnick, Michael A. (2010): Altered-function p53 missense mutations identified in breast cancers can have subtle effects on transactivation. In *Molecular cancer research : MCR* 8 (5), pp. 701–716. DOI: 10.1158/1541-7786.MCR-09-0442.

Joruiz, Sebastien M.; Bourdon, Jean-Christophe (2016): p53 Isoforms: Key Regulators of the Cell Fate Decision. In *Cold Spring Harbor perspectives in medicine* 6 (8). DOI: 10.1101/cshperspect.a026039.

Junttila, Melissa R.; Karnezis, Anthony N.; Garcia, Daniel; Madriles, Francesc; Kortlever, Roderik M.; Rostker, Fanya et al. (2010): Selective activation of p53-mediated tumour suppression in high-grade tumours. In *Nature* 468 (7323), pp. 567–571. DOI: 10.1038/nature09526.

Kaar, Joel L.; Basse, Nicolas; Joerger, Andreas C.; Stephens, Elaine; Rutherford, Trevor J.; Fersht, Alan R. (2010): Stabilization of mutant p53 via alkylation of cysteines and effects on DNA binding. In *Protein science : a publication of the Protein Society* 19 (12), pp. 2267–2278. DOI: 10.1002/pro.507.

Kafri, T.; van Praag, H.; Gage, F. H.; Verma, I. M. (2000): Lentiviral vectors: regulated gene expression. In *Molecular therapy : the journal of the American Society of Gene Therapy* 1 (6), pp. 516–521. DOI: 10.1006/mthe.2000.0083.

Kakudo Y.; Hiroyuki Shibata; Kazunori Otsuka; Shunsuke Kato; Chikashi Ishioka. (2005): Lack of Correlation between p53-Dependent Transcriptional Activity and the Ability to Induce Apoptosis among 179 Mutant p53s. In *Cancer research* (65), pp. 2108–2114.

Kamijo, T.; Weber, J. D.; Zambetti, G.; Zindy, F.; Roussel, M. F.; Sherr, C. J. (1998): Functional and physical interactions of the ARF tumor suppressor with p53 and Mdm2. In *Proceedings of the National Academy of Sciences of the United States of America* 95 (14), pp. 8292–8297. DOI: 10.1073/pnas.95.14.8292.

Kang, Hyo Jeong; Chun, Sung-Min; Kim, Kyu-Rae; Sohn, Insuk; Sung, Chang Ohk (2013): Clinical relevance of gain-of-function mutations of p53 in high-grade serous ovarian carcinoma. In *PloS one* 8 (8), e72609. DOI: 10.1371/journal.pone.0072609.

Kang, Ju-Gyeong; Lago, Cory U.; Lee, Ji-Eun; Park, Ji-Hoon; Donnelly, Matthew P.; Starost, Matthew F. et al. (2020): A Mouse Homolog of a Human TP53 Germline Mutation Reveals a Lipolytic Activity of p53. In *Cell reports* 30 (3), 783-792.e5. DOI: 10.1016/j.celrep.2019.12.074.

Kastenhuber, Edward R.; Lowe, Scott W. (2017): Putting p53 in Context. In *Cell* 170 (6), pp. 1062–1078. DOI: 10.1016/j.cell.2017.08.028.

Kato, Shunsuke; Han, Shuang-Yin; Liu, Wen; Otsuka, Kazunori; Shibata, Hiroyuki; Kanamaru, Ryunosuke; Ishioka, Chikashi (2003): Understanding the function-structure and function-mutation relationships of p53 tumor suppressor protein by high-resolution missense mutation analysis. In *Proceedings of the National Academy of Sciences of the United States of America* 100 (14), pp. 8424–8429. DOI: 10.1073/pnas.1431692100.

Kato S.; Shuang-Yin Han; Wen Liu; Kazunori Otsuka; Hiroyuki Shibata; Ryunosuke Kanamaru; Chikashi Ishioka. (2003): Understanding the function–structure and function– mutation relationships of p53 tumor suppressor protein by high-resolution missense mutation analysis. In *PNAS* 100 (14), pp. 8424–8429.

Kern, S. E.; Pietenpol, J. A.; Thiagalingam, S.; Seymour, A.; Kinzler, K. W.; Vogelstein, B. (1992): Oncogenic forms of p53 inhibit p53-regulated gene expression. In *Science (New York, N.Y.)* 256 (5058), pp. 827–830. DOI: 10.1126/science.1589764.

Keshelava, N.; Zuo, J. J.; Chen, P.; Waidyaratne, S. N.; Luna, M. C.; Gomer, C. J. et al. (2001): Loss of p53 function confers high-level multidrug resistance in neuroblastoma cell lines. In *Cancer research* 61 (16), pp. 6185–6193.

Keshelava, Nino; Zuo, Juan Juan; Waidyaratne, N. Sitara; Triche, Timothy J.; Reynolds, C. Patrick (2000): p53 mutations and loss of p53 function confer multidrug resistance in neuroblastoma. In *Med. Pediatr. Oncol.* 35 (6), pp. 563–568. DOI: 10.1002/1096-911X(20001201)35:6<563::AID-MPO15>3.0.CO;2-J.

Khoury, Marie P.; Bourdon, Jean-Christophe (2011): p53 Isoforms: An Intracellular Microprocessor? In *Genes & cancer* 2 (4), pp. 453–465. DOI: 10.1177/1947601911408893.

Kim, A. L.; Raffo, A. J.; Brandt-Rauf, P. W.; Pincus, M. R.; Monaco, R.; Abarzua, P.; Fine, R. L. (1999): Conformational and molecular basis for induction of apoptosis by a p53 C-terminal peptide in human cancer cells. In *The Journal of biological chemistry* 274 (49), pp. 34924–34931. DOI: 10.1074/jbc.274.49.34924.

Kim, Ella; Günther, Willy; Yoshizato, Kimio; Meissner, Hildegard; Zapf, Srenja; Nüsing, Rolf M. et al. (2003): Tumor suppressor p53 inhibits transcriptional activation of invasion gene thromboxane synthase mediated by the proto-oncogenic factor ets-1. In *Oncogene* 22 (49), pp. 7716–7727. DOI: 10.1038/sj.onc.1207155.

Kim, Michael P.; Lozano, Guillermina (2018): Mutant p53 partners in crime. In *Cell death and differentiation* 25 (1), pp. 161–168. DOI: 10.1038/cdd.2017.185.

Kitayner, Malka; Rozenberg, Haim; Kessler, Naama; Rabinovich, Dov; Shaulov, Lihi; Haran, Tali E.; Shakked, Zippora (2006): Structural basis of DNA recognition by p53 tetramers. In *Molecular cell* 22 (6), pp. 741–753. DOI: 10.1016/j.molcel.2006.05.015.

Klimovich, Boris; Mutlu, Samet; Schneikert, Jean; Elmshäuser, Sabrina; Klimovich, Maria; Nist, Andrea et al. (2019): Loss of p53 function at late stages of tumorigenesis confers ARF-dependent vulnerability to p53 reactivation therapy. In *Proceedings of the National Academy of Sciences of the United States of America* 116 (44), pp. 22288–22293. DOI: 10.1073/pnas.1910255116.

Köbel, Martin; Piskorz, Anna M.; Lee, Sandra; Lui, Shuhong; LePage, Cecile; Marass, Francesco et al. (2016): Optimized p53 immunohistochemistry is an accurate predictor of TP53 mutation in ovarian carcinoma. In *The journal of pathology. Clinical research* 2 (4), pp. 247–258. DOI: 10.1002/cjp2.53.

Kortlever, Roderik M.; Higgins, Paul J.; Bernards, René (2006): Plasminogen activator inhibitor-1 is a critical downstream target of p53 in the induction of replicative senescence. In *Nature cell biology* 8 (8), pp. 877–884. DOI: 10.1038/ncb1448.

Kotagama, Kasuen; Babb, Cody S.; Wolter, Justin M.; Murphy, Ronan P.; Mangone, Marco (2015): A human 3'UTR clone collection to study post-transcriptional gene regulation. In *BMC genomics* 16, p. 1036. DOI: 10.1186/s12864-015-2238-1.

Kotler, Eran; Shani, Odem; Goldfeld, Guy; Lotan-Pompan, Maya; Tarcic, Ohad; Gershoni, Anat et al. (2018): A Systematic p53 Mutation Library Links Differential Functional Impact to Cancer Mutation Pattern and Evolutionary Conservation. In *Molecular cell* 71 (1), 178-190.e8. DOI: 10.1016/j.molcel.2018.06.012.

Kracikova, M.; Akiri, G.; George, A.; Sachidanandam, R.; Aaronson, S. A. (2013): A threshold mechanism mediates p53 cell fate decision between growth arrest and apoptosis. In *Cell death and differentiation* 20 (4), pp. 576–588. DOI: 10.1038/cdd.2012.155.

Kravchenko, J. E.; Ilyinskaya, G. V.; Komarov, P. G.; Agapova, L. S.; Kochetkov, D. V.; Strom, E. et al. (2008): Small-molecule RETRA suppresses mutant p53-bearing cancer cells through a p73-dependent salvage pathway. In *Proceedings of the National Academy of Sciences of the United States of America* 105 (17), pp. 6302–6307. DOI: 10.1073/pnas.0802091105.

Kruse, Jan-Philipp; Gu, Wei (2009): Modes of p53 regulation. In *Cell* 137 (4), pp. 609–622. DOI: 10.1016/j.cell.2009.04.050.

Kussie, P. H.; Gorina, S.; Marechal, V.; Elenbaas, B.; Moreau, J.; Levine, A. J.; Pavletich, N. P. (1996): Structure of the MDM2 oncoprotein bound to the p53 tumor suppressor transactivation domain. In *Science (New York, N.Y.)* 274 (5289), pp. 948–953. DOI: 10.1126/science.274.5289.948.

Kweon, Jiyeon; Jang, An-Hee; Shin, Ha Rim; See, Ji-Eun; Lee, Woochang; Lee, Jong Won et al. (2020): A CRISPR-based base-editing screen for the functional assessment of BRCA1 variants. In *Oncogene*, pp. 30–35. DOI: 10.1038/s41388-019-0968-2.

Lai, M. Y.; Chang, H. C.; Li, H. P.; Ku, C. K.; Chen, P. J.; Sheu, J. C. et al. (1993): Splicing mutations of the p53 gene in human hepatocellular carcinoma. In *Cancer research* 53 (7), pp. 1653–1656.

Lambert, Jeremy M. R.; Gorzov, Petr; Veprintsev, Dimitry B.; Söderqvist, Maja; Segerbäck, Dan; Bergman, Jan et al. (2009): PRIMA-1 reactivates mutant p53 by covalent binding to the core domain. In *Cancer cell* 15 (5), pp. 376–388. DOI: 10.1016/j.ccr.2009.03.003.

Lang, Gene A.; Iwakuma, Tomoo; Suh, Young-Ah; Liu, Geng; Rao, V. Ashutosh; Parant, John M. et al. (2004): Gain of function of a p53 hot spot mutation in a mouse model of Li-Fraumeni syndrome. In *Cell* 119 (6), pp. 861–872. DOI: 10.1016/j.cell.2004.11.006.

Lanni, J. S.; Lowe, S. W.; Licitra, E. J.; Liu, J. O.; Jacks, T. (1997): p53-independent apoptosis induced by paclitaxel through an indirect mechanism. In *Proceedings of the National Academy of Sciences of the United States of America* 94 (18), pp. 9679–9683. DOI: 10.1073/pnas.94.18.9679.

Laptenko, Oleg; Shiff, Idit; Freed-Pastor, Will; Zupnick, Andrew; Mattia, Melissa; Freulich, Ella et al. (2015): The p53 C terminus controls site-specific DNA binding and promotes structural changes within the central DNA binding domain. In *Molecular cell* 57 (6), pp. 1034–1046. DOI: 10.1016/j.molcel.2015.02.015.

Laverdière, M.; Beaudoin, J.; Lavigueur, A. (2000): Species-specific regulation of alternative splicing in the C-terminal region of the p53 tumor suppressor gene. In *Nucleic acids research* 28 (6), pp. 1489–1497. DOI: 10.1093/nar/28.6.1489.

Lavra, Luca; Ulivieri, Alessandra; Rinaldo, Cinzia; Dominici, Roberto; Volante, Marco; Luciani, Emidio et al. (2009): Gal-3 is stimulated by gain-of-function p53 mutations and modulates chemoresistance in anaplastic thyroid carcinomas. In *The Journal of pathology* 218 (1), pp. 66–75. DOI: 10.1002/path.2510.

Le Cong; Ran, F. Ann; Cox, David; Lin, Shuailiang; Barretto, Robert; Habib, Naomi et al. (2013): Multiplex genome engineering using CRISPR/Cas systems. In *Science (New York, N.Y.)* 339 (6121), pp. 819–823. DOI: 10.1126/science.1231143.

Le Jiang; Kon, Ning; Li, Tongyuan; Wang, Shang-Jui; Su, Tao; Hibshoosh, Hanina et al. (2015): Ferroptosis as a p53-mediated activity during tumour suppression. In *Nature* 520 (7545), pp. 57–62. DOI: 10.1038/nature14344.

Ledford, Heidi (2020): CRISPR gene therapy shows promise against blood diseases. In *Nature* 588 (7838), p. 383. DOI: 10.1038/d41586-020-03476-x.

Lee, J. M.; Bernstein, A. (1993): p53 mutations increase resistance to ionizing radiation. In *Proceedings of the National Academy of Sciences of the United States of America* 90 (12), pp. 5742–5746. DOI: 10.1073/pnas.90.12.5742.

Lee, Ming Kei; Teoh, Wei Wei; Phang, Beng Hooi; Tong, Wei Min; Wang, Zhao Qi; Sabapathy, Kanaga (2012): Cell-type, dose, and mutation-type specificity dictate mutant p53 functions in vivo. In *Cancer cell* 22 (6), pp. 751–764. DOI: 10.1016/j.ccr.2012.10.022.

Lee, Seo-Young; Park, Jung-Hyun; Jeong, Sangkyun; Kim, Bu-Yeo; Kang, Yong-Kook; Xu, Yang; Chung, Sun-Ku (2019): K120R mutation inactivates p53 by creating an aberrant splice site leading to nonsense-mediated mRNA decay. In *Oncogene* 38 (10), pp. 1597–1610. DOI: 10.1038/s41388-018-0542-3.

Lee, Y. I.; Lee, S.; Das, G. C.; Park, U. S.; Park, S. M. (2000): Activation of the insulin-like growth factor II transcription by aflatoxin B1 induced p53 mutant 249 is caused by activation of transcription complexes; implications for a gain-of-function during the formation of hepatocellular carcinoma. In *Oncogene* 19 (33), pp. 3717–3726. DOI: 10.1038/sj.onc.1203694.

Leroy, Bernard; Anderson, Martha; Soussi, Thierry (2014a): TP53 mutations in human cancer: database reassessment and prospects for the next decade. In *Human mutation* 35 (6), pp. 672–688. DOI: 10.1002/humu.22552.

Leroy, Bernard; Ballinger, Mandy L.; Baran-Marszak, Fanny; Bond, Gareth L.; Braithwaite, Antony; Concin, Nicole et al. (2017): Recommended Guidelines for Validation, Quality Control, and Reporting of TP53 Variants in Clinical Practice. In *Cancer research* 77 (6), pp. 1250–1260. DOI: 10.1158/0008-5472.CAN-16-2179.

Leroy, Bernard; Fournier, Jean Louis; Ishioka, Chikashi; Monti, Paola; Inga, Alberto; Fronza, Gilberto; Soussi, Thierry (2013): The TP53 website: an integrative resource centre for the TP53 mutation database and TP53 mutant analysis. In *Nucleic acids research* 41 (Database issue), D962-9. DOI: 10.1093/nar/gks1033.

Leroy, Jef L.; Ruel, Marie; Habicht, Jean-Pierre; Frongillo, Edward A. (2014b): Linear growth deficit continues to accumulate beyond the first 1000 days in low- and middle-income countries: global evidence from 51 national surveys. In *The Journal of nutrition* 144 (9), pp. 1460–1466. DOI: 10.3945/jn.114.191981.

Lev Bar-Or, R.; Maya, R.; Segel, L. A.; Alon, U.; Levine, A. J.; Oren, M. (2000): Generation of oscillations by the p53-Mdm2 feedback loop: a theoretical and

experimental study. In *Proceedings of the National Academy of Sciences of the United States of America* 97 (21), pp. 11250–11255. DOI: 10.1073/pnas.210171597.

Levine, Arnold J.; Vosburgh, Evan (2008): P53 mutations in lymphomas: position matters. In *Blood* 112 (8), pp. 2997–2998. DOI: 10.1182/blood-2008-07-167718.

Levy, Claudia B.; Stumbo, Ana C.; Ano Bom, Ana P. D.; Portari, Elisabeth A.; Cordeiro, Yraima; Carneiro, Yraima et al. (2011): Co-localization of mutant p53 and amyloid-like protein aggregates in breast tumors. In *The international journal of biochemistry & cell biology* 43 (1), pp. 60–64. DOI: 10.1016/j.biocel.2010.10.017.

Li, Dun; Marchenko, Natalia D.; Schulz, Ramona; Fischer, Victoria; Velasco-Hernandez, Talia; Talos, Flaminia; Moll, Ute M. (2011): Functional inactivation of endogenous MDM2 and CHIP by HSP90 causes aberrant stabilization of mutant p53 in human cancer cells. In *Molecular cancer research : MCR* 9 (5), pp. 577–588. DOI: 10.1158/1541-7786.MCR-10-0534.

Li, Guoli; Guo, Xinwu; Chen, Ming; Tang, Lili; Jiang, Hui; Day, Julia X. et al. (2018): Prevalence and spectrum of AKT1, PIK3CA, PTEN and TP53 somatic mutations in Chinese breast cancer patients. In *PloS one* 13 (9), e0203495. DOI: 10.1371/journal.pone.0203495.

Li, Y.; Prives, C. (2007): Are interactions with p63 and p73 involved in mutant p53 gain of oncogenic function? In *Oncogene* 26 (15), pp. 2220–2225. DOI: 10.1038/sj.onc.1210311.

Lin, Steven; Staahl, Brett T.; Alla, Ravi K.; Doudna, Jennifer A. (2014): Enhanced homology-directed human genome engineering by controlled timing of CRISPR/Cas9 delivery. In *eLife* 3, e04766. DOI: 10.7554/eLife.04766.

Ling, Xinyu; Xie, Bingteng; Gao, Xiaoqin; Chang, Liying; Zheng, Wei; Chen, Heqi et al. (2020): Improving the efficiency of precise genome editing with site-specific Cas9-oligonucleotide conjugates. In *Science advances*, eaaz0051. DOI: 10.1126/sciadv.aaz0051.

Lisek, Kamil; Campaner, Elena; Ciani, Yari; Walerych, Dawid; Del Sal, Giannino (2018): Mutant p53 tunes the NRF2-dependent antioxidant response to support

survival of cancer cells. In *Oncotarget* 9 (29), pp. 20508–20523. DOI: 10.18632/oncotarget.24974.

Liu, Bin; Chen, Yumin; St Clair, Daret K. (2008): ROS and p53: a versatile partnership. In *Free radical biology & medicine* 44 (8), pp. 1529–1535. DOI: 10.1016/j.freeradbiomed.2008.01.011.

Liu, David S.; Duong, Cuong P.; Haupt, Sue; Montgomery, Karen G.; House, Colin M.; Azar, Walid J. et al. (2017): Inhibiting the system xC-/glutathione axis selectively targets cancers with mutant-p53 accumulation. In *Nature communications* 8, p. 14844. DOI: 10.1038/ncomms14844.

Liu, Geng; Parant, John M.; Lang, Gene; Chau, Patty; Chavez-Reyes, Arturo; El-Naggar, Adel K. et al. (2004): Chromosome stability, in the absence of apoptosis, is critical for suppression of tumorigenesis in Trp53 mutant mice. In *Nature genetics* 36 (1), pp. 63–68. DOI: 10.1038/ng1282.

Liu, Mingjie; Rehman, Saad; Tang, Xidian; Gu, Kui; Fan, Qinlei; Chen, Dekun; Ma, Wentao (2018): Methodologies for Improving HDR Efficiency. In *Frontiers in genetics*, p. 691. DOI: 10.3389/fgene.2018.00691.

Liu, Ying; Bodmer, Walter F. (2006): Analysis of P53 mutations and their expression in 56 colorectal cancer cell lines. In *Proceedings of the National Academy of Sciences of the United States of America* 103 (4), pp. 976–981. DOI: 10.1073/pnas.0510146103.

Liu, Yu; Chen, Chong; Xu, Zhengmin; Scuoppo, Claudio; Rillahan, Cory D.; Gao, Jianjiong et al. (2016): Deletions linked to TP53 loss drive cancer through p53-independent mechanisms. In *Nature* 531 (7595), pp. 471–475. DOI: 10.1038/nature17157.

Liu, Yunhua; Zhang, Xinna; Han, Cecil; Wan, Guohui; Huang, Xingxu; Ivan, Cristina et al. (2015): TP53 loss creates therapeutic vulnerability in colorectal cancer. In *Nature* 520 (7549), pp. 697–701. DOI: 10.1038/nature14418.

Loh, Stewart N. (2010): The missing zinc: p53 misfolding and cancer. In *Metallomics : integrated biometal science* 2 (7), pp. 442–449. DOI: 10.1039/c003915b.

Lozano, Guillermina (2010): Mouse models of p53 functions. In *Cold Spring Harbor perspectives in biology* 2 (4), a001115. DOI: 10.1101/cshperspect.a001115.

Ludes-Meyers, J. H.; Subler, M. A.; Shivakumar, C. V.; Munoz, R. M.; Jiang, P.; Bigger, J. E. et al. (1996): Transcriptional activation of the human epidermal growth factor receptor promoter by human p53. In *Molecular and cellular biology* 16 (11), pp. 6009–6019. DOI: 10.1128/MCB.16.11.6009.

Ludwig, R. L.; Bates, S.; Vousden, K. H. (1996): Differential activation of target cellular promoters by p53 mutants with impaired apoptotic function. In *Molecular and cellular biology* 16 (9), pp. 4952–4960. DOI: 10.1128/mcb.16.9.4952.

Lynch, C. J.; Milner, J. (2006): Loss of one p53 allele results in four-fold reduction of p53 mRNA and protein: a basis for p53 haplo-insufficiency. In *Oncogene* 25 (24), pp. 3463–3470. DOI: 10.1038/sj.onc.1209387.

Ma, Buyong; Levine, Arnold J. (2007): Probing potential binding modes of the p53 tetramer to DNA based on the symmetries encoded in p53 response elements. In *Nucleic acids research* 35 (22), pp. 7733–7747. DOI: 10.1093/nar/gkm890.

Ma, Buyong; Pan, Yongping; Zheng, Jie; Levine, Arnold J.; Nussinov, Ruth (2007): Sequence analysis of p53 response-elements suggests multiple binding modes of the p53 tetramer to DNA targets. In *Nucleic acids research* 35 (9), pp. 2986–3001. DOI: 10.1093/nar/gkm192.

Ma, Leyuan; Boucher, Jeffrey I.; Paulsen, Janet; Matuszewski, Sebastian; Eide, Christopher A.; Ou, Jianhong et al. (2017): CRISPR-Cas9-mediated saturated mutagenesis screen predicts clinical drug resistance with improved accuracy. In *Proceedings of the National Academy of Sciences of the United States of America*, pp. 11751–11756. DOI: 10.1073/pnas.1708268114.

Madhumalar, Arumugam; Lee, Hui Jun; Brown, Christopher J.; Lane, David; Verma, Chandra (2009): Design of a novel MDM2 binding peptide based on the p53 family. In *Cell cycle (Georgetown, Tex.)*, pp. 2828–2836. DOI: 10.4161/cc.8.17.9516.

Mali, Prashant; Yang, Luhan; Esvelt, Kevin M.; Aach, John; Guell, Marc; DiCarlo, James E. et al. (2013): RNA-guided human genome engineering via Cas9. In *Science (New York, N.Y.)* 339 (6121), pp. 823–826. DOI: 10.1126/science.1232033.

Malkin, D.; Li, F. P.; Strong, L. C.; Fraumeni, J. F.; Nelson, C. E.; Kim, D. H. et al. (1990): Germ line p53 mutations in a familial syndrome of breast cancer, sarcomas, and other neoplasms. In *Science (New York, N.Y.)* 250 (4985), pp. 1233–1238. DOI: 10.1126/science.1978757.

Manfredi, James J. (2019): p53 and Development: Shedding Light on an Evolutionary Enigma. In *Developmental cell* 50 (2), pp. 128–129. DOI: 10.1016/j.devcel.2019.07.004.

Mantovani, Fiamma; Collavin, Licio; Del Sal, Giannino (2019): Mutant p53 as a guardian of the cancer cell. In *Cell death and differentiation* 26 (2), pp. 199–212. DOI: 10.1038/s41418-018-0246-9.

Mantovani, Fiamma; Walerych, Dawid; Sal, Giannino Del (2017): Targeting mutant p53 in cancer: a long road to precision therapy. In *The FEBS journal* 284 (6), pp. 837–850. DOI: 10.1111/febs.13948.

Marcel, V.; Dichtel-Danjoy, M-L; Sagne, C.; Hafsi, H.; Ma, D.; Ortiz-Cuaran, S. et al. (2011): Biological functions of p53 isoforms through evolution: lessons from animal and cellular models. In *Cell death and differentiation* 18 (12), pp. 1815–1824. DOI: 10.1038/cdd.2011.120.

Marine, Jean-Christophe; Jochemsen, Aart G. (2004): Mdmx and Mdm2: brothers in arms? In *Cell cycle (Georgetown, Tex.)* 3 (7), pp. 900–904.

Martins, Carla P.; Brown-Swigart, Lamorna; Evan, Gerard I. (2006): Modeling the therapeutic efficacy of p53 restoration in tumors. In *Cell* 127 (7), pp. 1323–1334. DOI: 10.1016/j.cell.2006.12.007.

Maruyama, Takeshi; Dougan, Stephanie K.; Truttmann, Matthias C.; Bilate, Angelina M.; Ingram, Jessica R.; Ploegh, Hidde L. (2015): Increasing the efficiency of precise genome editing with CRISPR-Cas9 by inhibition of nonhomologous end joining. In *Nature biotechnology* 33 (5), pp. 538–542. DOI: 10.1038/nbt.3190.

Mateo, Joaquin; Seed, George; Bertan, Claudia; Rescigno, Pasquale; Dolling, David; Figueiredo, Ines et al. (2020): Genomics of lethal prostate cancer at diagnosis and castration resistance. In *The Journal of clinical investigation* 130 (4), pp. 1743–1751. DOI: 10.1172/JCI132031.

Matoulkova, Eva; Michalova, Eva; Vojtesek, Borivoj; Hrstka, Roman (2012): The role of the 3' untranslated region in post-transcriptional regulation of protein expression in mammalian cells. In *RNA biology* 9 (5), pp. 563–576. DOI: 10.4161/rna.20231.

Meisler, M. H. (1975): Inhibition of human liver beta-galactosidases and beta-glucosidase by n-bromoacetyl-beta-D-galactosylamine. In *Biochimica et biophysica acta* 410 (2), pp. 347–353. DOI: 10.1016/0005-2744(75)90236-3.

Mello, S. S.; Attardi, L. D. (2013): Not all p53 gain-of-function mutants are created equal. In *Cell death and differentiation* 20 (7), pp. 855–857. DOI: 10.1038/cdd.2013.53.

Menendez, Daniel; Inga, Alberto; Resnick, Michael A. (2006): The biological impact of the human master regulator p53 can be altered by mutations that change the spectrum and expression of its target genes. In *Molecular and cellular biology* 26 (6), pp. 2297–2308. DOI: 10.1128/MCB.26.6.2297-2308.2006.

Metsalu, Tauno; Vilo, Jaak (2015): ClustVis: a web tool for visualizing clustering of multivariate data using Principal Component Analysis and heatmap. In *Nucleic acids research* 43 (W1), W566-70. DOI: 10.1093/nar/gkv468.

Meyers, F. J.; Chi, S. G.; Fishman, J. R.; deVere White, R. W.; Gumerlock, P. H. (1993): p53 mutations in benign prostatic hyperplasia. In *Journal of the National Cancer Institute* 85 (22), pp. 1856–1858. DOI: 10.1093/jnci/85.22.1856.

Michalovitz, Dan; Halevy, Orna; Oren, Moshe (1990): Conditional inhibition of transformation and of cell proliferation by a temperature-sensitive mutant of p53. In *Cell* 62 (4), pp. 671–680. DOI: 10.1016/0092-8674(90)90113-s.

Michele Harvey; Hannes VogeF; Danna Morris; Allan Bradley; Alan Bernstein; Lawrence A. Donehower. (1995): A mutant p53 transgene accelerates tumour development in heterozygous but not nullizygous p53-deficient mice. In *Nature genetics* 9.

Mighell, Taylor L.; Evans-Dutson, Sara; O'Roak, Brian J. (2018): A Saturation Mutagenesis Approach to Understanding PTEN Lipid Phosphatase Activity and Genotype-Phenotype Relationships. In *American journal of human genetics* 102 (5), pp. 943–955. DOI: 10.1016/j.ajhg.2018.03.018.

Mihara, Motohiro; Erster, Susan; Zaika, Alexander; Petrenko, Oleksi; Chittenden, Thomas; Pancoska, Petr; Moll, Ute M. (2003): p53 Has a Direct Apoptogenic Role at the Mitochondria. In *Molecular cell* 11 (3), pp. 577–590. DOI: 10.1016/s1097-2765(03)00050-9.

Milner, Jo; Medcalf, E. A. (1991): Cotranslation of activated mutant p53 with wild type drives the wild-type p53 protein into the mutant conformation. In *Cell* 65 (5), pp. 765–774. DOI: 10.1016/0092-8674(91)90384-B.

Mina, Marco; Raynaud, Franck; Tavernari, Daniele; Battistello, Elena; Sungalee, Stephanie; Saghafinia, Sadegh et al. (2017): Conditional Selection of Genomic Alterations Dictates Cancer Evolution and Oncogenic Dependencies. In *Cancer cell* 32 (2), 155-168.e6. DOI: 10.1016/j.ccell.2017.06.010.

Moll, Ute M.; Wolff, Sonja; Speidel, Daniel; Deppert, Wolfgang (2005): Transcription-independent pro-apoptotic functions of p53. In *Current opinion in cell biology* 17 (6), pp. 631–636. DOI: 10.1016/j.ceb.2005.09.007.

Monti, Paola; Perfumo, Chiara; Bisio, Alessandra; Ciribilli, Yari; Menichini, Paola; Russo, Debora et al. (2011): Dominant-negative features of mutant TP53 in germline carriers have limited impact on cancer outcomes. In *Molecular cancer research : MCR* 9 (3), pp. 271–279. DOI: 10.1158/1541-7786.MCR-10-0496.

Morton, Jennifer P.; Timpson, Paul; Karim, Saadia A.; Ridgway, Rachel A.; Athineos, Dimitris; Doyle, Brendan et al. (2010): Mutant p53 drives metastasis and overcomes growth arrest/senescence in pancreatic cancer. In *Proceedings of the National Academy of Sciences of the United States of America* 107 (1), pp. 246–251. DOI: 10.1073/pnas.0908428107.

Muhlinen, Natalia von; Horikawa, Izumi; Alam, Fatima; Isogaya, Kazunobu; Lissa, Delphine; Vojtesek, Borek et al. (2018): p53 isoforms regulate premature aging in human cells. In *Oncogene* 37 (18), pp. 2379–2393. DOI: 10.1038/s41388-017-0101-3.

Mullany, Lisa K.; Wong, Kwong-Kwok; Marciano, David C.; Katsonis, Panagiotis; King-Crane, Erin R.; Ren, Yi Athena et al. (2015): Specific TP53 Mutants Overrepresented in Ovarian Cancer Impact CNV, TP53 Activity, Responses to

Nutlin-3a, and Cell Survival. In *Neoplasia (New York, N.Y.)* 17 (10), pp. 789–803. DOI: 10.1016/j.neo.2015.10.003.

Muller, Patricia A. J.; Vousden, Karen H. (2013): p53 mutations in cancer. In *Nature cell biology* 15 (1), pp. 2–8. DOI: 10.1038/ncb2641.

Muller, Patricia A. J.; Vousden, Karen H. (2014): Mutant p53 in cancer: new functions and therapeutic opportunities. In *Cancer cell* 25 (3), pp. 304–317. DOI: 10.1016/j.ccr.2014.01.021.

Muller, Patricia A. J.; Vousden, Karen H.; Norman, Jim C. (2011): p53 and its mutants in tumor cell migration and invasion. In *The Journal of cell biology* 192 (2), pp. 209–218. DOI: 10.1083/jcb.201009059.

Murakami, I.; Hiyama, K.; Ishioka, S.; Yamakido, M.; Kasagi, F.; Yokosaki, Y. (2000): p53 gene mutations are associated with shortened survival in patients with advanced non-small cell lung cancer: an analysis of medically managed patients. In *Clinical cancer research : an official journal of the American Association for Cancer Research* 6 (2), pp. 526–530.

Murray-Zmijewski, Fiona; Slee, Elizabeth A.; Lu, Xin (2008): A complex barcode underlies the heterogeneous response of p53 to stress. In *Nature reviews. Molecular cell biology* 9 (9), pp. 702–712. DOI: 10.1038/nrm2451.

Nambiar, Tarun S.; Billon, Pierre; Diedenhofen, Giacomo; Hayward, Samuel B.; Taglialatela, Angelo; Cai, Kunheng et al. (2019): Stimulation of CRISPR-mediated homology-directed repair by an engineered RAD18 variant. In *Nature communications*, p. 3395. DOI: 10.1038/s41467-019-11105-z.

Ng, Pauline C.; Henikoff, Steven (2003): SIFT: Predicting amino acid changes that affect protein function. In *Nucleic acids research* 31 (13), pp. 3812–3814. DOI: 10.1093/nar/gkg509.

Olive, Kenneth P.; Tuveson, David A.; Ruhe, Zachary C.; Yin, Bob; Willis, Nicholas A.; Bronson, Roderick T. et al. (2004): Mutant p53 gain of function in two mouse models of Li-Fraumeni syndrome. In *Cell* 119 (6), pp. 847–860. DOI: 10.1016/j.cell.2004.11.004.

Oliveira, Guilherme A. P. de; Petronilho, Elaine C.; Pedrote, Murilo M.; Marques, Mayra A.; Vieira, Tuane C. R. G.; Cino, Elio A.; Silva, Jerson L. (2020): The Status of p53 Oligomeric and Aggregation States in Cancer. In *Biomolecules* 10 (4). DOI: 10.3390/biom10040548.

Olivier, Magali; Eeles, Ros; Hollstein, Monica; Khan, Mohammed A.; Harris, Curtis C.; Hainaut, Pierre (2002): The IARC TP53 database: new online mutation analysis and recommendations to users. In *Human mutation* 19 (6), pp. 607–614. DOI: 10.1002/humu.10081.

Olivier, Magali; Hainaut, Pierre; Børresen-Dale, Anne-Lise (2007): Prognostic and Predictive Value of TP53 Mutations in Human Cancer. In Pierre Hainaut, Klas G. Wiman (Eds.): 25 Years of p53 Research, vol. 2. Dordrecht: Springer Netherlands, pp. 321–338.

Olivier, Magali; Hollstein, Monica; Hainaut, Pierre (2010): TP53 mutations in human cancers: origins, consequences, and clinical use. In *Cold Spring Harbor perspectives in biology* 2 (1), a001008. DOI: 10.1101/cshperspect.a001008.

Ory, K.; Legros, Y.; Auguin, C.; Soussi, T. (1994): Analysis of the most representative tumour-derived p53 mutants reveals that changes in protein conformation are not correlated with loss of transactivation or inhibition of cell proliferation. In *EMBO J* 13 (15), pp. 3496–3504.

Paek, Andrew L.; Liu, Julia C.; Loewer, Alexander; Forrester, William C.; Lahav, Galit (2016): Cell-to-Cell Variation in p53 Dynamics Leads to Fractional Killing. In *Cell* 165 (3), pp. 631–642. DOI: 10.1016/j.cell.2016.03.025.

Paola Monti; Paola Campomenosi; Yari Ciribilli; Raffaella Iannone; Alberto Inga; Angelo Abbondandolo et al. (2002): Tumour p53 mutations exhibit promoter selective dominance over wild type p53 21, pp. 1641–1648. DOI: 10.1038/sj/onc/1205250.

Parrales, Alejandro; Iwakuma, Tomoo (2015): Targeting Oncogenic Mutant p53 for Cancer Therapy. In *Frontiers in oncology* 5, p. 288. DOI: 10.3389/fonc.2015.00288.

Parrales, Alejandro; Ranjan, Atul; Iyer, Swathi V.; Padhye, Subhash; Weir, Scott J.; Roy, Anuradha; Iwakuma, Tomoo (2016): DNAJA1 controls the fate of misfolded

mutant p53 through the mevalonate pathway. In *Nature cell biology* 18 (11), pp. 1233–1243. DOI: 10.1038/ncb3427.

Parrales, Alejandro; Thoenen, Elizabeth; Iwakuma, Tomoo (2018): The interplay between mutant p53 and the mevalonate pathway. In *Cell death and differentiation* 25 (3), pp. 460–470. DOI: 10.1038/s41418-017-0026-y.

Peller, S.; Kopilova, Y.; Slutzki, S.; Halevy, A.; Kvitko, K.; Rotter, V. (1995): A novel polymorphism in intron 6 of the human p53 gene: a possible association with cancer predisposition and susceptibility. In *DNA and cell biology* 14 (12), pp. 983–990. DOI: 10.1089/dna.1995.14.983.

Peng, X.; Zhang, M-Q-Z; Conserva, F.; Hosny, G.; Selivanova, G.; Bykov, V. J. N. et al. (2013): APR-246/PRIMA-1MET inhibits thioredoxin reductase 1 and converts the enzyme to a dedicated NADPH oxidase. In *Cell death & disease* 4, e881. DOI: 10.1038/cddis.2013.417.

Polyak, K.; Waldman, T.; He, T. C.; Kinzler, K. W.; Vogelstein, B. (1996): Genetic determinants of p53-induced apoptosis and growth arrest. In *Genes & development* 10 (15), pp. 1945–1952. DOI: 10.1101/gad.10.15.1945.

Pomerantz, Jason; Schreiber-Agus, Nicole; Liégeois, Nanette J.; Silverman, Adam; Alland, Leila; Chin, Lynda et al. (1998): The Ink4a Tumor Suppressor Gene Product, p19Arf, Interacts with MDM2 and Neutralizes MDM2's Inhibition of p53. In *Cell* 92 (6), pp. 713–723. DOI: 10.1016/s0092-8674(00)81400-2.

Puca, Rosa; Nardinocchi, Lavinia; Porru, Manuela; Simon, Amos J.; Rechavi, Gideon; Leonetti, Carlo et al. (2011): Restoring p53 active conformation by zinc increases the response of mutant p53 tumor cells to anticancer drugs. In *Cell cycle (Georgetown, Tex.)* 10 (10), pp. 1679–1689. DOI: 10.4161/cc.10.10.15642.

Purvis, Jeremy E.; Karhohs, Kyle W.; Mock, Caroline; Batchelor, Eric; Loewer, Alexander; Lahav, Galit (2012): p53 dynamics control cell fate. In *Science (New York, N.Y.)* 336 (6087), pp. 1440–1444. DOI: 10.1126/science.1218351.

Quante, Timo; Otto, Benjamin; Brázdová, Marie; Kejnovská, Iva; Deppert, Wolfgang; Tolstonog, Genrich V. (2012): Mutant p53 is a transcriptional co-factor that binds to

G-rich regulatory regions of active genes and generates transcriptional plasticity. In *Cell cycle (Georgetown, Tex.)* 11 (17), pp. 3290–3303. DOI: 10.4161/cc.21646.

Ramensky, Vasily; Bork, Peer; Sunyaev, Shamil (2002): Human non-synonymous SNPs: server and survey. In *Nucleic acids research* 30 (17), pp. 3894–3900.

Ranjan, Atul; Iwakuma, Tomoo (2016): Non-Canonical Cell Death Induced by p53. In *International journal of molecular sciences* 17 (12). DOI: 10.3390/ijms17122068.

Ray-Coquard, Isabelle; Braicu, Ioana; Berger, Regina; Mahner, Sven; Sehouli, Jalid; Pujade-Lauraine, Eric et al. (2019): Part I of GANNET53: A European Multicenter Phase I/II Trial of the Hsp90 Inhibitor Ganetespib Combined With Weekly Paclitaxel in Women With High-Grade, Platinum-Resistant Epithelial Ovarian Cancer-A Study of the GANNET53 Consortium. In *Frontiers in oncology* 9, p. 832. DOI: 10.3389/fonc.2019.00832.

Reva, Boris; Antipin, Yevgeniy; Sander, Chris (2007): Determinants of protein function revealed by combinatorial entropy optimization. In *Genome Biology* 8 (11), R232. DOI: 10.1186/gb-2007-8-11-r232.

Reva, Boris; Antipin, Yevgeniy; Sander, Chris (2011): Predicting the functional impact of protein mutations: application to cancer genomics. In *Nucleic acids research* 39 (17), e118. DOI: 10.1093/nar/gkr407.

Ribeiro, R. C.; Sandrini, F.; Figueiredo, B.; Zambetti, G. P.; Michalkiewicz, E.; Lafferty, A. R. et al. (2001): An inherited p53 mutation that contributes in a tissue-specific manner to pediatric adrenal cortical carcinoma. In *Proceedings of the National Academy of Sciences of the United States of America* 98 (16), pp. 9330–9335. DOI: 10.1073/pnas.161479898.

Ribi, Sebastian; Baumhoer, Daniel; Lee, Kristy; Edison; Teo, Audrey S. M.; Madan, Babita et al. (2015): TP53 intron 1 hotspot rearrangements are specific to sporadic osteosarcoma and can cause Li-Fraumeni syndrome. In *Oncotarget* 6 (10), pp. 7727–7740. DOI: 10.18632/oncotarget.3115.

Richter-Pechańska, P.; Kunz, J. B.; Hof, J.; Zimmermann, M.; Rausch, T.; Bandapalli, O. R. et al. (2017): Identification of a genetically defined ultra-high-risk

group in relapsed pediatric T-lymphoblastic leukemia. In *Blood cancer journal* 7 (2), e523. DOI: 10.1038/bcj.2017.3.

Riemenschneider, M. J.; Büschges, R.; Wolter, M.; Reifenberger, J.; Boström, J.; Kraus, J. A. et al. (1999): Amplification and overexpression of the MDM4 (MDMX) gene from 1q32 in a subset of malignant gliomas without TP53 mutation or MDM2 amplification. In *Cancer research* 59 (24), pp. 6091–6096.

Riley, Todd; Sontag, Eduardo; Chen, Patricia; Levine, Arnold (2008): Transcriptional control of human p53-regulated genes. In *Nature reviews. Molecular cell biology* 9 (5), pp. 402–412. DOI: 10.1038/nrm2395.

Robles, Ana I.; Harris, Curtis C. (2010): Clinical outcomes and correlates of TP53 mutations and cancer. In *Cold Spring Harbor perspectives in biology* 2 (3), a001016. DOI: 10.1101/cshperspect.a001016.

Rowan, S.; Ludwig, R. L.; Haupt, Y.; Bates, S.; Lu, X.; Oren, M.; Vousden, K. H. (1996): Specific loss of apoptotic but not cell-cycle arrest function in a human tumor derived p53 mutant. In *EMBO J* 15 (4), pp. 827–838.

Ryan, K. M.; Vousden, K. H. (1998): Characterization of structural p53 mutants which show selective defects in apoptosis but not cell cycle arrest. In *Molecular and cellular biology* 18 (7), pp. 3692–3698. DOI: 10.1128/mcb.18.7.3692.

Sabapathy, Kanaga (2015): The Contrived Mutant p53 Oncogene - Beyond Loss of Functions. In *Frontiers in oncology* 5, p. 276. DOI: 10.3389/fonc.2015.00276.

Sabapathy, Kanaga; Lane, David P. (2018): Therapeutic targeting of p53: all mutants are equal, but some mutants are more equal than others. In *Nature reviews. Clinical oncology* 15 (1), pp. 13–30. DOI: 10.1038/nrclinonc.2017.151.

Sablina, Anna A.; Budanov, Andrei V.; Ilyinskaya, Galina V.; Agapova, Larissa S.; Kravchenko, Julia E.; Chumakov, Peter M. (2005): The antioxidant function of the p53 tumor suppressor. In *Nature medicine* 11 (12), pp. 1306–1313. DOI: 10.1038/nm1320.

Saiki, Anne Y.; Caenepeel, Sean; Cosgrove, Elissa; Su, Cheng; Boedigheimer, Michael; Oliner, Jonathan D. (2015): Identifying the determinants of response to

MDM2 inhibition. In *Oncotarget* 6 (10), pp. 7701–7712. DOI: 10.18632/oncotarget.3116.

Sailaja, K.; Rao, V. R.; Yadav, Satish; Reddy, R. Rajasekhar; Surekha, D.; Rao, D. Nageswara et al. (2012): Intronic SNPs of TP53 gene in chronic myeloid leukemia: Impact on drug response. In *Journal of natural science, biology, and medicine* 3 (2), pp. 182–185. DOI: 10.4103/0976-9668.101910.

Sallman, David A. (2020): To target the untargetable: elucidation of synergy of APR-246 and azacitidine in TP53 mutant myelodysplastic syndromes and acute myeloid leukemia. In *Haematologica* 105 (6), pp. 1470–1472. DOI: 10.3324/haematol.2020.249060.

Sane, Sanam; Rezvani, Khosrow (2017): Essential Roles of E3 Ubiquitin Ligases in p53 Regulation. In *International journal of molecular sciences* 18 (2). DOI: 10.3390/ijms18020442.

Sargent, R. G.; Brenneman, M. A.; Wilson, J. H. (1997): Repair of site-specific double-strand breaks in a mammalian chromosome by homologous and illegitimate recombination. In *Molecular and cellular biology* 17 (1), pp. 267–277. DOI: 10.1128/MCB.17.1.267.

Schlereth, Katharina; Beinoraviciute-Kellner, Rasa; Zeitlinger, Marie K.; Bretz, Anne C.; Sauer, Markus; Charles, Joël P. et al. (2010a): DNA binding cooperativity of p53 modulates the decision between cell-cycle arrest and apoptosis. In *Molecular cell* 38 (3), pp. 356–368. DOI: 10.1016/j.molcel.2010.02.037.

Schlereth, Katharina; Charles, Joël P.; Bretz, Anne C.; Stiewe, Thorsten (2010b): Life or death: p53-induced apoptosis requires DNA binding cooperativity. In *Cell cycle (Georgetown, Tex.)*, pp. 4068–4076. DOI: 10.4161/cc.9.20.13595.

Schlereth, Katharina; Heyl, Charlotte; Krampitz, Anna-Maria; Mernberger, Marco; Finkernagel, Florian; Scharfe, Maren et al. (2013): Characterization of the p53 cistrome--DNA binding cooperativity dissects p53's tumor suppressor functions. In *PLoS genetics* 9 (8), e1003726. DOI: 10.1371/journal.pgen.1003726.

Schon, Katherine; Tischkowitz, Marc (2018): Clinical implications of germline mutations in breast cancer: TP53. In *Breast cancer research and treatment* 167 (2), pp. 417–423. DOI: 10.1007/s10549-017-4531-y.

Schulz-Heddergott, Ramona; Moll, Ute M. (2018): Gain-of-Function (GOF) Mutant p53 as Actionable Therapeutic Target. In *Cancers* 10 (6). DOI: 10.3390/cancers10060188.

Schulz-Heddergott, Ramona; Stark, Nadine; Edmunds, Shelley J.; Li, Jinyu; Conradi, Lena-Christin; Bohnenberger, Hanibal et al. (2018): Therapeutic Ablation of Gain-of-Function Mutant p53 in Colorectal Cancer Inhibits Stat3-Mediated Tumor Growth and Invasion. In *Cancer cell* 34 (2), 298-314.e7. DOI: 10.1016/j.ccell.2018.07.004.

Sekine, Shigeki; Shibata, Tatsuhiro; Sakamoto, Michiie; Hirohashi, Setsuo (2002): Target disruption of the mutant beta-catenin gene in colon cancer cell line HCT116: preservation of its malignant phenotype. In *Oncogene* 21 (38), pp. 5906–5911. DOI: 10.1038/sj.onc.1205756.

Senturk, Serif; Yao, Zhan; Camiolo, Matthew; Stiles, Brendon; Rathod, Trushar; Walsh, Alice M. et al. (2014): p53Ψ is a transcriptionally inactive p53 isoform able to reprogram cells toward a metastatic-like state. In *Proceedings of the National Academy of Sciences of the United States of America* 111 (32), E3287-96. DOI: 10.1073/pnas.1321640111.

Shapiro, M. B.; Senapathy, P. (1987): RNA splice junctions of different classes of eukaryotes: sequence statistics and functional implications in gene expression. In *Nucleic acids research* 15 (17), pp. 7155–7174. DOI: 10.1093/nar/15.17.7155.

Shaulian, E.; Zauberman, A.; Ginsberg, D.; Oren, M. (1992): Identification of a minimal transforming domain of p53: negative dominance through abrogation of sequence-specific DNA binding. In *Molecular and cellular biology* 12 (12), pp. 5581–5592. DOI: 10.1128/mcb.12.12.5581.

Shi, Xu-Bao; Nesslinger, Nancy J.; Deitch, Arline D.; Gumerlock, Paul H.; deVere White, Ralph W. (2002): Complex functions of mutant p53 alleles from human prostate cancer. In *The Prostate* 51 (1), pp. 59–72. DOI: 10.1002/pros.10072.

Shirole; Pal D; Kastenhuber ER; Senturk S. (2016): TP53 exon-6 truncating mutations produce separation of function isoforms with pro-tumorigenic functions. Elife (5).

Sigalas, I.; Calvert, A. H.; Anderson, J. J.; Neal, D. E.; Lunec, J. (1996): Alternatively spliced mdm2 transcripts with loss of p53 binding domain sequences: transforming ability and frequent detection in human cancer. In *Nature medicine* 2 (8), pp. 912–917. DOI: 10.1038/nm0896-912.

Silden, Elisabeth; Hjelle, Sigrun M.; Wergeland, Line; Sulen, André; Andresen, Vibeke; Bourdon, Jean-Christophe et al. (2013): Expression of TP53 isoforms p53β or p53γ enhances chemosensitivity in TP53(null) cell lines. In *PloS one* 8 (2), e56276. DOI: 10.1371/journal.pone.0056276.

Siloto, Rodrigo M.P.; Weselake, Randall J. (2012): Site saturation mutagenesis: Methods and applications in protein engineering. In *Biocatalysis and Agricultural Biotechnology* 1 (3), pp. 181–189. DOI: 10.1016/j.bcab.2012.03.010.

Silva, Jerson L.; Moura Gallo, Claudia V. de; Costa, Danielly C. F.; Rangel, Luciana P. (2014): Prion-like aggregation of mutant p53 in cancer. In *Trends in biochemical sciences* 39 (6), pp. 260–267. DOI: 10.1016/j.tibs.2014.04.001.

Sim, Ngak-Leng; Kumar, Prateek; Hu, Jing; Henikoff, Steven; Schneider, Georg; Ng, Pauline C. (2012): SIFT web server: predicting effects of amino acid substitutions on proteins. In *Nucleic acids research* 40 (Web Server issue), W452-7. DOI: 10.1093/nar/gks539.

Sinn, Marianne; Sinn, Bruno V.; Treue, Denise; Keilholz, Ulrich; Damm, Frederik; Schmuck, Rosa et al. (2020): TP53 Mutations Predict Sensitivity to Adjuvant Gemcitabine in Patients with Pancreatic Ductal Adenocarcinoma: Next-Generation Sequencing Results from the CONKO-001 Trial. In *Clinical cancer research : an official journal of the American Association for Cancer Research* 26 (14), pp. 3732–3739. DOI: 10.1158/1078-0432.CCR-19-3034.

Smeby, Jørgen; Sveen, Anita; Bergsland, Christian H.; Eilertsen, Ina A.; Danielsen, Stine A.; Eide, Peter W. et al. (2019): Exploratory analyses of consensus molecular subtype-dependent associations of TP53 mutations with immunomodulation and

prognosis in colorectal cancer. In *ESMO open* 4 (3), e000523. DOI: 10.1136/esmoopen-2019-000523.

Solomon, H.; Sharon, M.; Rotter, V. (2014): Modulation of alternative splicing contributes to cancer development: focusing on p53 isoforms, p53β and p53γ. In *Cell death and differentiation* 21 (9), pp. 1347–1349. DOI: 10.1038/cdd.2014.99.

Soragni, Alice; Janzen, Deanna M.; Johnson, Lisa M.; Lindgren, Anne G.; Thai-Quynh Nguyen, Anh; Tiourin, Ekaterina et al. (2016): A Designed Inhibitor of p53 Aggregation Rescues p53 Tumor Suppression in Ovarian Carcinomas. In *Cancer cell* 29 (1), pp. 90–103. DOI: 10.1016/j.ccell.2015.12.002.

Sorrentino, Giovanni; Ruggeri, Naomi; Specchia, Valeria; Cordenonsi, Michelangelo; Mano, Miguel; Dupont, Sirio et al. (2014): Metabolic control of YAP and TAZ by the mevalonate pathway. In *Nature cell biology* 16 (4), pp. 357–366. DOI: 10.1038/ncb2936.

Soussi, Thierry (2014): The TP53 gene network in a postgenomic era. In *Human mutation* 35 (6), pp. 641–642. DOI: 10.1002/humu.22562.

Soussi, Thierry; Kato, Shunsuke; Levy, Pierre P.; Ishioka, Chikashi (2005): Reassessment of the TP53 mutation database in human disease by data mining with a library of TP53 missense mutations. In *Human mutation* 25 (1), pp. 6–17. DOI: 10.1002/humu.20114.

Srivastava, S.; Wang, S.; Tong, Y. A.; Hao, Z. M.; Chang, E. H. (1993): Dominant negative effect of a germ-line mutant p53: a step fostering tumorigenesis. In *Cancer research* 53 (19), pp. 4452–4455.

Srivastava S.; Wang S.; Tong Y.A, Hao Zheng-Mei, and Chang E. H. (1993): Dominant Negative Effect of a Germ-line Mutant p53: A Step Fostering Tumorigenesis. In *Cancer research* (53), pp. 4452–44555.

Steckel, Michael; Molina-Arcas, Miriam; Weigelt, Britta; Marani, Michaela; Warne, Patricia H.; Kuznetsov, Hanna et al. (2012): Determination of synthetic lethal interactions in KRAS oncogene-dependent cancer cells reveals novel therapeutic targeting strategies. In *Cell research* 22 (8), pp. 1227–1245. DOI: 10.1038/cr.2012.82.

Stein, Yan; Aloni-Grinstein, Ronit; Rotter, Varda (2020): Mutant p53 oncogenicity: dominant-negative or gain-of-function? In *Carcinogenesis* 41 (12), pp. 1635–1647. DOI: 10.1093/carcin/bgaa117.

Stewart-Ornstein, Jacob; Iwamoto, Yoshiko; Miller, Miles A.; Prytyskach, Mark A.; Ferretti, Stephane; Holzer, Philipp et al. (2021): p53 dynamics vary between tissues and are linked with radiation sensitivity. In *Nature communications* 12 (1), p. 898. DOI: 10.1038/s41467-021-21145-z.

Stiewe, Thorsten; Haran, Tali E. (2018): How mutations shape p53 interactions with the genome to promote tumorigenesis and drug resistance. In *Drug resistance updates : reviews and commentaries in antimicrobial and anticancer chemotherapy* 38, pp. 27–43. DOI: 10.1016/j.drup.2018.05.001.

Stoner, Christopher S.; Pearson, George D.; Koç, Ahmet; Merwin, Jason R.; Lopez, Nathan I.; Merrill, Gary F. (2009): Effect of thioredoxin deletion and p53 cysteine replacement on human p53 activity in wild-type and thioredoxin reductase null yeast. In *Biochemistry* 48 (38), pp. 9156–9169. DOI: 10.1021/bi900757q.

Strasser, A.; Harris, A. W.; Jacks, T.; Cory, S. (1994): DNA damage can induce apoptosis in proliferating lymphoid cells via p53-independent mechanisms inhibitable by Bcl-2. In *Cell* 79 (2), pp. 329–339. DOI: 10.1016/0092-8674(94)90201-1.

Sturm, I.; Bosanquet, A. G.; Hermann, S.; Güner, D.; Dörken, B.; Daniel, P. T. (2003): Mutation of p53 and consecutive selective drug resistance in B-CLL occurs as a consequence of prior DNA-damaging chemotherapy. In *Cell death and differentiation* 10 (4), pp. 477–484. DOI: 10.1038/sj.cdd.4401194.

Suh, Young-Ah; Post, Sean M.; Elizondo-Fraire, Ana C.; Maccio, Daniela R.; Jackson, James G.; El-Naggar, Adel K. et al. (2011): Multiple stress signals activate mutant p53 in vivo. In *Cancer research* 71 (23), pp. 7168–7175. DOI: 10.1158/0008-5472.CAN-11-0459.

Sulak, Michael; Fong, Lindsey; Mika, Katelyn; Chigurupati, Sravanthi; Yon, Lisa; Mongan, Nigel P. et al. (2016): TP53 copy number expansion is associated with the evolution of increased body size and an enhanced DNA damage response in elephants. In *eLife* 5. DOI: 10.7554/eLife.11994.

Sullivan, Kelly D.; Galbraith, Matthew D.; Andrysik, Zdenek; Espinosa, Joaquin M. (2018): Mechanisms of transcriptional regulation by p53. In *Cell death and differentiation* 25 (1), pp. 133–143. DOI: 10.1038/cdd.2017.174.

Sun, Xiao-Xin; Dai, Mu-Shui; Lu, Hua (2007): 5-fluorouracil activation of p53 involves an MDM2-ribosomal protein interaction. In *The Journal of biological chemistry* 282 (11), pp. 8052–8059. DOI: 10.1074/jbc.M610621200.

Sun, Y.; Dong, Z.; Nakamura, K.; Colburn, N. H. (1993): Dosage-dependent dominance over wild-type p53 of a mutant p53 isolated from nasopharyngeal carcinoma. In *FASEB journal : official publication of the Federation of American Societies for Experimental Biology* 7 (10), pp. 944–950. DOI: 10.1096/fasebj.7.10.8344492.

Sunyaev, S. R.; Eisenhaber, F.; Rodchenkov, I. V.; Eisenhaber, B.; Tumanyan, V. G.; Kuznetsov, E. N. (1999): PSIC: profile extraction from sequence alignments with position-specific counts of independent observations. In *Protein engineering* 12 (5), pp. 387–394. DOI: 10.1093/protein/12.5.387.

Sur, Surojit; Pagliarini, Raymond; Bunz, Fred; Rago, Carlo; Diaz, Luis A.; Kinzler, Kenneth W. et al. (2009): A panel of isogenic human cancer cells suggests a therapeutic approach for cancers with inactivated p53. In *Proceedings of the National Academy of Sciences of the United States of America* 106 (10), pp. 3964–3969. DOI: 10.1073/pnas.0813333106.

Surget, Sylvanie; Khoury, Marie P.; Bourdon, Jean-Christophe (2013): Uncovering the role of p53 splice variants in human malignancy: a clinical perspective. In *OncoTargets and therapy* 7, pp. 57–68. DOI: 10.2147/OTT.S53876.

Takahashi, T.; D'Amico, D.; Chiba, I.; Buchhagen, D. L.; Minna, J. D. (1990): Identification of intronic point mutations as an alternative mechanism for p53 inactivation in lung cancer. In *The Journal of clinical investigation* 86 (1), pp. 363–369. DOI: 10.1172/JCI114710.

Tanikawa, Chizu; Zhang, Yao-Zhong; Yamamoto, Ryuta; Tsuda, Yusuke; Tanaka, Masami; Funauchi, Yuki et al. (2017): The Transcriptional Landscape of p53

Signalling Pathway. In *EBioMedicine* 20, pp. 109–119. DOI: 10.1016/j.ebiom.2017.05.017.

Teng, Lianghong; Deng, Wanglong; Lu, Junliang; Zhang, Jing; Ren, Xinyu; Duan, Huanli et al. (2017): Hobnail variant of papillary thyroid carcinoma: molecular profiling and comparison to classical papillary thyroid carcinoma, poorly differentiated thyroid carcinoma and anaplastic thyroid carcinoma. In *Oncotarget* 8 (13), pp. 22023–22033. DOI: 10.18632/oncotarget.15786.

Teoh, P. J.; Chung, T. H.; Sebastian, S.; Choo, S. N.; Yan, J.; Ng, S. B. et al. (2014): p53 haploinsufficiency and functional abnormalities in multiple myeloma. In *Leukemia*, pp. 2066–2074. DOI: 10.1038/leu.2014.102.

Terzian, Tamara; Suh, Young-Ah; Iwakuma, Tomoo; Post, Sean M.; Neumann, Manja; Lang, Gene A. et al. (2008): The inherent instability of mutant p53 is alleviated by Mdm2 or p16INK4a loss. In *Genes & development* 22 (10), pp. 1337–1344. DOI: 10.1101/gad.1662908.

Timofeev, Oleg; Klimovich, Boris; Schneikert, Jean; Wanzel, Michael; Pavlakis, Evangelos; Noll, Julia et al. (2019): Residual apoptotic activity of a tumorigenic p53 mutant improves cancer therapy responses. In *EMBO J* 7, p. 606. DOI: 10.15252/embj.2019102096.

Timofeev, Oleg; Koch, Lukas; Niederau, Constantin; Tscherne, Alina; Schneikert, Jean; Klimovich, Maria et al. (2020): Phosphorylation control of p53 DNA binding cooperativity balances tumorigenesis and aging. In *Cancer research*. DOI: 10.1158/0008-5472.CAN-20-2002.

Timofeev, Oleg; Schlereth, Katharina; Wanzel, Michael; Braun, Attila; Nieswandt, Bernhard; Pagenstecher, Axel et al. (2013): p53 DNA binding cooperativity is essential for apoptosis and tumor suppression in vivo. In *Cell reports* 3 (5), pp. 1512–1525. DOI: 10.1016/j.celrep.2013.04.008.

Tisato, Veronica; Voltan, Rebecca; Gonelli, Arianna; Secchiero, Paola; Zauli, Giorgio (2017): MDM2/X inhibitors under clinical evaluation: perspectives for the management of hematological malignancies and pediatric cancer. In *Journal of hematology & oncology* 10 (1), p. 133. DOI: 10.1186/s13045-017-0500-5.

Tollini, Laura A.; Jin, Aiwen; Park, Jikyoung; Zhang, Yanping (2014): Regulation of p53 by Mdm2 E3 ligase function is dispensable in embryogenesis and development, but essential in response to DNA damage. In *Cancer cell* 26 (2), pp. 235–247. DOI: 10.1016/j.ccr.2014.06.006.

Tonelli, C.; Morelli, M. J.; Sabò, A.; Verrecchia, A.; Rotta, L.; Capra, T. et al. (2017): Genome-wide analysis of p53-regulated transcription in Myc-driven lymphomas. In *Oncogene* 36 (21), pp. 2921–2929. DOI: 10.1038/onc.2016.443.

Tonnessen-Murray, Crystal; Ungerleider, Nathan A.; Rao, Sonia G.; Wasylishen, Amanda R.; Frey, Wesley D.; Jackson, James G. (2018): p53 Mediates Vast Gene Expression Changes That Contribute to Poor Chemotherapeutic Response in a Mouse Model of Breast Cancer. In *Translational oncology* 11 (4), pp. 930–940. DOI: 10.1016/j.tranon.2018.05.003.

Tovar, Christian; Graves, Bradford; Packman, Kathryn; Filipovic, Zoran; Higgins, Brian; Xia, Mingxuan et al. (2013): MDM2 small-molecule antagonist RG7112 activates p53 signaling and regresses human tumors in preclinical cancer models. In *Cancer research* 73 (8), pp. 2587–2597. DOI: 10.1158/0008-5472.CAN-12-2807.

Tuladhar, Rubina; Yeu, Yunku; Tyler Piazza, John; Tan, Zhen; Rene Clemenceau, Jean; Wu, Xiaofeng et al. (2019): CRISPR-Cas9-based mutagenesis frequently provokes on-target mRNA misregulation. In *Nature communications* 10 (1), p. 4056. DOI: 10.1038/s41467-019-12028-5.

Tutuska, Karis; Parrilla-Monge, Laura; Di Cesare, Erica; Nemajerova, Alice; Moll, Ute M. (2020): Statin as anti-cancer therapy in autochthonous T-lymphomas expressing stabilized gain-of-function mutant p53 proteins. In *Cell death & disease* 11 (4), p. 274. DOI: 10.1038/s41419-020-2466-4.

Valente, L. J.; Grabow, S.; Vandenberg, C. J.; Strasser, A.; Janic, A. (2016a): Combined loss of PUMA and p21 accelerates c-MYC-driven lymphoma development considerably less than loss of one allele of p53. In *Oncogene* 35 (29), pp. 3866–3871. DOI: 10.1038/onc.2015.457.

Valente, Liz J.; Aubrey, Brandon J.; Herold, Marco J.; Kelly, Gemma L.; Happo, Lina; Scott, Clare L. et al. (2016b): Therapeutic Response to Non-genotoxic Activation of

p53 by Nutlin3a Is Driven by PUMA-Mediated Apoptosis in Lymphoma Cells. In *Cell reports* 14 (8), pp. 1858–1866. DOI: 10.1016/j.celrep.2016.01.059.

Valente, Liz J.; Gray, Daniel H. D.; Michalak, Ewa M.; Pinon-Hofbauer, Josefina; Egle, Alex; Scott, Clare L. et al. (2013): p53 efficiently suppresses tumor development in the complete absence of its cell-cycle inhibitory and proapoptotic effectors p21, Puma, and Noxa. In *Cell reports* 3 (5), pp. 1339–1345. DOI: 10.1016/j.celrep.2013.04.012.

Valenti, Fabio; Fausti, Francesca; Biagioni, Francesca; Shay, Tal; Fontemaggi, Giulia; Domany, Eytan et al. (2011): Mutant p53 oncogenic functions are sustained by Plk2 kinase through an autoregulatory feedback loop. In *Cell cycle (Georgetown, Tex.)* 10 (24), pp. 4330–4340. DOI: 10.4161/cc.10.24.18682.

Varley, J. M.; Chapman, P.; McGown, G.; Thorncroft, M.; White, G. R.; Greaves, M. J. et al. (1998): Genetic and functional studies of a germline TP53 splicing mutation in a Li-Fraumeni-like family. In *Oncogene* 16 (25), pp. 3291–3298. DOI: 10.1038/sj.onc.1201878.

Vaser, Robert; Adusumalli, Swarnaseetha; Leng, Sim Ngak; Sikic, Mile; Ng, Pauline C. (2016): SIFT missense predictions for genomes. In *Nature protocols* 11 (1), pp. 1–9. DOI: 10.1038/nprot.2015.123.

Vassilev, Lyubomir T.; Vu, Binh T.; Graves, Bradford; Carvajal, Daisy; Podlaski, Frank; Filipovic, Zoran et al. (2004): In vivo activation of the p53 pathway by small-molecule antagonists of MDM2. In *Science (New York, N.Y.)* 303 (5659), pp. 844–848. DOI: 10.1126/science.1092472.

Venkatachalam, S.; Tyner, S. D.; Pickering, C. R.; Boley, S.; Recio, L.; French, J. E.; Donehower, L. A. (2001): Is p53 haploinsufficient for tumor suppression? Implications for the p53+/- mouse model in carcinogenicity testing. In *Toxicologic pathology* 29 Suppl, pp. 147–154. DOI: 10.1080/019262301753178555.

Verselis, S. J.; Rheinwald, J. G.; Fraumeni, J. F.; Li, F. P. (2000): Novel p53 splice site mutations in three families with Li-Fraumeni syndrome. In *Oncogene* 19 (37), pp. 4230–4235. DOI: 10.1038/sj.onc.1203758.

Vieira, Igor Araujo; Andreis, Tiago Finger; Fernandes, Bruna Vieira; Achatz, Maria Isabel; Macedo, Gabriel S.; Schramek, Daniel; Ashton-Prolla, Patricia (2021): Prevalence of the Brazilian TP53 Founder c.1010GA (p.Arg337His) in Lung Adenocarcinoma: Is Genotyping Warranted in All Brazilian Patients? In *Frontiers in genetics* 12, p. 606537. DOI: 10.3389/fgene.2021.606537.

Vieler, Maximilian; Sanyal, Suparna (2018): p53 Isoforms and Their Implications in Cancer. In *Cancers* 10 (9). DOI: 10.3390/cancers10090288.

Vislovukh, Andrii; Vargas, Thaiz Rivera; Polesskaya, Anna; Groisman, Irina (2014): Role of 3'-untranslated region translational control in cancer development, diagnostics and treatment. In *World journal of biological chemistry* 5 (1), pp. 40–57. DOI: 10.4331/wjbc.v5.i1.40.

Vogiatzi, Fotini; Brandt, Dominique T.; Schneikert, Jean; Fuchs, Jeannette; Grikscheit, Katharina; Wanzel, Michael et al. (2016): Mutant p53 promotes tumor progression and metastasis by the endoplasmic reticulum UDPase ENTPD5. In *Proceedings of the National Academy of Sciences of the United States of America* 113 (52), E8433-E8442. DOI: 10.1073/pnas.1612711114.

Vries, Annemieke de; Flores, Elsa R.; Miranda, Barbara; Hsieh, Harn-Mei; van Oostrom, Conny Th M.; Sage, Julien; Jacks, Tyler (2002): Targeted point mutations of p53 lead to dominant-negative inhibition of wild-type p53 function. In *Proceedings of the National Academy of Sciences of the United States of America* 99 (5), pp. 2948–2953. DOI: 10.1073/pnas.052713099.

Walerych, Dawid; Lisek, Kamil; Del Sal, Giannino (2015): Mutant p53: One, No One, and One Hundred Thousand. In *Frontiers in oncology* 5, p. 289. DOI: 10.3389/fonc.2015.00289.

Walerych, Dawid; Lisek, Kamil; Sommaggio, Roberta; Piazza, Silvano; Ciani, Yari; Dalla, Emiliano et al. (2016): Proteasome machinery is instrumental in a common gain-of-function program of the p53 missense mutants in cancer. In *Nature cell biology* 18 (8), pp. 897–909. DOI: 10.1038/ncb3380.

Walerych, Dawid; Napoli, Marco; Collavin, Licio; Del Sal, Giannino (2012): The rebel angel: mutant p53 as the driving oncogene in breast cancer. In *Carcinogenesis* 33 (11), pp. 2007–2017. DOI: 10.1093/carcin/bgs232.

Wang, B.; Niu, D.; Lam, T. H.; Xiao, Z.; Ren, E. C. (2013): Mapping the p53 transcriptome universe using p53 natural polymorphs. In *Cell death and differentiation* 21 (4), pp. 521–532. DOI: 10.1038/cdd.2013.132.

Wang, Shaomeng; Sun, Wei; Zhao, Yujun; McEachern, Donna; Meaux, Isabelle; Barrière, Cédric et al. (2014): SAR405838: an optimized inhibitor of MDM2-p53 interaction that induces complete and durable tumor regression. In *Cancer research* 74 (20), pp. 5855–5865. DOI: 10.1158/0008-5472.CAN-14-0799.

Wang, Yao; Wang, Mingrui; Zheng, Ting; Hou, Yingzi; Zhang, Pingjing; Tang, Tao et al. (2020): Specificity profiling of CRISPR system reveals greatly enhanced off-target gene editing. In *Scientific reports* 10 (1), p. 2269. DOI: 10.1038/s41598-020-58627-x.

Wang, Zefeng; Rolish, Michael E.; Yeo, Gene; Tung, Vivian; Mawson, Matthew; Burge, Christopher B. (2004): Systematic identification and analysis of exonic splicing silencers. In *Cell* 119 (6), pp. 831–845. DOI: 10.1016/j.cell.2004.11.010.

Wasserman, Jonathan D.; Novokmet, Ana; Eichler-Jonsson, Claudia; Ribeiro, Raul C.; Rodriguez-Galindo, Carlos; Zambetti, Gerard P.; Malkin, David (2015): Prevalence and functional consequence of TP53 mutations in pediatric adrenocortical carcinoma: a children's oncology group study. In *Journal of clinical oncology : official journal of the American Society of Clinical Oncology* 33 (6), pp. 602–609. DOI: 10.1200/JCO.2013.52.6863.

Wassman, Christopher D.; Baronio, Roberta; Demir, Özlem; Wallentine, Brad D.; Chen, Chiung-Kuang; Hall, Linda V. et al. (2013): Computational identification of a transiently open L1/S3 pocket for reactivation of mutant p53. In *Nature communications* 4, p. 1407. DOI: 10.1038/ncomms2361.

Webster, Marie R.; Fane, Mitchell E.; Alicea, Gretchen M.; Basu, Subhasree; Kossenkov, Andrew V.; Marino, Gloria E. et al. (2020): Paradoxical Role for Wild-Type p53 in Driving Therapy Resistance in Melanoma. In *Molecular cell* 77 (3), 633-644.e5. DOI: 10.1016/j.molcel.2019.11.009.

Weinberg, Richard L.; Veprintsev, Dmitry B.; Fersht, Alan R. (2004): Cooperative binding of tetrameric p53 to DNA. In *Journal of molecular biology* 341 (5), pp. 1145–1159. DOI: 10.1016/j.jmb.2004.06.071.

Weissmueller, Susann; Manchado, Eusebio; Saborowski, Michael; Morris, John P.; Wagenblast, Elvin; Davis, Carrie A. et al. (2014): Mutant p53 drives pancreatic cancer metastasis through cell-autonomous PDGF receptor β signaling. In *Cell* 157 (2), pp. 382–394. DOI: 10.1016/j.cell.2014.01.066.

Weisz, L.; Oren, M.; Rotter, V. (2007): Transcription regulation by mutant p53. In *Oncogene* 26 (15), pp. 2202–2211. DOI: 10.1038/sj.onc.1210294.

West, Alina Nico; Ribeiro, Raul C.; Jenkins, Jesse; Rodriguez-Galindo, Carlos; Figueiredo, Bonald C.; Kriwacki, Richard; Zambetti, Gerard P. (2006): Identification of a novel germ line variant hotspot mutant p53-R175L in pediatric adrenal cortical carcinoma. In *Cancer research* 66 (10), pp. 5056–5062. DOI: 10.1158/0008-5472.CAN-05-4580.

Whitesell, L.; Sutphin, P. D.; Pulcini, E. J.; Martinez, J. D.; Cook, P. H. (1998): The physical association of multiple molecular chaperone proteins with mutant p53 is altered by geldanamycin, an hsp90-binding agent. In *Molecular and cellular biology* 18 (3), pp. 1517–1524. DOI: 10.1128/mcb.18.3.1517.

Wiedenheft, Blake; Sternberg, Samuel H.; Doudna, Jennifer A. (2012): RNA-guided genetic silencing systems in bacteria and archaea. In *Nature* 482 (7385), pp. 331–338. DOI: 10.1038/nature10886.

Williams, Ashley B.; Schumacher, Björn (2016): p53 in the DNA-Damage-Repair Process. In *Cold Spring Harbor perspectives in medicine* 6 (5). DOI: 10.1101/cshperspect.a026070.

Wong, K. B.; DeDecker, B. S.; Freund, S. M.; Proctor, M. R.; Bycroft, M.; Fersht, A. R. (1999): Hot-spot mutants of p53 core domain evince characteristic local structural changes. In *Proceedings of the National Academy of Sciences of the United States of America* 96 (15), pp. 8438–8442. DOI: 10.1073/pnas.96.15.8438.

Wong, Ronald Pak Cheung; Tsang, Wing Pui; Chau, Pui Yee; Co, Ngai Na; Tsang, Tsun Yee; Kwok, Tim Tak (2007): p53-R273H gains new function in induction of drug

resistance through down-regulation of procaspase-3. In *Molecular cancer therapeutics* 6 (3), pp. 1054–1061. DOI: 10.1158/1535-7163.MCT-06-0336.

Wong, Terrence N.; Ramsingh, Giridharan; Young, Andrew L.; Miller, Christopher A.; Touma, Waseem; Welch, John S. et al. (2015): Role of TP53 mutations in the origin and evolution of therapy-related acute myeloid leukaemia. In *Nature* 518 (7540), pp. 552–555. DOI: 10.1038/nature13968.

Wu, W.; Xu, C.; Ling, X.; Fan, C.; Buckley, B. P.; Chernov, M. V. et al. (2015): Targeting RING domains of Mdm2-MdmX E3 complex activates apoptotic arm of the p53 pathway in leukemia/lymphoma cells. In *Cell death & disease* 6, e2035. DOI: 10.1038/cddis.2015.358.

Wu, X.; Bayle, J. H.; Olson, D.; Levine, A. J. (1993): The p53-mdm-2 autoregulatory feedback loop. In *Genes & development* 7 (7A), pp. 1126–1132. DOI: 10.1101/gad.7.7a.1126.

Xie, Tian; Peng, Wei; Yan, Chuangye; Wu, Jianping; Gong, Xinqi; Shi, Yigong (2013): Structural insights into RIP3-mediated necroptotic signaling. In *Cell reports* 5 (1), pp. 70–78. DOI: 10.1016/j.celrep.2013.08.044.

Xu, Dandan; Tong, Xin; Sun, Leyu; Li, Haonan; Jones, Ryan D.; Liao, Jie; Yang, Guang-Yu (2019): Inhibition of mutant Kras and p53-driven pancreatic carcinogenesis by atorvastatin: Mainly via targeting of the farnesylated DNAJA1 in chaperoning mutant p53. In *Molecular carcinogenesis* 58 (11), pp. 2052–2064. DOI: 10.1002/mc.23097.

Xu, Jie; Qian, Jin; Hu, Ye; Wang, Jilin; Zhou, Xiaolin; Chen, Haoyan; Fang, Jing-Yuan (2014): Heterogeneity of Li-Fraumeni syndrome links to unequal gain-of-function effects of p53 mutations. In *Scientific reports* 4, p. 4223. DOI: 10.1038/srep04223.

Xu, Jie; Reumers, Joke; Couceiro, José R.; Smet, Frederik de; Gallardo, Rodrigo; Rudyak, Stanislav et al. (2011): Gain of function of mutant p53 by coaggregation with multiple tumor suppressors. In *Nature chemical biology* 7 (5), pp. 285–295. DOI: 10.1038/nchembio.546.

Xue, Wen; Zender, Lars; Miething, Cornelius; Dickins, Ross A.; Hernando, Eva; Krizhanovsky, Valery et al. (2007): Senescence and tumour clearance is triggered by p53 restoration in murine liver carcinomas. In *Nature* 445 (7128), pp. 656–660. DOI: 10.1038/nature05529.

Xu-Monette, Zijun Y.; Wu, Lin; Visco, Carlo; Tai, Yu Chuan; Tzankov, Alexander; Liu, Wei-min et al. (2012): Mutational profile and prognostic significance of TP53 in diffuse large B-cell lymphoma patients treated with R-CHOP: report from an International DLBCL Rituximab-CHOP Consortium Program Study. In *Blood* 120 (19), pp. 3986–3996. DOI: 10.1182/blood-2012-05-433334.

Yamamoto, Satomi; Iwakuma, Tomoo (2018): Regulators of Oncogenic Mutant TP53 Gain of Function. In *Cancers* 11 (1). DOI: 10.3390/cancers11010004.

Yemelyanova, Anna; Vang, Russell; Kshirsagar, Malti; Lu, Dan; Marks, Morgan A.; Shih, Ie Ming; Kurman, Robert J. (2011): Immunohistochemical staining patterns of p53 can serve as a surrogate marker for TP53 mutations in ovarian carcinoma: an immunohistochemical and nucleotide sequencing analysis. In *Modern pathology : an official journal of the United States and Canadian Academy of Pathology, Inc* 24 (9), pp. 1248–1253. DOI: 10.1038/modpathol.2011.85.

Yu, De-Hua; Xu, Zhi-Yuan; Mo, Shaowei; Yuan, Li; Cheng, Xiang-Dong; Qin, Jiang-Jiang (2020): Targeting MDMX for Cancer Therapy: Rationale, Strategies, and Challenges. In *Frontiers in oncology* 10, p. 1389. DOI: 10.3389/fonc.2020.01389.

Yu, Qiong; Li, Yan; Mu, Kun; Li, Zhishuang; Meng, Qingyong; Wu, Xiaojuan et al. (2014a): Amplification of Mdmx and overexpression of MDM2 contribute to mammary carcinogenesis by substituting for p53 mutations. In *Diagnostic pathology* 9, p. 71. DOI: 10.1186/1746-1596-9-71.

Yu, Xin; Blanden, Adam R.; Narayanan, Sumana; Jayakumar, Lalithapriya; Lubin, David; Augeri, David et al. (2014b): Small molecule restoration of wildtype structure and function of mutant p53 using a novel zinc-metallochaperone based mechanism. In *Oncotarget* 5 (19), pp. 8879–8892. DOI: 10.18632/oncotarget.2432.

Yu, Xin; Vazquez, Alexei; Levine, Arnold J.; Carpizo, Darren R. (2012): Allele-specific p53 mutant reactivation. In *Cancer cell* 21 (5), pp. 614–625. DOI: 10.1016/j.ccr.2012.03.042.

Yue, Xuetian; Zhao, Yuhan; Huang, Grace; Li, Jun; Zhu, Junlan; Feng, Zhaohui; Hu, Wenwei (2016): A novel mutant p53 binding partner BAG5 stabilizes mutant p53 and promotes mutant p53 GOFs in tumorigenesis. In *Cell discovery* 2, p. 16039. DOI: 10.1038/celldisc.2016.39.

Yue, Xuetian; Zhao, Yuhan; Liu, Juan; Zhang, Cen; Yu, Haiyang; Wang, Jiabei et al. (2015): BAG2 promotes tumorigenesis through enhancing mutant p53 protein levels and function. In *eLife* 4. DOI: 10.7554/eLife.08401.

Yue, Xuetian; Zhao, Yuhan; Xu, Yang; Zheng, Min; Feng, Zhaohui; Hu, Wenwei (2017): Mutant p53 in Cancer: Accumulation, Gain-of-Function, and Therapy. In *Journal of molecular biology* 429 (11), pp. 1595–1606. DOI: 10.1016/j.jmb.2017.03.030.

Zandi, Roza; Selivanova, Galina; Christensen, Camilla Laulund; Gerds, Thomas Alexander; Willumsen, Berthe Marie; Poulsen, Hans Skovgaard (2011): PRIMA-1Met/APR-246 induces apoptosis and tumor growth delay in small cell lung cancer expressing mutant p53. In *Clinical cancer research : an official journal of the American Association for Cancer Research* 17 (9), pp. 2830–2841. DOI: 10.1158/1078-0432.CCR-10-3168.

Zhang, Cen; Liu, Juan; Xu, Dandan; Zhang, Tianliang; Hu, Wenwei; Feng, Zhaohui (2020): Gain-of-function mutant p53 in cancer progression and therapy. In *Journal of molecular cell biology* 12 (9), pp. 674–687. DOI: 10.1093/jmcb/mjaa040.

Zhang, Qiang; Bykov, Vladimir J. N.; Wiman, Klas G.; Zawacka-Pankau, Joanna (2018): APR-246 reactivates mutant p53 by targeting cysteines 124 and 277. In *Cell death & disease* 9 (5), p. 439. DOI: 10.1038/s41419-018-0463-7.

Zhang, Wensheng; Edwards, Andrea; Flemington, Erik K.; Zhang, Kun (2017): Significant Prognostic Features and Patterns of Somatic TP53 Mutations in Human Cancers. In *Cancer informatics* 16, 1176935117691267. DOI: 10.1177/1176935117691267.

Zhang, Xiao-Hui; Tee, Louis Y.; Wang, Xiao-Gang; Huang, Qun-Shan; Yang, Shi-Hua (2015): Off-target Effects in CRISPR/Cas9-mediated Genome Engineering. In *Molecular therapy. Nucleic acids* 4, e264. DOI: 10.1038/mtna.2015.37.

Zhang, Yanping; Xiong, Yue; Yarbrough, Wendell G. (1998): ARF Promotes MDM2 Degradation and Stabilizes p53: ARF-INK4a Locus Deletion Impairs Both the Rb and p53 Tumor Suppression Pathways. In *Cell* 92 (6), pp. 725–734. DOI: 10.1016/s0092-8674(00)81401-4.

Zheng, Tongsen; Wang, Jiabei; Zhao, Yuhan; Zhang, Cen; Lin, Meihua; Wang, Xiaowen et al. (2013): Spliced MDM2 isoforms promote mutant p53 accumulation and gain-of-function in tumorigenesis. In *Nature communications* 4, p. 2996. DOI: 10.1038/ncomms3996.

Zhou, Xiang; Hao, Qian; Lu, Hua (2019): Mutant p53 in cancer therapy-the barrier or the path. In *Journal of molecular cell biology* 11 (4), pp. 293–305. DOI: 10.1093/jmcb/mjy072.

Zhu, Gaoyang; Pan, Chaoyun; Bei, Jin-Xin; Li, Bo; Liang, Chen; Xu, Yang; Fu, Xuemei (2020): Mutant p53 in Cancer Progression and Targeted Therapies. In *Frontiers in oncology* 10, p. 595187. DOI: 10.3389/fonc.2020.595187.

Zhu, J.; Zhang, S.; Jiang, J.; Chen, X. (2000): Definition of the p53 functional domains necessary for inducing apoptosis. In *The Journal of biological chemistry* 275 (51), pp. 39927–39934. DOI: 10.1074/jbc.M005676200.

Zhu, Jiajun; Sammons, Morgan A.; Donahue, Greg; Dou, Zhixun; Vedadi, Masoud; Getlik, Matthäus et al. (2015): Gain-of-function p53 mutants co-opt chromatin pathways to drive cancer growth. In *Nature* 525 (7568), pp. 206–211. DOI: 10.1038/nature15251.

Zilfou, Jack T.; Lowe, Scott W. (2009): Tumor suppressive functions of p53. In *Cold Spring Harbor perspectives in biology* 1 (5), a001883. DOI: 10.1101/cshperspect.a001883.

Zuber, Johannes; Radtke, Ina; Pardee, Timothy S.; Zhao, Zhen; Rappaport, Amy R.; Luo, Weijun et al. (2009): Mouse models of human AML accurately predict

chemotherapy response. In *Genes & development* 23 (7), pp. 877–889. DOI: 10.1101/gad.1771409.

Appendix

Curriculum Vitae

Personal data

Name	Mariia Klimovich
Adress	Maiengasse 4/1, 72144 Dußlingen
Date of birth	25 September 1985
Place of birth	Leningrad, USSR

Academic education and degrees

Jan 2014 - July 2020	Doctoral study, PD Dr. Oleg Timofeev, Molecular Oncology Institute (director Prof. Dr. Thorsten Stiewe), Marburg
2008-2010	Master of Science (**Public health**) St. Petersburg State University, Russia
2003-2007	Bachelor of Science (Biology) St. Petersburg State University, Russia
1999-2003	526 Gymnasium of the St.-Petersburg State University, Russia

Professional experience

2009-2014	Research Associate (ELISA group), Alkor Bio, St.-Petersburg, Russia
2008-2009	Technical Assistant, Laboratory of Radiation Genetics, Russian Research Center for Radiology and Surgical Technologies St.-Petersburg, Russia

Training

2018	FELASA B Course. Philipps University, Marburg

Supplementary materials

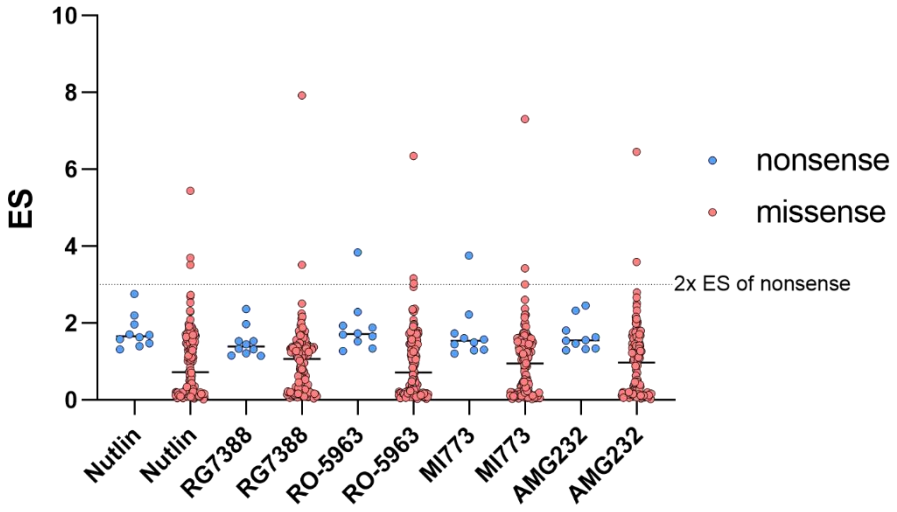

Figure 1. Comparison of enrichment scores of nonsense and missense variants in libraries treated with MDM2 inhibitors. Means of triplicates are shown. Dotted line: 2x mean ES of nonsense variants. Note that only single missense variants are enriched above this threshold. The most enriched missense variant in each library is P177D.

List of publications

Klimovich B, Mutlu S, Schneikert J, Elmshäuser S, **Klimovich M**, Nist A, Mernberger M, Timofeev O, Stiewe T. **Loss of p53 function at late stages of tumorigenesis confers ARF-dependent vulnerability to p53 reactivation therapy.** Proc Natl Acad Sci USA (PNAS). 2019, Oct 14. PMID: 31611375

Timofeev, Oleg; Koch, Lukas; Niederau, Constantin; Tscherne, Alina; Schneikert, Jean; **Klimovich, Maria** et al. (2020): **Phosphorylation control of p53 DNA binding cooperativity balances tumorigenesis and aging**. In *Cancer research*. DOI: 10.1158/0008-5472.CAN-20-2002.

Maria Klimovich, Marco Mernberger, Andrea Nist, Rajkumar Savai, Thorsten Stiewe, Michael Wanzel: ***Genomeditierung als Werkzeug für die Exploration von genetischen Einflussfaktoren in der personalisierten Tumortherapie***, Röhn 2017 (Poster)

List of academic teachers

My academic teachers at the Philipps University Marburg was Prof. Dr. Stiewe.

My academic teachers at the St.-Petersburg State University were:
Mmes and Messrs Barabanova, Buzovkina, Inge-Vechtomov, Lutova, Mironova, Mylnikov, Pendina, Tihodeev, Volkov, Vorobzova, Zhuravleva.

Acknowledgments

First, I would like to thank my supervisor Prof. Dr. Thorsten Stiewe, for giving me a chance to do my PhD thesis in his laboratory, for his advice, ideas, critic, support, and trust.

I am grateful to my colleagues from Stiewe lab for their excellent technical support, help, and compassion: Dr. Andrea Nist, Dr. Marco Mernberger for performing NGS, data analysis, helpful hints after our long discussion, and for the patience. Geli Filmer and Alexandra Schneider for helping with purifications and preparations of hundreds of samples for NGS. Without you, my work would have never be completed. Dr. Sabrina Elmshäuser for the help with an animal proposal, documents, and the steady-going support with my animal experiments. Björn Geißert for rendering invaluable assistance with minis and midis. Julia Funk, Michelle Neuman, and Pascal Hunold for being the best master students, your contribution is significant for my work, and I learned from you a lot.

I appreciate Siggi Bischofsberger, Miriam Rehberger, Anjela Mühling Aaron Dort and Antje Grzeschiczek for supporting laboratory's life in the very comfortable conditions. Nasti, Avanee, Laura, Anna Bo, Evangelos, Lukas, Constantin for making the lab a very pleasing place to work in.

Many thanks to former members of AG Stiewe: Martina, Anne, Jöel for helping me on the very beginning in the lab.

I would like to thank other University members for their help: Gavin Giel for his inestimable help with sorting, Dr. Andrea Arenz, and other members of the irradiation core facility for helping with setting up irradiation experiments.

I am especially thankful to my cousin Lilah Toker for the help with the text editing.

I am endlessly thankful to my colleagues who became much more than just colleagues for me: Michael (my first supervisor), Tini, Siggi, Oleg, Samet, Berni, Pier, Anna, Katha, Niklas. Thank you for everything.

I also thank my friends Maria, Frank, Vasili, and Anna for the friendship and lovely time in Marburg.

Last but not least, my deepest appreciation to my family, my beloved sister, and especially to my adorable husband Boris: your constant support, invaluable help with the databases analysis, clearness of purpose, and sense of humor made all this possible.

Ehrenwörtliche Erklärung

Ich erkläre ehrenwörtlich, dass ich die dem Fachbereich Medizin Marburg zur Promotionsprüfung eingereichte Arbeit mit dem Titel „Functional characterization of the TP53 mutome using CRISPR/Cas9 saturating mutagenesis“ im Institut für Molekulare Onkologie unter Leitung von Prof. Dr. Thorsten Stiewe ohne sonstige Hilfe selbst durchgeführt und bei der Abfassung der Arbeit keine anderen als die in der Dissertation aufgeführten Hilfsmittel benutzt habe. Ich habe bisher an keinem in- oder ausländischen Medizinischen Fachbereich ein Gesuch um Zulassung zur Promotion eingereicht, noch die vorliegende oder eine andere Arbeit als Dissertation vorgelegt.
Ich versichere, dass ich sämtliche wörtlichen oder sinngemäßen Übernahmen und Zitate kenntlich gemacht habe.

Mit dem Einsatz von Software zur Erkennung von Plagiaten bin ich einverstanden.

Vorliegende Arbeit wurde in Teilen in folgenden Publikationsorganen veröffentlicht:

Timofeev, Oleg; Koch, Lukas; Niederau, Constantin; Tscherne, Alina; Schneikert, Jean; Klimovich, Maria et al. (2020): Phosphorylation control of p53 DNA binding cooperativity balances tumorigenesis and aging. In *Cancer research*. DOI: 10.1158/0008-5472.CAN-20-2002

Ort, Datum, Unterschrift Doktorandin/Doktorand

_____

Die Hinweise zur Erkennung von Plagiaten habe ich zur Kenntnis genommen.

Ort, Datum, Unterschrift Referentin/Referent

_____